NASA TECHNICAL TRANSLATION

NASA TT F-805

NASA TT F-805

HEAT-MASS TRANSFER AND FRICTION IN A TURBULENT BOUNDARY LAYER

by S. S. Kutateladze and A. I. Leont'yev

"Energiya" Press
Moscow, 1972

NATIONAL AERONAUTICS AND SPACE ADMINISTRATION • WASHINGTON, D. C. • SEPTEMBER 1974

1. Report No.	2. Government Accession No.	3. Recipient's Catalog No.
NASA TT F-805		

4. Title and Subtitle	5. Report Date
HEAT-MASS AND FRICTION IN A TURBULENT BOUNDARY LAYER	September 1974
	6. Performing Organization Code

7. Author(s)	8. Performing Organization Report No.
S. S. Kutateladze and A. I. Leont'yev	
	10. Work Unit No.

9. Performing Organization Name and Address	11. Contract or Grant No.
Scripta Technica, Inc. 1511 K Street, N. W. Washington, D.C. 20005	NASw-2484
	13. Type of Report and Period Covered
12. Sponsoring Agency Name and Address	Translation
National Aeronautics and Space Administration Washington, D.C. 20546	14. Sponsoring Agency Code

15. Supplementary Notes

Translation of Teplo-Massoobmen i Treniye v Turbulentnom Pogranichnom Sloye, "Energiya" Press, Moscow, 1972, 344 pages

16. Abstract

The book analyses some conservative properties of the turbulent boundary layer at a wall. The concept of an ideal turbulent boundary layer with a degenerate viscous region is introduced, its properties are analyzed, and the theory of limiting friction and heat exchange at the surfaces of bodies immersed in flows with Reynolds numbers approaching infinity is presented. Problems connected with application of this theory of finite Reynolds numbers are discussed, experimental data are cited, and practical applications are indicated.

The projected audience for the book are specialists in hydro- and aerodynamics and convective heat transfer.

17. Key Words (Selected by Author(s))	18. Distribution Statement
	Unclassified -Unlimited STAR Category 01

19. Security Classif. (of this report)	20. Security Classif. (of this page)	21. No. of Pages	22. Price *
Unclassified	Unclassified	288	$6.75

*For sale by the National Technical Information Service, Springfield, Virginia 22151

FOREWORD

Turbulent flow is the most common form of motion of fluids, gases and plasma. /3* Nevertheless, the essence of this phenomenon became clear, if only in its most general aspects, only after the classical investigations of O. Reynolds, and turbulence was gradually perceived as a phenomenon inherent in nature and in various engineering processes.

Turbulence theory still remains one of the most fundamental and least developed problems of physical mechanics.

The ideas of L. Prandtl, K. Taylor and A. N. Kolmogorov regarding the existence of certain internal scales of turbulence led to the development of semi-empirical methods that are presently the only sound methods of extending the empirical knowledge in this area beyond the immediate context of the experimental data.

Most difficulty is encountered in the treatment of wall turbulence, i.e., the turbulent flow around a rigid body.

Two circumstances are paramount here: first, the significant structural inhomogeneity of the flow and its time-averaged parameter fields, and second, the existence of a flow region in the immediate vicinity of a rigid surface in which molecular friction is unconditionally dominant.

The turbulent boundary layer, just as any other stable statistical system, has some quite conservative properties; the significance of these properties in the development of a theory and practical computing methods have been accorded too little attention until recently.

The laws of wall turbulence in the immediate vicinity of a rigid body, but /4 outside the viscous region, are the most stable.

A change in conditions at the rigid surface exerts a significant influence on the viscous portion of the flow, and a change in conditions in the undisturbed flow reacts on the flow in the outer region of the turbulent boundary layer.

The circumstance that the dimensions of the viscous region diminish with decreasing viscosity more rapidly than does the size of the total turbulent boundary layer is also of much importance. In this connection it is necessary to consider some idealized turbulent flow with a degenerate viscous sublayer. It is noteworthy that in this boundary layer the integral characteristics of the transfer of momentum, heat and mass are determined by the properties of the conservative portion of the turbulent core and their relative changes when acted upon by disturbing factors (pressure gradient, compressibility, temperature non-uniformity, permeability of the rigid surface, physico-chemical transformations, etc.) do not depend on the

---

*Numbers in the margin indicate pagination in the foreign text.

empirical constants and are not linked to any special form of semi-empirical theory.

This text treats the fundamental theory of the turbulent boundary layer with vanishing viscosity and methods for its application in computing real flows. Also considered are the limiting properties of the thermal boundary layer at an adiabatic surface, the interaction of a submerged jet and a rigid body and certain other problems of thermal screens. Thus this monograph does not cover by any means all questions of turbulent boundary layer theory, but primarily only the results obtained in the main directions developed by the authors.

It is assumed that the reader is adequately equipped with the fundamentals of the modern theory of the boundary layer and the theory of convective heat-mass transfer.

We are most indebted to our colleagues of the Institute of Thermophysics and to the Air Transport Institute, Academy of Sciences, USSR, particularly to E. P. Volchkov and B. P. Mironov, who took direct part in the development of these new ideas and contributed directly to their development.

B. S. Petukhov and V. D. Vilenskiy are due thanks for their many valuable comments and discussions.

The Authors

TABLE OF CONTENTS

PRINCIPAL NOTATION

x, y—coordinates directed downstream along the surface and along the surface normal, respectively. /5

w_x, w_y—projections of average velocity on the x- and y-axes.

δ—thickness of dynamic boundary layer.

δ_T—thickness of thermal boundary layer.

δ_D—thickness of diffusion boundary layer.

P—pressure.

ρ—density.

τ—shearing stress in the xz-plane.

v_x, v_y, v_z—components of the fluctuating component of the velocity.

θ—fluctuating component of temperature.

B_x—magnetic field induction in the z-direction.

δ^*—displacement thickness.

δ^{**}—momentum loss thickness.

y_1—thickness of viscous sublayer.

$c_f = \frac{2\tau_w}{\rho_\infty w_\infty^2}$—coefficient of friction.

μ—coefficient of dynamic viscosity.

$\nu = \mu/\rho$—coefficient of kinematic viscosity.

$\bar{j}_{ot} = \frac{j_w}{\rho_\infty w_\infty}$—relative mass velocity through surface of body.

j_y—stream in direction of y-axis.

$v^*_w = \sqrt{\frac{\tau_w}{\rho_\infty}}$—friction velocity.

$\varphi = \frac{w_\infty}{v^*_w}$—dimensionless velocity.

a—velocity of sound.

$\eta = \frac{y v^*_w}{\nu}$—dimensionless coordinate.

$\xi = \frac{y}{\delta}$, $\xi_T = \frac{y}{\delta_T}$, $\xi_i = \frac{y}{\delta_i}$, $\xi_D = \frac{y}{\delta_D}$ —dimensionless distances from wall.

$b = \frac{j_w}{\rho_e w_e} \frac{2}{c_{fo}}$; $b_i = \frac{j_w}{\rho_e w_e} \frac{2}{c_f}$—permeability parameters. /6

$$b_T = \frac{j_w}{\rho_e w_e} \frac{1}{St_e}; \quad b_D = \frac{j_w}{\rho_e w_e} \frac{1}{St_D}.$$

c_{fo}—coefficient of friction on a plane impermeable plate in a non-isothermal flow (standard conditions").

$\tilde{\tau} = \frac{\tau}{\tau_w}$—dimensionless shearing stress under conditions considered.

$\tilde{\tau}_e = \frac{\tau_e}{\tau_{wo}}$—dimensionless shearing stress under "standard conditions."

$Re^{**} = \frac{\rho_e w_e \delta^{**}}{\mu^*}$—Reynolds number formed in accordance with the momentum loss thickness.

$f_k = \frac{\delta}{w_e} \frac{dw_e}{dx}$; $f = \frac{\delta^{**}}{w_e} \frac{dw_e}{dx}$; $f^* = \frac{\delta^*}{w_e} \frac{dw_e}{dx}$—shape parameters.

q—energy flux due to molecular and turbulent heat transfer.

q_v—volume density of all energy sources.

i—specific enthalpy.

T—temperature.

λ—coefficient of heat conductivity.

C_p—specific heat at constant pressure.

i^*—stagnation enthalpy.

i^*_Σ—total enthalpy.

c_i—concentration by weight of i-th component.

i^o_i—heat production of i-th component.

$Pr = \frac{\mu C_p}{\lambda}$—Prandtl number.

$Pr_T = C_p \frac{\mu_T}{\lambda_T}$—turbulent Prandtl number.

$M = \frac{w_e}{a}$—Mach number.

$\omega = \frac{w_x}{w_e}$—dimensionless velocity.

i_w^*—equilibrium enthalpy at wall.

T_w^*—equilibrium temperature at wall.

r—recovery coefficient.

$Sc = \frac{\nu}{D}$—Schmidt number.

$Sc_T = \frac{\nu_T}{D_T}$—turbulent Schmidt number.

$\psi = \frac{i_{cT}}{i_e}\left(\frac{T_{cT}}{T_e}\right)$—enthalpy (temperature) factor. /7

$\psi_e^* = \frac{i^*_{wo}}{i_e}\left(\frac{T^*_{wo}}{T_e}\right)$—adiabatic kinetic enthalpy (temperature) factor.

$\Delta\psi = \psi - \psi^*$—heat-transfer factor.

$\psi^* = \frac{i^*_w}{i_e}\left(\frac{T^*_w}{T_e}\right)$—kinetic enthalpy (temperature) factor.

ε—non-similarity factor of velocity and enthalpy profiles.

$\delta^{**}_{i\Sigma}$—energy-loss thickness.

$Re^{**}_{\Sigma} = \frac{\rho_e w_e \delta^{**}_{\Sigma}}{\mu_{ee}}$—Reynolds number formed from energy-loss thickness.

$St_x = \frac{q_{cT\,x}}{\rho_e w_e (i_w - i^*_w)}$—generalized Stanton number.

δ^{**}_D—mass-loss thickness.

$St_D = \frac{j_{cr_1}}{\rho_e w_e (c_w - c_e)}$ —Stanton diffusion number.

$\bar{q} = \frac{q}{q_w}$; $\bar{j}_1 = \frac{j_1}{j_{w1}}$—dimensionless energy and mass flows.

θ^*, Δc^* —heat- and diffusion-analogs of frictional velocity.
i

β—coefficient accounting for the effects of density fluctuations on τ_T.

$\Psi = \left(\frac{c_f}{c_{fe}}\right)_{Re^{**}}$; $\Psi_S = \left(\frac{St}{St_e}\right)_{Re^{**}_{\Omega}}$; $\Psi_D = \left(\frac{St_D}{St_{D_e}}\right)_{Re^{**}_D}$ — relative laws of friction, heat-transfer and mass-transfer.

ω_e, ϑ_e, $\overline{\Delta c_e}$—dimensionless velocity, enthalpy and concentration in "standard" conditions.

Ψ_∞, $\Psi_{S\infty}$, $\Psi_{D\infty}$—limiting relative laws of friction, heat- and mass-transfer.

α—degree of dissociation of gas.

i^o_α—heat of dissociation.

b_{crit}—critical injection parameter.

$U = w_o/w_{max}$—ratio of velocity at outer edge of boundary layer to maximum velocity $w_{max} = \sqrt{2gi_{oo}}$.

F—nozzle throat area.

F_{crit}—area of critical nozzle section.

$Pe^{**}_T = Re^{**}_T Pr$—Peclet number according to energy-loss thickness.

q(U)—flow-rate function.

δ^*_D—displacement thickness in Dorodnitsin variables.

Ψ_1—relative law of friction for laminar boundary layer. /8

G—gas flow rate.

a—non-uniformity factor of the velocity distribution over the tube cross section.

Θ—effectiveness of the gas screen.

Δ—roughness height.

c^*_i—concentration of i-th component at a given point of the boundary layer at an ideal wall.

$(c_{co})_w$—concentration of CO_2 at wall.

Main Subscripts

w—parameters at wall.

0—parameters at outer edge of boundary layer or "standard" conditions.

—parameters with $Re \rightarrow \infty$.

crit—critical parameters.

l—parameters of substance introduced into the boundary layer at intersection with the wall surface.

00—parameters with adiabatic stagnation of gas.

PART I: BOUNDARY LAYER WITH VANISHING VISCOSITY

CHAPTER 1
THE DYNAMIC BOUNDARY LAYER

1.1. Equations of Motion of the Plane Boundary Layer

/9

When a fluid flows around a rigid surface a dynamic boundary layer is formed, i.e., a region in which the velocity of the fluid varies from the wall velocity to a velocity quite close to that of the undisturbed flow. If the dimensions of this region are significantly greater than the molecular free path, the relative velocity of the medium at the surface of the rigid body is, practically, zero.

The usual flow region in which the gas may be considered to be a continuous medium "attached" to the surface in the flow, is described by the condition

$$M < 0{,}01 \sqrt{\mathrm{Re}}. \quad (1\text{-}1\text{-}1)$$

*

When separating out the dynamic boundary layer for $y \approx \delta$, the exact boundary conditions are replaced by approximate conditions. Then

$$y \to \delta,\ w_x \to (1-\varepsilon) w_0;$$
$$y \to 0,\ w_x \to 0;$$

where ε is a small quantity.

We refer to a boundary layer of finite thickness in this sense (Fig. 1.1).

As first shown by Prandtl, the conditions

$$\frac{\partial P}{\partial x} \gg \frac{\partial P}{\partial y},\ \frac{\partial^2 w_x}{\partial x^2} \ll \frac{\partial^2 w_x}{\partial y^2}. \quad (1\text{-}1\text{-}2)$$

are satisfied in a plane boundary layer in the absence of significant transverse forces (e.g. centrifugal forces). /10

In view of this the equation of motion is considerably simplified and takes the form

$$-\frac{dP}{dx} + \frac{\partial \tau}{\partial y} = \rho w_x \frac{\partial w_x}{\partial x} + \rho w_y \frac{\partial w_x}{\partial y} - j_y B_z. \quad (1\text{-}1\text{-}3)$$

With $j_y B_z = 0$,

$$-\frac{dP}{dx} + \frac{\partial \tau}{\partial y} = \rho w_x \frac{\partial w_x}{\partial x} + \rho w_y \frac{\partial w_x}{\partial y}. \quad (1\text{-}1\text{-}4)$$

*Translator's Note: In Russian practice, the comma indicates a decimal point.

The equation of continuity retains its usual form, i.e., for a plane, steady flow it is

$$\frac{\partial(\rho w_x)}{\partial x}+\frac{\partial(\rho w_y)}{\partial y}=0. \tag{1-1-5}$$

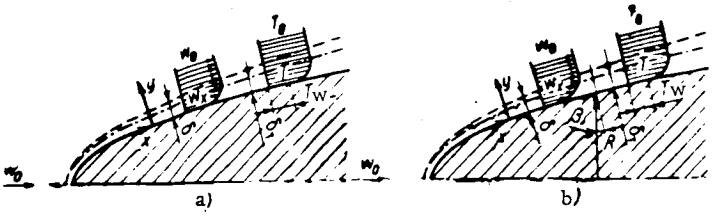

FIG. 1.1. Diagram of boundary layer at the surface of a body; a) plane boundary layer; b) axi-symmetric boundary layer.

These and all subsequent equations, unless specifically stated, refer to steady, mean motion, that is, all quantities appearing are averaged over a period of time considerably longer than the period of the turbulent fluctuations, where, for a conducting liquid, the fluctuations in the electric and magnetic quantities are neglected in a first approximation.

In the laminar boundary layer

$$\tau=\mu\frac{\partial w_x}{\partial y}, \tag{1-1-6}$$

and in the turbulent boundary layer

$$\tau=\mu\frac{\partial w_x}{\partial y}-\rho\overline{v_x v_y}\,(1-\tilde{\beta}), \tag{1-1-7}$$

where

$$\tilde{\beta}=\beta\frac{w_y\overline{v_x\theta}+\overline{v_x v_y\theta}}{\overline{v_x v_y}}$$

is a coefficient accounting for density fluctuations ascribable to temperature fluctuations and β is the temperature coefficient of volume expansion. /11

Outside the boundary layer ($y>\delta$) the frictional forces are almost absent, and for a steady flow with $B_z = 0$

$$-\frac{dP}{dx}=\rho_0 w_0\frac{dw_0}{dx}. \tag{1-1-8}$$

1.2. Integral Momentum Relations

Term-by-term integration of the equation of motion of the plane boundary layer (1-1-3) from 0 to δ, taking into account the equation of continuity and (1-1-7), reduces to the so-called integral momentum relations (the Karman equation). If we assume $j_y B_z$ = const. over the boundary layer cross section for conducting fluids, then

$$\rho_0 w_0\frac{dw_0}{dx}=-\frac{dP}{dx}+j_y B_x; \tag{1-2-1}$$

$$\frac{d\delta^{**}}{dx}+\frac{2\delta^{**}+\delta^{*}}{w_e}\frac{dw_e}{dx}+\frac{\delta^{**}}{\rho_e}\frac{d\rho_e}{dx}-\frac{j_w}{\rho_e w_e}=\frac{\tau_w}{\rho_e w_0^2}. \tag{1-2-2}$$

Here

$$\delta^{*}=\int_0^{\delta}\left(1-\frac{\rho w_x}{\rho_e w_e}\right)dy \tag{1-2-3}$$

is the displacement thickness;

$$\delta^{**}=\int_0^{\delta}\frac{\rho w_x}{\rho_e w_e}\left(1-\frac{w_x}{w_e}\right)dy$$

is the momentum loss thickness.

In dimensionless form

$$\tilde{\delta}^{*}=\delta^{*}/\delta \quad \text{and} \quad \tilde{\delta}^{**}=\delta^{**}/\delta. \tag{1-2-4}$$

Integral characteristics such as δ^* and δ^{**} have the remarkable property that an increase in the upper limit of integration in the range $y > \delta$ yields essentially no change in their magnitudes. In experimental determinations with sufficiently accurate measurements such "internal" linear characteristics of the boundary layer are practically insensitive to a further improvement in instrumental accuracy, while the boundary layer thickness δ is directly related to the choice of the quantity ε. /12

Stated differently, we can write for the boundary layer

$$\int_0^{\delta}\left(1-\frac{\rho w_x}{\rho_e w_e}\right)\frac{dy}{\delta}\approx\frac{1}{\delta}\int_0^{\infty}\left(1-\frac{\rho w_x}{\rho_e w_e}\right)dy. \tag{1-2-5}$$

The quantity j_v in (1-2-2) represents the mass velocity through the rigid surface considered. If this surface is impermeable (not porous, or if no physico-chemical transformations take place in it), $j_w = 0$.

We introduce the following notation:

$$c_f=\frac{2\tau_w}{\rho_e w_0^2}; \tag{1-2-6}$$

$$H=\frac{\delta^{*}}{\delta^{**}}; \tag{1-2-7}$$

$$f=\frac{\delta^{**}}{w_e}\frac{dw_e}{dx}; \tag{1-2-8}$$

$$\mathrm{Re}^{**}=\frac{\rho_e w_e \delta^{**}}{\mu^{*}}; \tag{1-2-9}$$

where μ^* is the characteristic viscosity, not dependent on x.

Then the integral momentum relation can be written as

$$\frac{d\,\mathrm{Re}^{**}}{d\bar{x}} + \mathrm{Re}_L (1+H) f - \bar{j}_w \mathrm{Re}_L = \mathrm{Re}_L \frac{c_f}{2}. \qquad (1\text{-}2\text{-}10)$$

Here $\bar{x} = x/L$ is the relative longitudinal distance (L = characteristic length of body) $\bar{j}_w = j_w/(\rho_0 \omega_0)$ is the relative mass velocity through the surface of the body; $\mathrm{Re}_L = \rho_0 \omega_0 L/\mu^*$ is the Reynolds number set up for the characteristic length of the body and the local flow velocity outside the boundary layer.

For a flow without pressure or magnetic field gradients (f = 0, since dP/dx = 0, $B_z = 0$) we have

$$\frac{d\,\mathrm{Re}^{**}}{d\,\mathrm{Re}_x} - \bar{j}_w = \frac{c_f}{2}, \qquad (1\text{-}2\text{-}11)$$

where

$$\mathrm{Re}_x = \omega_0 x/\nu_0, \quad \omega_0 = \mathrm{const}. \qquad /13$$

Thus the integral momentum relation interrelates the local coefficient of friction c_f, the local value of Reynolds number in the form Re** and the external flow parameters (wall permeability, pressure distribution along the flow, magnetic field intensity, current density).

The quantities H and f are related to body shape and are hence called shape factors. For a plane boundary layer of conducting fluid at an insulating wall

$$j_y \neq \mathrm{const} = j_y(z), \quad E_y = \mathrm{const},$$

and hence, after the appropriate conversions, we have

$$\frac{d\delta^{**}}{dx} + \delta^{**}\left[\frac{1}{x_0}\frac{dx_0}{dx}(H+2) + \frac{1}{\rho_0^*}\frac{d\rho_0}{dx} + \frac{B_z j_y^0}{\rho_0 \omega_0^2} H_j\right] - \frac{j_w}{\rho_0 \omega_0} = \frac{c_f}{2}, \qquad (1\text{-}2\text{-}12)$$

where

$$H_j = \Delta_j/\delta^{**}; \quad \Delta_j = \int_0^\delta \left(1 - \frac{j_y}{j_y^0}\right) dy;$$

j_y^0 is the stream at the outer edge of the boundary layer.

Going over to the Reynolds number, we have

$$\frac{d\,\mathrm{Re}^{**}}{d\bar{x}} + \mathrm{Re}_L (1+H) f + \mathrm{Re}^{**} \frac{B_z j_y^0}{\rho_0 \omega_0^2} H_j - \bar{j}_w \mathrm{Re}_L = \mathrm{Re}_L \frac{c_f}{2} \qquad (1\text{-}2\text{-}13)$$

For an axi-symmetric boundary layer, a diagram of which is shown in Fig. 1.1, with $\delta \ll R_x$, the integral momentum equation takes the form

$$\frac{d\delta^{**}}{dx} + f(2+H)\frac{\delta^{**}}{b_0}\frac{db_0}{dx} + \frac{\delta^{**}}{R_m}\frac{dR_m}{dx} - j_w = \frac{c_f}{2} \tag{1-2-14}$$

or /14

$$\frac{d(R_m \mathrm{Re}^{**})}{dx} + \mathrm{Re}_L R_x f(1+H) - \mathrm{Re}_L R_x j_w = \mathrm{Re}_L R_x \frac{c_f}{2}. \tag{1-2-15}$$

We assume

$$\tilde{\delta}^{*} = \int_0^1 (1-\tilde{\rho}\omega)\left(1 \pm \frac{y}{R_m}\cos\beta\right) d\xi; \tag{1-2-16}$$

$$\tilde{\delta}^{**} = \int_0^1 \tilde{\rho}\omega(1-\omega)\left(1 \pm \frac{y}{R_m}\cos\beta\right) d\xi, \tag{1-2-17}$$

where $\tilde{\rho} = \rho/\rho_0$ is the relative density of the medium at a given point; R_x is the radius of curvature of the body in the diametral plane; β is an angle (see Fig. 1.1).

In what follows, all considerations will relate basically to nonconducting fluids.

1.3. Turbulent Friction Near the Wall

On substituting the shearing stress from (1-1-7) into (1-1-4) we can write the equation of motion of a plane boundary layer as

$$-\frac{dP}{dx} + \frac{\partial}{\partial y}\left\{[\mathrm{Re}^{-1} + \chi^2(1-\tilde{\beta})]\rho\left(y\frac{\partial w_x}{\partial y}\right)^2\right\} = \rho w_x \frac{\partial w_x}{\partial x} + \rho w_y \frac{\partial w_x}{\partial y}. \tag{1-3-1}$$

Here

$$\mathrm{Re} = \frac{y^2}{\nu}\frac{\partial w_x}{\partial y} \tag{1-3-2}$$

is the local Reynolds number in the sense of L. G. Loitsyanskiy [58];

$$\chi^2 = -\frac{\overline{v_x v_y}}{\left(y\frac{\partial w_x}{\partial y}\right)^2} \tag{1-3-3}$$

is the characteristic of the intensity of the turbulent fluctuations in the sense of L. Prandtl.

At a rigid impermeable wall $v_y = 0$, and hence we have the conditions /15

$$y \to 0, \quad \overline{v_x v_y} \to 0, \quad \tau \to \tau_w = \mu \left(\frac{\partial w_x}{\partial y}\right)_w, \quad \mathrm{Re} \sim \frac{\rho_1}{\mu^2} y^2, \tag{1-3-4}$$

where τ_1 is the shearing stress due to molecular viscosity.

This region is called the viscous sublayer of the turbulent boundary layer. We denote its nominal thickness as y_1, and the velocity at its edge as w_1. With large enough Reynolds numbers, $y_1 \ll \delta$.

In the region $y > y_1$, the role of molecular friction reduces to the dissipation of the flow of mechanical energy from large-scale turbulence fluctuations into small-scale fluctuations, and turbulent friction is essentially independent of the molecular viscosity of the medium. From this it follows that the quantity χ in the outer periphery of the viscous sublayer does not depend materially on Re or on the conditions at the outer edge of the turbulent boundary layer:

$$y_1 < y \ll \delta, \quad \chi \approx \varkappa = \text{const}. \tag{1-3-5}$$

Accordingly, the law of turbulent friction near a rigid wall, but outside the viscous sublayer, is defined by the Prandtl formula*

$$\tau_T = \rho \left(\varkappa y \frac{\partial w_x}{\partial y}\right)^2 (1 - \tilde{\beta}). \tag{1-3-6}$$

As will be shown later, formula (1-3-6) is of fundamental importance in the theory of the turbulent boundary layer with vanishing molecular viscosity.

In the immediate vicinity of the wall, i.e., within the viscous sublayer, the turbulent fluctuations are strongly damped by molecular friction and their magnitude is directly related to Re.

1.4. Logarithmic Velocity Profile /16

Consider a plane, turbulent boundary layer of an incompressible fluid with $f = 0$. Then, in the region $y_1 < y \ll \delta$, with good accuracy

$$\tau = \tau_T = \tau_w = \rho \left(\varkappa y \frac{\partial w_x}{\partial y}\right)^2 \tag{1-4-1}$$

and accordingly

$$w_x = w_1 + \frac{v^*_w}{\varkappa} \ln \frac{y}{y_1}. \tag{1-4-2}$$

---

*Strictly speaking this formula has the form

$$\tau_T = \rho (\varkappa y)^2 \left|\frac{\partial w_x}{\partial y}\right| \frac{\partial w_x}{\partial y}.$$

This velocity distribution law was first defined by Prandtl and Nikuradze. Its universal form is

$$\varphi = c_* + \frac{1}{\varkappa} \ln \eta, \qquad (1\text{-}4\text{-}3)$$

where $\varphi = \frac{w_*}{v^*_w}$ is the dimensionless velocity; $c_* = \varphi_1 - \frac{1}{\varkappa} \ln \eta_1$ is some constant; $\eta = v^*_w y/\nu$ is the dimensionless distance from the wall; φ_1 and η_1 are the values of these parameters at the boundary of the viscous sublayer.

The quantities φ_1 and η_1 correspond to the common intersection of the logarithmic velocity profile in the turbulent core of the boundary layer and the linear velocity distribution in the viscous sublayer

$$\varphi = \eta. \qquad (1\text{-}4\text{-}4)$$

This arrangement of the turbulent boundary layer is called the "double layer", and it suffices for solution of the friction problem.

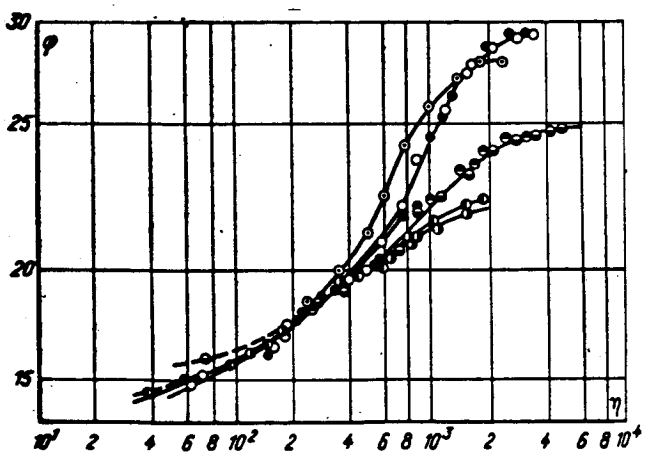

FIG. 1.2. Influence of free stream turbulence on the velocity profile in the turbulent boundary layer.
Test data [258]: ◑ ◐ ◓ ◒ – low turbulence (up to 1%); ⊙ ● ○ – high turbulence (up to 10%).

Figure 1.2 shows experimental data on the effect of external turbulence on the velocity profile in the turbulent boundary layer, with f = 0. It can be seen clearly that the velocity profile is significantly deformed in the outer portion of the boundary layer with high levels of turbulence in the main flow ($y > \delta$). But near the wall the logarithmic velocity distribution is maintained. /17

The same picture is also observed in the flow of an incompressible fluid with $f \neq 0$ (Fig. 1.3). However, in this case $\tau \neq \tau_w$ near the wall and the presence of the logarithmic section of the velocity profile requires special treatment.

According to the test data $\varkappa = 0.4$* and (in the two-layer scheme) $\eta_1 = 11.6$.

With these coefficients the Prandtl-Nikuradze formula takes the form

$$\varphi = 5{,}5 + 2{,}5 \ln \eta. \qquad (1\text{-}4\text{-}5)$$

*The theoretical value of this quantity is 0.395, as computed by M. A. Gol'shtik and S. S. Kutateladge [22].

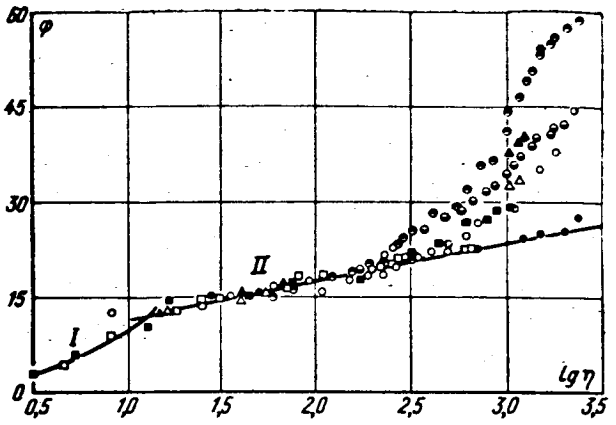

FIG. 1.3. Effect of longitudinal pressure gradient on the velocity profile in the turbulent boundary layer. Experimental points from data: o. ●– Shubauer and Klebanov [211]; □. ■ – Fage [137]; △. ▲ – Badley and Brebner [108]; ◓. ◒ – A. I. Leont'ev, P. N. Romanenko, A. N. Oblivin [66]. Curve 1—$\varphi = \eta$; curve II—$\varphi = 5.5 + 2.5 \lg \eta$.

1.5. Quadratic Law of Friction in the Core of a Turbulent Boundary Layer

Formulas (1-4-1) and (1-4-5) reflect the basic regularity of the developed turbulent flow—the quadratic law of friction. In this case the magnitude of the friction depends only on a single physical property of the medium—the density. The unique relationship between turbulent friction and the field of average flow velocities is the next fundamental factor. Here the magnitude of τ_T is definitively fixed by the derivative $\partial\omega_x/\partial_y$ in the region of significant velocity changes. /18

This result is confirmed experimentally by the fact of the existence of a logarithmic section of the velocity profile near a body in a flow of incompressible fluid.

But the inequality $|\partial w_x/\partial x| \gg |\partial w_x/\partial y|$ may also exist in the outer portion of the boundary layer, for $f \neq 0$, with $y \to \delta$ $\partial w_x/\partial y \to 0$, $\partial w_x/\partial x \to dw_0/dx$. Therefore, for a plane turbulent boundary layer of incompressible fluid, we must have in the general case

$$\overline{v_x v_y} = \Phi\left(\frac{\partial w_x}{\partial x};\ \frac{\partial w_x}{\partial y};\ y;\ \delta\right). \tag{1-5-1}$$

Keeping in mind (1-4-1), we can write

$$\frac{\overline{v_x v_y}}{\left(y\dfrac{\partial w_x}{\partial y}\right)^2} = \chi\left(\frac{\partial w_x/\partial x}{\partial w_x/\partial y};\ \xi\right), \tag{1-5-2}$$

where $\xi = y/\delta$ so that $\chi \to \varkappa$ as $\xi \to 1$.

If we introduce the parameter

$$l = \left|\frac{\sqrt{\overline{v_x v_y}}}{\partial w_x/\partial y}\right|, \tag{1-5-3}$$

then

$$\tau_T = \rho\left(l\frac{\partial w_x}{\partial y}\right)^2, \tag{1-5-4}$$

where

$$l = \delta \tilde{l}\left(\frac{\partial w_x/\partial x}{\partial w_x/\partial y}; \xi\right). \qquad (1\text{-}5\text{-}5)$$

Expression (1-5-4) is known as the Prandtl-Taylor formula, and, as can be seen from the above discussion, it is not related to any specific representation of the mechanism of turbulent transfer.*

The quantity l can be considered to be some integral linear scale of turbulence that retains the imprecise but traditional name of mixing path length. /19

In the vicinity of the viscous sublayer we have the law (1-3-6).

1.6. Shearing Stress Profile Approximations

We know that the distribution of shearing stress over the boundary layer cross section depends weakly on the fluid flow state. Thus, for example, with a steady, stable flow of an incompressible fluid of constant properties in a duct of constant cross section, the shearing stresses vary linearly over the duct width, independently of the fluid flow state, i.e.

$$\tilde{\tau} = \frac{\tau}{\tau_w} = 1 - \xi, \qquad (1\text{-}6\text{-}1)$$

where $\xi = y/h$; h is the half-width, or radius, of the duct.

In the general case the distribution of shearing stresses over the cross section of the boundary layer can be found from the equations of motion and continuity [18].

By integrating the equation of motion over the boundary layer section from 0 to y, we find

$$\tau - \tau_w = \frac{d}{dx}\int_0^y \rho w_y^2\, dy -$$

$$- w_x \frac{d}{dx}\int_0^y \rho w_x\, dy + \rho_w w_{y\,w} w_{x} - \rho_0 w_0 \frac{dw_0}{dx}\, y. \qquad (1\text{-}6\text{-}2)$$

For standard conditions (ρ= const, $j_w = 0$, $d\omega_0/dx = 0$) we have from Eq. (1-6-2):

$$\tau_0 = \tau_{wo} + \rho \frac{d}{dx}\int_0^y w_x^2\, dy - \rho w_x \frac{d}{dx}\int_0^y w_x\, dy. \qquad (1\text{-}6\text{-}3)$$

* Prandtl derived this formula from the somewhat inexact analogy between the transfer of certain "turbulent blobs" of fluid and the motion of gas molecules. Taylor proceeded from the more tenable hypothesis of the transfer of vorticity.

Going over to dimensionless form, we have /20

$$\tilde{\tau}_0 = \frac{\tilde{\tau}_0}{\tau_{w0}} = 1 - \frac{2}{c_{f0}}\left[\omega \frac{d}{dx}\left(\delta \int_0^\xi \omega d\xi\right) - \frac{d}{dx}\left(\delta \int_0^\xi \omega^2 d\xi\right)\right], \qquad (1\text{-}6\text{-}4)$$

where $\xi = y/\delta$.

For a self-similar flow $\omega = f(\xi)$, and then, taking into account the fact that $\frac{c_{f0}}{2} = \frac{d\delta}{dx}\int_0^1 \omega(1-\omega)\,d\xi$, we can write

$$\tilde{\tau}_0 = 1 - \frac{\delta}{\delta^{**}}\left(\omega \int_0^\xi \omega\, d\xi - \int_0^\xi \omega^2\, d\xi\right). \qquad (1\text{-}6\text{-}5)$$

Accordingly, in the general case, we have from (1-6-2):

$$\frac{\tau}{\tau_w} = Z_1 + b_1 Z_2 + \left(-\frac{2f}{c_f \tilde{\delta}^{**}}\right) Z_3, \qquad (1\text{-}6\text{-}6)$$

where

$$Z_1 = 1 - \frac{\delta}{\delta^{**}}\left(\omega \int_0^\xi \tilde{\rho}\omega\, d\xi - \int_0^\xi \tilde{\rho}\omega^2\, d\xi\right);$$

$$Z_2 = \omega - \frac{\delta}{\delta^{**}}\left(\omega \int_0^\xi \tilde{\rho}\omega\, d\xi - \int_0^\xi \tilde{\rho}\omega^2\, d\xi\right);$$

$$Z_3 = \xi - H\left(\omega \int_0^\xi \tilde{\rho}\omega\, d\xi - \int_0^\xi \tilde{\rho}\omega^2\, d\xi\right) - \omega \int_0^\xi \tilde{\rho}\omega\, d\xi$$

or

$$\frac{\tilde{\tau}}{\tilde{\tau}_0} = \varphi_1 + b_1\varphi_2 + \Lambda\varphi_3, \qquad (1\text{-}6\text{-}7)$$

where

$$\varphi_1 = \frac{Z_1}{Z_{10}},\ \varphi_2 = \frac{Z_2}{Z_{10}},\ \varphi_3 = \frac{Z_3}{Z_{10}};$$

$$Z_{10} = \tilde{\tau}_0 = 1 - \frac{\delta}{\delta^{**}}\left(\omega_0 \int_0^\xi \omega_0\, d\xi - \int_0^\xi \omega_0^2\, d\xi\right);$$

$$\Lambda = \frac{\delta}{\tau_w}\frac{dP}{dx} = -\frac{2f}{c_f \tilde{\delta}^{**}}.$$

Thus, for the general case with self-similar flow, the functions φ_1, φ_2 and φ_3 depend on the coordinate ξ, and on the velocity and density distributions in the boundary layer. /21

For more practical cases, a power-law approximation of the shearing stress distribution over the boundary layer cross section yields satisfactory results.

From the definition of a dynamic boundary layer of finite thickness we have the condition

$$\xi=0,\ \tilde{\tau}=1;\ \xi=1,\ \tilde{\tau}=0. \tag{1-6-8}$$

Very close to the wall $w_x \longrightarrow 0$ and the equation of motion can be written as

$$-\frac{dP}{dx}+\frac{\partial \tau}{\partial y}\sim \rho w_y \frac{\partial w_x}{\partial y}. \tag{1-6-9}$$

Integrating (1-6-9) with the condition $\rho\omega_y = j_w$, we find

$$\tau \sim \tau_w + \frac{dP}{dx} y + j_w w_x. \tag{1-6-10}$$

With $y \longrightarrow \delta$ $w_x \longrightarrow w_0$, $\partial w_x/\partial y \longrightarrow 0$, and taking (1-1-4) into account, we can write $\partial\tau/\partial y \longrightarrow 0$. From this the set of conditions follow

$$\left.\begin{aligned} &\xi\to 0,\ \tilde{\tau}\sim 1+\Lambda\xi+b_1\omega;\\ &\xi\to 1,\ \tilde{\tau}\to 0,\ \frac{\partial\tilde{\tau}}{\partial\xi}\to 0. \end{aligned}\right\} \tag{1-6-11}$$

Here

$$\Lambda=\frac{\delta}{\tau_w}\frac{dP}{dx}=-\frac{2f}{c_f\tilde{\delta}^{**}}; \tag{1-6-12}$$

$$b_1=\frac{2\bar{j}_w}{c_f}. \tag{1-6-13}$$

The first of these represents a certain modification of the shape parameter (aerodynamic body curvature parameter).

The second quantity describes the effect of supply or loss of matter through the surface of the body. We shall refer to this quantity as the wall permeability parameter.

In what follows we shall treat some additional modifications of the shape- and permeability parameters. /22

Conditions (1-6-1) are satisfied by a cubic parabola

$$\tilde{\tau}=1-3\xi^2+2\xi^3+(\Lambda\xi+b_1\omega)(1-\xi)^2 \tag{1-6-14}$$

or

$$\tilde{\tau}=\tilde{\tau}_0\left(1+\frac{\Lambda\xi+b_1\omega}{1+2\xi}\right), \tag{1-6-15}$$

where

$$\tilde{\tau}_0 = 1 - 3\xi^2 + 2\xi^3. \qquad (1\text{-}6\text{-}16)$$

The quantity τ_0 represents the distribution of shearing stress over the thickness of the boundary layer at a smooth impermeable plate in the absence of a pressure gradient.

The quantity $\omega = w_x/w_0$ represents the dimensionless longitudinal velocity component.

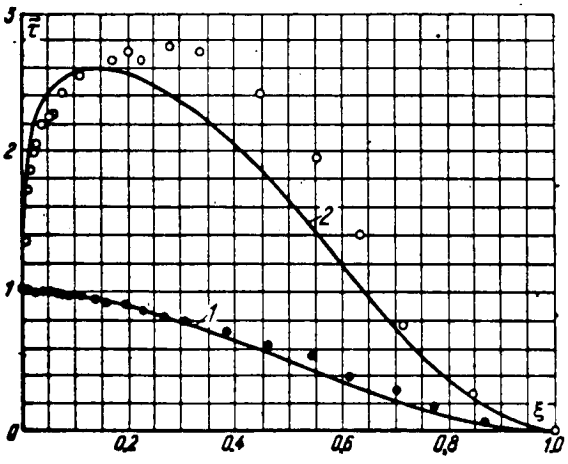

FIG. 1.4. Comparison of formulas (1-6-15) with test data.

Curves calculated from (1-6-15) (for $\lambda = 0$): 1—$\tilde{\tau} = \tilde{\tau}_0 = 1 + 3\xi^2 + 2\xi^3$; 2—$\tilde{\tau} = \tilde{\tau}_0 (1 + b_1 \omega)$. Points—tests by Mickley and others [180] and the treatment of Leadon [169]: o - $\bar{j}_w = 0.003$; b = 1.3; $\Psi = 0.455$, • - $\bar{j}_w = 0$; values of ω are experimental values.

It follows from (1-6-14) that the maximum shearing stress is found at a distance from the wall of /23

$$\xi_m = \frac{2\Lambda + 3}{2\Lambda + 2} - \sqrt{\left(\frac{2\Lambda + 3}{3\Lambda + 2}\right)^2 - \frac{\Lambda}{3\Lambda + 6}}. \qquad (1\text{-}6\text{-}17)$$

in the boundary layer at an impermeable surface, with $\Lambda > 0$.

As $\Lambda \to \infty$, $\xi_m \to 1/3$, i.e. with diffusor flow ($dP/dx > 0$), the maximum shearing stresses in the boundary layer at an impermeable surface lie in the range $0 < \xi < 1/3$.

Figure 1-4 gives a comparison of formula (1-6-15) with the test data. It can be seen clearly that this approximation yields not only a qualitatively correct representation of the function $\tilde{\tau}$, but also agrees with the quantitative results, particularly in the most effective wall region of the boundary layer, where we can take $1/(1+2\xi) \approx 1$.

1.7. Separation and Displacement of the Boundary Layer

In a convergent flow ($dP/dx < 0$) the stream is accelerated, the direction of motion of the fluid coincides with the direction of action of the pressure forces and the boundary layer at an impermeable surface is always stable in the sense that it does not separate from the body.

In diverging flow ($dP/dx > 0$) the stream is slowed down, the pressure increases and its action is counter to the direction of motion of the fluid. Since the pressure gradient remains the same over the entire cross section of the boundary layer, but the flow

velocity is decreased toward the wall, the supply of kinetic energy of the flow inside the boundary layer is insufficient completely to overcome the counteraction of the pressure field. As a result the positive pressure gradient produces drag in the boundary layer, and then stagnation and a return flow of fluid around the body. This phenomenon is known as separation of the boundary layer.

Formally, separation is associated with the fact that with $dP/dx>0$ the requirement $\tau > 0$ near the rigid surface is also satisfied even when $\tau_w = 0$.

Since the flow reversal occurs in the region of greatest stagnation, i.e., in the immediate vicinity of the wall, the point at which separation begins is defined by the condition /24

$$\left(\frac{\partial w_x}{\partial y}\right)_w = 0. \qquad (1\text{-}7\text{-}1)$$

Accordingly, $c_f = 0$ at the separation point and friction at the wall disappears.

In reality, boundary layer separation of course does not take place at a point but in some region.

With $b_1 = 0$ and $c_f = 0$, we have from (1-6-10) with $y \longrightarrow 0$

$$\tau \sim \frac{dP}{dx} y \qquad (1\text{-}7\text{-}2)$$

and in the viscous sublayer region

$$\delta = \frac{y^2}{2\nu} \frac{dw_e}{dx}. \qquad (1\text{-}7\text{-}3)$$

Boundary layer displacement due to intense injection is possible with an impermeable surface in the flow. An interference pattern of the boundary layer in the state of displacement from a permeable surface is shown in Fig. 1.5.

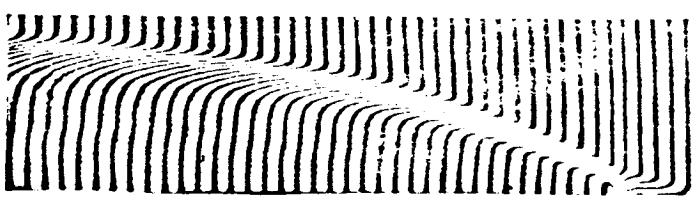

FIG. 1.5. Interferogram of a turbulent boundary layer at an impermeable surface in the state of displacement according to V. P. Motulevich [80].

Injection of CO_2 into air, $w_0 = 1.2$ m/sec, $\bar{j}_w = 0.17$.

In the Prandtl approximation the equation of motion in a viscous sublayer at a permeable plate with $dP/dx = 0$ is in the form

$$\mu \frac{\partial w_x}{\partial y} \sim \tau_w + j_w w_x \qquad (1\text{-}7\text{-}4)$$

and

$$\delta = \frac{c_f \rho_e w_e}{2 j_w} \left[\exp\left(\frac{j_w y}{\mu}\right) - 1\right]. \qquad (1\text{-}7\text{-}5)$$

With $j_w = 0$ this formula yields a linear velocity distribution. At the displacement point $c_f = 0$, and with some finite critical injection a flow is produced in the viscous sublayer that is slowed down in the x-direction, i.e., an effect somewhat similar to "forced drought" in jet processes is created. /25

1.8. Velocity Profile Near an Impermeable Wall with Pressure Gradient

With $b=0$ and $y \longrightarrow 0$

$$\tau \sim \tau_w + \frac{dP}{dx} y. \tag{1-8-1}$$

A quadratic velocity distribution is equivalent to this distribution of shearing stresses in the viscous sublayer:

$$\varphi = \eta - \frac{\dot{\gamma}}{2} \eta^2, \tag{1-8-2}$$

where

$$\dot{\gamma} = \left(\frac{2}{c_f}\right)^{3/2} \frac{f}{\mathrm{Re}^{**}}. \tag{1-8-3}$$

With $\xi_1 < \xi \ll 1$ the joint solution of Eqs. (1-3-6) and (1-8-1) yields a velocity profile

$$\varphi = \eta_1 - \frac{\dot{\gamma}}{2} \eta_1 + \frac{1}{\varkappa}\left(\sqrt{1-\dot{\gamma}\eta_1} - \sqrt{1-\dot{\gamma}\eta_1}\right) + \\ + \frac{1}{\varkappa} \ln \frac{\left(\sqrt{1-\dot{\gamma}\eta} - 1\right)\left(\sqrt{1-\dot{\gamma}\eta_1} + 1\right)}{\left(\sqrt{1-\dot{\gamma}\eta} + 1\right)\left(\sqrt{1-\dot{\gamma}\eta_1} - 1\right)}. \tag{1-8-4}$$

With $\dot{\gamma} \longrightarrow 0$ the profile (1-8-4) approaches the profile (1-4-3), i.e., the logarithmic section in Fig. 1-3, strictly speaking, exists both with small $\dot{\gamma}$ and with large Re^{**}.

1.9. Velocity Profiles at a Plate and in a Tube with the Flow of an Incompressible Fluid

From (1-5-4) we have for this case

$$\varphi - \varphi_1 = \int_{\xi_1}^{\xi} \sqrt{\frac{\tau}{\tau_0}} \frac{d\xi}{l} \tag{1-9-1}$$

or /26

$$1 - \varphi = \int_{\xi}^{1} \sqrt{\frac{\tau}{\tau_0}} \frac{d\xi}{l} \tag{1-9-2}$$

Hence, by virtue of the existence of the well-defined dependencies of $\tilde{l}$ and $\tilde{\tau}_0$ on ξ, the velocity defect is defined by a function in the form

$$\frac{w_0 - w_x}{v^*_w} = f(\xi) \tag{1-9-3}$$

or

$$\frac{w_x}{w_0} = 1 - \sqrt{\frac{c_f}{2}} f(\xi). \tag{1-9-4}$$

The function

$$f(\xi) = \frac{1}{\chi_0} \ln \xi \tag{1-9-5}$$

corresponds to the law of turbulent friction (1-3-6).

Actually, the well-defined relationship between the velocity defect ($w_0 - w_x$) and distance along the normal to the wall in the form (1-9-3) is a fundamental property of turbulent flow in ducts and at a plate. Figures 1.6 and 1.7 present the experimental data and computed results.

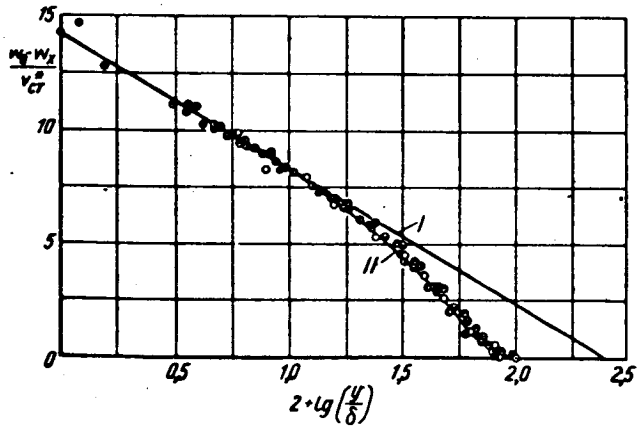

FIG. 1.6. Velocity distribution in the turbulent boundary layer at a flat plate.

I—computed from (1-9-3); II—curve drawn through test points of reference [213]. Values of $Re_x \cdot 10^{-6}$: ○—0.7; ●—1.3; ◑—1.9; ◐—3.2; ◒—4.1; ⊙—5.0; ◓—6.8.

If we resolve the function $\tilde{\tau}_0^{1/2} l^{-1}$ into a power series in ξ in the region of small ξ, we find

$$\varphi = \varphi_1 + \int_{\xi_1}^{\xi} \left(1 - \sum a_i \xi^i\right) \frac{d\xi}{\chi_0 \xi}, \tag{1-9-6}$$

which follows directly from the properties of the functions $\tau_0(\xi)$ and $l(\xi)$ considered above. From (1-3-6) and (1-6-5) we get

/27

$$\left.\begin{aligned} &\xi \to 0, \ \frac{\sqrt{\tilde{\tau}_0}}{l} \sim \frac{1}{\chi_0 \xi}, \\ &\xi \to 1, \ \frac{\sqrt{\tilde{\tau}_0}}{l} \to 0, \ \sum a_i = 1. \end{aligned}\right\} \tag{1-9-7}$$

Noting that

$$\left(\frac{2}{c_f}\right)^{1/2} = \varphi_{\xi=1}, \tag{1-9-8}$$

we obtain from (1-9-6):

$$\left(\frac{2}{c_f}\right)^{1/2} = -\frac{1}{\chi_0} \ln \xi_1 + f_1(\xi_1). \tag{1-9-9}$$

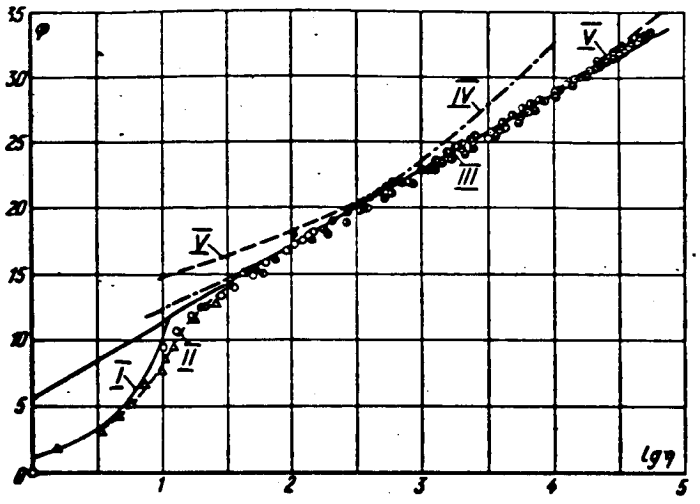

FIG. 1.7. Universal logarithmic law for the distribution of velocities in a smooth tube.

I—$\varphi = \eta$ - laminar sublayer; II—buffer layer; III—Eq. (1-10-2); IV, V—eq. (1-11-1) for n = 1/7 and n = 1/10. Experimental data (Nikuradze), ○—Re = 4.1×10^3; ●—2.3×10^4; ◐—1.1×10^5; ◑—4.0×10^5; ⊙—1.1×10^6; ◒—2.0×10^6; ◓—3.2×10^6; △—Experimental data (Reichardt).

where $f_1 = \varphi_1 - \frac{1}{\chi_0}\int_{\xi_1}^{1}\sum a_i \xi^{i-1} d\xi$ is the limiting value. /28

With dP/dx = 0, $\varphi_1 = \eta_1$, and for the two-layer boundary layer (see Section 1.4)

$$\xi_1 = \frac{11.6\tilde{\delta}^{**}}{\mathrm{Re}^{**}}\sqrt{\frac{2}{c_f}}. \qquad (1\text{-}9\text{-}10)$$

Hence, with $\mathrm{Re} \to \infty$ $\xi_1 \to 0$, and, by virtue of the boundedness of f_1

$$\left(\frac{2}{c_f}\right)^{1/2} \sim \left(-\frac{1}{\chi_0}\ln\xi\right) \sim \frac{1}{\chi_0}\ln \mathrm{Re}^{**}. \qquad (1\text{-}9\text{-}11)$$

1.10. "Logarithmic" Boundary Layer

It has been shown above that the actual velocity distribution for the flow of an incompressible fluid in a tube differs little from logarithmic. The deviation is more significant in the boundary layer at an impermeable plate. Nonetheless, in this case also the logarithmic velocity distribution satisfactorily describes the actual distribution up to $\omega = 0.9$. This circumstance allows the introduction of the concept of a model turbulent boundary layer with a distribution law for the mixing path length:

$$l = \chi_0 \xi \sqrt{\tilde{\tau}_0}. \qquad (1\text{-}10\text{-}1)$$

Such a boundary layer, with f = b = 0 and ρ = const. has a logarithmic velocity distribution over the entire range $y_1 < y < \delta$ and relatively simple characteristics, which in many instances satisfactorily describe a real flow both qualitatively and quantitatively. We shall call this model the "logarithmic boundary layer." The logarithmic boundary layer of an incompressible fluid at a smooth impermeable plate is described by the following characteristic relationships:

$$f = 0,\ b = 0;\ \rho = \mathrm{const};$$

$$\varphi = c_0 + \frac{1}{\chi_0}\ln\eta;$$

$$\omega = 1 - \frac{1}{\chi_0}\sqrt{\frac{c_f}{2}}\ln\xi;$$

$$\tilde{\tau}_0 = \frac{1}{\chi_0}\sqrt{\frac{c_f}{2}};$$

$$\gamma^{**} = \frac{1}{\chi_0}\sqrt{\frac{c_f}{2}} - \frac{c_f}{\chi_0^2};$$
$$H = \left(1 - \frac{1}{\chi_0}\sqrt{2c_f}\right)^{-1};$$
$$\sqrt{\frac{2}{c_f}} = c_* - \frac{1}{\chi_0}\ln\frac{\chi_0^2}{\chi_0 - \sqrt{2c_f}} + \frac{1}{\chi_0}\ln \mathrm{Re}^{**}. \qquad (1\text{-}10\text{-}2)$$

With $c_* = 5.5$ and $X_0 = 0.4$ the last relationship of (1-10-2) is well approximated by the relatively simple Karman formula /29

$$\sqrt{\frac{2}{c_f}} = 2{,}5\ln \mathrm{Re}^{**} + 3{,}8. \qquad (1\text{-}10\text{-}3)$$

As can be seen the law of friction of the logarithmic boundary layer (1-10-3) is a particular case of (1-9-9), where as the Reynolds member increases the laws of friction for the model and actual flows tend to the same limit, expressed by formula (1-9-11).

1.11. Power-law Velocity Profiles

The logarithmic velocity profile is the envelope of a family of power-law profiles

$$\varphi = A\eta^n, \qquad (1\text{-}11\text{-}1)$$

where $0 < n < 1$.

In many cases the use of a power-law approximation for the velocity profile is quite useful.

For the conditions $f = b = 0$, $\tilde{\rho} = 1$, we have the following relationships:

$$\left.\begin{aligned}
&\omega = \xi^n;\\
&\gamma^* = \frac{n}{1+n};\\
&\tilde{\delta}^{**} = \frac{n}{(1+n)(1+2n)};\\
&H = 1 + 2n;\\
&c_f = \frac{B}{\mathrm{Re}^{**m}};\\
&m = \frac{2n}{1+n},\\
&B = 2\left(A\tilde{\delta}^{**n}\right)^{-\frac{2}{1+n}}.
\end{aligned}\right\} \qquad (1\text{-}11\text{-}2)$$

In this case the momentum Eq. (1-2-2) takes the form

$$\frac{d\delta^{**}}{dx} = \frac{c_f}{2}. \qquad (1\text{-}11\text{-}3)$$

On substituting the value of the coefficient of friction from (1-11-2) into (1-11-3) and assuming that the turbulence layer sets in at point $x = x_{crit}$, we find

$$\mathrm{Re}^{**1+m} - \mathrm{Re}_{crit}^{**1+m} = \frac{1+m}{2} B (\mathrm{Re}_x - \mathrm{Re}_{x\,crit}). \qquad (1\text{-}11\text{-}4)$$

Here Re_{crit}^{**} is the Reynolds number set up from the thickness of the momentum loss at which boundary layer turbulence is generated; $\mathrm{Re}_x = w_0 x/\nu$ is the Reynolds number set up in accordance with distance from the leading edge of the plate. /30

If the turbulent boundary layer develops on the entire plate ($x_{crit} = 0$), then

$$\left.\begin{aligned} \mathrm{Re}^{**} &= \left(\frac{1+m}{2} B \mathrm{Re}_x\right)^{\frac{1}{1+m}}; \\ c_f &= B_1 \mathrm{Re}_x^{-m_1}; \\ m_1 &= \frac{m}{1+m}; \\ B_1 &= \left(\frac{2B^{1/m}}{1+m}\right)^{\frac{m}{1+m}}. \end{aligned}\right\} \qquad (1\text{-}11\text{-}5)$$

The values of the coefficients in (1-11-2) and (1-11-5) for various values of n are given in Table 1.1.

TABLE 1.1. Values of Coefficients in Formulas (1-11-2) and (1-11-5)

Coefficient	n			
	1/7	1/8	1/9	1/10
A	8,74	9,71	10,6	11,5
ϑ^{**}	0,0975	0,0890	0,0818	0,0757
H	1,28	1,25	1,22	1,20
m	0,250	0,222	0,200	0,182
B	0,0252	0,0206	0,0190	0,0148
m_1	0,200	0,182	0,167	0,154
B_1	0,0576	0,0450	0,0362	0,0308

In practice the formulas for n = 1/7 can be used in the range $\mathrm{Re}^{**} < 10^4$. Figure 1.8 gives a comparison of the available test data with formulas (1-10-3) and (1-11-2).

1.12. Wall Turbulence near a Rough Surface /31

When the order of the thickness of the viscous sublayer becomes equal to that of the height of the roughness, the flow conditions near the wall change. However, this is not reflected in the laws of friction in the turbulent core flow.

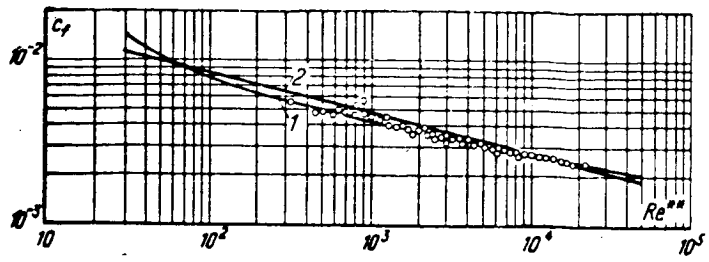

FIG. 1.8. Law of friction for the turbulent boundary layer at a flat plate: 1—formula (1-10-3); 2—formula (1-11-2); B = 0.0256; m = 0.25; points—experimental data [164].

As a consequence, the only change is the definition of the wall region which is the limit of developed turbulent flow.

For flow over a smooth impermeable surface this limit is of the order

$$y_1 \sim \frac{\nu}{v^*_w}, \qquad (1\text{-}12\text{-}1)$$

while for a rough surface it is

$$y_1 \sim \varepsilon, \qquad (1\text{-}12\text{-}2)$$

where ε is the roughness height for a uniform roughness or some "effective height" for nonuniform roughness.

Obviously, the measure of the effect of roughness on the turbulent flow around an impermeable surface will be

$$\eta_\varepsilon = \frac{v^*_w \varepsilon}{\nu}. \qquad (1\text{-}12\text{-}3)$$

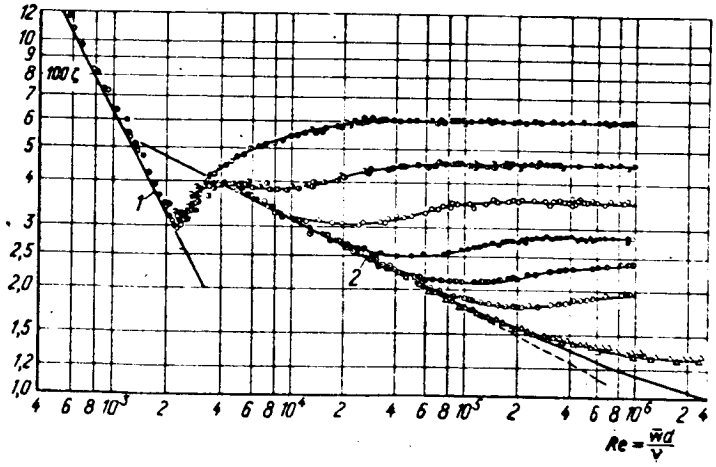

FIG. 1.9. Drag law for rough pipes. 1—laminar flow; 2—turbulent flow in a smooth pipe. Experimental data of Nikuradze (sandy surface): ⊙—R/Δ = 507; ◐—252; ●—126; ◑—30.6; ◔—15. Experimental data of Galavich (industrial roughness): Δ^{-R}/Δ= 1300.

So long as the roughness protuberances are "submerged" in the viscous sublayer they do not influence the transfer process. /32

Therefore with η_ε less than some value, the surface roughness is "hydrodynamically smooth." The laws of flow around a rough surface were first investigated in their pure form by Nikuradze, based on a uniform granular roughness.

The generalized result of these investigations for flow in circular pipes is shown in Fig. 1.9. In the region $\eta_\varepsilon < 5$, i.e., when the roughness does not protrude beyond the limits of the region in which molecular viscosity is completely dominant, the surface is hydrodynamically smooth.

In the region $\eta_\varepsilon > 40$ molecular friction essentially has no effect on the overall hydrodynamic drag and the quadratic drag law is clearly expressed.

CHAPTER 2
THERMAL AND DIFFUSION BOUNDARY LAYERS

2.1. The Differential Equations of Energy and Diffusion

The equation of heat propagation in a steady, homogeneous, plane boundary layer has the form

$$-\frac{\partial q}{\partial y}+q_V+\mu\left(\frac{\partial w_x}{\partial y}\right)^2+w_x\frac{\partial P}{dx}=\rho w_x\frac{\partial i}{\partial x}+\rho w_y\frac{\partial i}{\partial y}. \tag{2-1-1}$$

Here q is the heat flux in the direction of the y-axis attributable to the molecular and turbulent heat transfer; q_V is the volumetric density of all energy sources and sinks at a given point with the exception of heat evolved due to work performed by the flow.

In the laminar boundary layer

$$q=-\lambda\frac{\partial T}{\partial y}, \tag{2-1-2}$$

and in the turbulent boundary layer

$$q=-\lambda\frac{\partial T}{\partial y}-C_p\rho\overline{v_y\theta}\,(1-\widetilde{\beta}_T), \tag{2-1-3}$$

where $\widetilde{\beta}_T=\beta\frac{\overline{w_y\theta^2}+\overline{v_y\theta^2}}{\overline{v_y\theta}}$ is the thermal analogue of the coefficient $\widetilde{\beta}$ in (1-1-6).

For the actual quantities it is convenient to represent the equation of heat propagation in the form given by M. F. Shirokov [99]:

$$\frac{\partial}{\partial y}\left\{\frac{\lambda}{C_p}\frac{\partial}{\partial y}\left[i^*+(\mathrm{Pr}-1)\frac{w_x^2}{2}\right]\right\}+q_V=\rho w_x\frac{\partial i^*}{\partial x}+\rho w_y\frac{\partial i^*}{\partial y} \tag{2-1-4}$$

or, with C_p = const. /33

$$\frac{\partial}{\partial y}\left\{\lambda\frac{\partial}{\partial y}\left[T^*+(\mathrm{Pr}-1)\frac{w_x^2}{2}\right]\right\}+q_V=$$
$$=C_p\rho w_x\frac{\partial T^*}{\partial x}+C_p\rho w_y\frac{\partial T^*}{\partial y}. \tag{2-1-5}$$

Here

$$i^*=i+\frac{w_x^2}{2} \tag{2-1-6}$$

is the stagnation enthalpy,

$$T^*=T+\frac{w_x^2}{2C_p} \tag{2-1-7}$$

is the stagnation temperature.

$$\mathrm{Pr} = \frac{C_p \mu}{\lambda} \tag{2-1-8}$$

is Prandtl's number, which describes the ratio of the intensity of molecular friction and molecular heat conductivity. In the case of gases this quantity depends primarily on the valency of the molecules.

The energy equation for the turbulent boundary layer of a compressible gas, with chemical reactions taking place, is conveniently written in the form [77]:

$$\begin{aligned} \rho w_x \frac{\partial i^*_\Sigma}{\partial x} + \rho w_y \frac{\partial i^*_\Sigma}{\partial y} = \frac{\partial}{\partial y}(q_\Sigma) + \\ + q_V + \frac{\partial}{\partial y}\left\{\left[\frac{\lambda}{\bar{C}_P}(\mathrm{Le}-1) + \frac{\lambda_\tau}{\bar{C}_P}(\mathrm{Le}_\tau - 1)\right]\sum i_i \frac{\partial c_i}{\partial y}\right\} + \\ + \frac{\partial}{\partial y}\left\{\left[\mu\left(1-\frac{1}{\mathrm{Pr}}\right) + \mu_\tau\left(1-\frac{1}{\mathrm{Pr}_\tau}\right)\right]\frac{1}{2}\frac{\partial w_x^2}{\partial y}\right\} \end{aligned} \tag{2-1-9}$$

or, for the case $\mathrm{Pr} = \mathrm{Pr}_T = \mathrm{Le} = \mathrm{Le}_T = 1$,

$$\rho w_x \frac{\partial i^*_\Sigma}{\partial x} + \rho w_y \frac{\partial i^*_\Sigma}{\partial y} = \frac{\partial}{\partial y}(q_\Sigma) + q_V, \tag{2-1-10}$$

where

$$\left.\begin{aligned} q_\Sigma &= \left(\frac{\mu}{\mathrm{Pr}} + \frac{\mu_\tau}{\mathrm{Pr}_\tau}\right)\frac{\partial i^*_\Sigma}{\partial y}; \\ i^*_\Sigma &= i_\Sigma + \frac{w_x^2}{2}, \; i_\Sigma = \sum_i c_i i_i; \\ i_i &= \int_0^T C_{P_i}\, dT + i_i^0; \end{aligned}\right\} \tag{2-1-11}$$

c_i is the concentration by weight of the i-th component; i_i^0 is the heat of formation of the i-th component. /34

Taking account of Eq. (2-1-11) we have:

$$q_\Sigma = q_{\Sigma 1} + q_{\Sigma\tau}, \tag{2-1-12}$$

where

$$q_{\Sigma 1} = -\frac{\lambda}{\bar{C}_P}\frac{\partial i^*_\Sigma}{\partial y}; \; q_{\Sigma\tau} = \frac{\rho l^2 \frac{\partial w_x}{\partial y}}{\mathrm{Pr}_\tau}\frac{\partial i^*_\Sigma}{\partial y}(1-\tilde{\beta}_\tau),$$

where $\mathrm{Pr}_\tau = \bar{C}_P \frac{\mu_\tau}{\lambda_\tau}$ is the turbulent Prandtl number, $\bar{C}_P = \sum_{i=1}^{n} c_i C_{P_i}$. For a flow of

conducting fluid in an electric field, in the region of small magnetic Reynolds numbers and Hall parameters, we have

$$q_v = -j_y E_y,$$

where E_y is the electric field intensity in the y-axis direction.

The equation for the dispersion of matter in a stationary, plane boundary layer takes the form

$$\rho w_x \frac{\partial c_i}{\partial x} + \rho w_y \frac{\partial c_i}{\partial y} = -\frac{\partial j_i}{\partial y} + \dot{c}_i, \tag{2-1-13}$$

where j_i is the specific flow rate of the i-th component in the y-axis direction attributable to molecular and turbulent diffusion; $\dot{c}_i$ is the rate of formation of the i-th component due to chemical reactions; c_i is the concentration by weight of the i-th component.

In the laminar boundary layer of a binary mixture

$$j_i = -\rho D_{12}\left[\frac{\partial c_i}{\partial y} + \frac{\alpha c_i (1-c_i)}{T}\frac{\partial T}{\partial y}\right]. \tag{2-1-14}$$

In cases of interest in practice the terms defining thermal diffusion are small in comparison with the diffusion term (less than 10%). Therefore, we can assume, with adequate accuracy

$$j_i = -\rho D_{12}\frac{\partial c_i}{\partial y}. \tag{2-1-15}$$

In the turbulent boundary layer

$$j_i = -\rho D_{12}\frac{\partial c_i}{\partial y} - \rho\overline{v_y c_i}(1-\tilde{\beta}_D), \tag{2-1-16}$$

where $\tilde{\beta}_D = \frac{\overline{v_y\theta c_i} + \overline{\theta v_x c_i}}{\overline{v_x c_i}}$ is the diffusion analogue of the coefficient $\tilde{\beta}$ in (1-1-7). Prandtl's formula (1-3-6), applied to the diffusion problem, is written as

$$j_T = \rho l l_D \frac{\partial w_x}{\partial y}\frac{\partial c_i}{\partial y}(1-\tilde{\beta}_D). \tag{2-1-17}$$

where l_D is the diffusion mixing path length. The quantity $\mu_T/\rho D_T = Sc_T$ has the sense of the turbulent Schmidt number. Correspondingly, $\rho D_T C_p/\lambda_T = Le_T$ is called the turbulent Lewis-Semenov number. If we introduce the concentration of the i-th chemical element $\bar{c}_i$, ignoring the chemical compound in which it is found, then, in the absence of intra-nuclear transformations, we have from (2-1-13):

$$\rho w_x \frac{\partial \bar{c}_i}{\partial x} + \rho w_y \frac{\partial \bar{c}_i}{\partial y} = -\frac{\partial \bar{j}_i}{\partial y}, \tag{2-1-18}$$

where $\bar{j}_i$ is the specific flow rate of the i-th element in the y-axis direction.

2.2. Similarity of the Enthalpy-, Concentration- and Velocity-Fields

As follows from Eqs. (1-1-3), (2-1-4) and (2-1-18), if the condition $Pr = Sc = Pr_T = Sc_T = 1$ is satisfied, and also with $f = 0$, $i^*_{\Sigma 0} = \text{const}$, $\overline{C}_{i0} = \text{const}$, $i_w = \text{const}$, $\overline{C}_{iw} = \text{const}$, $q_v = 0$, similarity must exist between the distributions of velocity, total enthalpy and concentration of the chemical elements

$$\bullet = \frac{i_{\Sigma w} - i^*_{\Sigma}}{i_{\Sigma w} - i^*_{\Sigma 0}} = \frac{\bar{c}_i - \bar{c}_{iw}}{\bar{c}_{i0} - \bar{c}_{iw}}. \qquad (2\text{-}2\text{-}1)$$

With $q_v = 0$, $\overline{Cp} = \text{const}$, $\overline{C}_i = 0$, $M_0 \ll 1$, and without chemical reactions, we have from (2-2-1)

$$\bullet = \frac{T_w - T}{T_w - T_0} = \frac{c - c_w}{c_0 - c_w}. \qquad (2\text{-}2\text{-}2)$$

Consequently, for the conditions stated, the three-fold Reynolds analogue is satisfied:

$$\frac{\tau_w}{\rho_0 w_0^2} = \frac{q_{\Sigma w}}{\rho_0 w_0 (i^*_{\Sigma 0} - i_{\Sigma w})} = \frac{j_{iw}}{\rho_0 w_0 (\bar{c}_{i0} - \bar{c}_{iw})}, \qquad (2\text{-}2\text{-}3)$$

where

$$\frac{\tau_w}{\rho_0 w_0^2} = \frac{c_f}{2}; \quad \frac{q_{\Sigma w}}{\rho_0 w_0 (i^*_{\Sigma 0} - i_{\Sigma w})} = St_{\Sigma};$$

$$\frac{j_{iw}}{\rho_0 w_0 (\bar{c}_{i0} - \bar{c}_{iw})} = St_D.$$

In the absence of chemical reactions in the boundary layer

$$St_{\Sigma} = \frac{q_w}{\rho_0 w_0 (i^*_0 - i_w)} = St_D = \frac{j_{iw}}{\rho_0 w_0 (c_{i0} - c_{iw})}, \qquad (2\text{-}2\text{-}4)$$

and with constant specific heat /36

$$St_{\Sigma} = \frac{q_w}{C_p \rho_0 w_0 (T^*_0 - T_w)}. \qquad (2\text{-}2\text{-}5)$$

If $Pr \neq 1$, as a first approximation we should replace $i^*_{\Sigma 0}$ by $i^*_{\Sigma w}$ (equilibrium enthalpy) in Eqs. (2-2-3) and (2-2-4), and T^*_0 by T^*_w (equilibrium wall temperature) in (2-2-5). In this way i^*_w and T^*_w are the enthalpy and temperature at the thermally isolated wall surface.

It is known that

$$i^*_w = i_e + r\frac{w_0^2}{2}, \tag{2-2-6}$$

for the case C_p = const

$$T^*_w = T_e + r\frac{w_0^2}{2C_p}, \tag{2-2-7}$$

where r is the stagnation enthalpy (or temperature) recovery coefficient. In the general case the recovery coefficient r depends on many factors [43]. For an impermeable plate, for the laminar boundary layer

$$r \approx Pr^{1/2} \tag{2-2-8}$$

and for the turbulent boundary layer

$$r \approx Pr^{1/3}. \tag{2-2-9}$$

Also, the correction factor K

$$St_z = St_D = \frac{c_f}{2}K. \tag{2-2-10}$$

must be inserted in the three-fold analogue (2-2-3) with $Pr \neq Sc \neq 1$.

For gases, with $Pr_T = Sc_T \approx 1$, this factor is adequately approximated by the formula

$$K \approx Pr^{-2/3} \approx Sc^{-2/3}. \tag{2-2-11}$$

The Prandtl and Schmidt numbers are a qualitative measure of the ratio between the thicknesses of the dynamic-, diffusion- and thermal boundary layers, as given in Table 2.

TABLE 2.1. Relationship between the Thickness of the Thermal-, Diffusion- and Dynamic-Boundary Layers

/37

Pr, Sc	<1,0	1	>1
$\frac{\delta_T}{\delta}, \frac{\delta_D}{\delta}$	>1,0	1	<1

Differing from the molecular Prandtl and Schmidt numbers, which should be viewed as physical parameters of fluids, the corresponding turbulence analogues depend not only on the physical properties of the fluid, but also on the hydrodynamic state in the flow. This presents a major difficulty in the solution of problems in turbulent heat- and mass transfer.

The experimental values of the turbulent Prandtl and Schmidt numbers for the wall turbulence region lie in the range 0.85-0.90. Values of the order of 0.5 are found for plane turbulent jets. In more complex situations—for example in the boundary layer separation region—the turbulent Prandtl numbers, as shown by the measurements made by Z. Zaric [255], may be considerably less than unity.

In addition, in the general case the turbulent Pr_T- and Sc_T- numbers are not constant over the boundary layer cross section. Experiment has shown that the turbulent Prandtl number may depend significantly on the magnitude of the molecular Prandtl number, the level of the free-stream turbulence and on the Re number. However, for fluids with $Pr \approx Sc \approx 1$, the condition $Pr_T \approx Sc_T \approx 1$, first formulated by O. Reynolds in 1874, remains a good approximation for calculations of the turbulent thermal- and diffusion boundary layers.

2.3. Enthalpy Factor in a Gas Boundary Layer

In the boundary layer of a gas obeying the Clapyron-Mendeleev equation of state, by virtue of the condition $dP/dy = 0$, the gas density is unambiguously related to the thermodynamic enthalpy by the relationship

$$\tilde{\rho} = \frac{\rho}{\rho_0} = \frac{i_0}{i}. \tag{2-3-1}$$

For a homogeneous gas ($Pr \approx 1$), without chemical reactions, and with $C_p = C_{po}$, /38 using Eqs. (1-1-4) and (2-1-4), we find

$$\frac{i^* - i_w}{i^*_0 - i_w} = \omega; \tag{2-3-2}$$

$$\frac{i}{i_0} = \frac{T}{T_0} = \psi - \Delta\psi\omega - (\psi^*_0 - 1)\omega^2, \tag{2-3-3}$$

where $\psi = i_w/i_0 = T_w/T_0$ is the enthalpy (temperature) factor; $\psi^*_0 = i^*_0/i_0 = T^*_0/T_0$ is the adiabatic kinetic enthalpy (temperature) factor; $\Delta\psi = \psi - \psi^*_0$ the heat transfer factor.

The case $\Delta\psi = 0$ relates to flow around a thermally-insulated body; with $\Delta\psi > 0$ the body gives up heat to the gas flow, and with $\Delta\psi < 0$ the body takes up heat from the gas flow.

With $Pr \neq 1$, and also with $dP/dx \neq 0$, Eqs. (2-3-2) and (2-3-3) are inaccurate. Taking Eqs. (2-3-2) as a basis, we write

$$\frac{i^* - i_w}{i^*_w - i_w} = \varepsilon(\xi)\omega, \tag{2-3-4}$$

$$i^* = i + r(\xi)\frac{A\omega_x^2}{2g}. \tag{2-3-5}$$

The forms of the functions $r(\xi)$ and $\varepsilon(\xi)$ in the general case depend on the Pr number, the pressure gradient, the mass transfer and other "perturbing" factors appearing in the boundary conditions for the dynamic- and thermal boundary layers.

Taking Eq. (2-3-2) into account, we can write

$$\frac{i^* - i_w}{i^*_0 - i_w} = \left[1 + (1 - r)\frac{\psi^*_0 - 1}{\Delta\psi}\right]\varepsilon\omega - (1 - r)\frac{\psi^*_0 - 1}{\Delta\psi}\omega^2. \qquad (2\text{-}3\text{-}6)$$

With $\varepsilon = r = 1$, Eq. (2-3-6) goes over into the known Crocco integral (2-3-2).

At the limits of the thermal boundary layer, we shall require that the quantity

$$\vartheta = \frac{i - i_w}{i^*_w - i_w}$$

satisfy the same conditions as does ω at the limits of the dynamic layer. Then, with $y = \delta_T$, $D = 1$ and with $i^* = i^*_w$, $r(\delta_T) = r$. As pointed out above, in the turbulent boundary layer the recovery coefficient is about $\sqrt[3]{Pr}$, i.e. for gases, close to unity. /39
Therefore, without significant error, we can take $r(\xi) \approx r$, and

$$i^* \approx i + r\frac{Aw_x^2}{2g}. \qquad (2\text{-}3\text{-}7)$$

Then, from Eq. (2-3-4), we have

$$i/i_0 = \psi - \Delta\psi\varepsilon\omega - (\psi^* - 1)\omega^2, \qquad (2\text{-}3\text{-}8)$$

where $\psi^* = i^*_w/i_0$ is the kinetic enthalpy factor. With a power-law approximation for the velocity- and enthalpy fields

$$\omega = \xi^n, \quad \vartheta = \xi_T^{n_T} \qquad (2\text{-}3\text{-}9)$$

we find that

$$\vartheta = \varepsilon_1\omega^{n/n_T}, \qquad (2\text{-}3\text{-}10)$$

where

$$\varepsilon_1 = (\delta/\delta_T)^{n_T}.$$

Far from the boundary layer separation point $n \approx n_T$, and the relative similarity

$$\vartheta = \varepsilon\omega. \qquad (2\text{-}3\text{-}11)$$

exists.

Figure 2.1 gives a comparison between formulas (2-3-2), (2-3-6) and the tests of Danberg [125] and Hill [155]. The tests covered a rather broad range of Mach numbers (up to 9.1). As can be seen from the diagram, the tests on the plate [125] agree with

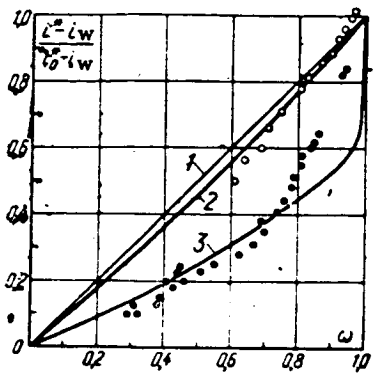

Fig. 2.1. Comparison between formulas (2-3-2), (2-3-6) and experiment. 1—Computed with (2-3-2); 2—computed from (2-3-6), $\varepsilon = 1.0$; 3—computed from (2-3-6), $\varepsilon = 0.5$; o—Danberg's tests [125], flat plate, $M_o = 6.4$; ●—Hill's tests [155], conical nozzle, $M_o = 9.1$.

the adopted relationship with $\varepsilon = 1.0$. The tests in conical nozzles [155] agree satisfactorily with Eq. (2-3-6), with $\varepsilon = 0.5$, in the wall region.

2.4. Integral Energy and Diffusion Relations /40

On integrating Eq. (2-1-10) with respect to the y-coordinate over the boundary layer thickness, and taking account of the equation of continuity (1-1-5), we obtain an integral energy relationship for the two-dimensional boundary layer

$$\frac{d\delta^{**}_i}{dx}+\frac{\delta^{**}_i}{w_0\Delta i^*_\Sigma}\frac{d}{dx}(w_0\Delta i^*_\Sigma)+\frac{\delta^{**}_i}{\rho_0}\frac{d\rho_0}{dx}+ \\ +\frac{q_V\delta_2}{\rho_0 w_0\Delta i^*_\Sigma}-\tilde{j}_w=\frac{q_{0\tau}}{\rho_0 w_0\Delta i^*_\Sigma}, \tag{2-4-1}$$

where $\Delta i^*_\Sigma = i_w - i^*_{\Sigma w}$ is the difference in total enthalpies and

$$\delta^{**}_i=\int_\delta^{\delta_T}\tilde{\rho}\omega\left(1-\frac{i^*_\Sigma-i_w}{i^*_w-i_w}\right)dy \tag{2-4-2}$$

is the total energy loss thickness, similar in its properties to the momentum loss thickness δ^{**} (see (1-2-4)).

With C_p = const and in the absence of chemical reactions, we have from (2-4-1):

$$\frac{d\delta^{**}_T}{dx}+\frac{\delta^{**}_T}{w_0\Delta T}\frac{d}{dx}(w_0\Delta T)+\frac{\delta^{**}_T d\rho_0}{\rho_0 dx}+ \\ +\frac{q_V\delta_T}{C_p\rho_0 w_0\Delta T}-\tilde{j}_w=\frac{q_{0\tau}}{C_p\rho_0 w_0\Delta T}, \tag{2-4-3}$$

where

$$\Delta T=T_w-T^*_w;\quad \delta^{**}_T=\int_\delta^{\delta_T}\tilde{\rho}\omega\left(1-\frac{T^*-T_w}{T^*_w-T_w}\right)dy.$$

We introduce the following notation:

$$\mathrm{Re}^{**}_{i\Sigma}=\frac{\rho_0 w_0\delta^{**}_{i\Sigma}}{\mu^*}; \tag{2-4-4}$$

$$f_i=\frac{1}{\Delta i_\Sigma}\frac{d\Delta i_\Sigma}{dx}; \tag{2-4-5}$$

$$\tilde{q}_V = \frac{q_V \delta_T}{\rho_0 w_0 \Delta i_\Sigma}; \quad \mathrm{Re}_L = \frac{\rho_0 w_0 L}{\mu^*}. \tag{2-4-6}$$

Then, in analogy with (1-2-10), we find /41

$$\frac{d\,\mathrm{Re}^{**}_{i\Sigma}}{d\bar{x}} + \mathrm{Re}^{**}_{i\Sigma} f_i + (\tilde{q}_V - \tilde{j}_w)\,\mathrm{Re}_L = \mathrm{St}_\Sigma \mathrm{Re}_L. \tag{2-4-7}$$

Similarly, for the axi-symmetric case, we have

$$f_{i\Phi} = \frac{1}{\Delta i_\Sigma}\frac{d(\Delta i_\Sigma)}{d\bar{x}} + \frac{1}{R}\frac{dR}{d\bar{x}} = \frac{d}{d\bar{x}}[\ln(\Delta i_\Sigma R)]. \tag{2-4-8}$$

For flows of conducting fluids in electric and magnetic fields, in the region of small magnetic Reynolds numbers and Hall parameters, and taking the expression for q_V (see Section 2.1) into account, we obtain the integral energy relationship in the form [18]:

a) for the electrode wall

$$\frac{d\delta^{**}_i}{dx} + \delta^{**}_i\left[\frac{1}{\rho_0 w_0 \Delta i}\frac{d(\rho_0 w_0 \Delta i)}{dx} + \frac{1}{\Delta i}\frac{di^*_e}{dx}(-H_E + H)\right] - \tilde{j}_w = \mathrm{St}_\Sigma \tag{2-4-9}$$

or

$$\frac{d\,\mathrm{Re}^{**}_{i\Sigma}}{d\bar{x}} + \mathrm{Re}^{**}_{i\Sigma} f_{i\Sigma} - \tilde{j}_w \mathrm{Re}_L = \mathrm{Re}_L \mathrm{St}_\Sigma, \tag{2-4-10}$$

where

$$H_E = \int_0^{\delta_i} \frac{\left(1 - \frac{E}{E_0}\right) dy}{\delta^{**}_{i\Sigma}}; \tag{2-4-11}$$

$$f_{T\Sigma} = \frac{1}{\Delta i}\frac{d\Delta i}{d\bar{x}} + \frac{1}{\Delta i}\frac{di^*_e}{d\bar{x}}(H - H_E); \tag{2-4-12}$$

b) For the insulator wall

$$\frac{d\delta^{**}_i}{dx} + \delta^{**}_i\left[\frac{1}{\rho_0 w_0 \Delta i}\frac{d}{dx}(\rho_0 w_0 \Delta i) + \frac{1}{\Delta i}\frac{di^*_e}{dx}(H - H_j)\right] - \tilde{j}_w = \mathrm{St}_\Sigma \tag{2-4-13}$$

or

$$\frac{d\,\mathrm{Re}^{**}_{i\Sigma}}{d\bar{x}} + \mathrm{Re}^{**}_{i\Sigma} f_{T\Sigma} - \tilde{j}_w\,\mathrm{Re}_L = \mathrm{Re}_L \mathrm{St}_\Sigma, \tag{2-4-14}$$

where /42

$$H_j = \frac{\int_0^{\delta_1} \left(1 - \frac{j}{j_0}\right) dz}{\delta^{**}_1}.$$

For the axi-symmetric boundary layer, in analogy with (2-4-8), an additional term $\frac{1}{R}\frac{dR}{dx}$ appears in (2-4-12).

Integrating the diffusion Eq. (2-1-18) over the boundary layer cross section, taking into account the continuity equation, we obtain

$$\frac{d\delta^{**}_D}{dx} + \frac{\delta^{**}_D}{\rho_0 w_0 \Delta\bar{c}_1}\frac{d}{dx}(\rho_0 w_0 \Delta\bar{c}_1) - \frac{j_w}{\rho_0 w_0} = St_D, \qquad (2\text{-}4\text{-}15)$$

where $\Delta\overline{C}_1 = \overline{C}_w - \overline{C}_0$ is the difference in weight concentrations of the diffusing element at the wall and in the flow; $\delta^{**}_D = \int_0^{\delta_D} \frac{\bar{\rho}}{\rho_\infty}\left(1 - \frac{\bar{c} - \bar{c}_w}{\bar{c}_0 - \bar{c}_w}\right) dy$ is the mass loss thickness;

$St_D = \frac{j_{1w}}{\rho_0 w_0 (\bar{c}_w - \bar{c}_0)}$ is the Stanton diffusion number; j_{1w} is the flow of diffusing element at the wall. In the general case $j_{1w} \neq j_w$.

Introducing the nomenclature

$$\left.\begin{aligned} Re^{**}_D &= \frac{\rho_0 w_0 \delta^{**}_D}{\mu^*}; \quad f_D = \frac{1}{\Delta\bar{c}}\frac{d(\Delta\bar{c})}{dx}; \\ Re_L &= \frac{\rho_0 w_0 L}{\mu^*}, \end{aligned}\right\} \qquad (2\text{-}4\text{-}16)$$

we find

$$\frac{dRe^{**}_D}{dx} + Re^{**}_D f_D - j_w Re_L = Re_L St_D. \qquad (2\text{-}4\text{-}17)$$

For an axi-symmetric boundary layer

$$f_{D0} = \frac{d}{dx}[\ln(\Delta\bar{c}R)]. \qquad (2\text{-}4\text{-}18)$$

For a given thermal load and diffusing substance at the wall, from Eq. (2-4-7) and (2-4-17) we have (with $q_v = 0$)

$$Re^{**}_{iz} = \frac{1}{\Delta i^*_z}\left\{(Re^{**}_{iz}\Delta i^*_z)_{x=x_0} + \right.$$

$$\left. + \frac{1}{\mu^*}\int_{x_0}^{x} [q_{iw} + \Delta i^*_z j_w]\, dx\right\}; \qquad (2\text{-}4\text{-}19)$$ /43

$$\mathrm{Re}^{**}_D = \frac{1}{\Delta\bar{c}}\left\{(\mathrm{Re}^{**}_D \Delta\bar{c})_{x=x_0} + \right.$$
$$\left. + \frac{1}{\mu^*}\int_{x_0}^{x} [j_{1w} + \Delta\bar{c} j_w]\, dx \right\}. \qquad (2\text{-}4\text{-}20)$$

2.5. Approximations of the Distribution of Thermal- and Diffusion- Flows over the Boundary Layer Cross Section

We shall approximate the distribution of thermal and diffusion flows over the boundary layer cross section by a third-order polynomial, whose coefficients are found from the differential energy and diffusion equations, with boundary conditions

$$\left.\begin{array}{ll} \text{with } y=0, & q_\Sigma = q_{\Sigma w},\\ & j_1 = j_{1w};\\ \text{with } y=\delta_i & q_\Sigma = 0;\\ \text{with } y=\delta_D & j_1 = 0. \end{array}\right\} \qquad (2\text{-}5\text{-}1)$$

Integrating Eqs. (2-1-4) and (2-1-13) over y, with $y \to 0$, we find

$$q_\Sigma \sim q_{w\Sigma} - \int_0^y q_V\, dy + j_w (i^* - i^*_w); \qquad (2\text{-}5\text{-}2)$$

$$j_1 \sim j_{1w} - \int_0^y c_1^0\, dy + j_w (c_1 - c_{1w}). \qquad (2\text{-}5\text{-}3)$$

Conditions (2-5-1), (2-5-2) and (2-5-3) are satisfied by the following approximations:

$$\tilde{q} = \tilde{q}_0\left(1 + \frac{\mathrm{St}_\Sigma^{-1}\int_0^1 \tilde{q}_V\, d\xi_i + b_{1i}\vartheta}{1+2\xi_i}\right); \qquad (2\text{-}5\text{-}4)$$

$$\tilde{j}_1 = \tilde{j}_{10}\left(1 + \frac{\mathrm{St}_D^{-1}\int_0^1 c_1\, d\xi_D + b_{1D}\tilde{c}}{1+2\xi_D}\right), \qquad (2\text{-}5\text{-}5)$$

where $\tilde{q} = q_\Sigma/q_{\Sigma w}$; $\tilde{j}_1 = j_1/j_{1w}$ are the relative thermal and diffusion flows; $b_{1i} = \tilde{j}_w/\mathrm{St}_\Sigma$; /44
$b_{1D} = j_{1w}/\mathrm{St}_D$ are the thermal and diffusion permeability parameters, $\tilde{q}_0$ and $\tilde{j}_{10}$ are the distributions of thermal- and diffusion flows under "standard" conditions in the absence of perturbing factors; $\tilde{c} = (\bar{c}-\bar{c}_w)/(\bar{c}_0-\bar{c}_w)$ is the dimensionless weight concentration of the diffusing element.

In conformity with the adopted approximations

$$\tilde{q}_0 = \tilde{j}_{10} = 1 - 3\xi^2 + 2\xi^3. \qquad (2\text{-}5\text{-}6)$$

2.6. "Logarithmic" Thermal- and Diffussion-Boundary Layers

We introduce the thermal and diffusion analogues of the "logarithmic" boundary layer considered in Section 1.4.

It follows from Eqs. (2-1-17) and (2-1-12) that the ratio $\tau/q = \tau/j_1$ is constant over the boundary layer cross section for the case of flow of a fluid having constant physical parameters around an impermeable plate. With boundary conditions T_w = const and c_w = const. Then, with $Pr = Sc = Pr_T = Sc_T = 1$, taking into account (2-1-11) and (2-1-17), we find

$$\varphi^* = c^* + \frac{1}{\chi_0} \ln \eta^*, \tag{2-6-1}$$

where, for the thermal layer

$$\varphi^* = \varphi_T = \frac{\theta}{\theta^*}, \quad \eta^* = \eta_T = \frac{q_w y}{\lambda \Pr \theta^*}, \tag{2-6-2}$$

and $\theta^* = \sqrt{q_{0T}\Delta T/(\rho_0 w_0 C_p)}$ is the thermal analogue of the friction velocity; and, for the diffusion boundary layer

$$\varphi^* = \varphi_D = \frac{c_1 - c_{1w}}{\Delta c^*}; \quad \eta^* = \eta_D = \frac{j_{1w} y}{D \Delta c^*}; \tag{2-6-3}$$

$\Delta c^* = \sqrt{j_{1oT}\Delta c/(\rho_0 w_0 \mathrm{Sc}_T)}$ is the diffusion analogue of the friction velocity.

The computational formulas for all parameters of the thermal- and diffusion "logarithmic" boundary layers are established in analogy with the dynamic boundary layer and have the same form as Eqs. (1-10-2), (1-11-1), (1-11-2) and (1-4-3), only in the case of the thermal boundary layer φ_T should replace φ and, for the diffusion boundary layer, φ_D should replace φ, in conformity with (2-6-2) and (2-6-3).

With $Pr \neq 1$ and $Sc \neq 1$ a correction (see Sect. 2.2) should be inserted into the laws of heat- and mass transfer. For gases ($Pr \approx Sc \approx 1$), with a power-law approximation of Eq. (1-10-3), these laws can be written in the form

$$\mathrm{St}_0 = \frac{B}{2} \Pr^{-0.75} \mathrm{Re}_T^{**-m} \tag{2-6-4}$$

and

/45

$$\mathrm{St}_D = \frac{B}{2} \mathrm{Sc}^{-0.75} \mathrm{Re}_D^{**-m}, \tag{2-6-5}$$

where the values of B and m are selected from Table 1-2. For the region $\mathrm{Re}^{**}_T = \mathrm{Re}^{**}_D < 10^4$, $B/2 = 0.0128$, $m = 0.25$. With simultaneous development of the dynamic, thermal and diffusion boundary layers at a plate, using the integral

energy and diffusion relationships (2-4-7) and (2-4-5), for $\bar{j} = 0$, $q_v = 0$ and boundary conditions $T_w = \text{const}$, $c_w = \text{const}$, we obtain

$$Nu_x = 0{,}0288 \cdot Re_x^{0.8} Pr^{0.4}; \qquad (2\text{-}6\text{-}6)$$

$$Nu_{Dx} = 0{,}0288 \cdot Re_x^{0.8} Sc^{0.4}. \qquad (2\text{-}6\text{-}7)$$

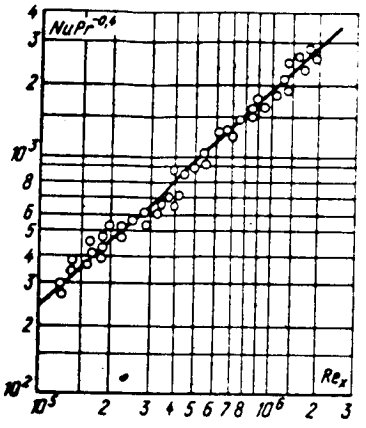

Fig. 2.2. Local values of Nu_x with a subsonic flow of air around a plate. Straight line—computed from formula (2-6-6); points—data from B. S. Petukhov [86].

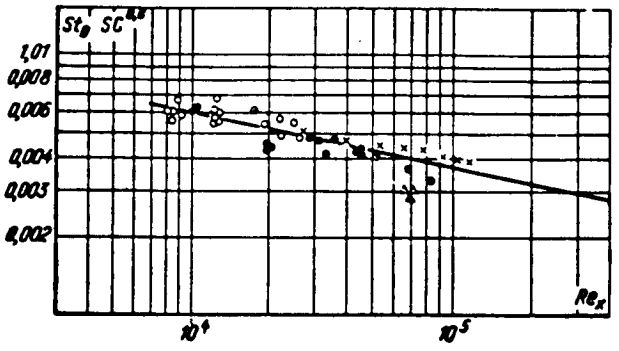

Fig. 2.3. Mass transfer at a flat plate. Straight line—calculated from formula $St_D Sc^{0.6} = 0.036\ Re_x^{-0.2}$, derived from (2-6-7); Points: O—Wade, ×—Pascual, ⊙—Powell, ●—Powell and Griffiths, Δ—Lur'e and Mikhailov.

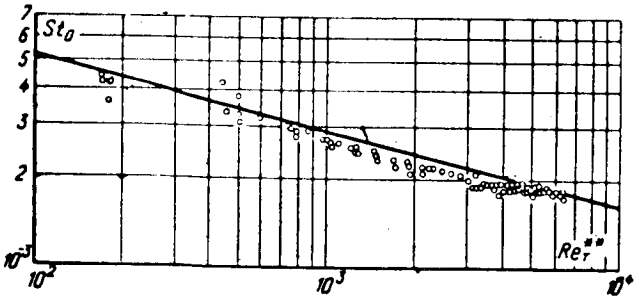

Fig. 2.4. Law of heat transfer at a flat plate. Straight line—calculated from formula (2-6-4); Points—test data [182].

Figures 2.2 and 2.3 show comparisons of the data of B. S. Petukchov, A. A. Detlaf, V. V. Kirilov [86] with formula (2-6-6) and the test data of various authors with formula (2-6-7). /46

Figure 2.4 presents the test data of Whitten, Moffat and Kays [182] on the heat transfer at a flat impermeable plate, for the condition $T_w = \text{const}$ compared with the calculated values from formula (2-6-4).

CHAPTER 3
THE BOUNDARY LAYER WITH VANISHING VISCOSITY

3.1. Degeneration of the Viscous Sublayer

As the viscosity decreases, with other conditions remaining unchanged, the dynamic layer becomes thinner, and the flow increasingly takes on the characteristics of the flow of an ideal fluid. However, in such a situation the rates of change of the thicknesses of the turbulent core and viscous sublayer turn out to be unequal.

As has been shown in Section 1.9, as $\mathrm{Re} \to \infty$, $\xi_1 \to 0$; i.e., the thickness of the viscous sublayer falls off more rapidly than does the thickness of the entire boundary layer as the Reynolds number increases.

For a more general consideration of this problem it becomes necessary to introduce the concept of a fluid with vanishing viscosity.

A characteristic feature of this model fluid is that its viscosity $\mu \to 0$, but never actually goes to zero. Hence any fluid flow with vanishing viscosity has $\mathrm{Re} \to \infty$ and forms a turbulent boundary layer around a rigid surface. /47

For the laminar sublayer it follows from (1-6-10) that as $\xi \to 0$

$$\omega \sim \frac{\bar{j}_w \mathrm{Re}^{**} c_f - 2\tilde{\delta}^{**-1} f}{2\bar{j}_w^2 \mathrm{Re}^{**}} (e^{Z\xi} - 1) + \tilde{\delta}^{**-1} \frac{f}{\bar{j}_w} \xi, \tag{3-1-1}$$

where

$$Z = \bar{j}_w \mathrm{Re}^{**} \tilde{\delta}^{**-1}.$$

With $\bar{j}_w = 0$, we have from (3-1-1)

$$\omega \sim \mathrm{Re}^{**} \tilde{\delta}^{**-1} \left(\frac{c_f}{2} \xi - f \tilde{\delta}^{**-1} \xi^2 \right) \tag{3-1-2}$$

and with $f = 0$

$$\omega \sim \frac{c_f}{2\bar{j}_w} (e^{Z\xi} - 1). \tag{3-1-3}$$

Further, by definition, we know

$$0 < \omega < 1; \; 0 < \tilde{\delta}^{**} < \infty. \tag{3-1-4}$$

Hence, if we attach the subscript 1 to the quantities ω and ξ to describe the nominal limit of the viscous sublayer and of the turbulent core, we see that for any condition, as $\mathrm{Re} \to \infty$, $\xi_1 \to 0$.

Thus, in a fluid with vanishing viscosity the viscous sublayer degenerates, and the role of viscosity reduces only to the creation of the effect of "attachment" of fluid to the wall, i.e., assuring the conditions $\omega = 0$ with $\xi = 0$ and the dissipation of the energy of turbulent motion.

These properties distinguish a fluid with vanishing viscosity from an ideal fluid and allow the formation in it of an ideal turbulent boundary layer—i.e., a layer with $\tau_1 \to 0$.

3.2. Degeneration of Density Fluctuations

The effect of density fluctuations attributable to the inhomogeneity of the temperature field on the Reynolds stresses is expressed by the quantity

$$\tilde{\beta} = \beta \frac{\overline{w_y \theta} + \overline{v_x v_y \theta}}{\overline{v_x v_y}}.$$

Since the turbulent Prandtl number $Pr_T \approx 1$, we can take as an estimate [44] /48

$$\theta \approx v_x \frac{\Delta T}{w_0} \approx v^* \frac{\Delta T}{w_0}. \qquad (3\text{-}2\text{-}1)$$

Then

$$\tilde{\beta} \approx \left(\frac{w_y}{w_0} + \sqrt{\frac{c_f}{2}} \right) \beta \Delta T. \qquad (3\text{-}2\text{-}2)$$

From the equation of continuity we find

$$\frac{w_y}{w_0} \sim \frac{d\delta}{dx} \sim \frac{\delta}{\delta^{**}} \frac{d\delta^{**}}{dx}, \qquad (3\text{-}2\text{-}3)$$

i.e., in view of the momentum equation we can assume that $w_y/w_0 \sim c_f$.

Thus $\tilde{\beta}$ decreases as the coefficient of friction decreases, and, since the latter tends to zero as $Re \to \infty$, then also $\tilde{\beta} \to 0$.

3.3. Relative Drag Law

We introduce the quantity

$$\Psi = \left(\frac{c_f}{c_{f0}} \right)_{Re^{**}}, \qquad (3\text{-}3\text{-}1$$

where c_{fo} is the coefficient of friction for some standard boundary layer, and comparison is made with Re^{**} = idem.

We shall choose the simplest possible boundary layer as the standard--namely, a turbulent, isothermal boundary layer, without pressure gradient, at a smooth and impermeable plate.

We integrate Eq. (1-3-6) so that

$$Z\Psi^{1/2} = \int_{\eta_1}^{1} \left(\frac{\tilde{\rho} \tilde{\tau}_0}{\tilde{\tau}} \right)^{1/2} d\eta, \qquad (3\text{-}3\text{-}2)$$

where

$$Z=\left(\frac{c_{f_0}}{2}\right)^{1/2}\int_{\xi_1}^{1}\left(\frac{\tilde{\tau}_0}{1-\tilde{\beta}}\right)^{1/2}\frac{d\xi}{\tilde{l}}.$$

With Re $\to \infty$, in accordance with (1-9-6) and (1-9-11) and with $\tilde{\beta} \to 0$. /49

$$Z \to \frac{-\ln \xi_1}{\ln \mathrm{Re}^{**}}, \tag{3-3-3}$$

or, if $\xi_1 \sim \mathrm{Re}^{**-n}$,

$$Z \to n. \tag{3-3-4}$$

With f = 0, n = 1; with $f = f_{crit}$, $n \approx 2/3$, i.e. as Re $\to \infty$

$$\frac{2}{3} < Z < 1. \tag{3-3-5}$$

Thus, in an ideal turbulent boundary layer—with a gradient-free flow rigorously, and otherwise approximately,

$$\int_0^1 \left(\frac{\tilde{\rho}\tilde{\tau}_0}{\tilde{\Psi}\tilde{\tau}}\right)^{1/2} d\omega = 1. \tag{3-3-6}$$

This integral expresses the remarkable circumstance that although the absolute magnitude of the coefficient of friction also tends to zero in fluids with vanishing viscosity, its relative changes when influenced by perturbing factors (nonisothermal state, compressibility, wall permeability, etc) remain finite.

Equation (3-3-6) defines the limiting relative drag laws of the turbulent boundary layer. Here special attention should be given the circumstance that this equation (which describes a set of important properties of the turbulent boundary layer), in its general formulation, does not depend on any empirical constant.

3.4. Relative Law of Heat Transfer

From (2-1-12) it follows that

$$Z_T \Psi_S^{1/2} = \int_{\xi_{T_1}}^{1}\left(\frac{\tilde{\rho}\tilde{q}}{\tilde{q}_0}\frac{\partial\omega}{\partial\xi_T}\frac{\partial\vartheta}{\partial\xi_T}\right)^{1/2} d\xi_T, \tag{3-4-1}$$

where /50

$$Z_T = \left(\frac{\mathrm{St}_0}{\mathrm{Pr}_T}\right)^{1/2}\int_{\xi_{T1}}^{1}\left(\frac{\tilde{q}_0}{1-\tilde{\beta}_T}\right)^{1/2}\frac{d\xi_T}{\tilde{l}_T}; \tag{3-4-2}$$

$\Psi_s = \left(\frac{St}{St_0}\right)_{Re=\infty_T}$ and ϑ are defined over Δi.

The properties of the quantities ξ_{T_1}, $\tilde{\beta}_T$ and Z_T are the same as those of their hydrodynamical analogues. With $Re \to \infty$

$$\Psi_s \to \left[\int_0^1 \left(\frac{\tilde{\rho}\tilde{q}}{q_0}\frac{\partial\omega}{\partial\xi_T}\frac{\partial\vartheta}{\partial\xi_T}\right)^{1/2} d\xi_T\right]^2. \qquad (3\text{-}4\text{-}3)$$

If the temperature and velocity fields are similar, then $\xi = \xi_T$, $\partial\omega/\partial\xi = \partial\vartheta/\partial\xi_T$, Eq. (3-4-3) goes over into (3-3-6) and $\Psi_s = \Psi$.

But in the general case, with substantial infringements of similarity of the temperature and velocity fields, the functions Ψ and Ψ_s do not agree. Thus, for example, in the diffusor-flow region of the turbulent boundary layer ($f < 0$), Ψ can be considerably less than unity, while with finite Reynolds numbers Ψ_s in the diffusor-flow region may change very little.

3.5. Relative Law of Mass Transfer

From (2-1-17) it follows that

$$Z_D \Psi_D^{1/2} = \int_{\xi_{D1}}^1 \left(\frac{\tilde{\rho}\tilde{j}}{j_0}\frac{\partial\omega}{\partial\xi_D}\frac{\partial\tilde{c}}{\partial\xi_D}\right)^{1/2} d\xi_D, \qquad (3\text{-}5\text{-}1)$$

where

$$Z_D = \left(\frac{St_{D0}}{Sc_2}\right)^{1/2} \int_{\xi_{D1}}^1 \left(\frac{\tilde{j}_0}{1-\tilde{\beta}_D}\right)^{1/2} \frac{d\xi_D}{\tilde{l}_D}; \qquad (3\text{-}5\text{-}2)$$

$\Psi_D = \left(\frac{St_D}{St_{D0}}\right)_{Re}$ is the relative law of mass transfer.

It is not difficult to show that the properties of the quantities ξ_{D_1}, $\tilde{\beta}_D$ and Z_D are like those of their hydrodynamical analogues. Hence, with $Re \to \infty$, we have /51

$$\Psi_D \to \left[\int_0^1 \left(\frac{\tilde{\rho}\tilde{j}}{j_0}\frac{\partial\omega}{\partial\xi_D}\frac{\partial\tilde{c}}{\partial\xi_D}\right)^{1/2} d\xi_D\right]^2. \qquad (3\text{-}5\text{-}3)$$

If condition (2-2-1) is satisfied, i.e., if similarity exists between the velocities, enthalpies and concentrations, then

$$\Psi_D = \Psi_S = \Psi. \tag{3-5-4}$$

However, in the general case this similarity may be infringed. In particular, in the case of a gradient gas flow, the law of friction can differ considerably from the laws for heat- and mass transfer. The analogy between heat- and mass transfer, i.e., the equality $\Psi_S = \Psi_D$, is maintained over a wide range of change in the determining parameters.

3.6. Distributions of Velocity, Temperature and Concentration over a Turbulent Boundary Layer Cross Section at High Reynolds Numbers

Equation (1-5-4) can be reduced to the form

$$\sqrt{\frac{\widetilde{\rho\tau_0}}{\widetilde{\Psi\tau}}}\, d\omega = \sqrt{\frac{\widetilde{c_{f0}\tau_0}}{2(1-\widetilde{\beta})}}\, \frac{d\xi}{\widetilde{l}} \tag{3-6-1}$$

or

$$\frac{d\omega}{d\omega_0} = \sqrt{\frac{\Psi}{\widetilde{\rho}}\, \frac{\widetilde{\tau}}{\widetilde{\tau}_0(1-\widetilde{\beta})}}, \tag{3-6-2}$$

where ω_0 is the dimensionless velocity under standard conditions.

Integrating, we find

$$\int_0^1 \sqrt{\frac{\widetilde{\rho\tau_0}}{\widetilde{\Psi\tau}}}\, d\omega = \int_\xi^1 \sqrt{\frac{\widetilde{c_{f0}}}{2}\, \frac{\widetilde{\tau}_0}{(1-\widetilde{\beta})}}\, \frac{d\xi}{\widetilde{l}}. \tag{3-6-3}$$

With $\mathrm{Re} \to \infty$, as a consequence of the increasing fill-in of the outer portions of the turbulent boundary layer, the velocity profile begins to be decisively determined by Prandtl's law—i.e., a situation is produced such that the quantity $\tilde{\tau}$ becomes essentially independent of perturbation factors in the derivation of the laws of friction and heat transfer. If we also take into account the asymptotic properties of the boundary layer ($\tilde{\beta} \to 0$), we obtain /52

$$\int_\xi^1 \sqrt{\frac{\widetilde{c_{f0}}}{2}\widetilde{\tau}_0}\, \frac{d\xi}{\widetilde{l}}\Big|_{\mathrm{Re}\to\infty} = 1 - \omega_0. \tag{3-6-4}$$

Consequently

$$\int_0^1 \sqrt{\frac{\widetilde{\rho\tau_0}}{\widetilde{\Psi\tau}}}\, d\omega = 1 - \omega_0. \tag{3-6-5}$$

If we set $\xi = \xi_1$ in Eq. (3-6-4), then, as $\mathrm{Re} \to \infty$, $\xi_1 \to 0$, and formula (3-6-4) goes over into the limiting formula. Hence, for large Reynolds numbers we have, approximately

$$\int_{\omega}^{1} \frac{\tilde{\rho}^{1/2}\, d\omega}{\sqrt{\frac{\tilde{\tau}}{\tau_0}}} = \sqrt{\Psi_\infty}\,(1-\omega_0) \tag{3-6-6}$$

or, in consideration of Eq. (1-4-3)

$$\int_{\omega}^{1} \frac{\tilde{\rho}^{1/2}\, d\omega}{\sqrt{\frac{\tilde{\tau}}{\tau_0}}} = -\sqrt{\Psi_\infty}\,\frac{1}{\chi_0}\sqrt{\frac{c_{f0}}{2}}\ln\xi_0. \tag{3-6-7}$$

Similarly, formulas for the distributions of enthalpy and concentration can be found:

$$\int_{\theta}^{1} \frac{d\theta}{\sqrt{\frac{\rho_0 q}{\tilde{\rho} q_0}}} = -\sqrt{\Psi_{S\infty}}\,\frac{1}{\chi_0}\sqrt{\mathrm{St}_{S0}}\ln\xi_{T0} \tag{3-6-8}$$

and

$$\int_{\chi}^{1} \frac{d\tilde{c}}{\sqrt{\frac{\rho_0 j}{\tilde{\rho} j_0}}} = -\sqrt{\Psi_{D\infty}}\,\frac{1}{\chi_0}\sqrt{\mathrm{St}_{D0}}\ln\xi_{D0}. \tag{3-6-9}$$

Henceforth, Eqs. (3-6-7), (3-6-8) and (3-6-9) will be used to derive the limiting distributions of velocity, temperature and concentration under the action of various perturbing factors. /53

CHAPTER 4
LIMITING RELATIVE LAWS OF FRICTION AND HEAT TRANSFER WITH A LONGITUDINAL GAS FLOW AROUND AN IMPERMEABLE PLATE

4.1. Limiting Law of Friction for a Non-isothermal Boundary Layer on a Flat Plate

For the conditions being considered, it follows from Eq. (1-6-15) that $\tilde{\tau}/\tilde{\tau}_0 = 1$, i.e. the non-isothermal state and gas compressibility should not affect the distribution of the turbulent shearing stress over the boundary layer cross section with the approximations adopted.

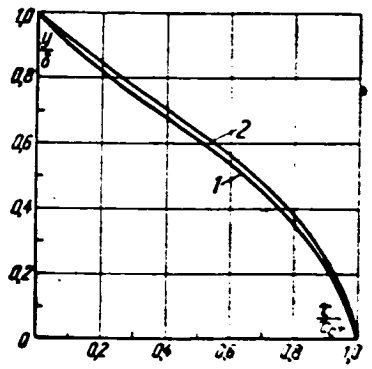

FIG. 4.1. Effect of compressibility on the distribution of turbulent shearing stress over the boundary layer cross section (according to [175]). 1—M = 0; 2—M = 5.

The results of an analysis of the effect of compressibility on the distribution of τ given in [175] (Fig. 4.1) are a direct confirmation of this deduction.

Taking into account Eqs. (1-6-15), (2-3-1) and (2-3-8), for $\varepsilon = 1$, we have from Eq. (3-3-2): /54

$$\Psi = \frac{1}{(\psi^* - 1)\, Z}\left[\arcsin\frac{2(\psi^* - 1) + \Delta\psi}{E} - \arcsin\frac{2(\psi^* - 1)\,\omega_1 + \Delta\psi}{E}\right]^2, \tag{4-1-1}$$

where

$$E = \sqrt{4(\psi^* - 1)(\psi^* + \Delta\psi) + \Delta\psi^2}.$$

With $R \to \infty$, $\omega_1 \to 0$ and $Z \to 1$. As a result, we have

$$\Psi_\infty = \frac{1}{\psi^* - 1}\left[\arcsin\frac{2(\psi^* - 1) + \Delta\psi}{E} - \arcsin\frac{\Delta\psi}{E}\right]^2. \tag{4-1-2}$$

Formula (4-1-2) defines the relative limiting law of friction for a non-isothermal turbulent boundary layer at an impermeable plate. It does not contain empirical turbulence constants and is not related to any semiempirical theory of turbulence. The quantity c_{fo} in the limit laws can be established both on theoretical grounds (for example, in terms of some semiempirical theory of turbulence for non-isothermal flow) and directly from the experimental data. For a supersonic gas flow around a thermally-insulated plate, ($\Delta\psi = 0$), we have from (4-1-2):

$$\Psi_\infty = \frac{\left(\arcsin\sqrt{\frac{\psi^* - 1}{\psi^*}}\right)^2}{\psi^* - 1} \tag{4-1-3}$$

or since

$$\psi^* - 1 = r\frac{k-1}{2}M_0^2,$$

$$\Psi_\infty = \left(\frac{\operatorname{arctg} M_0\sqrt{r\frac{k-1}{2}}}{M_0\sqrt{r\frac{k-1}{2}}}\right)^2. \qquad (4\text{-}1\text{-}4)$$

For subsonic gas flow ($\psi^* \to 1$), we find from (4-1-2) /55

$$\Psi_\infty = \left[\frac{2}{\sqrt{\psi}+1}\right]^2 \qquad (4\text{-}1\text{-}5)$$

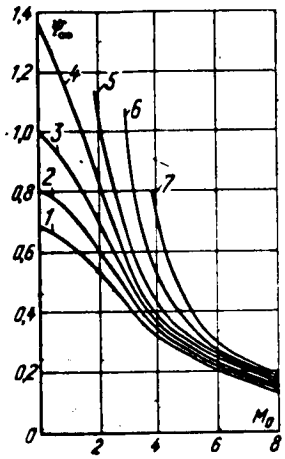

FIG. 4.2. Dependence of ψ_∞ on M_0 and $\Delta\psi$ according to the limit formula (4-1-2). 1—$\Delta\psi = 1$; 2—$\Delta\psi = 0.5$; 3—$\Delta\psi = 0$; 4—$\Delta\psi = -0.5$; 5—$\Delta\psi = -1$; 6—$\Delta\psi = -2$; 7—$\Delta\psi = -3$.

Figure 4.2 illustrates the dependence of ψ_∞ on M_0 and $\Delta\psi$, as computed from (4-1-2), in which case $\psi^* = 1 + r\frac{k-1}{2}M_0^2$.

Spalding [164] has proposed a relatively simple approximation of (4-1-2) which, to within a few percent, is valid up to $M_0 \approx 6.0$, and has the form:

$$\Psi_\infty \approx \left\{\frac{1}{4}\left[\left(\frac{T_{0r}}{T_0}\right)^{1/2}+1\right]^2 + \frac{1}{6}r\frac{k-1}{2}M_0^2\right\}^{-1}. \qquad (4\text{-}1\text{-}6)$$

Assuming r = 0.9 and k = 1.4, we obtain

$$\Psi_\infty \approx \left\{\frac{1}{4}\left[\left(\frac{T_{0r}}{T_0}\right)^{1/2}+1\right]^2 + 0{,}03M_0^2\right\}^{-1}. \qquad (4\text{-}1\text{-}7)$$

For the subsonic gas flow region we can assume

$$\Psi_\infty \approx \psi^{-0.5}. \qquad (4\text{-}1\text{-}8)$$

in the range $0.5 < \psi < 3.0$.

Under some conditions it is convenient to introduce the relative coefficient of friction $\overline{\Psi}_\infty = \left(\frac{c_f}{c_{fM}}\right)_{Re^{**}, M_0}$, which involves only the effect of the non-isothermal state. Here c_{fm} is the coefficient of friction with $\Delta\psi = 0$, with the same values of Re^{**} and Mo.

From Eq. (4-1-2) and (4-1-3) we can write two limit expressions for $\overline{\Psi}_\infty$:

$$\text{with } \psi^* \to 1 \quad \overline{\Psi}_\infty = \left(\frac{2}{\sqrt{\psi}+1}\right)^2; \qquad (4\text{-}1\text{-}9)$$

$$\text{with } \psi^* \to \infty \quad \overline{\Psi}_\infty = \left(\frac{2}{\pi}\arccos\frac{\overline{\psi}-1}{\overline{\psi}+1}\right)^2, \qquad (4\text{-}1\text{-}10) \quad /56$$

where $\overline{\psi} = \psi/\psi^* = T_w/T^*_w$ is a generalized temperature factor.

TABLE 4.1. Effect of the generalized temperature factor on the relative laws of friction and heat-transfer with Re → ∞

$\bar{\psi}$	0	0,25	0,5	0,75	1	2	3
$\bar{\Psi}_{\psi^*\to 1}$	4	1,78	1,38	1,15	1	0,68	0,54
$\bar{\Psi}_{\psi^*\to\infty}$	4	2,02	1,49	1,18	1	0,62	0,44

Table 4.1 shows the comparative results of computing with formulas (4-1-9) and (4-1-10).

As can be seen from the table, the relative influence of the temperature factor on the limiting law of friction is almost identical for both subsonic and supersonic flows. Therefore, in practical calculations with large Re numbers we can adopt a comparatively simple interpolation formula. /57

$$\Psi \approx \left[\frac{2\operatorname{arctg} M_e\sqrt{r\frac{k-1}{2}}}{\left(\sqrt{\frac{T_w}{T^*_w}}+1\right)M_e\sqrt{r\frac{k-1}{2}}}\right]^2. \qquad (4\text{-}1\text{-}11)$$

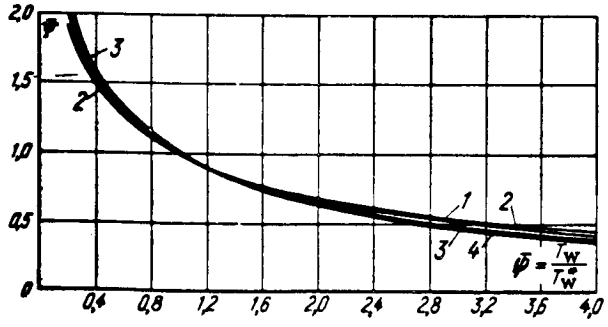

FIG. 4.3. Comparison of calculations with formulas (4-1-2) and (4-1-12). Calculations with (4-1-2): $\bar{\psi} = \psi/\psi_M$, with ψ according to (4-1-2) and W_M according to (4-1-3); 1—$\psi^* = 1$; 2—$\psi^* = 2$; 3—$\psi^* = 18$; 4—calculated from (4-1-12), i.e. $\bar{\Psi}=\left(\frac{2}{\sqrt{\frac{T_w}{T^*_w}}+1}\right)$.

With Re → ∞, $\omega_1 \to 0$, Z → 1 we have

(a) With ε < 1

For the case r = 0.9 and k = 1.4, we have

$$\Psi \approx \left[\frac{4{,}7\operatorname{arctg}(0{,}424M_e)}{\left(\sqrt{\frac{T_w}{T^*_w}}+1\right)M_e}\right]^2. \qquad (4\text{-}1\text{-}12)$$

A comparison of calculations with (4-1-12) and the exact formula (4-1-2) is shown in Fig. 4.3.

With relative similarity of velocities and enthalpies we find

$$\Psi = \frac{1}{(\psi^*-1)Z}\left[\arcsin\frac{2(\psi^*-1)+\varepsilon\Delta\psi}{E} - \arcsin\frac{2(\psi^*-1)\omega_1+\varepsilon\Delta\psi}{E}\right]^2, \qquad (4\text{-}1\text{-}13)$$

where ε is the off-similarity factor.

$$\Psi = \frac{1}{\psi^* - 1}\left[\arcsin\frac{2(\psi^* - 1) + \varepsilon\Delta\psi}{\sqrt{4(\psi^* - 1)(\psi^* + \Delta\psi) + (\varepsilon\Delta\psi)^2}} - \arcsin\frac{\varepsilon\Delta\psi}{\sqrt{4(\psi^* - 1)(\psi^* + \Delta\psi) + (\varepsilon\Delta\psi)^2}}\right]^2; \quad (4\text{-}1\text{-}14)$$

(b) With $\varepsilon > 1$

$$\Psi = \frac{1}{\psi^* - 1}\left[\arcsin\frac{2(\psi^* - 1)\varepsilon^{-1} + \varepsilon\Delta\psi}{\sqrt{4(\psi^* - 1)(\psi^* + \Delta\psi) + (\varepsilon\Delta\psi)^2}} - \arcsin\frac{\varepsilon\Delta\psi}{\sqrt{4(\psi^* - 1)(\psi^* + \Delta\psi) + (\varepsilon\Delta\psi)^2}} + \arcsin\sqrt{\frac{\psi^* - 1}{\psi^*}} - \arcsin\sqrt{\frac{\psi^* - 1}{\varepsilon^2\psi^*}}\right]^2. \quad (4\text{-}1\text{-}15)$$

For subsonic velocities

(a) With $\varepsilon < 1$

$$\Psi_\infty = \left[\frac{2}{\sqrt{\psi} + \sqrt{\psi - (\psi - 1)\varepsilon}}\right]^2; \quad (4\text{-}1\text{-}16)$$

(b) With $\varepsilon > 1$

$$\Psi_\infty = \left[\frac{2}{\varepsilon(\sqrt{\psi} + 1)} + \frac{\varepsilon - 1}{\varepsilon}\right]^2. \quad (4\text{-}1\text{-}17)$$

From (4-1-14), (4-1-16) and (4-1-17) it follows that the magnitude of ε most markedly affects the relative change in the coefficient of friction at subsonic velocities. The degree of this effect can be seen from Table 4.2. /58

TABLE 4.2. Value of $(C_f/C_{fo})_{Re}$** at subsonic velocities from the limit formulas (4-1-16) and (4-1-17)

x/b_T	ε	Ψ						
		0,25	0,5	1	2	3	4	5
0	0	4	2	1	0,5	0,33	0,25	0,25
0,25	0,71	2,65	2,35	1	0,62	0,45	0,35	0,29
0,5	0,9	1,88	1,45	1	0,65	0,5	0,41	0,35
0,8	0,97	1,81	1,41	1	0,67	0,52	0,43	0,37
1	1	1,78	1,38	1	0,69	0,54	0,45	0,38
2	1,1	1,69	1,33	1	0,71	0,58	0,47	0,43
5	1,26	1,59	1,29	1	0,75	0,63	0,54	0,49
10	1,39	1,54	1,26	1	0,77	0,65	0,58	0,54
∞	∞	1	1	1	1	1	1	1

ε is found from (2-3-10), with n = 1/7. It is interesting to note that the effect of the non-similarity in the velocity and temperature fields on the magnitude of ψ, with gas heating and cooling, is not large and is opposite in sense.

4.2. Velocity Distribution in the Non-isothermal Boundary Layer at a Plate with High Re numbers

For our conditions, Eq. (3-6-7) yields

$$\arcsin\frac{2(\psi^*-1)\omega+\Delta\psi}{\sqrt{4\psi(\psi^*-1)+\Delta\psi^2}}=$$
$$=\sqrt{\psi^*-1}\sqrt{\Psi_\infty}\left(1-\frac{1}{\chi_0}\sqrt{\frac{c_{f_0}}{2}}\ln\xi_0\right)+\arcsin\frac{\Delta\psi}{\sqrt{4\psi(\psi^*-1)+\Delta\psi^2}}. \quad (4\text{-}2\text{-}1)$$

With $\Delta\psi = 0$

$$\arcsin\left(\sqrt{\frac{\psi^*-1}{\psi^*}}\,\omega\right)=$$
$$=\sqrt{\psi^*-1}\sqrt{\Psi_\infty}\left(1-\frac{1}{\chi_0}\sqrt{\frac{c_{f_0}}{2}}\ln\xi_0\right) \quad (4\text{-}2\text{-}2)$$

or

$$\omega=\sqrt{\frac{\psi^*}{\psi^*-1}}\sin\left\{\sqrt{\psi^*-1}\sqrt{\Psi_\infty}\times\left(1-\frac{1}{\chi_0}\sqrt{\frac{c_{f_0}}{2}}\ln\xi_0\right)\right\}. \quad (4\text{-}2\text{-}3)$$

/59

For the subsonic gas flow region

$$\omega=\sqrt{\Psi_\infty}\omega_0\left[\omega_0\frac{1-\sqrt{\psi}}{2}+\sqrt{\psi}\right]. \quad (4\text{-}2\text{-}4)$$

Assuming $\omega_0=1+\frac{1}{\chi_0}\sqrt{\frac{c_{f_0}}{2}}\ln\xi_0$, we find

$$\omega=\sqrt{\Psi_\infty}\left[1+\frac{1}{\chi_0}\sqrt{\frac{c_{f_0}}{2}}\ln\xi_0\right]\left[\frac{1-\sqrt{\psi}}{2}\times\left(1+\frac{1}{\chi_0}\sqrt{\frac{c_{f_0}}{2}}\ln\xi_0\right)+\sqrt{\psi}\right]. \quad (4\text{-}2\text{-}5)$$

For the limiting cases, we have

(a) With $\psi \to 0$

$$\omega=\omega_0^2=\left(1+\frac{1}{\chi_0}\sqrt{\frac{c_{f_0}}{2}}\ln\xi_0\right)^2; \quad (4\text{-}2\text{-}6)$$

(b) With $\psi \to \infty$

$$\omega=\omega_0(2-\omega_0)=\left[1-\left(\frac{1}{\chi_0}\sqrt{\frac{c_{f_0}}{2}}\ln\xi_0\right)^2\right]. \quad (4\text{-}2\text{-}7)$$

With $\psi = 1$, naturally, $\omega = \omega_0$.

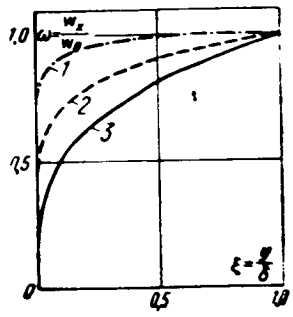

FIG. 4.4. Effect of non-isothermicity on the limiting velocity profile (M ≪ 1). 1—$\omega = \omega_0 = \xi^{1/7}(\psi=\infty)$; 2—$\omega_0 = \xi^{1/7}(\psi = 1)$; 3—$\omega = \omega_0^2 = \xi^{2/7}$ ($\psi = 0$).

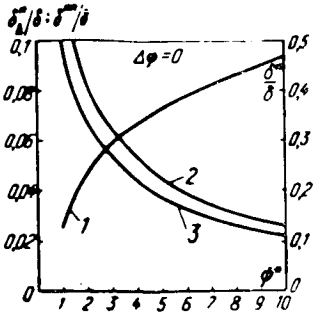

FIG. 4.5. Effect of gas compressibility on the integral characteristics of the turbulent boundary layer. 1—δ^*/δ; 2—δ^*_Δ/δ; 3—δ^{**}/δ.

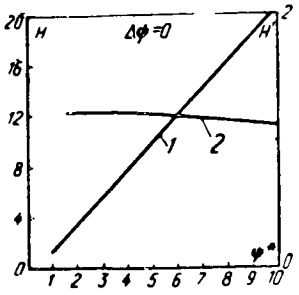

FIG. 4.6. Effect of compressibility on the shape parameters H and H'. 1—H; 2—H'.

Figure 4.4 shows comparative results for calculations made with (4-2-6) and (4-2-7), with $\omega_0 = \xi^{1/7}$. As can be seen from the diagram, the limiting velocity profile becomes less full with an increase in the intensity of cooling of the wall.

In consideration of (4-2-1), (4-2-3) and (4-2-4), we find the limiting expressions for the displacement—and momentum-loss—thicknesses and the shape parameter H. /60

Figures 4.5 and 4.6 illustrate the calculations of δ^*/δ, δ^{**}/δ, δ^*_Δ/δ, H and H', using (4-2-3), for the case $\Delta\psi = 0$.

Here $\delta^*_\Delta/\delta = \int_\delta^\xi (1-\omega)\bar{\rho}\, d\xi$ and $H' = \delta^*_\Delta/\delta^{**}$.

As can be seen from the graphs, gas compressibility has a considerable influence on the integral characteristics of the boundary layer and shape parameter H. On the other hand, the influence of compressibility on the shape parameter $H' = \delta^*_\Delta/\delta^{**}$ is inconsequential.

To an adequate approximation, the computed results can be represented by the following formulas

(a) For $\psi^* \approx 1$

$$H = \psi H_0; \qquad (4\text{-}2\text{-}8)$$

(b) For $10 > \psi^* > 1$, $\Delta\psi = 0$

$$H = H_0(1{,}67\psi^* - 0{,}67); \qquad (4\text{-}2\text{-}9)$$

(c) For $10>\psi^*>1$, $\Delta\psi\neq 0$

$$H=\psi H_0(1{,}67\psi^*-0{,}67), \tag{4-2-10}$$

where $\overline{\psi} = T_w/T_w^*$.

4.3. Limiting Law of Heat Transfer for a Non-isothermal Boundary Layer on a Flat Plate /61

For the similarity region of the distributions of enthalpy and concentration over the boundary layer cross section, and for the diffusion of gases of like valency, taking into account (2-2-1), (2-3-1), (2-3-4), (2-5-4), (2-5-5), (3-4-3) and (3-5-3), we have

(a) With $\delta<\delta_T(\delta_D)$ (i.e. $\varepsilon<1$)

$$\Psi_{S\infty}=\Psi_{D\infty}=\left\{\frac{\varepsilon}{\sqrt{\psi^*-1}}\left[\arcsin\frac{2\frac{\psi^*-1}{\varepsilon}+\Delta\psi}{\sqrt{4\frac{\psi^*-1}{\varepsilon^2}(\psi^*+\Delta\psi)+(\Delta\psi)^2}}-\arcsin\frac{\Delta\psi}{\sqrt{4\frac{\psi^*-1}{\varepsilon^2}(\psi^*+\Delta\psi)+(\Delta\psi)^2}}\right]+\frac{2}{\Delta\psi}\left[\sqrt{1+\Delta\psi(1-\varepsilon)}-\sqrt{1+\Delta\psi}\right]\right\}^2; \tag{4-3-1}$$

(b) With $\delta>\delta_T(\delta_D)$ (i.e. $\varepsilon>1$)

$$\Psi_{S\infty}=\Psi_{D\infty}=\frac{\varepsilon^2}{\psi^*-1}\left[\arcsin\frac{2\frac{\psi^*-1}{\varepsilon^2}+\Delta\psi}{\sqrt{4\frac{\psi^*-1}{\varepsilon^2}(\psi^*+\Delta\psi)+(\Delta\psi)^2}}-\arcsin\frac{\Delta\psi}{\sqrt{4\frac{\psi^*-1}{\varepsilon^2}(\psi^*+\Delta\psi)+(\Delta\psi)^2}}\right]^2. \tag{4-3-2}$$

For the case $\varepsilon=1$

$$\Psi_{S\infty}=\Psi_{D\infty}=\Psi_\infty$$
$$=\frac{1}{\psi^*-1}\left[\arcsin\frac{2(\psi^*-1)+\Delta\psi}{\sqrt{4(\psi^*-1)(\psi^*+\Delta\psi)+(\Delta\psi)^2}}-\arcsin\frac{\Delta\psi}{\sqrt{4(\psi^*-1)(\psi^*+\Delta\psi)+(\Delta\psi)^2}}\right]^2. \tag{4-3-3}$$

As Spalding [164] has shown, Eqs. (4-3-1) and (4-3-2) can be approximated to within a few percent by the following simple formula:

$$\Psi_S=\Psi_D=\left[\frac{1}{4}\{\psi^{1/2}+1\}^2+\frac{1}{6}(\psi^*-1)\varepsilon^{-2}\right]^{-1}. \tag{4-3-4}$$

Assuming r = 0.9 and k = 1.4, we have

$$\Psi_S=\Psi_D\approx\left[\frac{1}{4}\{\psi^{1/2}+1\}^2+0{,}03\left(\frac{M_e}{e}\right)^2\right]^{-1}. \tag{4-3-5}$$

The gas flow velocity for the subsonic region is

$$\Psi_S=\Psi_D=\left[\frac{2}{\sqrt{\psi}+1}\right]^2. \tag{4-3-6}$$

The limiting temperature and concentration-distributions of the gas diffusing over the boundary layer cross section are found from Eqs. (3-6-9) and (3-6-10), with the condition

$$\tilde{q}/q_0=\tilde{j}/\tilde{j}_0=1.$$

In particular, for the subsonic region and diffusion of gases of like valency, with the main flow from Eqs. (3-6-8) and (3-6-9), we find

$$\vartheta=\sqrt{\Psi_{S\infty}}\left[1+\frac{1}{\chi_0}\sqrt{\mathrm{St}_0}\ln\xi_T\right]\left[\frac{1-\sqrt{\psi}}{2}\left(1+\frac{1}{\chi_0}\sqrt{\mathrm{St}_0}\ln\xi_T\right)+\sqrt{\psi}\right] \tag{4-3-7}$$

and

$$\tilde{c}=\sqrt{\Psi_{D\infty}}\left[1+\frac{1}{\chi_0}\sqrt{\mathrm{St}_{D0}}\ln\xi_D\right]\left[\frac{1-\sqrt{\psi}}{2}\left(1+\frac{1}{\chi_0}\sqrt{\mathrm{St}_{D0}}\ln\xi_D\right)+\sqrt{\psi}\right]. \tag{4-3-8}$$

The limiting laws of heat- and mass transfer for more complicated conditions of diffusion and injection of an inhomogeneous gas, with chemical reactions at the surface, will be derived in Chapter 5.

4.4. Limiting Law of Friction for a Non-isothermal Boundary Layer of a Dissociating Gas on a Flat Plate

/63

Gas dissociation processes in the boundary layer are possible in the high-temperature region.

We shall assume that the dissociating gas is a binary mixture of atoms and molecules. Using the familiar approximation of the ideal dissociating gas, we introduce the mass concentration of atoms as a given point, $\alpha = \rho_a/\rho$, and then the mass concentration of molecules will be $\rho_M/\rho = 1 - \alpha$. In this case

$$i_\Sigma=\Sigma c_i i_i=C_{P_M}T+(C_{P_a}-C_{P_M})\alpha T+\alpha i_a^0. \tag{4-4-1}$$

Introducing the specific heat of the mixture $C_p = \Sigma c_i C_{pi}$, we find

$$i_\Sigma = C_p T + \alpha i_a^0, \tag{4-4-2}$$

where i_a^0 is the heat of dissociation.

From the equation of conservation of atomic components (2-1-13), we find

$$\rho w_x \frac{\partial \alpha}{\partial x} + \rho w_y \frac{\partial \alpha}{\partial y} = \frac{\partial}{\partial y}\left[\left(\frac{\mu}{Sc} + \varepsilon_\tau\right)\frac{\partial \alpha}{\partial y}\right] + \dot{w}_\alpha, \tag{4-4-3}$$

where w_α is the mass rate of formation of an atomic component.

For the "ideal dissociating gas" we can assume [73]:

$$\dot{w}_\alpha = \rho^2 M_\alpha^{-2} K_r (1+\alpha)\frac{\alpha_e^2 - \alpha^2}{1-\alpha_e^2}, \tag{4-4-4}$$

where M_α is the atomic weight of the gas; α_e is the equilibrium degree of dissociation; K_r is the dissociation rate constant.

Converting (4-4-3) to dimensionless form, we have

$$\bar{\rho}\bar{w}_x \frac{\partial \alpha}{\partial \bar{x}} + \bar{\rho}\bar{w}_y \frac{\partial \alpha}{\partial \bar{y}} - \frac{1}{Re_L}\frac{\partial}{\partial y}\left[\left(\frac{\mu}{Sc} + \varepsilon_\tau\right)\frac{\partial \alpha}{\partial \bar{y}}\right] = -Da\,\bar{\rho}^2 (1+\alpha)\frac{\alpha_e^2 - \alpha^2}{1-\alpha_e^2}, \tag{4-4-5}$$

where $Re_L = \rho_0 w_0 L/\mu_0$; $Da = \frac{L\rho_0^2 K_r}{w_0 a^2}$ is the Damköhler number characterizing the ratio of the time of existence of particles in the flow (diffusion time) to the chemical reaction time.

When Da → 0 the effect of gas phase chemical reactions on the flow in the boundary layer is slight. In this case $w_\alpha = 0$, the mixture of gases in the boundary layer can be considered to be chemically inert; such a boundary layer is called "frozen-in."

If Da → ∞ the chemical reaction time turns out to be much less than the time particles remain in the boundary layer, and local thermo-chemical equilibrium will be established at each point.

The distributions of the concentration of each component will depend only on the local thermodynamic parameters T and P. This boundary layer is termed "equilibrium." In this case the diffusion equations are not needed to solve the problem. /64

If the rate of the chemical process and the transfer processes are of the same order, the conservation equations of the components must be used in their general forms.

Let us consider the "frozen-in" turbulent boundary layer with a catalytic wall.

Then, for Sc ≈ 1, we have from Eqs. (1-1-4) and (4-4-3)

$$\alpha = \alpha_w + (\alpha_0 - \alpha_w)\omega. \tag{4-4-6}$$

If we assume that only translatory degrees of freedom are perturbed in atoms, and both translatory and rotational degrees of freedom in molecules, we have

$$C_{Pa} = 2{,}5\frac{k}{m_a};\quad C_{PM} = 3{,}5\frac{k}{m_a};$$
$$i_a^0 = \frac{D}{m_M};\quad 2m_a = m_M. \tag{4-4-7}$$

Taking (4-4-1), (4-4-7) and the equation of state of an ideal gas into account, we obtain

$$i_\Sigma = (3{,}5 + 1{,}5\alpha)\frac{k}{2m_a}T + \alpha\frac{D}{2m_a}; \tag{4-4-8}$$

$$P = P_0 = \rho\frac{k}{m_a}(1+\alpha)T. \tag{4-4-9}$$

Hence

$$\frac{\rho}{\rho_0} = \frac{T_0}{T}\frac{1+\alpha_0}{1+\alpha}. \tag{4-4-10}$$

In view of (4-4-6), (4-4-8) and the similarity of the total enthalpies and velocities in the boundary layer, we find

$$\frac{T}{T_0} = \frac{7+3\alpha_w}{7+3\alpha}\psi + \left(\frac{7+3\alpha_0}{7+3\alpha} - \frac{7+3\alpha_w}{7+3\alpha}\psi\right)\omega + \omega(1-\omega)\frac{1{,}4M_0^2}{7+3\alpha}. \tag{4-4-11}$$

Substituting (4-4-6), (4-4-10) and (4-4-11) into (3-3-6), we obtain the limiting relative law of friction for the "frozen-in" turbulent boundary layer of a dissociated gas:

$$\Psi_{\infty\infty} = \left(\int_0^1\left[\left\{\frac{7+3\alpha_w}{7+3\alpha}\psi + \left(\frac{7+3\alpha_0}{7+3\alpha} - \frac{7+3\alpha_w}{7+3\alpha}\psi\right)\omega + \omega(1-\omega)\frac{1{,}4M_0^2}{7+3\alpha}\right\}^{-1}\left[\frac{1+\alpha_0}{1+\alpha}\right]^{1/2}d\omega\right)^2. \tag{4-4-12}$$

For the hypothetical case of an isothermal flow of a dissociated gas at subsonic speeds, we have /65

$$\Psi_{\infty\infty} = \left(\frac{2}{\sqrt{\psi_a}+1}\right)^2. \tag{4-4-13}$$

where

$$\psi_a = \frac{1 + a_w}{1 + a_e}.$$

The results of the numerical integration of (4-4-12) are satisfactorily approximated with the formula

$$\Psi_\infty = \Psi_{l\infty}\Psi_{M\infty}\Psi_{a\infty}, \qquad (4\text{-}4\text{-}14)$$

where

$$\Psi_{l\infty} = \left(\frac{2}{\sqrt{\frac{T_w}{T_w^*}} + 1}\right)^2;$$

$$\Psi_{a\infty} = \left(\frac{2}{\sqrt{\psi_a} + 1}\right)^2;$$

$$\Psi_{M\infty} = \left(\frac{\operatorname{arctg} M_e \sqrt{r\frac{k-1}{2}}}{M_e \sqrt{r\frac{k-1}{2}}}\right)^2.$$

Figure 4.7 gives a comparison between (4-4-13) and calculations made using the method of U. Kh. Dorrance [131]. The calculations covered the ranges of change of Re_x of 10^5-10^8, M_o-number from 0-4 and T_w/T_w^* from 0.04-1.0. The relationship between $(c_f/c_{fo})_{Re_x}$ and $(c_f/c_{fo})_{Re^{**}}$ is found from the momentum equation and, for the conditions being considered, is

$$\left(\frac{c_f}{c_{f0_{a=0}}}\right)_{Re_x} = \left(\frac{c_f}{c_{fo}}\right)^{\frac{1}{m+1}}_{Re^{**}}. \qquad (4\text{-}4\text{-}15)$$

As can be seen from the graph, the relative law of friction in the form $\left(c_f/c_{fo}\right)_{\alpha = 0}\Big)_{R_{e^{**}}, M, \psi}$ depends weakly on the temperature factor and M-number. The maximum effect of gas dissociation on the limiting laws lies within ±25%. For the case $Pr_T = Pr \approx 1$ the known analogue $\psi_\infty = \psi_{S\infty}$ can be used.

It should not be overlooked that in this case in the determination of the total heat flux to the surface of the plate the coefficient of heat-transfer should be multiplied by the drops in total enthalpy. /66

On substituting Eqs. (4-4-6), (4-4-10) and (4-4-11) into Eqs. (3-6-8) and (3-6-9), we obtain the limiting distributions of velocity, enthalpy and concentration over the cross section of a turbulent boundary layer of dissociated gas.

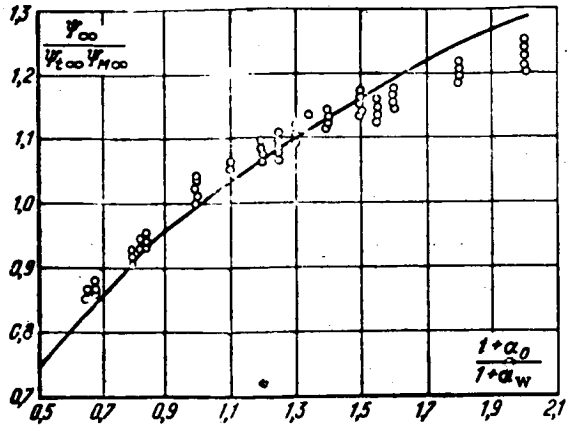

FIG. 4.7. Influence of gas dissociation on the relative law of friction in the turbulent boundary layer. Curve—computed from (4-4-13); Points—computed using the Dorrance method [131].

In particular, for the subsonic region of gas flow, under isothermal conditions, we have

$$\omega = \sqrt{\psi_{\infty}}\,\omega_0\left[\omega_0\frac{1-\sqrt{\psi_\alpha}}{2}+\sqrt{\psi_\alpha}\right]. \quad (4\text{-}4\text{-}16)$$

For the limiting cases: /67

(a) $\alpha_w = 0$, $\alpha_0 = 1.0$ (complete dissociation in the stream and complete recombination at the wall):

$$\omega = (0{,}17\omega_0 + 0{,}83)\,\omega_0; \quad (4\text{-}4\text{-}17)$$

(b) $\alpha_w = 1.0$, $\alpha_0 = 0$ (complete dissociation at the wall and complete recombination in the flow):

$$\omega = \omega_0(1{,}17 - 0{,}17\omega_0). \quad (4\text{-}4\text{-}18)$$

Comparison of (4-4-17) and (4-4-18) shows that the influence of gas dissociation on the limiting velocity profile is negligible (Fig. 4.8).

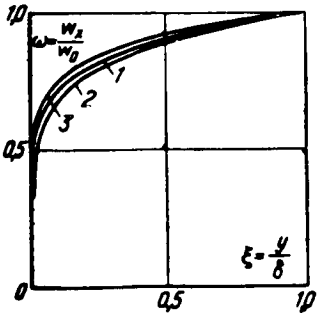

FIG. 4.8. Effect of gas dissociation on the distribution of velocities in the turbulent boundary layer. 1—ω_0; 2—$\psi_\alpha = 0.5$; 3—$\psi_\alpha = 2$.

CHAPTER 5
THE TURBULENT BOUNDARY LAYER ON A PERMEABLE SURFACE

5.1. Limiting Laws of Friction, Heat- and Mass Transfer on a Permeable Plate

The problem of calculating the turbulent boundary layer on a permeable surface is extremely important. Processes of this type arise in connection with the protection of machine elements from the action of high-temperature gas flows (the so-called "pore" cooling of gas-turbine blades, rocket engine combustion chambers, etc.) during evaporation and condensation, in the presence of chemical reactions at the surface of heat-exchangers (burn-out of heat-resistant coating), and in the freezing of liquids and the fusion of solid bodies.

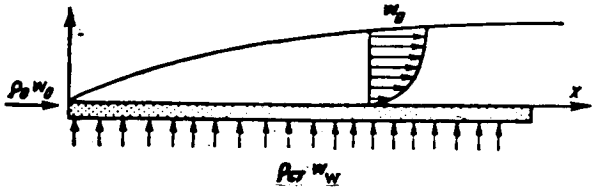

FIG. 5.1. Diagram of boundary layer on a permeable plate.

A diagram of the turbulent boundary layer on a permeable plate is shown in Fig. 5.1. We shall consider that the surface of the plate is penetrable at all points for one component of the flow. If gas is injected into the boundary layer, or sucked out from it, the openings are assumed to be small in size but in adequate number.

The distribution of shearing stress /68
over the boundary layer cross section, for the conditions being considered, follows from Eq. (1-6-15) as

$$\tilde{\tau}=\tilde{\tau}_0\left(1+\frac{b_1\omega}{1+2\xi}\right) \tag{5-1-1}$$

For the condition $\mathrm{Re}\to\infty$, the wall region, where $\xi \ll 1$, becomes most important for τ. Consequently

$$\tilde{\tau}=\tilde{\tau}_0(1+b_1\omega). \tag{5-1-2}$$

A comparison between the test data [140, 168] and the values computed with formula (5-1-2) is shown in Fig. 5.2. As can be seen from the diagram, the test data and formula (5-1-2) agree both qualitatively and quantitatively.

The relative limiting law of friction for a flow around a permeable plate is /69
written as

$$\Psi_\infty=\left(\int_0^1\frac{\tilde{\rho}^{1/2}\,d\omega}{\sqrt{1+b_1\omega}}\right)^2 \tag{5-1-3}$$

or

$$\int_0^1\frac{\tilde{\rho}^{1/2}\,d\omega}{(\Psi_\infty+b\omega)^{1/2}}=1. \tag{5-1-4}$$

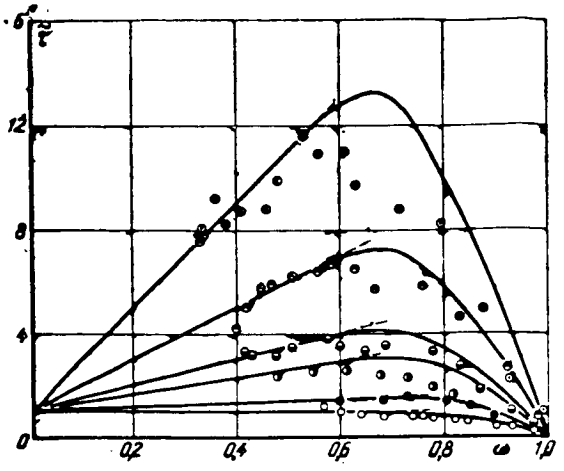

FIG. 5.2. Effect of gas injection on the distribution of turbulent shearing stress over the boundary layer cross section. Curves computed from formula (5-1-2):

Source	[140]				[168]	
Symbol	○	◒	◓	⊙	●	◑
b_1	0	5	10	20	0,8	3,25

The relative density $\tilde{\rho}$ is always finite, and the relative velocity ω varies from 0 to 1, and hence there exists some value of the permeability parameter b with which the integral (5-1-4) has the value $\psi_\infty = 0$. This value of the permeability parameter will be termed "critical" and symbolized as b_{crit}. This phenomenon can be identified with displacement of the boundary layer from the permeable surface.

The magnitude of the critical permeability parameter is found from Eq. (5-1-4), setting $\psi_\infty = 0$:

$$b_{crit\,\infty} = \left[\int_0^1 \left(\frac{\tilde{\rho}}{\omega}\right)^{1/2} d\omega\right]^2. \tag{5-1-5}$$

From Eq. (3-6-6) we find the limiting velocity distribution over the turbulent boundary layer cross section

$$\int_\omega^1 \frac{\tilde{\rho}^{1/2}\, d\omega}{\sqrt{1 + b_1\omega}} = \sqrt{\Psi_\infty}\,(1 - \omega_0). \tag{5-1-6}$$

In case of critical injection

$$\int_\omega^1 \frac{\tilde{\rho}^{1/2}}{\omega^{1/2}}\, d\omega = \sqrt{b_{crit}}\,(1 - \omega_0). \tag{5-1-7}$$

The properties of the gas injected through the wall are in general different from those of the gas in the main flow, and therefore we shall distinguish between injection of a homogeneous gas ($M_1 = M_2$) and an inhomogeneous gas ($M_1 \neq M_2$).

5.2. Injection of a Homogeneous Gas under Isothermal Conditions

/70

For the simplest case of injection of a homogeneous gas under isothermal conditions ($\tilde{\rho} = 1$) and from Eqs. (5-1-3), (5-1-5), (5-1-6) and (5-1-7), we have

$$\Psi_\infty = \left(1 - \frac{b}{4}\right)^2 \tag{5-2-1}$$

$$b_{crit} = 4{,}0; \tag{5-2-2}$$

$$\omega = \left(1 - \frac{b}{4}\right)\omega_0 + \frac{b}{4}\omega_0^2; \tag{5-2-3}$$

$$\omega_{crit} = \omega_0^2, \tag{5-2-4}$$

where ω_{crit} is the dimensionless velocity in the displacement section of the boundary layer.

In view of Eqs. (1-9-4) and (1-9-5).

$$\omega_{crit} = \left(1 + \frac{1}{\chi_0}\sqrt{\frac{c_{f_0}}{2}}\ln\xi\right)^2. \tag{5-2-5}$$

Table 5.1 gives values of the shape parameter $H = \delta^*/\delta^{**}$ computed from (5-2-5) for various values of Re^{**}:

$$\left(H = \int_0^1 (1 - \omega_{crit})\,d\xi \Big/ \int_0^1 \omega_{crit}(1 - \omega_{crit})\,d\xi\right)$$

TABLE 5.1. Values of the shape parameter H at the point of displacement

H	Re^{**}				
	2 000	10 000	100 000	1 000 000	∞
H with $b = b_{sep}$	1,53	1,44	1,4	1,33	1,0
H with $b = 0$	1,28	1,23	1,18	1,15	1
$\overline{H} = H/H_0$	1,19	1,17	1,18	1,15	1

In the case of gas suction through the porous plate, we have

$$\Psi_\infty = \left(1 + \frac{b}{4}\right)^2 \tag{5-2-6}$$

and

/71

$$\omega = \left(1 + \frac{b}{4}\right)\omega_0 - \frac{b}{4}\omega_0^2. \tag{5-2-7}$$

For the limiting suction of gas (see Section 8.1), b = 4, and

$$\omega = \omega_0(2 - \omega_0).$$

Figure 5.3 shows the effect of gas injection and suction on the limiting profiles of velocity and temperature. For the conditions in question, $\omega = \theta$. As can be seen from the diagram, the velocity profile becomes less full with gas injection into the boundary layer, and, with suction of gas, it becomes fuller.

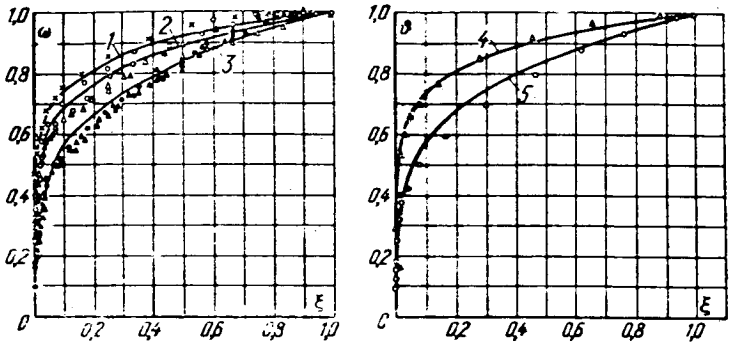

FIG. 5.3. Effect of injection and suction of gas on the limiting profiles of velocity and temperature. 1, 2, 3, —calculated from formula (5-2-3) and (5-2-7), respectively, for b = -0.43; b = 0.53, b = 3.07. 4, 5—calculated from formulas (5-2-3) and (5-2-7) for b = -0.38 and b = 2.91.

Source	[181]		[182]	
Symbol	△	▲	○	●, ×
b	0.53; −0.38	3.07	3.07; 2.91	−0.43

Taking Eq. (5-2-3) into account, the limiting formulas for the displacement thickness, momentum-loss thickness and shape parameter H can be derived. If we set $\omega_0 = \xi^n$, then

$$\tilde{\delta}^*_{\infty} = \frac{n\left(2n+1+\frac{b}{4}\right)}{(n+1)(2n+1)}; \quad (5\text{-}2\text{-}8)$$

$$\tilde{\delta}^*_{\infty\,\mathrm{crit}} = \frac{2n}{2n+1}; \quad (5\text{-}2\text{-}9)$$

$$\tilde{\delta}^{**}_{\infty} = \left(1-\frac{b}{4}\right)\frac{1}{n+1} + \left[\frac{b}{4} - \left(1-\frac{b}{4}\right)^2\right]\frac{1}{2n+1} - 2\frac{b}{4}\left(1-\frac{b}{4}\right)\frac{1}{3n+1} - \frac{b^2}{16}\frac{1}{4n+1}; \quad (5\text{-}2\text{-}10)$$

$$\tilde{\delta}^{**}_{\infty\,\mathrm{crit}} = \frac{2n}{(2n+1)(4n+1)}; \quad (5\text{-}2\text{-}11)$$

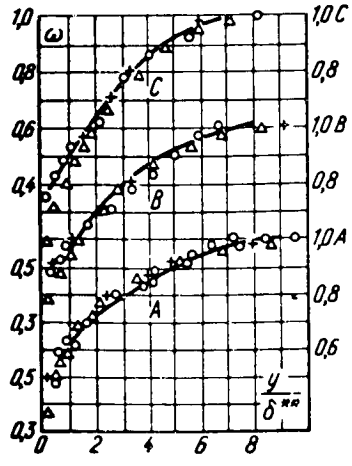

Symbol	b, Re^{**}_{∞}	A	B	C	Source
△	b	1.31	2.5	4.89	[63]
	Re^{**}_{∞}	5 860	7 200	8 410	
✦	b	1.1	2.2	4.9	[82]
	Re^{**}_{∞}	2 630	2 870	3 410	
○	b	1.25	2.4	4.72	[180]
	Re^{**}_{∞}	777	1 120	1 265	

FIG. 5.4. Comparison between formula (5-2-3) and the experimental data. Curves—computed from (5-2-3).

$$H_\infty = \frac{\delta^*_\infty}{\delta^{**}_\infty} = \frac{n\left(2n+1+\frac{b}{4}\right)}{\left(1-\frac{b}{4}\right)^{(2n+1)} + \left[\frac{b}{4} - \left(1-\frac{b}{4}\right)^2 (n+1) - 2\frac{b}{4}\left(1-\frac{b}{4}\right)\frac{(n+1)(2n+1)}{n+1} - \frac{b^2}{16}\frac{(n+1)(2n+1)}{4n+1}\right]^{\frac{1}{2}}}; \quad (5\text{-}2\text{-}12)$$

$$H_{\infty\,\mathrm{crit}} = 1 + 4n. \quad (5\text{-}2\text{-}13)$$

Figure 5.4 gives a comparison between formula (5-2-3) and the experimental data of various investigators. As can be seen from the curves, the limiting velocity distributions are in good agreement with the test data. /73

5.3. Injection of a Homogeneous Gas under Non-isothermal Conditions

The limiting relative laws of friction for the case of injection of a homogeneous gas into a subsonic flow of gas under non-isothermal conditions are found after substituting the expression for the density

$$\frac{\rho_0}{\rho} = \psi + (1-\psi)\,\omega \quad (5\text{-}3\text{-}1)$$

into (5-1-3). After integrating, we have

(a) with $\psi < 1$

$$\Psi_\infty = \frac{4}{(1-\psi)\,b_1}\left[\ln\frac{\sqrt{(1-\psi)(1+b_1)}+\sqrt{b_1}}{\sqrt{1-\psi}+\sqrt{b_1\psi}}\right]^2; \quad (5\text{-}3\text{-}2)$$

(b) with $\psi > 1$

$$\Psi_\infty = \frac{4}{(\psi-1)\,b_1}\left[\operatorname{arctg}\sqrt{\frac{b_1}{(\psi-1)(b_1+1)}} - \operatorname{arctg}\sqrt{\frac{b_1\psi}{\psi-1}}\right]^2. \quad (5\text{-}3\text{-}3)$$

As shown by Spalding [164], Eqs. (5-3-2) and (5-3-3) are satisfactorily approximated by the following simple formula:

$$\Psi_\infty \approx \left[\frac{1}{4}\left\{\psi^{1/2} + (1+b_1)^{1/2}\right\}^2 + \frac{1}{6}b_1(\psi-1)\right]^{-1}. \quad (5\text{-}3\text{-}4)$$

For the critical injection parameters, we obtain from Eq. (5-1-5), taking (5-3-1) into account: /74

(a) with $\psi < 1$

$$b_{\mathrm{crit}\,\infty} = \frac{1}{1-\psi}\left(\ln\frac{1+\sqrt{1-\psi}}{1-\sqrt{1-\psi}}\right)^2; \quad (5\text{-}3\text{-}5)$$

(b) with $\psi > 1$

$$b_{crit\infty} = \frac{1}{\psi - 1}\left(\arccos\frac{2-\psi}{\psi}\right)^2 \qquad (5\text{-}3\text{-}6)$$

In analogy with Eq. (5-3-4), Eqs. (5-3-5) and (5-3-6) are conveniently approximated with the formula

$$b_{crit\infty} \approx \frac{4}{\frac{1}{3} + \frac{2}{3}\psi}. \qquad (5\text{-}3\text{-}7)$$

Figure 5.5 illustrates the relationship between the critical injection parameter and the temperature factor.

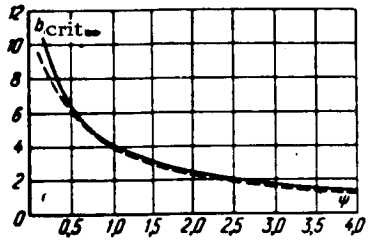

FIG. 5.5. Influence of non-isothermicity on the critical injection parameter. Solid line—computed from (5-3-5) and (5-3-6); Broken line—computed from (5-3-7).

The equation

$$\Psi_\infty = \Psi_{i\infty}\left(1 - \frac{b}{b_{crit\infty}}\right)^2, \qquad (5\text{-}3\text{-}8)$$

is an adequate approximation of Eqs. (5-3-2) and (5-3-3); where $\Psi_{i\infty} = \left(\frac{2}{\sqrt{\psi}+1}\right)^2$, and $b_{crit\infty}$ is found from (5-3-5) and (5-3-6).

Figure 5.6 shows the comparative results of calculations using (5-3-2), (5-3-3) and (5-3-8).

From an analysis of formula (5-3-8) we come to the interesting conclusion that gas injection is less effective than an increase in wall temperature, with other conditions being the same.

The limiting velocity distribution over the cross section of a non-isothermal turbulent boundary layer is found by substituting expression (5-3-1) into Eqs. (5-1-6) and (5-1-7). For $\psi < 1$ /75

$$\omega = \frac{K^2 - ac}{a(2K + d)}, \qquad (5\text{-}3\text{-}9)$$

where

$$a = (1-\psi)b;\quad d = (1-\psi)\Psi_\infty + \psi b;$$
$$c = \psi\Psi_\infty;$$
$$K = \left[\sqrt{a(a+d+c)} + a + \frac{1}{2}d\right]e^{\sqrt{a}(\omega_0 - 1)} - \frac{1}{2}d;$$

For $\psi > 1$

$$\operatorname{arctg}\sqrt{\frac{(\psi-1)(1+b_1\omega)}{\psi + (1-\psi)\omega}} = \operatorname{arctg}\sqrt{(\psi-1)(1+b_1)} - \frac{\sqrt{\psi-1}}{2}\sqrt{\Psi_\infty}(1-\omega_0). \qquad (5\text{-}3\text{-}10)$$

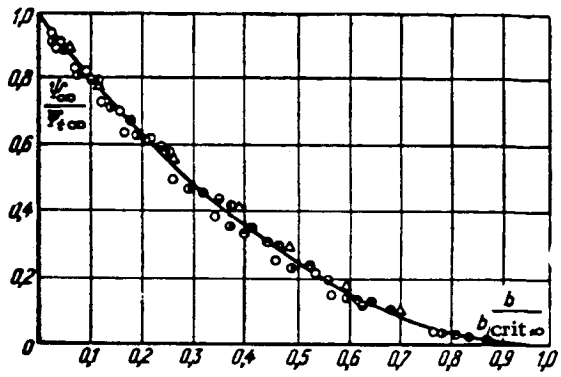

FIG. 5.6. Comparison of formulas (5-3-2), (5-3-3) and (5-3-8). Curve—calculated from (5-3-8).

Calc. from equation	(5-3-2)				(5-3-3)		
Symbol	○	◑	◐	◓	◒	●	△
ψ	0.2	0.4	0.6	0.8	2	4	8

In case of critical injection:

For $\psi < 1$:

$$\sqrt{\psi+(1-\psi)\omega}+\sqrt{(1-\psi)\omega}=[1+\sqrt{1-\psi}]\,e^{\frac{\sqrt{1-\psi}}{2}\sqrt{b_{\text{crit}\infty}}(\omega_0-1)}, \tag{5-3-11}$$

For $\psi > 1$: /76

$$\operatorname{arctg}\sqrt{\frac{(\psi-1)\omega}{\psi+(1-\psi)\omega}}=\operatorname{arctg}\sqrt{\psi-1}-\frac{\sqrt{\psi-1}}{2}\sqrt{b_{\text{crit}\infty}}(1-\omega_0).$$

Taking (5-3-9) into account, the integral characteristics δ^* and δ^{**}, and the shape parameter H, can be computed.

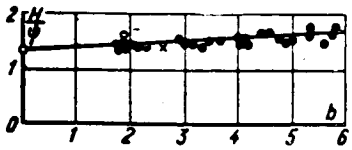

FIG. 5.7. Dependence of shape parameter H on non-isothermicity and injection. Straight line—computed from (5-3-12); Points—◒ plate ($\psi = 1$) [81]; o, x—initial section of tube ($\psi = 0.5$, 0.4) [69].

Figure 5.7 shows the computed shape parameter H and a comparison with the test data of various investigators. For the region $\psi < 1$, the calculation is satisfactorily approximated by the following formula

$$H = H_0\psi(1+0{,}05b), \tag{5-3-12}$$

where $H_0 = 1 + 2n$.

5.4. Injection of a Homogeneous Gas into a Supersonic Flow

For the region of supersonic gas flow:

$$\frac{\rho_0}{\rho}=\psi-\Delta\psi\omega-(\psi^*-1)\omega^2. \tag{5-4-1}$$

The limiting law of friction for the supersonic boundary layer is found by substituting this formula into Eqs. (5-1-4) and (5-1-5):

$$\Psi_\infty=\left(\int_0^1\frac{d\omega}{\sqrt{(1+b_1\omega)[\psi-\Delta\psi\omega-(\psi^*-1)\omega^2]}}\right)^2 \tag{5-4-2}$$

and for the critical injection parameter

$$b_{\text{crit}\infty}=\left[\int_0^1\frac{d\omega}{\sqrt{\omega[\psi-\Delta\psi\omega-(\psi^*-1)\omega^2]}}\right]^2. \tag{5-4-3}$$

Elliptic integrals are the result, and the final expressions for ψ_∞ and b_{crit} take /77
the forms:

$$\sqrt{\Psi_\infty} = \frac{1}{\sqrt{b_1(\psi^*-1)}} \frac{2}{\sqrt{|\omega_2|+|\omega_1|}} [F(\varphi_1, p) - F(\varphi_2, p)]. \quad (5\text{-}4\text{-}4)$$

and

$$\sqrt{b_{crit}} = \frac{1}{\sqrt{\psi^*-1}} \frac{2}{\sqrt{|\omega_2|+|\omega_1|}} F(\beta, n), \quad (5\text{-}4\text{-}5)$$

where F is an incomplete elliptic integral of the first kind:

$$\varphi_1 = \arcsin \sqrt{\frac{|\omega_2|}{|\omega_2|+\frac{1}{b_1}}}; \quad \varphi_2 = \arcsin \sqrt{\frac{|\omega_2|-1}{|\omega_2|+\frac{1}{b_1}}};$$

$$p = \sqrt{\frac{|\omega_2|+\frac{1}{b_1}}{|\omega_2|+|\omega_1|}}; \quad \beta = \arcsin \sqrt{\frac{|\omega_2|+|\omega_1|}{|\omega_2|(1+|\omega_1|)}};$$

$$n = \sqrt{\frac{|\omega_2|}{|\omega_2|+|\omega_1|}}$$

$\rho_0/\rho = 0.$

and ω_1 and ω_2 are the roots of Eq. (5-4-1) with $\rho_0/\rho = 0$.

The results of the numerical integration of (5-4-2), carried out by I. K. Ermolaev over a wide range of variation in ψ and ψ^*, are given in the Appendix. For the injection of helium into air the relationship between density and velocity is taken from (5-5-11).

As shown by N. I. Yarygin, Eq. (5-4-2) is approximated to within ±15% by the following formula

$$\Psi_\infty = \Psi_1 \Psi_M \left(1 - \frac{b}{b_{crit}}\right)^2, \quad (5\text{-}4\text{-}6)$$

where

$$\Psi_1 = \left(\frac{2}{\sqrt{\frac{T_w}{T_w^*}+1}}\right)^2; \quad \Psi_M = \left(\frac{\operatorname{arctg} M \sqrt{r\frac{k-1}{2}}}{M\sqrt{r\frac{k-1}{2}}}\right)^2.$$

The critical injection parameter is defined by the expression /78

$$b_{crit\infty} = b_{crit\psi} \Psi_M, \quad (5\text{-}4\text{-}7)$$

where $b_{crit\,\psi}$ is determined from formulas (5-3-5) and (5-3-6), with

$$\bar{\psi} = \psi/\psi^*.$$

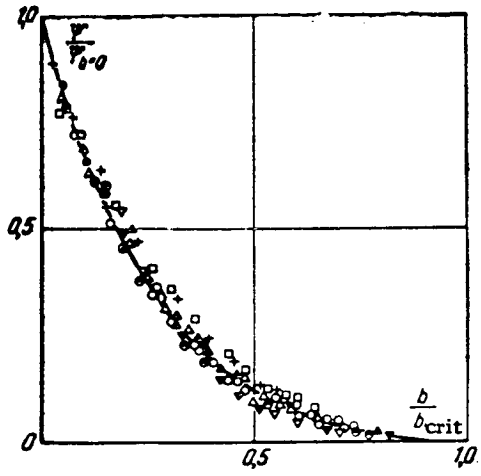

FIG. 5.8. Influence of compressibility and non-isothermicity on the relative law of friction. Curve—computed from (5-4-6); Points—computed from (5-4-4) and (5-4-5) in the M-number range from 0-12 and with $\Delta\psi$ from 0-30.

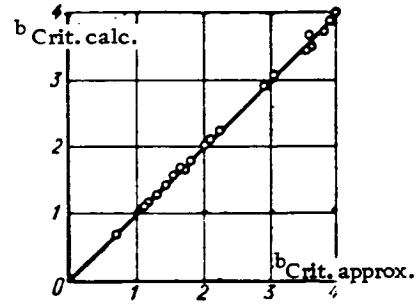

FIG. 5.9. Comparison of calculations of the critical injection parameter from (5-4-5) (ordinate) and (5-4-7) (abscissa) in the M-number range 0-12 and with $\Delta\psi$ from 0 to 30.

Figures 5.8 and 5.9 compare the results as computed from Eqs. (5-4-4) and (5-4-5) and from the approximation formulas (5-4-6) and (5-4-7).

Substituting (5-4-1) into Eq. (5-1-6), we obtain the limiting velocity profile for a supersonic gas flow over a permeable plate:

$$\int_{\omega}^{1} \frac{d\omega}{\sqrt{(1+b_1\omega)\,[\psi-\Delta\psi\omega-(\psi^*-1)\,\omega^2]}} = \Psi_\infty(1-\omega_0), \tag{5-4-8}$$

and for the section with critical injection /79

$$\int_{\omega}^{1} \frac{d\omega}{\sqrt{\omega\,[\psi-\Delta\psi\omega-(\psi^*-1)\,\omega^2]}} = \sqrt{b_{crit\infty}}(1-\omega_i). \tag{5-4-9}$$

For an adiabatic plate ($\Delta\psi = 0$) we have

$$\frac{\sqrt{\psi^*}+\sqrt{\psi^*-(\psi^*-1)\,\omega^2}}{\omega} = [1+\sqrt{\psi^*}\,]\,e^{\sqrt{\psi^*}\,\sqrt{b_{crit\infty}}(1-\omega_0)}. \tag{5-4-10}$$

5.5. Injection of a Foreign Gas

With the injection of a foreign gas through a permeable plate, under the conditions being considered (Le = Pr = 1; dP/dx = 0, i_w = const, $\bar{\rho}_w$ = const), similarity must exist between the distributions of total enthalpy, velocity and weight concentration of injected gas over the cross section of the boundary layer, i.e.

$$\frac{i^* - i_w}{i^*_w - i_w} = \frac{\bar{\rho}' - \bar{\rho}'_w}{\bar{\rho}'_e - \bar{\rho}'_w} = \omega, \tag{5-5-1}$$

where $\bar{\rho}'$ is the weight concentration of injected gas.

If the concentration of injected gas in the main flow is zero, then

$$\frac{i^* - i_w}{i^*_w - i_w} = 1 - \frac{\bar{\rho}'}{\bar{\rho}'_w} = \omega. \tag{5-5-2}$$

The gas constant for a binary mixture of gases is

$$\frac{R}{R_e} = \bar{\rho}'(\bar{R} - 1) + 1, \tag{5-5-3}$$

where $\bar{R} = R_1/R_0$; R_1 is the gas constant of the injected gas; R_0 the gas constant of the main gas. For a binary mixture of ideal gases (since $dP/dy = 0$) we have:

$$\frac{\rho_e}{\rho} = \frac{R}{R_e}\frac{T}{T_e}. \tag{5-5-4}$$

Hence, taking into account (5-5-2) and (5-5-3), we find

$$\frac{\rho_e}{\rho} = [1 + \bar{\rho}'_w(\bar{R} - 1)(1 - \omega)]\frac{T}{T_e}. \tag{5-5-5}$$

The mass balance of injected gas at the wall is written as

$$j_w = -D\rho_w\left(\frac{\partial \bar{\rho}'}{\partial y}\right)_w + \rho'_w w_{yw}. \tag{5-5-6}$$

In view of (5-5-2), (5-5-5) and (5-5-6), with Pr = Le = 1, we have

$$\bar{\rho}'_w = \frac{b_1}{1 + b_1}. \tag{5-5-7}$$

Hence

$$\frac{\rho_e}{\rho} = \frac{T}{T_e}\left[1 + \frac{b_1}{1 + b_1}(\bar{R} - 1)(1 - \omega)\right]. \tag{5-5-8}$$

Since in the absence of chemical reactions

$$\frac{T}{T_e} = \frac{C_{p0}i}{C_p i_e} = \frac{C_{p0}}{C_p}\left[\frac{i_w}{i_e} - \left(\frac{i_w}{i_e} - \psi^*\right)\omega - (\psi^* - 1)\omega^2\right] \tag{5-5-9}$$

and

$$\frac{C_p}{C_{p0}} = 1 - \frac{b_1}{1 + b_1}\left(\frac{C_{p1}}{C_{p0}} - 1\right)(1 - \omega), \tag{5-5-10}$$

then, for the conditions stipulated, we have

$$\frac{\rho}{\rho_0}=\left\{\frac{1+\frac{b_1}{1+b_1}(\bar{C}-1)(1-\omega)}{1+\frac{b_1}{1+b_1}(\bar{R}-1)(1-\omega)}\right\}$$
$$\left\{\frac{T_w}{T_0}\left[1+\frac{b_1}{1+b_1}(\bar{C}-1)\right]+\left[\psi^*-\frac{T_w}{T_0}\left(1+\frac{b_1}{1+b_1}(\bar{C}-1)\right)\right]\omega-(\psi^*-1)\omega^2\right\}^{-1}, \quad (5\text{-}5\text{-}11)$$

where $\bar{c} = c_{p_1}/c_{p_0}$.

For gas mixtures of like valency, $\bar{R} = \bar{c}$, we have /81

$$\frac{\rho_0}{\rho}=\frac{i_w}{i_0}-\left(\frac{i_w}{i_0}-\psi^*\right)\omega-(\psi^*-1)\omega^2 \quad (5\text{-}5\text{-}12)$$

or

$$\frac{\rho_0}{\rho}=\psi_1-(\psi_1-\psi^*)-(\psi^*-1)\omega^2, \quad (5\text{-}5\text{-}13)$$

where $\psi_1^* = \rho_0/\rho_w$.

Values of ψ_1 for some processes are compiled in Table 5.2.

TABLE 5.2. Value of ψ_1

Boundary Layer Characteristics	ψ_1
Homogeneous non-isothermal	$\psi = T_w/T_0$
Non-homogeneous isothermal	$1+\frac{b_1}{1+b_1}(\bar{R}-1)$
Non-homogeneous, mixture of gases of like valency, non-isothermal	$\frac{i_w}{i_0}=\psi\left[1+\frac{b_1}{1+b_1}(\bar{R}-1)\right]$

Thus all limiting formulas derived for the injection of a homogeneous gas under non-isothermal conditions can also be extended to the injection of a foreign gas if we substitute $\psi_1 = \rho_0/\rho_w$ for ψ in the formulas.

Specifically, for the injection of a foreign gas under isothermal conditions, we obtain from (5-3-5) and (5-3-6) a relationship between the critical injection parameter and the ratio of the molecular weights of the injected gas and the main gas flow. With critical injection $\psi_1 = \bar{R}$. Therefore for $\bar{R} < 1$

$$b_{crit\,\infty}=\frac{1}{1-\bar{R}}\left(\ln\frac{1+\sqrt{1-\bar{R}}}{1-\sqrt{1-\bar{R}}}\right)^2, \quad (5\text{-}5\text{-}14)$$

and for R > 1

$$b_{crit\infty} = \frac{1}{\bar{R}-1}\left(\arccos\frac{2-\bar{R}}{\bar{R}}\right)^2. \qquad (5\text{-}5\text{-}15)$$

The approximation formula is of the form

$$b_{crit\infty} = \frac{4}{\frac{1}{3}+\frac{2}{3}\bar{R}}. \qquad (5\text{-}5\text{-}16)$$

From Eqs. (5-5-14) and (5-5-15) we see that the critical injection parameter increases with the molecular weight of the injected gas. /82

As Spalding [164] has shown, Eqs. (5-4-2) and (5-4-3) may be approximated when $\bar{R} = c$ by the formulas:

$$\Psi_\infty \approx \left[\frac{1}{4}\left\{(\psi)^{1/2}\left(\frac{1+\bar{R}b_1}{1+b_1}\right)+(1+b_1\psi^*)^{1/2}\right\}^2 + \frac{1}{6}(\psi^*-1)+\frac{b_1}{6}\left\{\psi\left(\frac{1+\bar{R}b_1}{1+b_1}\right)-\psi^*\right\}\right]^{-1}; \qquad (5\text{-}5\text{-}17)$$

$$b_{crit\infty} = \frac{4}{\frac{1}{3}\psi^*+\frac{2}{3}\bar{R}\psi}. \qquad (5\text{-}5\text{-}18)$$

5.6. Limiting Law of Friction for the Non-isothermal Boundary Layer of a Dissociated Gas on a Flat Permeable Plate

For the "frozen-in" boundary layer of a dissociated ideal gas, taking (4-4-10) and (4-4-11) into account, we have

$$\frac{\rho}{\rho_e} = \frac{1+\alpha_e}{1+\alpha}\left\{\frac{7+3\alpha_w}{7+3\alpha}\psi+\left[\frac{7+3\alpha_e}{7+3\alpha}-\frac{7+3\alpha_w}{7+3\alpha}\psi\right]\omega + \omega(1-\omega)\frac{1{,}4M_0^2}{7+3\alpha}\right\}^{-1}. \qquad (5\text{-}6\text{-}1)$$

Substituting (5-6-1) into (5-1-3), and using (4-4-6), we obtain the limiting law of friction for the conditions being considered:

$$\Psi_\infty = \int_0^1 \frac{\sqrt{\left\{\frac{4+3(1+\alpha_e)[\psi_a+(1-\psi_a)\omega]}{\psi_a+(1-\psi_a)\omega}\right\}}\,d\omega}{\{(7+3\alpha_w)\psi+[7+3\alpha_e-(7+3\alpha_w)\psi]\omega+\omega(1-\omega)1{,}4M_0^2\}^{1/2}(1+b_1\omega)^{1/2}}. \qquad (5\text{-}6\text{-}2)$$

The critical injection parameter is found similarly from Eq. (5-1-5): /83

$$b_{crit\infty} = \left[\int_0^1 \sqrt{\frac{4 + 3(1 + \varkappa_0)\left[\psi_\alpha + (1 - \psi_\alpha)\,\omega\right]}{\psi_\alpha + (1 - \psi_\alpha)\,\omega}}\,\frac{d\omega}{\omega^{1/2}}\right]^{-2} \tag{5-6-3}$$

For the hypothetical case of the isothermal dissociation of a subsonic turbulent boundary layer ($\psi = 1$), we have

$$\frac{\rho}{\rho_0} = [\psi_\alpha + (1 - \psi_\alpha)\,\omega]^{-1}. \tag{5-6-4}$$

Consequently, for $\psi_\alpha < 1$:

$$\Psi_\infty = \frac{4}{b_1(1 - \psi_\alpha)}\left[\ln\frac{(1 - \psi_\alpha)^{1/2}(1 + b_1)^{1/2} + b_1^{1/2}}{(1 - \psi_\alpha)^{1/2} + (b_1\psi_\alpha)^{1/2}}\right]^2; \tag{5-6-5}$$

$$b_{crit\infty} = \frac{1}{1 - \psi_\alpha}\left[\ln\frac{1 + (1 - \psi_\alpha)^{1/2}}{1 - (1 - \psi_\alpha)^{1/2}}\right]^2, \tag{5-6-6}$$

and for $\psi_\alpha > 1$:

$$\Psi_\infty = \frac{4}{b_1(\psi_\alpha - 1)}\left\{\operatorname{arctg}\left[\frac{b_1}{(\psi_\alpha - 1)(1 + b_1)}\right]^{1/2} - \operatorname{arctg}\left[\frac{b_1\psi_\alpha}{\psi_\alpha - 1}\right]^{1/2}\right\}^2; \tag{5-6-7}$$

$$b_{crit\infty} = \frac{1}{\psi_\alpha - 1}\left(\arccos\frac{2 - \psi_\alpha}{\psi_\alpha}\right)^2. \tag{5-6-8}$$

In the Spalding approximation

$$\Psi_\infty = \left\{\frac{1}{4}\left[\psi_\alpha^{1/2} + (1 + b_1)^{1/2}\right]^2 + \frac{1}{6}b_1(\psi_\alpha - 1)\right\}^{-1}; \tag{5-6-9}$$

$$b_{crit\infty} = \frac{4}{1/3 + 2/3\psi_\alpha}. \tag{5-6-10}$$

It follows from Eq. (5-6-10) that gas dissociation may exert a marked effect on the limiting critical injection parameter. In particular, with $\psi_\alpha = 0.5$, $b_{crit\,\infty} = 6$, and with $\psi_\alpha = 2.0$, $b_{crit\,\infty} = 2.4$.

Formula (5-6-10) is conveniently expressed in the form /84

$$\frac{b_{crit\infty}}{b_{\substack{crit\infty \\ \alpha=0}}} = \frac{3}{1 + 2\psi_\alpha}, \tag{5-6-11}$$

where $b_{\substack{crit\,\infty \\ \alpha = 0}}$ is the critical injection parameter in the absence of dissociation.

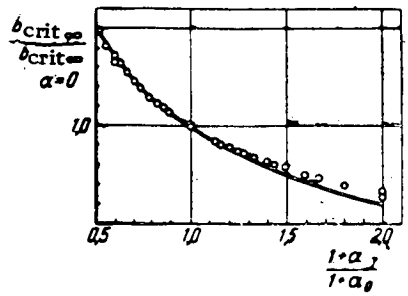

FIG. 5.10. Effect of gas dissociation on the critical injection parameter. Curve—calculated from (5-6-11); Points—calculated from (5-6-3) in the M-number range of 0-10; ψ from 0.1-1.0, α_0 from 0 to 1, α_w from 0-1.

Calculations show that formula (5-6-11) is more universal and may be extended to the flow of a compressible gas under non-isothermal conditions if the effect of these parameters on $b_{crit\infty}$ is accounted for in accordance with (5-4-7).

Figure 5.10 presents a comparison of calculations made with (5-6-11) and (5-6-3) in the M-number range 0-10, ψ from 0.1-10. The limiting law of friction may be approximated by the following simple formula over rather broad ranges of M, ψ, ψ_α, α_0 and α_w:

$$\Psi_\infty = \Psi_t \Psi_M \Psi_\alpha \left(1 - b_{crit\infty} \frac{b}{}\right)^2, \qquad (5\text{-}6\text{-}12)$$

where

$$\Psi_t = \left(\frac{2}{\sqrt{\frac{T_w}{T^*_w}} + 1}\right)^2; \quad \Psi_\alpha = \left(\frac{2}{\sqrt{\Psi_\alpha} + 1}\right)^2;$$

$$\Psi_M = \left(\frac{\operatorname{arctg} M \sqrt{r\frac{k-1}{2}}}{M \sqrt{r\frac{k-1}{2}}}\right)^2$$

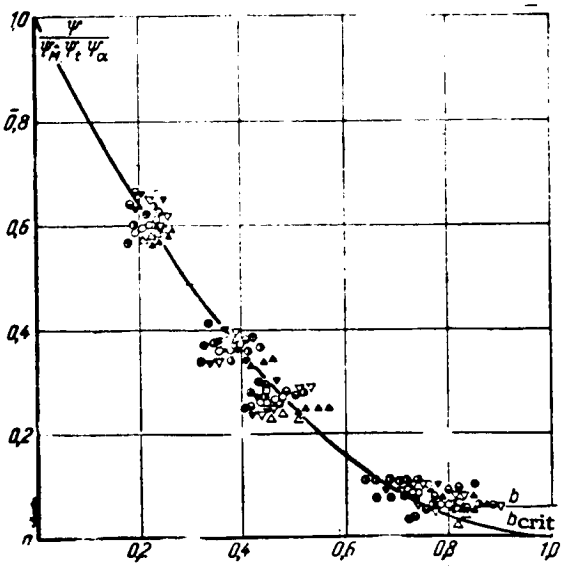

FIG. 5.11. Effect of non-isothermicity, compressibility and dissociation on the relative law of friction on a permeable plate: Curve—calculated from (5-6-12); Points—calculated from (5-6-2).

Figure 5.11 shows a comparison of the calculations using (5-6-2) and (5-6-12). As can be seen from the diagrams, the results with the exact and approximate formulas are in good agreement in the subsonic region. Formula (5-6-2) generalizes the computed results in the supersonic region somewhat less satisfactorily.

Taking (5-1-6), (5-1-7) and (5-6-1) into account we can derive the limiting velocity distributions over the cross section of a dissociated turbulent boundary layer of gas on a permeable plate. /85

M	0	2	6	10
$\phi=0,1$	○	◑	◒	◓
$\phi=0,2$	△	▲	▽	▼

5.7. Limiting Laws of Heat- and Mass Transfer for the Turbulent Boundary Layer on a Permeable Plate

The limiting relative laws of heat- and mass-transfer, in the general case as shown in Chapter 4, are in the form

$$\Psi_{S\infty} = \left[\int_0^1 \left(\frac{\tilde{\rho}\tilde{q}}{\tilde{q}_e}\frac{\partial\omega}{\partial\xi_T}\frac{\partial\vartheta}{\partial\xi_T}\right)^{1/2} d\xi_T\right]^2; \tag{5-7-1}$$

$$\Psi_{D\infty} = \left[\int_0^1 \left(\frac{\tilde{\rho}\tilde{j}_1}{j_{1e}}\frac{\partial\omega}{\partial\xi_D}\frac{\partial\tilde{c}}{\partial\xi_D}\right)^{1/2} d\xi_D\right]^2, \tag{5-7-2}$$

/86

where

$$\left(\frac{\tilde{q}}{\tilde{q}_e}\right)_{Re\to\infty} = 1 + St^{-1}\int_0^{\xi_T} q_\nu d\xi_T + b_{1T}\vartheta; \tag{5-7-3}$$

$$\left(\frac{\tilde{j}_1}{j_{1e}}\right)_{Re\to\infty} = 1 + b_{1D}\tilde{c} + St_D^{-1}\int_0^{\xi_D} c_1 d\xi_D. \tag{5-7-4}$$

If there are no chemical reactions or sources of heat or matter in the boundary layer, formula (5-5-11) remains valid for the gas density. Then the limiting laws of heat- and mass transfer, and the limiting distributions of total enthalpy and concentration will be given by Eqs. (5-4-2), (5-4-3), (5-4-8) and (5-4-9) except that ϑ and $\tilde{c}$ will appear in place of ω.

In more complicated cases, with chemical reactions inside the boundary layer, it is convenient to introduce the weight concentration $\tilde{c}_i$ of the individual chemical elements.

Then, with similarity of boundary conditions, and with $Pr = Pr_T = Le = Le_T = 1$, the similarity of the distributions of velocity, total enthalpy and generalized concentration is maintained.

$$\frac{i_\Sigma^\circ - i_{\Sigma w}^\circ}{i_{\Sigma 0}^\circ - i_{\Sigma w}^\circ} = \omega = \tilde{c}_i = \frac{\tilde{c}_i - \tilde{c}_{iw}}{\tilde{c}_{ie} - \tilde{c}_{iw}}. \tag{5-7-5}$$

However, in this case difficulty arises in deriving the gas density formula. Strictly speaking, to estimate the concentrations of all gas components at a given point we must resort to the equations of chemical kinetics, which markedly complicates the calculations. In some cases, estimates for two limiting cases are useful: equilibrium and "frozen-in" boundary layers. The case of the "frozen in" boundary layer of a dissociated gas has already been considered in Section 5.6, and the formulas derived in this section can be extended to the boundary layer with chemical reactions at a catalytic wall. In practice, the conditions when the chemical reaction rate in the boundary layer is infinitely large compared with the rate of diffusion of the components is also

/87

pertinent. The reaction zone can then be considered to be some surface (the flame front) at which chemical reactions also occur.

We shall assume that the injected gas reacts with the oxygen that diffuses to the heat transfer surface, in which case a stoichiometric relationship is established at some section (flame front) that determines the weight concentration of injected gas:

$$\bar{c}_c = \frac{1}{1+K}, \tag{5-7-6}$$

where K is the amount of oxidizer per unit mass of fuel.

The boundary layer will be divided into two sections by the flame front—the following conditions are satisfied for these regions:

$$\bar{c} < \bar{c}_c \begin{cases} c_T = 0, \\ c_o = 1 - (1+K)\,\bar{c}, \\ c_{pr} = (1+K)\,\bar{c}; \end{cases} \tag{5-7-7}$$

$$\bar{c} > \bar{c}_c \begin{cases} c_T = \left(1 + \frac{1}{K}\right)\bar{c} - \frac{1}{K}, \\ \bar{c}_o = 0, \\ c_{pr} = \left(1 + \frac{1}{K}\right)(1-\bar{c}), \end{cases} \tag{5-7-8}$$

where $\bar{c}_c$ is the stoichiometric concentration of injected gas; c_{pr} is the weight concentration of combustion products; $\bar{c}_T$ is the weight concentration of injected gas; c_o the weight concentration of the main gas.

The corresponding formulas for the molecular weights of the mixture have the following form:

For $\bar{c} < \bar{c}_{pr.c}$

$$\frac{1}{M} = \frac{1-(1+K)\,\bar{c}}{M_o} + \frac{(1+K)\,\bar{c}}{M_{pr}}; \tag{5-7-9}$$

For $\bar{c} > \bar{c}_{pr.c}$

$$\frac{1}{M} = \frac{\left(1+\frac{1}{K}\right)\bar{c} - \frac{1}{K}}{M_T} + \frac{\left(1+\frac{1}{K}\right)(1-\bar{c})}{M_{pr}}. \tag{5-7-10}$$

In determining the enthalpy of the gas mixture it is convenient to assume that the enthalpy of the main gas and reaction products is zero at absolute zero; the enthalpy of the injected gas is assumed to be positive and equal to i_{To}. Then /88

$$i = (\bar{c}_o C_{po} + \bar{c}_{pr} C_{ppr} + \bar{c}_T C_{pT})\,T + \bar{c}_T\, i_{To}. \tag{5-7-11}$$

Thus, for $c < c_{pr.c}$

$$i = \{[1-(1+K)\bar{c}]C_{P0} + (1+K)\bar{c}C_{Ppr}\}T, \tag{5-7-12}$$

and for $\bar{c} > \bar{c}_{pr.c}$

$$i = \left\{\left[\left(1+\frac{1}{K}\right)(1-\bar{c})\right]C_{Ppr} + \left[\left(1+\frac{1}{K}\right)\bar{c} - \frac{1}{K}\right]C_{PT}\right\}T + \left[\left(1+\frac{1}{K}\right)\bar{c} - \frac{1}{K}\right]i_{T0}. \tag{5-7-13}$$

Substituting (5-7-9), (5-7-10), (5-7-12) and (5-7-13) into Eq. (5-5-4) we have:

for $\bar{c} < \bar{c}_{pr.c}$

$$\frac{\rho_0}{\rho} = \left\{1-(1+K)\bar{c} + \frac{M_e}{M_{pr}}(1+K)\bar{c}\right\} \times \left\{[1-(1+K)\bar{c}] + \frac{C_{Ppr}}{C_{P0}}(1+K)\bar{c}\right\}^{-1}\frac{i}{i_e}; \tag{5-7-14}$$

and for $\bar{c} > \bar{c}_{pr.c}$

$$\frac{\rho_0}{\rho} = \left\{\frac{M_e}{M_T}\left[\left(1+\frac{1}{K}\right)\bar{c} - \frac{1}{K}\right] + \frac{\left(1+\frac{1}{K}\right)(1-\bar{c})\frac{M_e}{M_{pr}}}{}\right\} \times \left\{\left[\left(1+\frac{1}{K}\right)(1-\bar{c})\right]\frac{C_{Ppr}}{C_{P0}} + \left[\left(1+\frac{1}{K}\right)\bar{c} - \frac{1}{K}\right]\frac{C_{PT}}{C_{P0}}\right\}^{-1} \times \left\{\frac{i - \left[\left(1+\frac{1}{K}\right)\bar{c} - \frac{1}{K}\right]i_{T0}}{i_e}\right\}. \tag{5-7-15}$$

Making use of Eqs. (5-7-5) and (5-7-7), we get the ω-dependence of ρ. On substituting this relationship into Eqs. (5-1-3), (5-7-1) and (5-7-2), we find the limiting laws of friction, heat- and mass transfer for the turbulent boundary layer with chemical reactions. Spalding [226] has evaluated these integrals numerically for the case of injection of hydrogen and air.

CHAPTER 6
INFLUENCE OF A LONGITUDINAL PRESSURE GRADIENT ON THE LIMITING LAWS OF FRICTION, HEAT- AND MASS TRANSFER

/89

6.1. Limiting Separation Parameters of an Isothermal Boundary Layer on an Impermeable Surface

In the case of flow over a curved surface, the flow velocity at the outer edge of the boundary layer varies along the contour, and consequently $dP/dx \neq 0$.

A convergent flow, when $dP/dx < 0$ differs from a diffusor flow, when $dP/dx > 0$.

In Section 1.7 the conditions for separation of a turbulent boundary layer from a surface with diffusor flow were considered and the effect of a longitudinal pressure gradient on the stability of the viscous sublayer was analyzed. Let us derive the limiting formulas for the separation parameters. We can write the following conditions for the separation section of a two-dimensional, isothermal, turbulent boundary layer of incompressible fluid at an impermeable wall:

$$c_f = 0, \quad \rho = \rho_0, \quad \beta = 0. \tag{6-1-1}$$

Substituting these values into the Prandtl formula (1-5-4) and integrating over the cross section, we obtain

$$\omega = \omega_{1\,\mathrm{crit}} + \int_{\xi_{1\,\mathrm{crit}}}^{\xi} \left(\frac{\delta}{l}\right)_{\mathrm{crit}} \sqrt{\frac{\tau_{\mathrm{crit}}(\xi)}{\rho w_0^2}}\, d\xi. \tag{6-1-2}$$

The distribution of shearing stress over the boundary layer is defined by Eq. (1-6-14), which can be written as

$$\tilde{\tau} = \varphi_0(\xi) + \Lambda\xi\varphi_1(\xi), \tag{6-1-3}$$

where

$$\varphi_0(\xi) = 1 - 3\xi^2 + 2\xi^3 \quad \varphi_1(\xi) = (1-\xi)^2.$$

Taking (6-1-1) into account, we find

$$\frac{\tau_{\mathrm{crit}}}{\rho w_0^2} = \frac{\delta}{\rho w_0^2}\frac{dP}{dx}\xi\varphi_1(\xi) = \left(-f\frac{\delta}{\delta^{**}}\right)\xi\varphi_1(\xi). \tag{6-1-4}$$

where $f = \frac{\delta^{**}}{w_0}\frac{dw_0}{dx}$ is the shape parameter, which is independent of c_f.

We substitute τ_{crit} into (6-1-2) and find /90

$$\omega = \omega_{1\,\mathrm{crit}} + \left(-f\frac{\delta}{\delta^{**}}\right)^{1/2}_{\mathrm{crit}} \int_{\xi_{1\,\mathrm{crit}}}^{\xi} \left(\frac{\delta}{l}\right)_{\mathrm{crit}} \sqrt{\xi\varphi_1(\xi)}\, d\xi. \tag{6-1-5}$$

Assuming $\omega = 1$ and $\xi = 1$, we find the critical value of the shape parameter from (6-1-5):

$$\left(-f\frac{\delta}{\delta^{**}}\right)_{crit} = \left[\frac{\dot{1} - \omega_{crit}}{\int\limits_{\xi_{1\,crit}}^{1}\left(\frac{\delta}{l}\right)_{crit}\sqrt{\xi\varphi_1(\xi)}\,d\xi}\right]^2 \qquad (6\text{-}1\text{-}6)$$

With $Re \to \infty$, $\xi_1 \to 0$, $\omega_1 \to 0$

$$\left(-f\frac{\delta}{\delta^{**}}\right)_{crit} = \left[\int\limits_0^1\left(\frac{\delta}{l}\right)_{crit}\sqrt{\xi\varphi_1(\xi)}\,d\xi\right]^{-2}; \qquad (6\text{-}1\text{-}7)$$

$$\omega = \frac{\int\limits_0^{\xi}\left(\frac{\delta}{l}\right)_{crit}\sqrt{\xi\varphi_1(\xi)}\,d\xi}{\int\limits_0^1\left(\frac{\delta}{l}\right)_{crit}\sqrt{\xi\varphi_1(\xi)}\,d\xi}. \qquad (6\text{-}1\text{-}8)$$

Assuming that the distribution of mixing path length over the boundary layer cross section does not depend on the longitudinal pressure gradient and is defined by (1-10-1), we have from Eq. (6-1-8)

$$\omega = \frac{\ln\left(2\sqrt{4\xi^2 + 2\xi} + 4\xi + 1\right)}{\ln\left(2\sqrt{6} + 5\right)}. \qquad (6\text{-}1\text{-}9)$$

This same equation is obtained from (3-6-1), taking (6-1-4) into account. Accordingly

$$\left(-f\frac{\delta}{\delta^{**}}\right)_{crit} = 2\left[\frac{1}{\chi_0}\ln\left(2\sqrt{6} + 5\right)\right]^{-2} \qquad (6\text{-}1\text{-}10)$$

With the assumptions adopted, it follows from (6-1-9) and (6-1-10) that the limiting velocity profile in the separation section of the boundary layer does not depend on empirical turbulence constants. But the limiting critical value of the shape parameter f depends on the constant x_0. With $x_0 = 0.4$, we have, for the conditions being considered ($T_w = const$, $j_1 = 0$, $Re \to \infty$): /91

$$\left.\begin{aligned}\left(-f\frac{\delta}{\delta^{**}}\right) &= 0{,}062;\ \left(\frac{\delta^*}{\delta}\right)_{crit} = 0{,}3;\\ \left(\frac{\delta^{**}}{\delta}\right)_{crit} &= 0{,}16;\ H_{crit} = 1{,}87;\ f_{crit} = -0{,}01.\end{aligned}\right\} \qquad (6\text{-}1\text{-}11)$$

The velocity profile (6-1-9) is quite well approximated by the power-law relationship

$$\omega = \xi^{0.43}. \qquad (6\text{-}1\text{-}12)$$

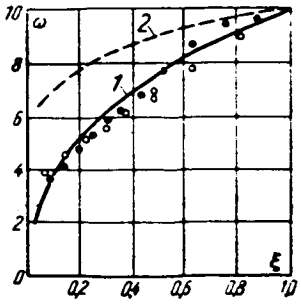

FIG. 6.1. Comparison of the limiting velocity profile at the separation point with experimental data: 1—calculated from (5-1-9); 2—calculated from the formula $\omega = \xi^{1/7}$; O—Nikuradze's tests [188]; ●—tests of A. I. Leont'ev, A. N. Oblivin and P. N. Romanenko [66].

From (6-1-11) it follows that the shape parameter f also maintains a finite critical value with Re-numbers approaching infinity, while the critical value of the Bury-Loitsyanskiy shape parameter ($\Gamma = 2f/c_{fo}$) tends to infinity as $Re \to \infty$.

Figure 6.1 gives a comparison of the limiting separated velocity profile [Eq. (6-1-9)] with the tests of N. Nikuradze [188] and A. I. Leont'ev, A. N. Oblivin, P. N. Romanenko [66]. As can be seen from the diagram, the limiting velocity distribution and the test data are in satisfactory agreement for finite Re-numbers. A comparison of the critical limiting values of the shape parameter H with the test data is of interest. According to I. Nikuradze's tests, $H_{crit} = 1.8$; according to E. Gruschwitz. $H_{crit} = 1.9$; in the paper by D. Khurai, $H_{crit} = 1.9$. These data all correlate quite satisfactorily with the theoretical limiting values. However, tests exist [202, 66] in which the measured values of the shape parameter H_{crit} reach 2-2.6.

This deviation from the theoretical value may possibly relate to surface roughness or other factors not allowed for in the assumptions adopted for the functions l(y) and $\tau(y)$. /92

In analogy with Section 1.7, we estimate the parameters of the viscous sublayer in the separation section of the turbulent boundary layer.

The velocity distribution in the viscous sublayer in the separation section of the boundary layer is defined by formula (1-7-3):

$$\omega = -\frac{1}{2} f_{crit} \left(\frac{\delta}{\delta^{**}}\right)^3 Re^{**} \xi^2. \qquad (6\text{-}1\text{-}13)$$

We shall assume that (6-1-9) also describes the velocity profile in the turbulent portion of the boundary layer with finite Re-numbers. Figure 6.1 serves to provide some basis for this assumption. It is clear that the assumption is more nearly correct as Re becomes larger.

In case the velocity profiles computed from (6-1-9) and (6-1-13) intersect, $\xi_{1\,crit}$ and $\omega_{1\,crit}$ are, to a first approximation

$$\xi_{1crit} \approx \frac{2,84}{Re^{**0,44}}; \qquad \omega_{1crit} \approx \frac{1,57}{Re^{**0,11}}. \qquad (6\text{-}1\text{-}14)$$

From this

$$Re_{1crit} = \omega_{1crit} \xi_{1\,crit} \left(\frac{\delta}{\delta^{**}}\right)_{crit} Re^{**} \approx 28. \qquad (6\text{-}1\text{-}15)$$

As was demonstrated in Section 1.3, the number $\mathrm{Re}_1 = \left(\frac{y^2 \partial w_x}{\nu \partial y}\right)_{y=y_1}$ may be taken as a measure of the thickness of the viscous region near the wall. With dP/dx = 0, the magnitude of $\dot{\mathrm{R}}\mathrm{e}_1$ is $\dot{\mathrm{R}}\mathrm{e}_1 = \eta_{10}^2 = 134$.

For the separation section of the turbulent boundary layer we have

$$\dot{\mathrm{R}}\mathrm{e}_{1\,\mathrm{crit}} = -f_{\mathrm{crit}} \left(\frac{\delta}{\delta^{**}}\right)^3_{\mathrm{crit}} \mathrm{Re}^{**2}_{\mathrm{crit}} \xi^3_{\mathrm{crit}} \qquad (6\text{-}1\text{-}16)$$

Taking (6-1-11) and (6-1-14) into account we find that $\dot{\mathrm{R}}\mathrm{e}_1 \approx 57$, i.e. the $\dot{\mathrm{R}}\mathrm{e}_1$-number is more conservative than Re with respect to the action of a longitudinal pressure gradient.

In the region of gradient flows we note that the condition $\dot{\mathrm{R}}\mathrm{e}_1 = \mathrm{const} = \eta_{10}^2$ is equivalent to the Szablewski condition [209] introduced earlier— $\left(\frac{y}{\nu}\sqrt{\frac{\tau}{\rho}}\right)_{y=y_1} = \mathrm{const} = \eta_{10}$. /93 We thus obtain the limiting values of all parameters of the turbulent boundary layer of incompressible fluid in the separation section.

6.2. Law of Friction of an Isothermal Boundary Layer on an Impermeable Surface with $dw_0/dx \neq 0$

The velocity profile in the turbulent core of an isothermal boundary layer on an impermeable curved surface, with (1-5-4) and (1-6-14) taken into account, has the form

$$w = w_1 + \int_{\xi_1}^{\xi} \left(\frac{\delta}{l}\right) \sqrt{\Psi \frac{c_{f0}}{2} \varphi_0(\xi) + \frac{c_{f0}}{2} \Lambda_0 \xi \varphi_1(\xi)}\, d\xi, \qquad (6\text{-}2\text{-}1)$$

where $\varphi_0(\xi)$ and $\varphi_1(\xi)$ are functions in the approximation of the distribution of shearing stress over the boundary layer cross section.

Specifically, for a third-order polynomial, we have:

$$\varphi_0(\xi) = \tilde{\tau}_0 = 1 - 3\xi^2 + 2\xi^3; \quad \varphi_1(\xi) = (1-\xi)^2;$$
$$\Lambda_0 = -\frac{2}{c_{f0}} \frac{\delta^{**}}{w_0} \frac{dw_0}{dx} = \frac{2}{c_{f0}} \frac{\delta^{**}}{\delta^{**}} f. \qquad (6\text{-}2\text{-}2)$$

For the velocity distribution in the viscous sublayer we have the equation

$$w = \mathrm{Re}^{**} \left(\frac{\delta}{\delta^{**}}\right) \left(\frac{c_f}{2}\xi - \frac{\delta}{\delta^{**}} f \frac{\xi^2}{2}\right). \qquad (6\text{-}2\text{-}3)$$

With the thickness of the viscous sublayer being defined by the stability criterion in the form

$$\dot{\mathrm{R}}\mathrm{e}_1 = \left(\frac{y^2}{\nu} \frac{dw_x}{dy}\right)_{y=y_1}, \qquad (6\text{-}2\text{-}4)$$

we have from (6-2-3)

$$\Psi \frac{c_{f0}}{2} \xi_1^2 + \frac{c_{f0}}{2} \Lambda_0 \xi_1^3 = \frac{\dot{\mathrm{Re}}_1}{\left(\mathrm{Re}^{**} \frac{\delta}{\delta^{**}}\right)^2}. \qquad (6\text{-}2\text{-}5)$$

At the boundary layer separation point $\psi = 0$, and condition (6-1-16) follows from (6-2-5).

Setting $\xi = 1$ and $\omega = 1$ in Eq. (6-2-1), and $\xi = \xi_1$ and $\omega = \omega_1$ in (6-2-3), we have the following system of equations: /94

$$1 - \omega_1 = \int_{\xi_1}^{1} \left(\frac{\delta}{l}\right) \sqrt{\Psi \frac{c_{f0}}{2} \varphi_0(\xi) + \frac{c_{f0}}{2} \Lambda_0 \xi \varphi_1(\xi)}\, d\xi; \qquad (6\text{-}2\text{-}6)$$

$$\omega_1 = \frac{\delta}{\delta^{**}} \mathrm{Re}^{**} \left(\Psi \frac{c_{f0}}{2} \xi_1 + \frac{1}{2} \frac{c_{f0}}{2} \Lambda_0 \xi_1^2\right); \qquad (6\text{-}2\text{-}7)$$

$$\left(\Psi \frac{c_{f0}}{2} \xi_1^2 + \frac{c_{f0}}{2} \Lambda_0 \xi_1^3\right) \left(\frac{\delta}{\delta^{**}} \mathrm{Re}^{**}\right)^2 = \dot{\mathrm{Re}}_1. \qquad (6\text{-}2\text{-}8)$$

To determine the law of friction ψ, we add to this system the relationships used earlier

$$\frac{l}{\delta} = \varkappa \xi \varphi_0(\xi); \qquad (6\text{-}2\text{-}9)$$

$$\frac{\delta^{**}}{\delta} = \int_0^1 \frac{\rho w}{\rho_0 w_0} (1 - \omega)\, d\xi; \qquad (6\text{-}2\text{-}10)$$

$$\frac{c_{f0}}{2} = (2{,}5 \ln \mathrm{Re}^{**} + 3{,}8)^{-2}. \qquad (6\text{-}2\text{-}11)$$

The stability criterion of the viscous sublayer $\dot{\mathrm{Re}}_1$ is defined by the formula

$$\sqrt{\dot{\mathrm{Re}}_1} = 11{,}6 - 4 \frac{\Lambda_0}{\Lambda_{0\,\mathrm{crit}}}. \qquad (6\text{-}2\text{-}12)$$

to a first approximation.

The parameters in the boundary layer separation section are defined from the system of Eqs. (6-2-6) - (6-2-12), with the conditions $\Psi = 0$ and $\Lambda_0 = \Lambda_{\mathrm{crit}}$.

The results of a numerical solution of the system (6-2-6) - (6-2-12) obtained by A. V. Fafurin on the "Minsk-22" computer, using an iteration method, are shown in Figs. 6.2, 6.3 and 6.4.

It should be noted that negative values of Λ_0 yield an unstable solution, and the iteration process diverges; therefore only the diffusor flow results are shown in the figures. /95

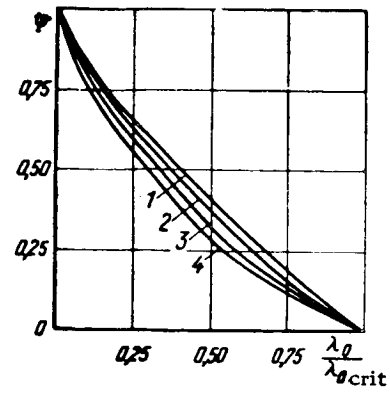

FIG. 6.2. Influence of the longitudinal pressure gradient on the relative law of friction. 1—$Re^{**} = 2 \times 10^3$; 2—$Re^{**} = 10^4$; 3—$Re^{**} = 10^5$; 4—$Re^{**} = 10^6$.

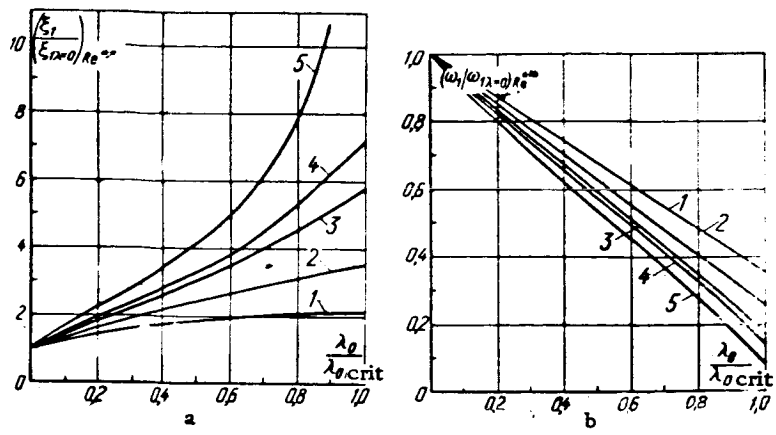

FIG. 6.3. Influence of longitudinal pressure gradient on the relative thickness of the viscous sublayer (a) and on the dimensionless velocity at the boundaries of the viscous sublayer (b). 1—$Re^{**} = 2 \times 10^3$; 2—$Re^{**} = 10^4$; 3—$Re^{**} = 5 \times 10^4$; 4—$Re^{**} = 10^5$; 5—$Re^{**} = 10^6$.

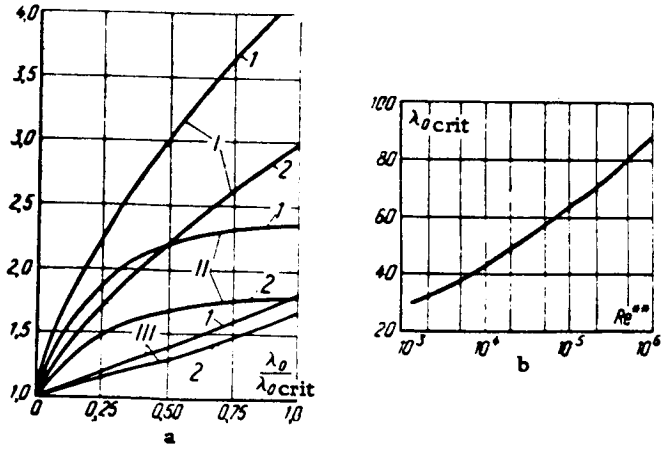

FIG. 6.4. Influence of various factors on the characteristics of the boundary layer. (a)—influence of longitudinal pressure gradient on the integral characteristics of the boundary layer: I—$\delta^*/\delta^*_{\lambda=0}$; II—$\delta^{**}/\delta^{**}_{\lambda=0}$; III—$H/H_{\lambda=0}$; 1—$Re^{**} = 10^4$; 2—$Re^{**} = 10^6$; (b)—influence of Re^{**}-number on the shape factor of the separation of the turbulent boundary layer ($\Delta_{o\,crit}$).

As can be seen from the figures, a positive longitudinal pressure gradient (or a negative longitudinal velocity gradient) significantly affects all characteristics of the turbulent boundary layer.

It is clear from Fig. 6.4a that Re^{**} exerts a weak influence on the dependence of the shape parameter H on $\Lambda_0/\Lambda_{0crit}$.

The calculated results can be approximated in the range of Re^{**} from 10^4-10^6 by the expression

$$H = H_0\left(1 + 0{,}75\frac{\Lambda_0}{\Lambda_{0crit}}\right), \qquad (6\text{-}2\text{-}13)$$

where H_0 is the shape parameter with $\Lambda_0 = 0$.

For the law of friction we find

$$\Psi = \left(1 - \frac{\Lambda_0}{\Lambda_{0crit}}\right)^{1,64}. \qquad (6\text{-}2\text{-}14)$$

6.3. Law of Heat Transfer in the Diffusor Region of a Quasi-isothermal Turbulent Boundary Layer at an Impermeable Wall

The presence of a longitudinal pressure gradient essentially disrupts the similarity between the frictional processes and heat transfer in the boundary layer. In this case the properties of the heat transfer are quite conservative with respect to the longitudinal pressure gradient, which has already been noted in comparing the distribution laws for shearing stress and density of heat flux over the boundary layer cross section. As seen from formulas (1-6-14) and (2-5-4), with the adopted assumptions the heat flux density in general does not depend on the longitudinal pressure gradient, while the distribution of shearing stress depends significantly on the magnitude of f.

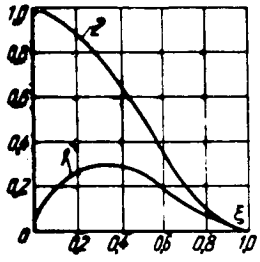

FIG. 6.5. Distributions of shearing stress $2\tau/\rho_0 w_0^2$ (1) and heat flux q/qw (2) at the boundary layer separation point.

The distribution of shearing stresses and heat flux over the boundary layer cross section is shown in Fig. 6.5 for the separation region. Let us estimate the intensity of heat transfer in the separation section of the boundary layer for the conditions $Pr = Pr_T \approx 1$ and $\delta_T < \delta$. In this case we can take $l_T \approx 1$, and we have from (2-1-12): /97

$$\tilde{q}St \approx \left(\frac{l}{\delta}\right)^2 \frac{\partial \omega}{\partial \xi} \frac{\partial \vartheta}{\partial \xi}. \qquad (6\text{-}3\text{-}1)$$

Assuming $\tilde{q} = \tilde{\tau}_0$, and using (1-10-1), we find

$$St \approx 0{,}16\xi^2 \frac{\partial \omega}{\partial \xi} \frac{\partial \vartheta}{\partial \xi}. \qquad (6\text{-}3\text{-}2)$$

Substituting the limiting velocity distribution (6-1-9) into (6-3-2) and integrating, we obtain

$$St \approx 0{,}0688 \frac{\int_{\vartheta_1}^{1} \frac{\partial \vartheta}{\partial \xi} d\xi}{\int_{\xi_T}^{\xi_1} \frac{d\xi}{\xi^{1{,}43}}} = 0{,}0295 \xi_T^{0{,}43} \frac{1-\vartheta_1}{1-\left(\frac{\delta}{\delta_T}\xi_1\right)^{0{,}43}}. \qquad (6\text{-}3\text{-}3)$$

Here

$$\vartheta_1 = \frac{\alpha y_1}{\lambda} = St\, Pr\, Re^{**} \frac{\delta}{\delta^{**}} \xi_1. \qquad (6\text{-}3\text{-}4)$$

Neglecting $[(\delta/\delta_T)\xi_1]^{0.43}$ in comparison with unity, we have

$$St_{crit} \approx \frac{0{,}0295\xi_1^{0{,}43}}{1 + 0{,}0295 (\delta/\delta^{**})_{crit} \xi_1^{1{,}43} Re^{**}}. \qquad (6\text{-}3\text{-}5)$$

On substituting $\delta^{**}/\delta = 0.16$ and ξ_1 from (6-1-14) into (6-3-5), we find

$$St_{crit} \approx \frac{0{,}046}{(1 + 0{,}71 Re^{**})^{0{,}1}}. \qquad (6\text{-}3\text{-}6)$$

Taking $St_0 = 0.0128\ Re^{**-0.25}$, we obtain

$$\frac{St_{crit}}{St_0} \approx \frac{3.5}{Re^{**0.12} + 0.7Re^{**0.12}}. \qquad (6\text{-}3\text{-}7)$$

From (6-3-7) it follows that the ratio St_{crit}/St_0 is close to unity in the Re^{**} range from 3×10^3 - 10^4.

With an increase in Re^{**} the critical value of the Stanton number becomes less than St_0. /98

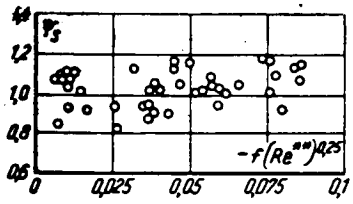

FIG. 6.6. Influence of longitudinal pressure gradient on the law of heat transfer according to the data of reference [66].

Thus the theoretical estimate shows that the law of heat transfer does not depend essentially on the longitudinal pressure gradient up to the boundary layer separation point for the practical range of Re^{**}. This important deduction is in quite satisfactory agreement with the experimental data in Figs. 6.6, 6.7 and 6.8. It is clear from the graphs that the St-number and the temperature profile are almost unchanged with a substantial decrease in coefficient of friction and a sharp deformation of the velocity profile with an increased positive pressure gradient. Nonetheless, it follows from this theory that as $Re^{**} \to \infty$ the St-number, although slowly, tends to zero. This tendency is also observed in tests. /99

Similar conclusions regarding the effect of a longitudinal pressure gradient are also easily arrived at for the law of mass transfer.

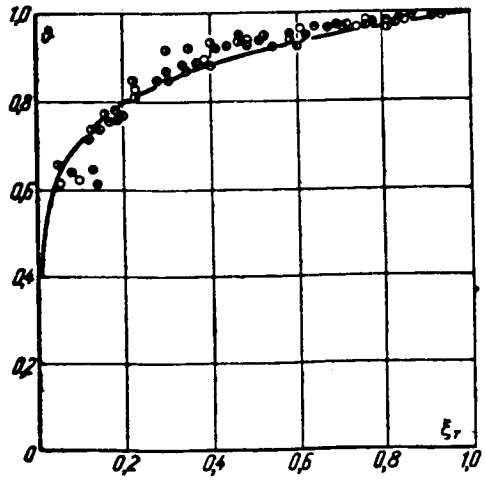

$f(Re^{**})^{0.25} \cdot 10^3$	−74	−55	−26	49	12,1
Symbol	○	●	◐	◑	◓

FIG. 6.7.- Influence of a longitudinal pressure gradient on the temperature distribution over the boundary layer cross section [66]. Curve—calculated from the formula $\vartheta = \xi_T^{1/7}$.

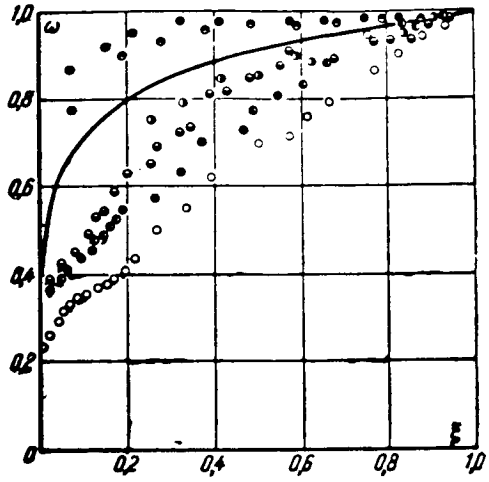

FIG. 6.8. Influence of a longitudinal pressure gradient on the velocity distribution over the boundary layer cross section [66]. Curve—calculated from formula $\omega = \xi^{1/7}$.

$f(\mathrm{Re}^{**})^{0,25} \cdot 10^3$	−9,06	−55	4,9	−28,2	−74	11,2
Symbol	◑	◐	◓	◒	○	●

6.4. Influence of Non-isothermicity on the Separation Parameters of a Turbulent Boundary Layer from an Impermeable Surface

The velocity distribution in the separation section of a non-isothermal layer at an impermeable wall, taking (1-5-4) and (6-1-4) into account, is defined by the equation /100

$$\int_{\omega_1}^{1} \sqrt{\frac{\rho}{\rho_0}(1-\beta)}\, d\omega = 2{,}5 \sqrt{\left(-\frac{\delta}{\delta^{**}} f\right)_{\text{crit}}} \int_{\xi_1}^{\xi} \frac{d\xi}{\sqrt{2\xi^2+\xi}}. \qquad (6\text{-}4\text{-}1)$$

In the limiting case when $\mathrm{Re} \to \infty$, $\xi_1 \to 0$, $\omega_1 \to 0$, $\beta \to 0$, we have

$$\left(-\frac{\delta}{\delta^{**}} f\right)_{\text{crit}} = \left(\frac{\int_0^1 \sqrt{\frac{\rho}{\rho_0}}\, d\omega}{2{,}5 \int_0^1 \frac{d\xi}{\sqrt{2\xi^2+\xi}}} \right)^2. \qquad (6\text{-}4\text{-}2)$$

With $\rho = \rho_0$ we obtain (6-1-10).

Thus, the ratio of the limiting critical values of the shape parameters for non-isothermal and isothermal flows is defined by the formula

$$\frac{\left(\frac{\delta}{\delta^{**}} f\right)_{\text{crit}}}{\left(\frac{\delta}{\delta^{**}} f\right)_{\text{crit}_0}} = \left(\int_0^1 \sqrt{\frac{\rho}{\rho_0}}\, d\omega\right)^2. \tag{6-4-3}$$

The value of this integral, with a constant coefficient of non-similarity of the temperature- and velocity-fields, has been calculated in Section 4.1. With a gradient flow, in the general case, $\varepsilon = \varepsilon(\xi)$. Thus with an isothermal flow the velocity profile in the separation section is defined by formula (6-1-9). At the same time, in the Re-number range to 10^4, the law of heat-transfer is almost independent of the longitudinal pressure gradient and $n_T = n_{To} = 1/7$.

For these conditions

$$\varepsilon = \varepsilon_0 \xi^{0.29}, \tag{6-4-4}$$

where ε_0 is the value of the non-similarity coefficient of the temperature- and velocity-fields with $dP/dx = 0$.

As was shown in Section 4.1, the magnitude of ε depends weakly on the value of the integral in (6-4-3). In addition, as $Re^{**} \to \infty$ and $St_{\text{crit}} \to 0$, the non-similarity between the frictional processes and heat transfer is reduced. If we take for these conditions $\varepsilon = \varepsilon_0 = 1$, we have*

(a) For a subsonic gas flow:

$$\frac{\left(\frac{\delta}{\delta^{**}} f\right)_{\text{crit}}}{\left(\frac{\delta}{\delta^{**}} f\right)_{\text{crit}_0}} = \left(\frac{2}{\sqrt{\psi} + 1}\right)^2. \tag{6-4-5}$$

(b) For a supersonic gas flow: /101

$$\frac{\left(\frac{\delta}{\delta^{**}} f\right)_{\text{crit}}}{\left(\frac{\delta}{\delta^{**}} f\right)_{\text{crit}_0}} \approx \frac{1}{\psi^* - 1}\left[\arcsin \frac{2(\psi^* - 1) + \Delta\psi}{\sqrt{4(\psi^* - 1)(\psi^* + \Delta\psi) + (\Delta\psi)^2}} - \arcsin \frac{\Delta\psi}{\sqrt{4(\psi^* - 1)(\psi^* + \Delta\psi) + (\Delta\psi)^2}}\right]^2. \tag{6-4-6}$$

Equation (6-4-6), as shown earlier, is quite closely approximated by the formula

$$\frac{\left(\frac{\delta}{\delta^{**}} f\right)_{\text{crit}}}{\left(\frac{\delta}{\delta^{**}} f\right)_{\text{crit}_0}} = \left[\frac{1}{4}\{(\psi)^{1,2} + 1\}^2 + \frac{1}{6} r \frac{k-1}{2} M_0^2\right]^{-1} \tag{6-4-7}$$

---

* Equations (6-4-5) and (6-4-6) were first derived by L. E. Kalikhman [36], but not as limiting equations.

Taking n_{crit} into account, as found earlier, we come to the limiting velocity distribution:

$$\int_{\delta}^{\infty} \sqrt{\frac{T_e}{T}}\, d\omega = \xi^{0.43} \int_{0}^{1} \sqrt{\frac{T_e}{T}}\, d\omega. \tag{6-4-8}$$

For subsonic velocities:

$$\omega = \frac{\psi - |\sqrt{\psi} - (\sqrt{\psi} - 1)\,\xi^{0.43}|^2}{\psi - 1}. \tag{6-4-9}$$

With $\psi = 0$, $\omega = \xi^{0.86}$; with $\psi \to \infty$, $\omega = \xi^{0.43} \cdot (2 - \xi^{0.43})$.

For supersonic velocities:

$$\omega \approx \frac{E}{2(\psi^* - 2)} \sin\left\{\left[\arcsin\frac{2(\psi^* - 1) + \Delta\psi}{E} - \arcsin\frac{\Delta\psi}{E}\right]\xi^{0.43} + \arcsin\frac{\Delta\psi}{E}\right\} - \frac{\Delta\psi}{2(\psi^* - 1)}, \tag{6-4-10}$$

where $E = \sqrt{4(\psi^* - 1)(\psi^* + \Delta\psi) + (\Delta\psi)^2}$.

Figure 6.9 illustrates the effect of the temperature factor on the limiting velocity profile at the boundary layer separation point, with subsonic flow. But here we cite the curves for the case of an adiabatic supersonic gas flow with $\psi^* = 6$. As can be seen from the graph, the temperature factor rather weakly distorts the velocity profile in the boundary layer.

Figures 6.10-6.12 present values of the critical parameters f_{crit}, H_{crit}, and $(\delta/\delta^{**})_{crit}$ as functions of the temperature factor ψ for subsonic velocities. H_{crit} changes almost linearly as the temperature factor increases. As can be seen from the graphs, cooling of the surface ($\psi < 1$) improves the stability of the boundary layer to separation in the case of diffusor flow. With surface heating ($\psi > 1$) the stability of the boundary layer to separation is lowered. As seen from the graphs, the region of existence of supersonic nonseparated flow, with $dP/dx > 0$, is strongly limited in supersonic gas flows. Figure 6.14 shows the dependence of the shape parameter on the non-isothermicity and compressibility. The results of computing the critical limiting values of the shape parameters (Figs. 6.10-6.14) can be quite closely approximated by the following simple formulas: /102

(a) For the subsonic flow region:

$$\left.\begin{aligned} &\frac{H_{crit}}{H_{crit_0}} = \psi; \quad \frac{f_{crit}}{f_{crit_0}} = \psi^{-0.8} \text{ for } \psi < 1; \\ &\frac{H_{crit}}{H_{crit_0}} = 1 + \frac{1.32}{H_{crit_0}}(\psi - 1); \quad \frac{f_{crit}}{f_{crit_0}} = \frac{1}{\psi} \text{ for } \psi > 1; \end{aligned}\right\} \tag{6-4-11}$$

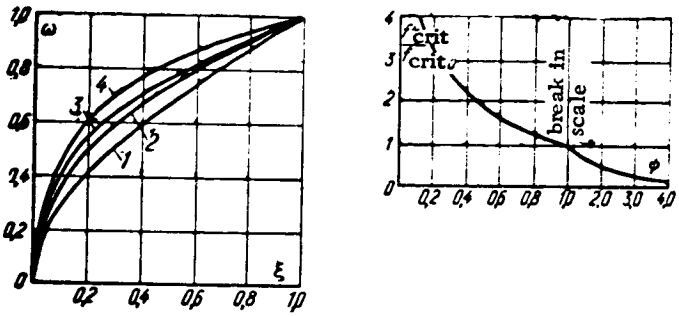

FIG. 6.9. Influence of heat-transfer on the limiting velocity profile at the separation point. 1—$\psi^* = 1$; $\psi = 0.25$; 2—$\psi^* = 1$, $\psi = 1.0$; 3—$\psi^* = 1$; $\psi = 2.0$; 4—$\psi^* = 6$, $\psi = 6.0$.

FIG. 6.10. Effect of non-isothermal conditions on f_{crit} (M << 1).

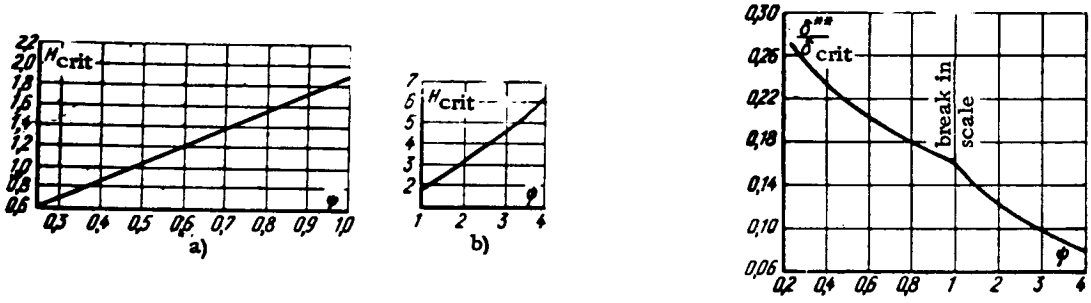

FIG. 6.11. Influence of non-isothermal conditions on the shape parameter H_{crit} (M << 1). a—cooled wall; b—heated wall.

FIG. 6.12. Influence of non-isothermal conditions on the momentum-loss thickness in the separation section of the boundary layer (M << 1).

/103

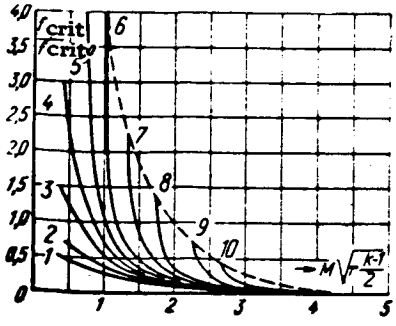

FIG. 6.13. Effect of compressibility and heat-transfer on the separation parameters of the boundary layer: 1 — $\Delta\psi = 1.0$; 2 — $\Delta\psi = 0$; 3 — $\Delta\psi = -0.5$; 4 — $\Delta\psi = -1.0$; 5 — $\Delta\psi = -1.5$; 6 — $\Delta\psi = -2.0$; 7 — $\Delta\psi = -3.0$; 8 — $\Delta\psi = -4.0$; 9 — $\Delta\psi = -6.0$; 10 — $\Delta\psi = -9.0$.

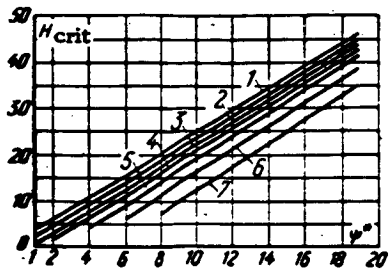

FIG. 6.14. Effect of compressibility and heat-transfer on the shape parameter H_{crit}. 1 – $\Delta\psi$=1; 2 – $\Delta\psi$=0; 3 – $\Delta\psi$ =–1; 4 – $\Delta\psi$=–2; 5 – $\Delta\psi$=–4; 6 – $\Delta\psi$=–6; 7 – $\Delta\psi$=–8.

(b) For the supersonic region:

$$\left.\begin{aligned} H_{crit} &= 2.41\psi^* + 1.38\Delta\psi - 0.52 \text{ for } \Delta\psi < 0; \\ f_{crit}/f_{crit_0} &= \psi^{*-1.43} \text{ for } \Delta\psi = 0. \end{aligned}\right\} \quad (6\text{-}4\text{-}12)$$

6.5. Joint Influence of Longitudinal Pressure Gradient and Transverse Mass Flow /104

As was demonstrated above, a longitudinal pressure gradient and a transverse mass flow at the surface of the body substantially affect the laws of friction and heat transfer and, under certain conditions, the boundary layer may be displaced from the wall. With the joint action of these two factors the problem is considerably more complex.

D. N. Vasil'ev [18] proposed a derivation of the limiting laws for this case, using the Van Dyke perturbation method [19].

Equation (3-6-2), together with (1-6-6), can be written in the form (for $\beta = 0$ and $\rho = \text{const}$):

$$\left(\frac{d\omega}{d\xi}\right)^2 = \{\Psi_1\varphi_1 + b\varphi_2 + \Lambda_0\varphi_3\}\left(\frac{d\omega_0}{d\xi}\right)^2 \quad (6\text{-}5\text{-}1)$$

or

$$\left(\frac{d\omega}{d\xi}\right)^2 = \left\{\frac{c_{f_0}}{2}[\Psi\varphi_1 + b\varphi_2] + (-f_3\varphi_3)\right\}\left(-\frac{dD_0}{d\xi}\right)^2,$$

where $D_0 = \dfrac{1-\omega_0}{\sqrt{\frac{c_{f_0}}{2}}}$.

In this way, if we take into account the expressions for φ_1, φ_2 and φ_3, the problem reduces to solving the integers-differential Eq. (6-5-1). with boundary conditions

$$\left.\begin{aligned} \omega_0 &= 0, \quad \omega = 0; \\ \omega_0 &= 1, \quad \omega = 1. \end{aligned}\right\} \quad (6\text{-}5\text{-}2)$$

With $\text{Re} \to \infty$, $c_{fo}/2 \to 0$, and Eq. (6-5-1) takes the form:

$$\left(\frac{d\omega}{d\xi}\right)^2 = (-f_3)\varphi_3\left(-\frac{dD_0}{d\xi}\right)^2. \quad (6\text{-}5\text{-}3)$$

This equation is not able to satisfy the boundary condition $\xi = 0$, $\omega = 0$.

Following Van Dyke, we introduce inner and outer solution regions and expand this solution into a series in the parameter $\gamma_0 = \sqrt{c_{f_0}/2}$.

The solution for the outer region is represented as

$$\omega = \omega^{e} = \sum \omega_{n}^{0} \gamma_{0}^{n}. \tag{6-5-4}$$

Substituting this expression in (6-5-1) and equating terms with like exponents in γ_0, we obtain (with an accuracy to within γ_0) the differential equation /105

$$\frac{d\omega_0^0}{d\xi} = \sqrt{(-f_w)\varphi_2}\left(-\frac{dD_0}{d\xi}\right) \tag{6-5-5}$$

with boundary condition $\xi = 1$ with $\omega = 1$.

Here ω_0^0 is the outer solution of zero order in γ_0.

Integrating (6-5-5) over ξ, we have

$$\omega_0^0 = 1 - \sqrt{-f_w}\int_{\xi}^{1} \sqrt{\varphi_2}\left(-\frac{dD_0}{d\xi}\right) d\xi. \tag{6-5-6}$$

For the inner region we introduce a new inner variable $\omega_0 = 1 - \gamma_0 D_0$, and represent the solution in the form

$$\omega^{i} = \sum \omega_{n}^{i} \omega_{0} \gamma_{0}^{n}. \tag{6-5-7}$$

We substitute this relationship in Eq. (6-5-1), equate terms with like powers of γ_0, and obtain (with an accuracy to within γ_0), the differential equation

$$\left(\frac{d\omega_0^i}{d\omega_0}\right)^2 = \Psi\varphi_1 + b\varphi_2 \tag{6-5-8}$$

with boundary condition $\omega_0 = 0$, $\omega = 0$.

Here ω_0^i is the inner solution of zero order in γ_0.

With $\xi \to 0$, $\varphi_1 \to 1$ and $\varphi_2 \to \omega$, and hence

$$\frac{d\omega_0^i}{d\omega_0} = \Psi + b\omega_0^i. \tag{6-5-9}$$

Taking the boundary conditions into account ($\omega_0 = 0$, $\omega_0^i = 0$) we obtain

$$\omega_0^i = \frac{1}{\sqrt{\Psi}}\omega_0 + \frac{b}{4}\omega_0^2. \tag{6-5-10}$$

The identical result was found earlier (Section 5.2) for the case of the injection of a gas with a smooth plate in the flow. In this case the relative law of friction (ψ) is as yet a free parameter, and it is defined by correlating the solutions for the inner and outer regions.

We use the principle of limit stitching of solutions formulated by Van Dyke as follows: "The inner limit of the outer solution is equal to the outer limit of the inner solution," i.e. /106

$$\omega_0^i(1) = \omega_0^0(0) \tag{6-5-11}$$

Then, from (6-5-6) and (6-5-10), we have

$$\sqrt{\Psi} + \frac{b}{4} = 1 - \sqrt{-f_2} \int_0^1 \sqrt{\varphi_2} \left(-\frac{dD_0}{d\xi} \right) d\xi. \tag{6-5-12}$$

In essence we have found the limiting relative law of friction with the joint action of a longitudinal pressure gradient and a transverse mass flow. In similar fashion, using the additive method [18], a composite solution of zero order in γ_0 can be set up in the entire region.

Following Van Dyke, we can write

$$\omega_0^c = \begin{cases} \omega_0^0 + \omega_0^i - \omega_0^0(0), \\ \omega_0^0 + \omega_0^i - \omega_0^i(1). \end{cases} \tag{6-5-13}$$

Here ω_0^c is the composite solution of zero-order in γ_0.

Consequently

$$\omega_0 = \sqrt{(-f_2)} \int_0^\xi \sqrt{\varphi_2} \left(-\frac{dD_0}{d\xi} \right) d\xi + \sqrt{\Psi}\,\omega_0 + \frac{b}{4}\omega_0^2. \tag{6-5-14}$$

Eliminating ψ using Eq. (6-5-12), we have

$$\begin{aligned} \omega_0^c = \sqrt{(-f_2)} \Bigg[& \int_0^\xi \sqrt{\varphi_2} \left(-\frac{dD_0}{d\xi} \right) d\xi \\ & - \omega_0 \int_0^1 \sqrt{\varphi_2} \left(-\frac{dD_0}{d\xi} \right) d\xi \Bigg] + \omega_0 \left(1 - \frac{b}{4} \right) + \frac{b}{4}\omega_0^2. \end{aligned} \tag{6-5-15}$$

It can be seen from (6-5-15) that the solution consists of two parts: a singular part $\left[\omega_0 \left(1 - \frac{b}{4} \right) + \frac{b}{4}\omega_0^2 \right]$, entirely concentrated in an infinitely small region around $\xi = 0$, and a regular part, in the interval $0 < \xi < 1$.

With $\mathrm{Re} \to \infty$, $\omega_0 \to 1$, and, for all $\xi > 0$ /107

$$\omega_0^c = \left(\sqrt{\Psi} + \frac{b}{4} \right) + \sqrt{-f_2} \int_0^\xi \sqrt{\varphi_2} \left(-\frac{dD_0}{d\xi} \right) d\xi. \tag{6-5-16}$$

If the function φ_3 does not depend on perturbing factors, from Eq. (6-5-16), taking $\omega_0^c = 1$ with $\xi = 1$, we obtain the limiting relative law of friction in the form

$$\sqrt{\Psi} = \left(1 - \frac{b}{4}\right)(1 - \sqrt{f}), \tag{6-5-17}$$

where

$$f = \frac{f_3}{f_{3\,\text{crit}}}, \quad \sqrt{(-f_{3\,\text{crit}})} = \frac{1 - \frac{b}{4}}{\int_0^1 \varphi_3\left(-\frac{dD_0}{d\xi}\right) d\xi}.$$

Thus the relative law of friction does not depend on a specific form of the function φ_3. The form of φ_3 determines the parameter Λ_{crit} with a given injection parameter b, or the critical injection b_{crit} with a given shape parameter Λ.

It should be noted that the functions φ_1, φ_2 and φ_3 depend implicitly on the perturbing factors by way of the velocity profile, and any method of calculation based on the self-similarity property of these functions for perturbations is inaccurate.

To determine the critical parameters we must solve the system of equations

$$\frac{d\omega}{d\xi} = \sqrt{(-f_3)}\sqrt{\varphi_3}\left(-\frac{dD_0}{d\xi}\right); \tag{6-5-18}$$

$$\frac{dJ_1}{d\xi} = \omega, \quad \frac{dJ_2}{d\xi} = \omega^2; \tag{6-5-19}$$

$$\varphi_3 = \frac{\xi - H(J_1\omega - J_2) - J_2}{D_0\xi - \int_0^\xi D_0\, d\xi}\left(1 - \frac{\int_0^\xi D_0\, d\xi}{D_0\xi - \int_0^\xi D_0\, d\xi}\right), \tag{6-5-20}$$

where /108

$$J_1 = \int_0^\xi \omega\, d\xi, \quad J_2 = \int_0^\xi \omega^2 d\xi,$$

with boundary conditions

$$\left.\begin{aligned} &\xi \to 0, \ \omega = \sqrt{\Psi} + \frac{b}{4}, \ J_1 = 0, \ J_2 = 0; \\ &\xi \to 1, \ \omega = 1, \ J_1 = 1 - \frac{\delta^*}{\delta}, \ J_2 = 1 - \frac{\delta^*}{\delta} - \frac{\delta^{**}}{\delta}. \end{aligned}\right\} \tag{6-5-21}$$

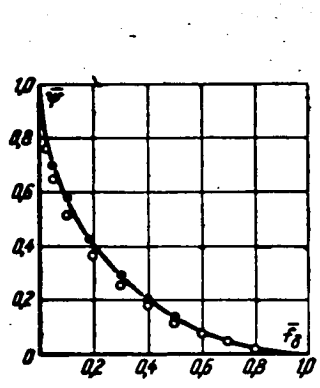

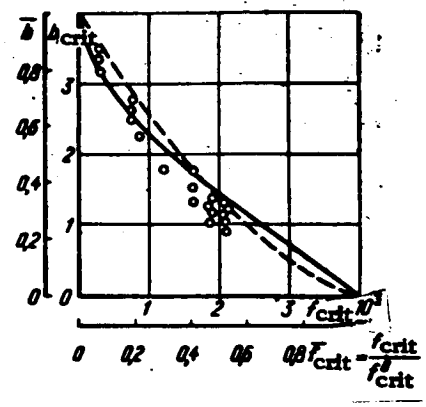

FIG. 6.15. Relative law of friction from the numerical integration of the system of Eqs. (6-5-18)-(6-5-20). $\bar{\psi} = \psi/\psi_b$, where $\psi_b = (1-0.25\,b)^2$; $\bar{f}\delta = f/f_{crit}$. Points: ●—b = 0; ○—b = 3; curve calculated from (6-5-22).

FIG. 6.16. Relationship between the permeability parameter b_{crit} and the shape parameter f_{crit} according to Eqs. (6-5-18) to (6-5-21). $\bar{b} = b_{crit}/b^0_{crit}$; $\bar{f}_{crit} = f_{crit}/f^0_{crit}$; f^0_{crit} is the critical shape parameter at an impermeable wall; b^0_{crit} is the critical injection parameter on a flat plate. ——) results of numerical solution of the system of equations; - - -) = calculation with (6-5-23); ○) test points of B. P. Mironov and P. P. Lugovskiy.

The relative law of friction $\psi(f, b)$ and the integral characteristics of the boundary layer, δ^*/δ, δ^{**}/δ, H, are found from the second boundary condition.

The system of Eqs. (6-5-18)-(6-5-21) was derived and numerically integrated by D. N. Kasil'ev [18]. He proposed a formula to approximate the results of the numerical integration /109

$$\Psi = \left(1 - \frac{b}{4}\right)^2 [1 - \sqrt{\bar{f}(2-\bar{f})}]. \qquad (6\text{-}5\text{-}22)$$

where $\bar{f} = f/f_{crit}$ and the parameter f_{crit} depends on the longitudinal pressure gradient and on the intensity of injection.

Figure 6.15 shows the results of the calculation of the relative limiting law of friction. As can be seen from the curves in the variables ψ, $\bar{f}_\delta$, gas injection does not have an appreciable effect on the relative law of friction. This effect is taken into account by the dependence of $f_{\delta crit}$ on b_{crit}, which is shown in Fig. 6.16. Also plotted

in this figure are the experimental data of B. P. Mironov and P. P. Lugovskiy [75] and a computation using the formula they proposed

$$\frac{b_{crit}}{b_{crit_0}} = (1 - f_{\delta crit})^{1,66}. \qquad (6\text{-}5\text{-}23)$$

As can be seen from the curves, the agreement between the assumed asymptotic solution and the test data is satisfactory.

As D. N. Vasil'ev [18] has shown, simple analytic expressions can be derived with the power-law approximation for the relative limiting laws of friction with joint action of a longitudinal pressure gradient and a transverse mass flow. In this case, from (6-5-20), it follows that

$$\varphi_\delta = \frac{(1-\omega^2)\,\xi}{Z_{1_0}}. \qquad (6\text{-}5\text{-}24)$$

Then, instead of Eq. (6-5-18), we have

$$\frac{d\omega}{d\xi} = \sqrt{(-f_\delta)}\sqrt{\frac{(1-\omega^2)\,\xi}{Z_{1_0}}}\left(-\frac{dD_0}{d\xi}\right). \qquad (6\text{-}5\text{-}25)$$

From this, integrating with limits from $\sqrt{\psi} + b/4$ to 1, and from 0 to ξ, we have

$$\int\limits_{\sqrt{\psi}+\frac{b}{4}}^{1} \frac{d\omega}{\sqrt{1-\omega^2}} = \sqrt{(-f_\delta)}\int\limits_0^1 \left(-\frac{dD_0}{d\xi}\right)\frac{\sqrt{\xi}}{Z_{1_0}}\,d\xi. \qquad (6\text{-}5\text{-}26)$$

The integral in the right-hand member of the equation depends only on the velocity profile under standard conditions. For boundary layer separation ($\psi = 0$) we have from (6-5-26) /110

$$\sqrt{(-f_\delta)_{crit}} = \frac{\arcsin\sqrt{\left[1-\left(\frac{b}{4}\right)^2\right]}}{L}, \qquad (6\text{-}5\text{-}27)$$

where

$$L = \int\limits_0^1 \left(-\frac{dD_0}{d\xi}\right)\frac{\sqrt{\xi}}{Z_{1_0}}\,d\xi.$$

From Prandtl's formula and Eq. (1-6-7) we have $I = \left(-\frac{dD_0}{d\xi}\right)^2 \Big/ \sqrt{Z_{1_0}}$, and hence $L = \int\limits_0^1 \frac{\sqrt{\xi}\,d\xi}{I}$. In case of an impermeable surface b = 0, and we have from Eq. (6-5-27):

$$\sqrt{(-f_{crit})_{b0}} = \frac{\pi}{2L}. \qquad (6\text{-}5\text{-}28)$$

Hence

$$\frac{\pi}{2}\sqrt{(f)_0} = \arccos f_0, \qquad (6\text{-}5\text{-}29)$$

where $(\bar{f})_0 = f_{\delta crit}/f_{\delta crit\ 0}$; $\bar{b}_0 = b_{crit}/b_{crit\ 0}$, $f_{\delta crit\ 0}$ is the critical shape parameter at an impermeable wall, $b_{crit\ 0}$ is the critical injection parameter with $f_\delta = 0$.

Formula (6-5-29) is in essential agreement with the numerical solution of the system of Eqs. (6-5-19)-(6-5-20). On substituting (6-5-27) into (6-5-26), after rearranging, we obtain

$$\arcsin\left[\sqrt{1-\left(\Psi+\frac{b}{4}\right)^2}\right]=\sqrt{\bar{f}}\arcsin\left[\sqrt{1-\left(\frac{b}{4}\right)^2}\right] \qquad (6\text{-}5\text{-}30)$$

or

$$\sqrt{\Psi}=\cos\left[\sqrt{\bar{f}}\arccos\frac{b}{4}\right]-\frac{b}{4}. \qquad (6\text{-}5\text{-}31)$$

Taking Spalding's formula [229] for $\bar{l}$, we have (with $Re \to \infty$): /111

$$\left.\begin{aligned} 0<\xi<a,\quad \bar{l}&=\varkappa\xi,\\ a<\xi<1,\quad \bar{l}&=\varkappa a,\end{aligned}\right\} \qquad (6\text{-}5\text{-}32)$$

where x and a are empirical constants (for an incompressible fluid x = 0.4, a = 0.2). Hence L = 9.8.

From Eq. (6-5-28) we have

$$\left.\begin{aligned}\sqrt{(-f_{\delta crit_0})}&=0{,}4\varkappa=0{,}16\\ (-f_{\delta crit_0})&=0{,}0257.\end{aligned}\right\} \qquad (6\text{-}5\text{-}33)$$

Integrating (6-5-26) over ω from $\sqrt{\psi} + b/4$ to ω and over ξ from 0 to ξ, we obtain the limiting velocity profile:

$$\arcsin\omega-\arcsin\left(\sqrt{\Psi}+\frac{b}{4}\right)=\sqrt{(-f_\delta)}\,L(\xi), \qquad (6\text{-}5\text{-}34)$$

where

$$L(\xi)=\int_0^\xi\frac{\sqrt{\xi}}{\bar{l}}\,d\xi.$$

After rearranging, we have

$$\omega=\cos\left[\sqrt{\bar{f}_\delta}\left(\arccos\frac{b}{4}\right)(1-\bar{L})\right], \qquad (6\text{-}5\text{-}35)$$

where $\bar{L} = L(\xi)/L(1)$, $f_\delta = f_\delta/f_{\delta crit}$.

It should be recalled that Eq. (6-5-35) is valid in the region $\xi > 0$ (outer solution).

In the separation section of the boundary layer $f_\delta = 1$

$$\bullet_{crit} = \cos\left[(1 - L)\arccos\frac{b}{4}\right]. \qquad (6\text{-}5\text{-}36)$$

For an impermeable plate (b = 0)

$$\bullet = \cos\left[(1 - L)\frac{\pi}{2}\sqrt{(\bar{f}_\delta)_\bullet}\right]. \qquad (6\text{-}5\text{-}37)$$

For the separation section, with b = 0 /112

$$\bullet_{crit} = \sin\left[\frac{\pi}{2}\bar{L}\right]. \qquad (6\text{-}5\text{-}38)$$

With $\bar{f}_\delta = 0$, $\omega = 1$, and, with Spalding's formula for l, we have

$$\left.\begin{aligned} L &= \frac{3a\sqrt{\xi}}{[1 + 2a\sqrt{a}]} \text{ with } 0 < \xi < a; \\ L &= \bar{L}(a) + \frac{[\xi\sqrt{\xi} - a\sqrt{a}]}{1 + 2a\sqrt{a}} \text{ with } a < \xi < 1. \end{aligned}\right\} \qquad (6\text{-}5\text{-}39)$$

Using Eqs. (6-5-34) and (6-5-39), D. N. Vasil'ev calculated the integral characteristics of the boundary layer for the conditions adopted.

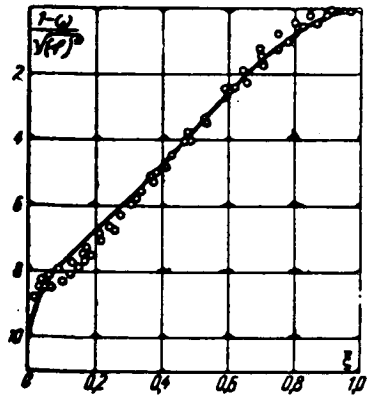

FIG. 6.17. Distribution of velocities in the separation section of the boundary layer (b = 0, $f = f_{crit}$). Curve—results of numerical integration; o-Stratford's experimental points [234]; f* = fH.

In particular, in the boundary layer separation section at an impermeable wall

$$\left.\begin{aligned} \frac{\delta^{**}}{\delta} &= 0{,}157; \quad \frac{\delta^{*}}{\delta} = 0{,}37; \\ H_{crit} &= 2{,}36; \\ (-f''_{crit}) &= \left(-f_\delta\frac{\delta^{*}}{\delta}\right) = 0{,}00946; \\ (-f'''_{crit}) &= \left(-f_\delta\frac{\delta^{**}}{\delta}\right) = 0{,}00401. \end{aligned}\right\} \qquad (6\text{-}5\text{-}40)$$

We see, on comparing these values with the formulas (6-1-11), that the more accurate accounting for the effect of the longitudinal pressure gradient on the distribution of shearing stress over the boundary layer cross section is essentially reflected in the limiting values of the shape parameters H_{crit} and f^{**}_{crit}, and has practically no effect on the parameter δ^{**}/δ. Figure 6.17 presents a comparison of the limiting velocity profile in the separation section at an impermeable wall with Stratford's data [234]. Note the satisfactory agreement between experiment and calculation. /113

PART II: PRACTICAL APPLICATIONS OF THE ASYMPTOTIC TURBULENT BOUNDARY-LAYER THEORY

CHAPTER 7
BOUNDARY LAYER ON AN IMPERMEABLE SURFACE

/114

7.1. The Influence of Finite Reynolds Numbers on the Relative Laws of Friction, Heat and Mass Transfer on an Impermeable Plate

The asymptotic theory of wall turbulence presented in the preceding chapters, as well as all the limit formulas ensuing from this theory, are applicable, strictly speaking, only in the realm of infinitely large Reynolds numbers.

The question as to whether the relative limit laws are applicable for turbulent boundary-layer calculations at finite Reynolds numbers remains open, and the final answer to this question can be obtained only by a direct comparison of the limit formulas with the existing experimental data.

The problem of the effect of compressibility and nonisothermicity on the laws of drag and mass transfer in a turbulent boundary layer of gas is of great practical significance in various branches of contemporary technology and has been attracting the attention of many researchers, both here and abroad.

Shown in Fig. 7.1 are the ranges of temperature factor and Mach number that have been covered by experimental research. The initial experimental data and conditions of the most fundamental research in this area are given in Table 7.1. As can be seen from the graph and table, a rather broad range of governing parameters (ψ, $\Delta\psi$, M_0 and Re^{**}) has been covered experimentally up to the present time for flow of a supersonic gas stream past a plate. For instance, the enthalpy factor ψ_i varies from 0.01 to 20, the Mach number up to 10 and the Re^{**} number up to 10^9.

/115

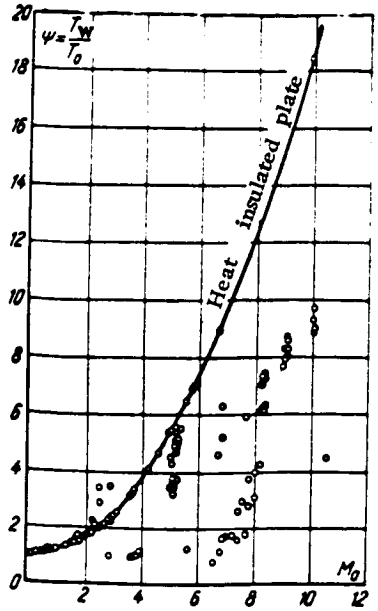

FIG. 7.1. Ranges of application of the parameters ψ and M_0 covered by experiments devoted to measurement of turbulent drag and heat transfer on an impermeable surface.

Table 7.1. Comparision of the experimental data on turbulent friction on a flat plate

Authors	M_∞	Re^{**}	$\frac{\psi^*}{\psi}$	ψ	Experimental Conditions	Method of determining c_f
Coles [18] $Re^{**} = idem$, $Re_x \approx 8 \cdot 10^6$	2,6	6 600	1,0	0,638	Thermally insulated plate	Direct measurement with a floating element
	2,6	10 200	1,0	0,641		
	3,7	4 100	1,0	0,516		
	3,7	7 560	1,0	0,499		
	4,5	2 900	1,0	0,460		
	4,5	3 470	1,0	0,455		
	4,5	5 240	1,0	0,424		
	4,5	6 590	1,0	0,429		
Hill [154] $Re^{**} = idem$	8,99	1 245	0,448	0,197	Cooled wall of a conical nozzle	From the velocity gradient at the wall
	9,04	1 607	0,460	0,235		
	9,07	1 908	0,474	0,234		
	9,10	2 287	0,495	0,227		
	8,22	2 081	0,493	0,257		
	8,35	2 498	0,497	0,265		
	8,27	2 885	0,500	0,259		
	8,29	3 202	0,500	0,247		
	8,29	3 451	0,502	0,239		
Korkegi [162] $Re^{**} = idem$	5,787	2 477	1,0	0,403	Thermally insulated plate	Direct measurement using a floating element
	5,77	2 780	1,0	0,400		
	5,793	3 429	1,0	0,400		
	5,805	4 040	1,0	0,397		
Lobb, Winkler and Persh [173] $Re^{**} = idem$	4,93	5 350	0,924	0,369	Cooled wall of a plane nozzle	From the velocity gradient at the wall and by Reynolds analogy from measurements of the heat fluxes in the test cross section
	5,01	6 480	0,713	0,381		
	5,03	7 950	0,575	0,341		
	5,06	7 370	0,535	0,329		
	6,83	8 550	0,613	0,251		
	6,83	12 640	0,508	0,234		
	6,78	8 400	0,513	0,244		
	6,78	7 960	0,457	0,251		
	7,67	8 440	0,465	0,217		
Wilson [245] $Re_x = idem$, $Re_x \approx 10^7$	1,55		1,0	0,885	Thermally insulated plate	From velocity profile measurements and the momentum equation.
	1,70		1,0	0,851		
	1,75		1,0	0,828		
	1,93		1,0	0,810		
	2,18		1,0	0,770		
Chapman and Kester [113] $Re_x = (6-16) \cdot 10^6$	0,51		1,0	0,985	Flow past a thermally insulated cylinder in the longitudinal direction	Direct measurement of mean cross sections.
	0,81		1,0	0,929		
	1,99		1,0	0,746		
	2,49		1,0	0,671		
	2,95		1,0	0,623		
	3,36		1,0	0,578		
	3,60		1,0	0,551		
Liepmann and Dhawan [113] $Re_x = idem$, $Re_x \approx 1 \cdot 10^6$	0,42		1,0	0,989	Flow past a thermally insulated plate	Direct measurement of local values
	0,63		1,0	0,966		
	0,82		1,0	0,965		
	1,28		1,0	0,829		
	1,45		1,0	0,790		

Table 7.1. Continued

Authors	M_0	Re^{**}	$\frac{\phi^*}{\phi}$	ψ	Experimental Conditions	Method of determining c_f
Sommer and Chort [223] Re_x = idem, $Re_x = (3-9)\cdot 10^6$	2,81 3,82 5,63 6,90 7,00 3,78 3,67		0,400 0,268 0,176 0,161 0,162 0,272 0,285	0,867 0,730 0,562 0,404—0,451 0,395—0,446 0,694 0,724	Hollow cylinder moving against the flow in a wind tunnel	From the change in model flight velocity
Monoghan [19] Re^{**} = idem	2,43		1,0	0,680		
Rubesin [113] Re_x = idem, $Re_x = 7\cdot 10^6$	2,55		1,0	0,705		From velocity profile measurements
Brinich [109] Re_x = idem, $Re_x = (3-18)\cdot 10^6$	3,05		1,0	0,625	Cylindrical surface	From velocity profiles
Abbot [154] Re_x = idem, $Re_x = 5\cdot 10^6$	3,80 7,20		0,278 0,173	0,720 0,340		

Comparison of experimental data on turbulent heat transfer on a flat plate (ratios of the Stanton numbers St/St_0 for Re_X = idem)

Authors	M	St/St_0	Experimental Conditions	Method of determining St
Bradfield and De Coursin [106]	2,586 8,180 3,410	0,67—0,77 0,535—0,700 0,547—0,610	Flow past a cone	Measurement of the heat transfer by a non-stationary method
Pappas [190]	1,823 2,290	0,795—0,900 0,675—0,790	Uniformly heated plate	From the expenditure of electric power and from the wall temperature
Schoulbey [106]*	2,00 2,50 3,09	0,763 0,675 0,600	Uniformly heated plate	From the expenditure of electrical power and from the wall temperature
Fallis [138]	2,5 2,5	0,744 0,745	Data not given	

*Data reduced to thermal-insulation conditions by the method of Van Driest.

The experimental data cited in Table 7.1 as compared in Fig. 7.2 with the limit formula (4-1-4). The experimental data obtained in the presence of heat transfer are reduced to thermal-insulation conditions by formula (4-1-2). The frictional-drag coefficient for standard condition (c_{fo}) was calculated by formula (1-10-3), the μ and ρ that occur in Re^{**} being determined from the free-stream temperature T_0.

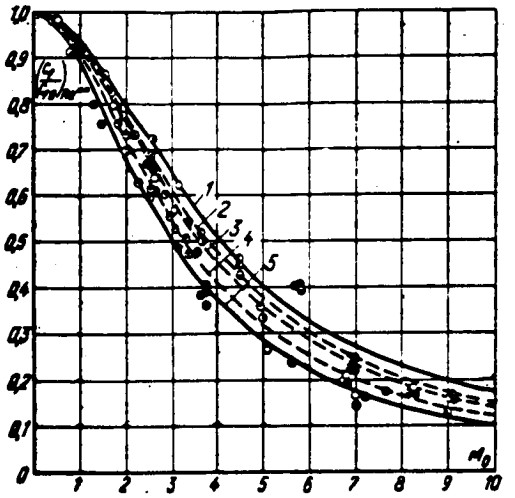

FIG. 7.2. Effect of gas compressibility on the relative drag law. 1—$Re^{**} = 10^3$; 2—$Re^{**} = 4 \cdot 10^3$; 3—$Re^{**} = 1.4 \cdot 10^4$; 4—$Re^{**} = 10^6$; 5—$Re^{**} = \infty$.

As can be seen from Fig. 7.2, the agreement observed between the experimental data of the various researchers concerning the influence of compressibility on the frictional-drag coefficient and the limit formula is not only qualitative, but, in some cases, quantitative as well. All the experimental points are found to be above the limit formula, and a tendency toward stratification of the experimental data according to Re^{**} number is noted. Considering the relatively weak influence of Re^{**} on the value of the relative friction coefficient, it is completely permissible to introduce the values of the parameters Z and ω corresponding to isothermal flow as a first approximation into Eqs. (4-1-1) and (4-1-13), that is,

$$\left.\begin{aligned} Z_0 &= 1 - \omega_{10}; \\ \omega_1 &= \omega_{10} = \varphi_{10}\sqrt{\frac{c_{f0}}{2}}. \end{aligned}\right\} \qquad (7\text{-}1\text{-}1)$$

For a plate, $\varphi_{10} = 11.6$. After substituting these values for Z_{10} and ω_{10} into Eq. (4-1-13), we get /120

$$\Psi = \frac{1}{(\psi^* - 1)(1 - 8.2\sqrt{c_{f0}})^2} \times \left[\arcsin\frac{2(\psi^* - 1) + \varepsilon\Delta\psi}{\sqrt{4(\psi^* - 1)(\psi^* + \Delta\psi) + (\varepsilon\Delta\psi)^2}} - \arcsin\frac{16.4(\psi^* - 1)\sqrt{c_{f0}} + \varepsilon\Delta\psi}{\sqrt{4(\psi^* - 1)(\psi^* + \Delta\psi) + (\varepsilon\Delta\psi)^2}}\right]^2. \qquad (7\text{-}1\text{-}2)$$

For adiabatic flow,

$$\Psi = \frac{1}{\psi^* - 1}\left(\frac{\arcsin\sqrt{\frac{\psi^*-1}{\psi^*}} - \arcsin 8{,}2\sqrt{\frac{\psi^*-1}{\psi^*}}\,c_{f_0}}{1 - 8{,}2\sqrt{c_{f_0}}}\right)^2. \tag{7-1-3}$$

At subsonic velocities,

$$\Psi = \left[\frac{2}{\sqrt{\psi} - 8{,}2(\psi - 1)\sqrt{c_{f_0}} + 1}\right]^2. \tag{7-1-4}$$

The results of calculating the parameter Ψ by formula (7-1-3) for various values of Re** are shown in Fig. 7.2. As can be seen from the graph, the very first approximation yields satisfactory agreement with the experiments. /121

Spalding [164] has proposed simple approximating formulas for Eqs. (7-1-3) and (4-1-4); they have the form

$$\Psi = \left[\frac{\Psi_\infty^{1/2} - \omega_{1\delta}\Psi_0^{1/2}}{1 - \omega_{1\delta}}\right]^2, \tag{7-1-5}$$

where Ψ_∞ is the limit friction law;

$$\Psi_0 = \left\{\frac{1}{4}\left[(\psi)^{1/2} + \left[\psi + \varepsilon\omega_{1\delta}(1-\psi) + \omega_{1\delta}(\varepsilon - \omega_{1\delta})\,r\frac{k-1}{2}\right.\right.\right.$$
$$\left.\left.\left.\times M_\delta^2\right]^{1/2}\right\}^2 + \frac{1}{6}\,r\frac{k-1}{2}M_\delta^2\omega_{1\delta}^2\Bigg]^{-1}. \tag{7-1-6}$$

Taking Eqs. (1-11-2) and (1-4-4) into account,

$$\omega_{1\delta} = 1{,}3\,(\mathrm{Re}^{**})^{-1/8}. \tag{7-1-7}$$

For the region of large but not infinite values of Re**, the value of $\omega_{1\delta}$ is significantly smaller than unity. From formula (7-1-6) it follows that in this case

$$\Psi_0 = (\psi)^{-1/2}. \tag{7-1-8}$$

Correspondingly, from Eq. (7-1-5) we get

$$\Psi = \left[\frac{\Psi_\infty^{1/2} - 1.3\,(\mathrm{Re}^{**})^{-1/8}\,\psi^{-1/2}}{1 - 1.3\,(\mathrm{Re}^{**})^{-1/3}}\right]^2. \tag{7-1-9}$$

Expanding into a binomial series, we have

$$\Psi = \Psi_\infty\left[1 + 2{,}6\,(\mathrm{Re}^{**})^{-1/8}\left(1 - \psi^{-1/2}\Psi_\infty^{-1/2}\right)\right]. \tag{7-1-10}$$

Let us examine three limit cases:

a) $M < 1$,

then, $\Psi_\infty \to 2/(1+\psi)$ as $\psi \to 1$,

and

$$\Psi \to \Psi_\infty \left[1 + 0{,}65\,(\mathrm{Re}^{**})^{-1/8}\left(1 - \frac{1}{\psi}\right)\right]. \tag{7-1-11}$$

Thus, when a wall is heated, $\Psi > \Psi_\infty$, and when it is cooled, $\Psi < \Psi_\infty$; /122

b) the Mach number is very large and the wall is thermally insulated; in this case

$$T_w = T^*_w,$$

$$\Psi_\infty = \frac{12}{5}\left(r\frac{k-1}{2}M_\infty^2\right)^{-1} = \frac{12}{5}\frac{1}{\psi^*} \tag{7-1-12}$$

and

$$\Psi = \Psi_\infty\,[1 + 0{,}927\,(\mathrm{Re}^{**})^{-1/8}]. \tag{7-1-13}$$

From Eq. (7-1-13) it is evident that $\Psi > \Psi_\infty$;

c) the case $\psi^* \longrightarrow \infty$, $\Delta\psi \neq 0$.

Taking into account Eqs. (7-1-3) and (7-1-11) we get

$$\overline{\Psi} = \left\{\frac{1 - \frac{2}{\pi}\arcsin\frac{\psi - 1 + 16{,}4\sqrt{c_{f_0}}}{\psi - 1}}{1 - \frac{2}{\pi}\arcsin 8{,}2\sqrt{c_{f_0}}}\right\}^2,$$

where

$$\overline{\Psi} = \left(\frac{c_f}{c_{f0\,(\Delta\psi=0)}}\right)_{\mathrm{Re}^{**}_T}; \tag{7-1-14}$$

$$\overline{\Psi} = \frac{T_w}{T^*_w}; \tag{7-1-15}$$

The experimental data of Matting, Chapman and Nycolm [176] are compared in Fig. 7.3 with (7-1-3). The experiments were carried out over a broad range of Re_x and Mach numbers. The frictional drag coefficient was measured by means of a floating element with a maximum error of 5%. The transition from Ψ to $\Psi_x = \left(\frac{c_f}{c_{f0}}\right)_{\mathrm{Re}_x}$ was realized by means of the integral momentum relation.

For a plate the integral momentum relation can be written as

$$\frac{d\mathrm{Re}^{**}}{d\bar{x}} = \mathrm{Re}_L\,\Psi\frac{c_{f_0}}{2} = \mathrm{Re}_L\,\Psi\frac{B}{2\,(\mathrm{Re}^{**})^m}. \tag{7-1-16}$$

After integrating and transforming, we get /123

$$\Psi_x = \Psi^{\frac{1}{n+1}} \tag{7-1-17}$$

As can be seen from Fig. 7.3, the first approximation yields friction coefficients which are somewhat too high, especially at high Mach numbers. The second approximation yields almost complete agreement with the experimental data, when

$$Z = 1 - \omega_1, \quad \omega_1 = 11{,}6\sqrt{\Psi_\infty \frac{c_{f_0}}{2}}. \tag{7-1-18}$$

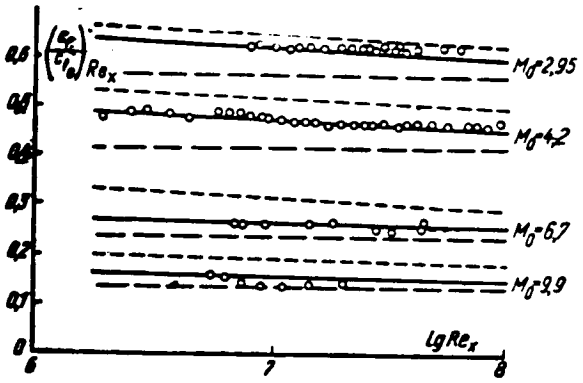

FIG. 7.3. Comparison of the limiting formulas with the experiments of Matting, Chapman and Nycolm [176]. – – –) calculated by formula (4-1-4): - - -) calculated by formula (7-1-3); ——) calculated by formula (7-1-20).

The final computational formula is

$$\Psi = \frac{1}{(\psi^* - 1)\left(1 - 8{,}2\sqrt{\Psi_\infty c_{f_0}}\right)^2} \times \left[\arcsin \frac{2(\psi^* - 1) + \Delta\psi}{\sqrt{4(\psi^* - 1)(\psi^* + \Delta\psi) + \Delta\psi^2}} - \arcsin \frac{16{,}4(\psi^* - 1)\sqrt{\Psi_\infty c_{f_0}} + \Delta\psi}{\sqrt{4(\psi^* - 1)(\psi^* + \Delta\psi) + (\Delta\psi)^2}}\right]^2. \tag{7-1-19}$$

For the case $\Delta\psi = 0$ /124

$$\Psi = \frac{1}{\psi^* - 1}\left(\frac{\arcsin\sqrt{\frac{\psi^* - 1}{\psi}} - \arcsin 8{,}2\sqrt{\frac{\psi^* - 1}{\psi^*}\Psi_\infty c_{f_0}}}{1 - 8{,}2\sqrt{\Psi_\infty c_{f_0}}}\right), \tag{7-1-20}$$

and for subsonic velocities

$$\Psi = \left[\frac{2}{\sqrt{\psi - 8{,}2(\psi - 1)\sqrt{\Psi_\infty c_{f_0}} + 1}}\right]^2. \tag{7-1-21}$$

For the case $\psi \to 0$ it follows from (7-1-21) that

$$\Psi_{\psi \to 0} \to \left[\frac{2}{4{,}05(c_{f_0})^{1/4} + 1}\right]^2. \tag{7-1-22}$$

The results of relative drag-law calculations by formula (7-1-21) are presented in Fig. 7.4. As can be seen from the graph, with strong wall cooling ($\psi \ll 1$) and heating ($\psi \gg 1$) the Re^{**} is observed to have an appreciable effect on the magnitude of the relative friction coefficient. Given in Fig. 7.5 is a comparison of the existing experimental data with formula (7-1-21). Despite the great scatter of the experimental data, /125 the agreement of the proposed computational method with experiment can be considered satisfactory.

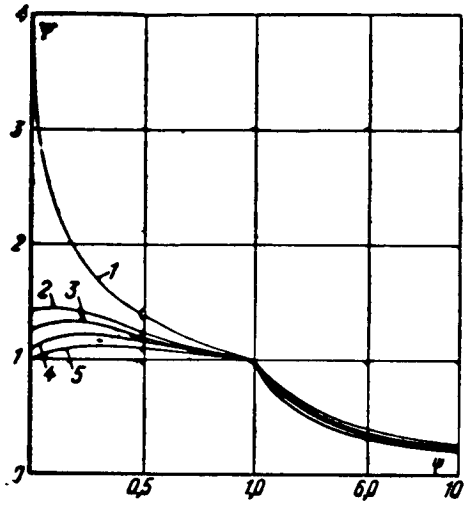

FIG. 7.4. The effect of non-isothermicity on the relative drag law: Curves calculated by formula (7-1-21): 1—$Re^{**} = \infty$; 2—$Re^{**} = 10^6$; 3—$Re^{**} = 10^5$; 4—$Re^{**} = 10^4$; 5—$Re^{**} = 10^3$.

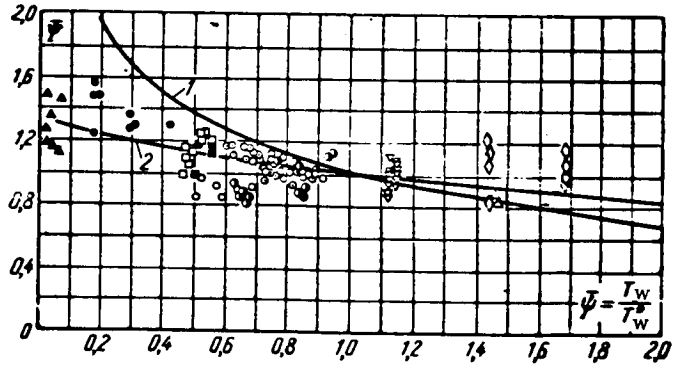

FIG. 7.5. Effect of non-isothermicity on the relative laws of drag and heat transfer on a flat plate: 1—calculated by formula (4-1-5); 2—calculated by formula (7-1-21) for $Re^{**} = 1,000$, $\Psi = \Psi/\Psi_M$; $\Psi = T_w/T^{**}_w$.

Source	[173]	[183]	[154]	[155]	[183]	[190]	[52]	[246]	[223]	[202]
Symbol	○	◇	□	■	△	▽	⊙	◑	●	▲

Equations (7-1-20) and (7-1-21) enable us to take into account the effect of the Reynolds number on the relative drag law, but this effect is not great in the practical range of Re**. For practical calculations, therefore, it is convenient to retain the relative laws of drag and heat transfer in the form of limiting relations (4-1-2), (4-1-3) and (4-1-5). In deriving the limiting laws the choice of the "standard" conditions, i.e. the friction coefficient c_{fo}, leaves unanswered the question as to the temperature at which the viscosity coefficient appearing in Re** should be defined, the friction coefficient c_{fo} being calculated in turn from Re**.

This question arises when practical calculations are being made and when the relative limiting laws are compared with experimental data.

In the computational method proposed above, based on the introduction of the second approximation, all the physical gas parameters appearing in Re** are determined from the thermodynamic temperature at the outer edge of the boundary layer. /126

As a result, it is possible to get good agreement between the computed and the experimental data, but the computational formulas have become complicated, compared to the limiting ones. The variable viscosity in the laminar sublayer can affect the relative laws of drag and heat transfer only with finite Re. Since $\vartheta_1 \to 0$ as $Re \to \infty$, as was demonstrated earlier, the temperature T, at the outer edge of the viscous sublayer tends to T_w, and in such a case the viscosity may show up in the wall layer having the temperature T_w.

If, taking these arguments into account, the gas viscosity assuming is Re** is determined from the wall temperature, the limit drag laws change to:

a)

$$\Psi = \left(\frac{\mu_w}{\mu_e}\right)^m \left(\frac{2}{\sqrt{\psi}+1}\right)^2; \qquad (7\text{-}1\text{-}23)$$

for the subsonic velocity region;

b)

$$\Psi = \left(\frac{\mu_w}{\mu_e}\right)^m \left(\frac{\operatorname{arctg} M_e \sqrt{r\frac{k-1}{2}}}{M_e \sqrt{r\frac{k-1}{2}}}\right)^2; \qquad (7\text{-}1\text{-}24)$$

for the supersonic velocity region on a heat-insulated plate;

c)

$$\Psi_\infty = \left(\frac{\mu_w}{\mu_e}\right)^m \left[\frac{2\operatorname{arctg} M_e \sqrt{r\frac{k-1}{2}}}{\left(\sqrt{\frac{T_{cr}}{T^*_{cr}}}+1\right) M_e \sqrt{r\frac{k-1}{2}}}\right]^2 \qquad (7\text{-}1\text{-}25)$$

for the supersonic velocity region and heat transfer, taking (4-1-11) into account.

Given in Fig. 7.6 is a comparison of formula (7-1-25) with the existing experimental data. The complex

$$\bar{\Psi} = \Psi_{\infty}\left(\frac{\mu_0}{\mu_w}\right)^{m}\left(\frac{\sqrt{\frac{T_w}{T^*_w}}+1}{2}\right)^{2}.$$

is plotted on the ordinate axis.

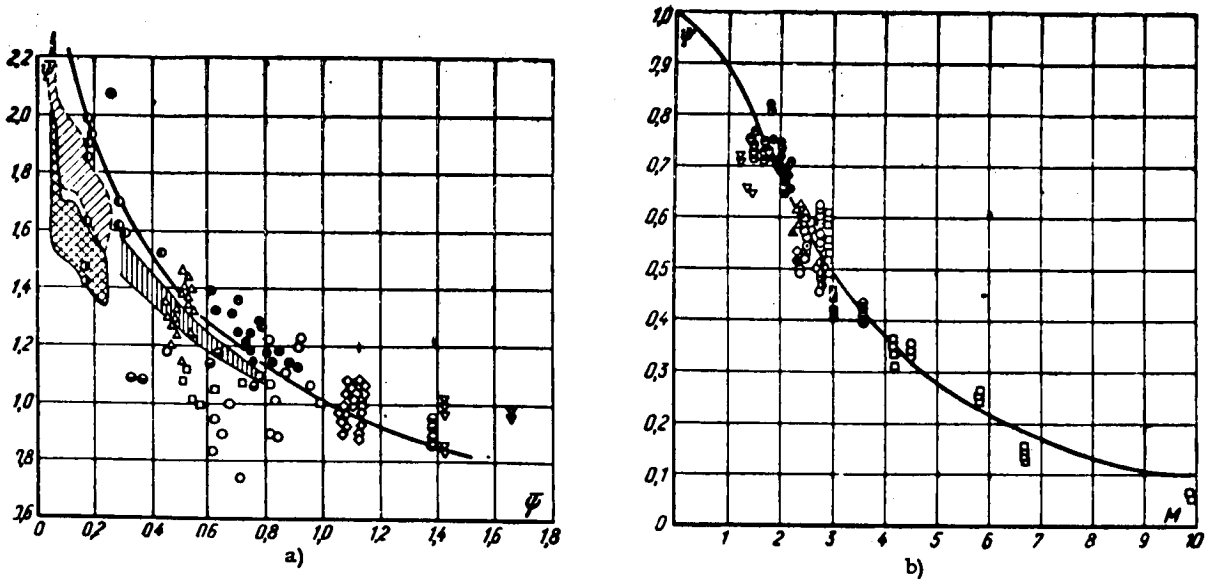

a)

Reference	[227]	[52]	[154]	[223]	[246]	[183]	[183]	[6]	[173]	[193]	[6]	[51]	[84]
Symbol	◑	●	△	◐	○	▽	◒	Vertical hatching	□	◇	Cross hatching	Oblique hatching	◓

b)

Reference	[227]	[124]	[183]	[183]	[118]	[147]	[176]	[129]	[204]	[245]	[113]	[109]	[183]	[162]	[190]	[173]	[106]
Symbol	○	▽	△	◑	◐	◓	□	◇	⊙	●	◒	■	×	+	▲	▼	◆

FIG. 7.6. Influence of non-isothermicity (a) and compressibility (b) on the relative laws of drag and heat transfer. The curves were calculated by formular (7-1-25).

As can be seen from the graph, all the experimental points are located along the curve describing the limiting relative drag law. /127

For the domain of existence of the triple Reynolds analogy, then recommendations can be applied to the laws of heat and mass transfer. The question of whether the laws of heat and mass transfer are conserved when the boundary conditions change will be examined in Chapter 7.

Thus, for engineering calculations of friction and heat transfer during the flow of a compressible gas under non-isothermal conditions, we can use the limit relative laws of drag and of heat and mass transfer if the standard values of the coefficients c_{fo}, St_o and St_{Do} are calculated from Re^{**}, in which the dynamic viscosity coefficient is determined from the wall temperature.

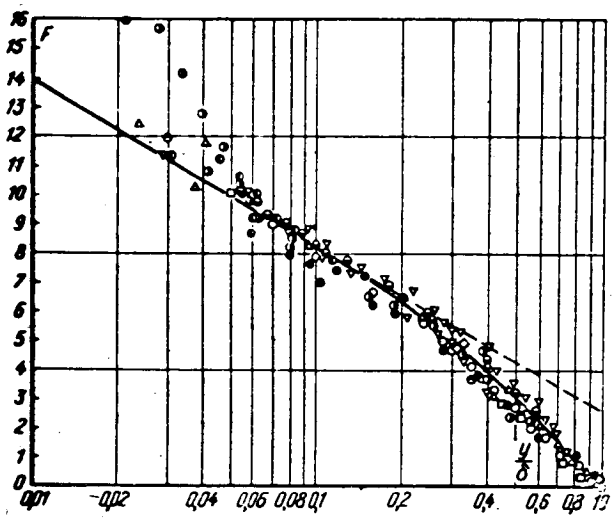

FIG. 7.7. Comparison of the limit velocity distribution in the turbulent boundary layer of a compressible gas with the experimental data of [175].

-------calculated by formula (4-2-2)

$$F = \frac{1}{\sqrt{\frac{c_1}{2}\sqrt{\psi^{*}-1}}}\left[\arcsin\sqrt{\frac{\phi^{*}-1}{\psi^{*}}}\omega - \arcsin\sqrt{\frac{\psi^{*}-1}{\phi^{*}}}\right].$$

M_e	1,47	2,7	2,9	4,93	1,85
Re^{**}	$4,6\cdot10^3$	$7\cdot10^3$	$5,4\cdot10^4$	$5,35\cdot10^3$	$3\cdot10^3$
Symbol	○	●	△	◑	▽

M_e	2,1	2,57	2,96	1,97	4,5
Re^{**}	$2,78\cdot10^3$	$3,24\cdot10^3$	$2,64\cdot10^3$	$2,98\cdot10^3$	$3,47\cdot10^3$
Symbol	□	◒	◐	◓	◇

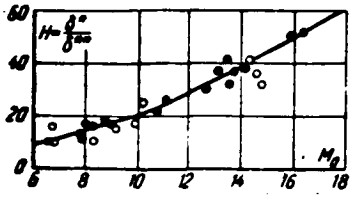

FIG. 7.8. Effect of compressibility of the gas on the value of the shape parameter H. Curve calculated by the formula $H = 1.28\psi^* 0.95$; experimental data: o—[134]; ●—[155].

Also possible are other recommendations for determining the parameters appearing in Re^{**}. Thus, for example, according to the calculations of Spalding and Chi [227], the limit formula gives a mean square error of 9.9% when compared with all the available experimental data of the formula is written as

$$\Psi_\infty = F_R \frac{1}{\psi^* - 1}\left[\arcsin \frac{2(\psi^* - 1) + \Delta\psi}{\sqrt{4(\psi^* - 1)(\psi + \Delta\psi) + (\Delta\psi)^2}} - \arcsin \frac{\Delta\psi}{\sqrt{4(\psi^* - 1)(\psi^* + \Delta\psi) + (\Delta\psi)^2}}\right]^2, \quad (7\text{-}1\text{-}26)$$

where $F_R = \psi^{-0.702}\psi^{-0.772}$.

A comparison of the limit velocity distributions with the experiments of various authors is given in Fig. 7.7, and the effect of gas compressibility on the value of the shape parameter H is shown in Fig. 7.8. As can be seen from the graphs, the limit velocity distributions in the turbulent boundary layer of a compressible gas are in satisfactory agreement with the experimental data.

Given in Table 7.2 are the results of comparing the experimental data on the friction coefficients on a flat plate with those calculated by I. K. Ermolaev using formulas (7-1-19) and (4-1-2). The table shows that the use of the limit formulas to determine viscosity from the wall temperature yields a mean square deviation of the calculated friction coefficients from the experimental ones, within the limits of the experimental accuracy of about 10%. /132

7.2. Solution of the Integral Momentum and Energy Relations for a Turbulent Boundary Layer on an Impermeable Surface

The integral momentum relation for a plane boundary layer is conveniently written in the following form:

$$\frac{d\,\mathrm{Re}^{**}_\infty}{dx} + \mathrm{Re}_L f(1 + H) = \Psi\,\mathrm{Re}_L \frac{c_{f_0}}{2}, \quad (7\text{-}2\text{-}1)$$

where

$$\mathrm{Re}^{**}_\infty = \rho_\infty w_\infty \delta^{**}/\mu_\infty;\ \mathrm{Re}_L = \rho_\infty w_\infty L/\mu_\infty;$$

Table 7.2. Table of mean square values $\Delta = \frac{c_{f\,exp} - c_{f\,theor}}{c_{f\,theor}}$

Author		M_∞	$\Delta\phi$	First approximation			From μ_w			Reference
				Acc. to each author separately Δ, %	Separately for $\Delta\phi=0$ and $\Delta\phi\neq0$, %	Total for all authors Δ, %	Accord. to each author separately Δ, %	Separately for $\Delta\phi=0$ and $\Delta\phi\neq0$, %	Total for all authors Δ, %	
Spivak	(1950)	2,8	0	6,915	8,740		4,709	9,1105		[259]
Brinich et al.	(1952)	3,05	0	7,582	8,740		10,67	9,1105		[109]
Dahwan	(1952)	0,35—1,45	0	13,69	8,740		12,76	9,1105		[124]
Monagan et al.	(1952)	2,82—2,43	0	6,806	8,740		8,266	9,1105		[261]
Coles	(1954)	2,6—4,5	0	11,09	8,740		8,117	9,1105		[118]
Wilson	(1950)	1,9—2,19	0	10,53	8,740		9,076	9,1105		[245]
Rubesin et al.	(1951)	2,5	0	8,881	8,740		5,715	9,1105		[203]
Chapman et al.	(1954)	0,81—3,6	0	5,652	8,740		6,406	9,1105		[113]
O'Donnel	(1954)	2,41	0	11,58	8,740		6,36	9,1105		[129]
Hakkinen	(1955)	0,18—1,76	0	9,007		10,94	8,269		10,05	[147]
Matting et al.	(1961)	2,95—9,9	0	6,567		10,94	8,87		10,05	[176]
Goddard	(1959)	0,7—4,54	0	12,71		10,94	15,4		10,05	[263]
Abbot	(1953)	3,9—7,25	1—1,8	17,06	14,81		23,44	11,99		[264]
Monagan et al.	(1953)	2,43—2,82	3—3,5	19,56	14,81		14,91	11,99		[262]
Pappas	(1954)	1,69—2,27	1,7—2,19	12,60	14,81		11,26	11,99		[190]
Sommer et al.	(1955)	2,81—7,0	1,05—1,75	8,720	14,81		13,21	11,99		[223]
Hill	(1959)	8,99—10	6,1—9,0	18,20	14,81		14,821	11,99		[155]
Winkler	(1961)	5,20	3,5—5,5	18,09	14,81		16,03	11,99		[246]
Jeromin	(1968)	2,5—3,5	2,2—3,5	8,20	14,81		4,90	11,99		[156]

μ_{**} is the dynamic viscosity coefficient at the stagnation temperature; and $f = \frac{\delta^{**}}{w_e}\frac{dw_e}{dx}$ is the shape parameter.

We represent Eq. (7-2-1) in the form

$$\frac{d\,\mathrm{Re}^{**}_{**}}{\mathrm{Re}_L d\bar{x}} = \Psi\frac{c_{f_0}}{2} - \tilde{f}(1+H)f_{\mathrm{crit}} \qquad (7\text{-}2\text{-}2)$$

and linearize the right-hand side of the equation. The relative drag law is represented as

$$\Psi = \Psi_t\Psi_f\Psi_M, \qquad (7\text{-}2\text{-}3)$$

where

$$\Psi_t = \left[\frac{2}{\left(\sqrt{\frac{T_w}{T^*_w}}+1\right)}\right]^2;$$

$$\Psi_M = \left[\frac{\operatorname{arctg} M_\infty\sqrt{r\frac{k-1}{2}}}{M_\infty\sqrt{r\frac{k-1}{2}}}\right]^2,$$

and Ψ_f is determined from the graph of Fig. 6.2.

We represent the right-hand side of Eq. (7-2-2) in the form

$$F = \Psi_t \Psi_M \frac{c_{f0}}{2} - (1 + H_{crit}) f_{crit} \tilde{f}; \tag{7-2-4}$$

this approximation is exact if $\tilde{f} = 0$; a small error is introduced when $\tilde{f} \to 1$, but since $\Psi_t \Psi_M (c_{f0}/2) \ll (1 + H_{crit}) f_{crit}$, this error is insignificant. Then the integral momentum relation, after appropriate transformations, reduces to /133

$$\frac{d\,\mathrm{Re}^{**}_{\infty}}{d\bar{x}} + (1 + H_{crit}) \frac{\mathrm{Re}^{**}_{\infty}}{w_e} \frac{dw_e}{d\bar{x}} = \Psi_t \Psi_M \frac{c_{f0}}{2} \mathrm{Re}_L. \tag{7-2-5}$$

Taking Eqs. (1-11-2) and (7-1-25) into account, we have

$$\frac{d\,\mathrm{Re}^{**}_{\infty}}{d\bar{x}} + (1 + H_{crit}) \frac{\mathrm{Re}^{**}_{\infty}}{w_e} \frac{dw_e}{d\bar{x}} = (\Psi_t \Psi_M)_{\infty} \times \left(\frac{\mu_w}{\mu_{\infty}}\right)^m \mathrm{Re}_L \frac{B}{2 (\mathrm{Re}^{**}_{\infty})^m}. \tag{7-2-6}$$

Integrating, we get

$$\mathrm{Re}^{**}_{\infty} = \exp\left(-\frac{J}{1+m}\right)\left[(m+1)\frac{B}{2}\mathrm{Re}_{L_0}\int_{\bar{x}_0}^{\bar{x}} (\Psi_t \Psi_M)_{\infty} \times \left(\frac{\mu_w}{\mu_{\infty}}\right)^m U (1 - U^n)^{\frac{1}{k-1}} \exp(J)\, dx + C\right]^{\frac{1}{m+1}}, \tag{7-2-7}$$

where $\mathrm{Re}_{00} = \rho_{00} \omega_{max} L/\mu_{00}$; $\rho_{00} = P_{00}/RT_{00}$; P_{00} is the total pressure;

$$J = (m+1) \int (1 + H_{crit})\, d\omega_e/\omega_e; \quad U = \omega_e/\omega_{max};$$
$$\omega_{max} = \sqrt{2 g i_{c0}}; \quad H_{crit} = 2{,}41\bar{\gamma}^* + 1{,}38\Delta\bar{\gamma} - 0{,}52.$$

Thus, for given laws of variation of wall temperature and velocity at the outer edge of the boundary layer with respect to the coordinate x, we determine the local values of Re^{**}_{00} from Eq. (7-2-7). The integration constant $C = (\mathrm{Re}^{**m+1}_{\omega 0} e')$ when $x = \bar{x}_0$, x_0 is the section at which integration begins.

In the particular case of the turbulent boundary layer beginning to grow at zero, C = 0. If the turbulent boundary layer is preceded by a laminar boundary layer, the laminar boundary layer is calculated upto the moment it changes into a turbulent one and the integration constant is determined from the value of Re^{**}_{00} for the laminar boundary layer in this section.

The local values of the frictional drag coefficient are determined by the formula /134

$$c_f = \Psi \Psi_f \frac{B}{\mathrm{Re}^{**m}_{\omega 0}} \left(\frac{\mu_w}{\mu_{\infty}}\right)^m, \tag{7-2-8}$$

where Ψ is calculated by formula (7-1-19) or by the approximating formula (7-1-25). The value of Ψ_f is taken from the graph in Fig. 6.2. The shape parameter f, which is needed for determination of $\bar{f}_{crit}=f/f_{crit}$ and subsequent determination of Ψ_f, is calculated by the formula

$$f=\frac{\mathrm{Re}^{**}_{00}}{\mathrm{Re}_{00}U^2(1-U^2)^{\frac{1}{k-1}}}\frac{dU}{d\bar{x}}. \qquad (7\text{-}2\text{-}9)$$

The quantity f_{crit} is determined by formulas (6-4-6), (6-4-7), (6-4-12) or by the graphs in Figs. 6.10 and 6.13. In the cross section where the shape parameter f reaches the value f_{crit}, the turbulent boundary layer separates from the wall.

For the subsonic gas flow region Eq. (7-2-7) is reduced to

$$\mathrm{Re}^{**}=\exp\left(-\frac{J}{m+1}\right)\left[\frac{(m+1)B}{2}\mathrm{Re}_0\int_{\bar{x}_0}^{\bar{x}}\Psi_t\bar{w}_0\exp(J)dx+C\right]^{\frac{1}{m+1}} \qquad (7\text{-}2\text{-}10)$$

where $\mathrm{Re}_0=\rho_0 w_{01}L/\mu_0$; w_{01} is the velocity at the outer edge of the boundary layer in the initial section $\bar{x}=\bar{x}_0$;

$$\bar{w}_0=w_0/w_{01};\quad J=(m+1)\int(1+H_{crit})\frac{d\bar{w}_0}{\bar{w}_0}.$$

The parameters H_{crit} and f_{crit} are found from formulas (6-4-11).

At constant wall temperature Ψ = const

$$\mathrm{Re}^{**}_w=\bar{w}_0^{-\varkappa}\left[\frac{1+m}{2}B\,\mathrm{Re}_{0w}\Psi_{t\infty}\int_{\bar{x}_0}^{\bar{x}}\bar{w}_0^{1+(1+m)\varkappa}dx+(\mathrm{Re}^{**}_w\bar{w}^{\varkappa}_0)^{1+m}_{\bar{x}_0}\right]^{\frac{1}{\varkappa(1+m)}} \qquad (7\text{-}2\text{-}11)$$

where

$$\mathrm{Re}^{**}_w=\rho_0 w_0\delta^{**}/\mu_w;\quad \mathrm{Re}_{0w}=\rho_0 w_{01}L/\mu_w;$$
$$\Psi_{t\infty}=\left(\frac{2}{\sqrt{\Psi}+1}\right)^2;\quad f=\mathrm{Re}^{**}_w/(\mathrm{Re}_{0w}\bar{w}_0)\,d\bar{w}_0/d\bar{x};\quad \varkappa=1+H_{crit}$$

The drag coefficient is calculated by the formula /135

$$c_f=\Psi_{t\infty}\Psi_f B(\mathrm{Re}^{**}_w)^{-m} \qquad (7\text{-}2\text{-}12)$$

For the case f flow around a plate (dP/dx = 0) the integral momentum relation has the form

$$\frac{d\,\mathrm{Re}^{**}}{d\bar{x}} = \mathrm{Re}_L \Psi \frac{B}{2\,\mathrm{Re}^{**m}} \tag{7-2-13}$$

Integrating we get

$$\mathrm{Re}^{**} = \left[\frac{B}{2}(m+1)\,\mathrm{Re}_L \int_{\bar{x}_0}^{\bar{x}} \Psi\, d\bar{x} + (\mathrm{Re}^{**}_T)^{m+1}_{\bar{x}_0} \right]^{\frac{1}{m+1}} \tag{7-2-14}$$

Taking Eq. (7-1-25) into account,

$$\mathrm{Re}^{**} = \left\{ \frac{(\bar{m}+1)B}{2} \mathrm{Re}_L \left[\frac{\operatorname{arctg} M_\infty \sqrt{r\frac{k-1}{2}}}{M_\infty \sqrt{r\frac{k-1}{2}}} \right] \int_{\bar{x}_0}^{\bar{x}} \left(\frac{2}{\sqrt{\Psi}+1} \right)^2 \times \left(\frac{\mu_w}{\mu_0} \right)^m d\bar{x} + (\mathrm{Re}^{**}_T)^{1+m}_{\bar{x}_0} \right\}^{\frac{1}{1+m}} \tag{7-2-15}$$

In the case of constant wall temperature

$$\mathrm{Re}^{**}_w = \left\{ \frac{(m+1)B}{2} \mathrm{Re}_{Lw} \left[\frac{\operatorname{arctg} M_\infty \sqrt{r\frac{k-1}{2}}}{M_\infty \sqrt{r\frac{k-1}{2}}} \right] \right.$$
$$\left. \times \left(\frac{2}{\sqrt{\Psi}+1} \right)^2 (\bar{x} - \bar{x}_0) + (\mathrm{Re}^{**}_w)^{1+m}_{\bar{x}=\bar{x}_0} \right\}^{\frac{1}{m+1}} \tag{7-2-16}$$

If the turbulent boundary layer grows from the leading edge of the plate,

$$\mathrm{Re}^{**}_w = \left\{ \frac{(m+1)B}{2} \left[\frac{\operatorname{arctg} M_\infty \sqrt{r\frac{k-1}{2}}}{M_\infty \sqrt{r\frac{k-1}{2}}} \right] \left(\frac{2}{\sqrt{\Psi}+1} \right)^2 \mathrm{Re}_{xw} \right\}^{\frac{1}{m+1}} \tag{7-2-17}$$

The local drag coefficient is determined from the equation /136

$$c_f = \Psi_\infty \frac{B}{\mathrm{Re}^{**m}_w} = B_1 \Psi_\infty^{\frac{1}{m+1}} \mathrm{Re}_{xw}^{-\frac{m}{m+1}} \tag{7-2-18}$$

Thus,

$$\left(\frac{c_f}{c_{f0}} \right)_{\mathrm{Re}_{xw}} = \Psi_\infty^{\frac{1}{m+1}}; \quad \left(\frac{c_f}{c_{f0}} \right)_{\mathrm{Re}_\infty} = \left(\frac{\mu_w}{\mu_0} \right)^{\frac{m}{m+1}} \Psi_\infty^{\frac{1}{m+1}} \tag{7-2-19}$$

For more accurate calculations we can use the second approximation, i.e. formula (7-1-19). In this case Eq. (7-2-18) is written as

$$c_f = \Psi \frac{B}{\mathrm{Re}^{**m}_w} \left(\frac{\mu_0}{\mu_w} \right)^m, \tag{7-2-20}$$

Ψ being determined by formula (7-1-19) and Re^{**}_{w} by formula (7-2-16). In the case of gas flow near the forward point of a blunt-nosed body, the velocity at the outer edge of the boundary layer varies according to the linear law

$$w_0 = cw_{01}\bar{x}, \tag{7-2-21}$$

where w_{01} is the free-stream velocity and $\bar{x} = x/D$.

The constant c depends on the shape of the body universed in the flow and is close to unity for blunt-nosed bodies. If it is assumed that $\Psi_f \approx 1$ for the accelerated flow region, then for the subsonic gas flow region at constant wall temperature

$$Re^{**} = 0{,}0136\Psi_t^{0.8} Re_{01}^{0.8} c^{0.8} \bar{x}^{1.62} \tag{7-2-22}$$

and the local friction coefficient is

$$\frac{c_f}{2} = 0{,}0375\Psi_t^{0.8} Re_{01}^{-0.2} c^{-0.2} \bar{x}^{-0.4}. \tag{7-2-23}$$

Thus, in contrast to longitudinal flow past a plate, where $c_f \sim \bar{x}^{-0.2}$, when the flow is crosswise to the plate, $c_f \sim \bar{x}^{-0.4}$. The mean drag coefficient is

a)
$$\bar{c}_{f_{long.}} = \frac{1}{L}\int_0^L c_f\, dx = 0{,}072\Psi_t^{0.8} Re_L^{-0.2}; \tag{7-2-24}$$

for longitudinal flow past a plate, and

b)
$$\bar{c}_{f_{trans}} = 0{,}125\Psi_t^{0.5} Re_L^{-0.2}; \tag{7-2-25}$$ /137

for a transverse flow.

Thus,

$$\frac{\bar{c}_{f\,trans}}{\bar{c}_{f\,long.}} = 1{,}732. \tag{7-2-26}$$

A number of other practical problems can be solved by means of the integral momentum relation. Thus, for example, it is not difficult to determine the law of change in area of a diffuser at whose walls the turbulent boundary layer is in the pre-separation state. In this case the frictional drag coefficient at the wall will equal zero and the integral momentum relation for the flow of an incompressible fluid in a plane diffuser is written as

$$\frac{d\delta^{**}}{dx} + \frac{\delta^{**}}{w_0}\frac{dw_0}{dx}(2 + H_{crit}) = 0 \tag{7-2-27}$$

or

$$\frac{d\delta^{**}}{\delta^{**}} = -(2 + H_{crit})\frac{dw_0}{w_0}. \tag{7-2-28}$$

Assuming in the first approximation that the boundary layer growing at the diffuser walls does not affect the parameter of the fluid in the flow case, the continuity equation can be written in the form

$$G=\rho_0 w_{01} F_1=\rho_0 w_0 F=\text{const}, \tag{7-2-29}$$

where F is the diffuser cross-sectional area, F_1 the area of the initial cross section beginning with which $f = f_{crit}$ and $cf = 0$, and w_{01} is the velocity of the fluid in the initial cross section.

After integrating, taking Eq. (7-2-29) into account, we have

$$\delta^{**}=\delta^{**}_1\left(\frac{F}{F_1}\right)^{2+H_{crit}} \tag{7-2-30}$$

where δ^{**}_1 is the momentum loss thickness in the initial section.

On the other hand, for the shape parameter f we have the formula

$$f_{crit}=\frac{\delta}{w_0}\frac{dw_0}{dx}=-\frac{\delta^{**}}{\bar{F}}\frac{d\bar{F}}{dx}, \tag{7-2-31}$$

where $\bar{F} = F/F_1$.

Taking Eq. (7-2-30) into account,

$$f_{crit}=-\delta^{**}_1(\bar{F})^{1+H_{crit}}\frac{d\bar{F}}{dx}. \tag{7-2-32}$$

After integrating we get

$$\bar{F}=\left[1-(2+H_{crit})\frac{f_{crit}}{\delta^{**}_1}(x-x_1)\right]^{\frac{1}{2+H_{crit}}} \tag{7-2-33}$$

If it is assumed that H_{crit} and f_{crit} are their limit values ($H_{crit} = 1.87$, $f_{crit} = -0.01$), then /138

$$\bar{F}=\left[1+\frac{0,0387}{\delta^{**}_1}(x-x_1)\right]^{\frac{1}{3,87}}. \tag{7-2-34}$$

The problem is solved analogously for a cooled diffuser, as well as for the flow of a compressible fluid. In particular, $H_{crit} \to 0$ for intense diffuser wall cooling conditions, when $\psi \to 0$, and it follows from (7-2-33) that

$$\bar{c}_f=\left[1+\frac{0,02}{\delta^{**}_1}(x-x_1)\right]^{1/2}. \tag{7-2-35}$$

Of great practical value for supersonic aviation is calculation of a supersonic diffuser without separation. The configuration of the throughput section of such diffuser,

corresponding to the pre-separation state of the boundary layer on the surface of a duct, can be determined by resorting to the integral momentum relation and the limit formulas for the critical shape parameters.

In the two-dimensional diffuser case the integral momentum relation for a boundary layer in the pre-separation state can be written as

$$\frac{d\delta^{**}}{dx}+\frac{\delta^{**}}{U}\frac{dU}{dx}(2+H_{crit})=0, \qquad (7\text{-}2\text{-}36)$$

where $U = w_0/w_{max}$.

The parameters U and ψ^* are interrelated by

$$\psi^*=\frac{1-(1-r)U^2}{1-U^2}. \qquad (7\text{-}2\text{-}37)$$

The dependence of H_{crit} on ψ^* and $\Delta\psi$, as was shown earlier (see (6-4-12)), can be approximated by the formula

$$H_{crit}=2{,}41\psi^*+1{,}38\psi^*(\bar{\psi}-1)-0{,}52. \qquad (7\text{-}2\text{-}38)$$

Integration of Eq. (7-2-36), with allowance for Eq. (7-2-38), yields

$$\frac{\delta^{**}}{\delta^{**}_1}=\left(\frac{U_1^2}{U^2}\right)^{[1{,}94-0{,}7(\bar{\psi}-1)]}\left(\frac{1-U^2}{1-U_1^2}\right)^{1{,}2+0{,}7(\bar{\psi}-1)}. \qquad (7\text{-}2\text{-}39)$$

The expression for the shape parameter f can be written in the form

$$f_{crit}=\frac{\delta^{**}}{2}\frac{1}{U^2}\frac{d(U^2)}{dx}. \qquad (7\text{-}2\text{-}40)$$

Substituting Eq. (7-2-39) into Eq. (7-2-40) and using the dependence of the shape parameter f_{crit} on ψ^* and $\Delta\psi$ obtained earlier (see Fig. 6.13), it is possible to determine the dependence of the dimensionless velocity U at the outer edge of the boundary layer on the longitudinal coordinate $\bar{x}$, corresponding to an attached gas flow in a supersonic, shockless diffuser. In particular, for the case of a heat-insulated wall we can use the formula /139

$$\frac{f_{crit}}{f_{crit_0}}\approx\psi^{*-1{,}88}=\left[\frac{1-(1-r)U^2}{1-U^2}\right]^{-1{,}88}. \qquad (7\text{-}2\text{-}41)$$

Then

$$\int_{a_1}^{a}\frac{[1-(1-r)U^2]^{1{,}88}}{(1-U^2)^{0{,}88}}\frac{d(U^2)}{(U^2)^{2{,}94}}=\frac{(1-U_1^2)^{1{,}2}}{(U_1^2)^{1{,}94}}\times\frac{2f_{crit_0}}{\delta^{**}_1}(x-x_1). \qquad (7\text{-}2\text{-}42)$$

The corresponding change in area of the duct throughput section is found from the continuity equation, which, for the conditions being considered, can be written conveniently as

$$U(1-U^2)^{\frac{k}{k-1}}F = U_1(1-U_1^2)^{\frac{1}{k-1}}F_1 = \text{const.} \tag{7-2-43}$$

The integral momentum relation for an axisymmetric boundary layer can be written in the form

$$\frac{d\mathrm{Re}^{**}_{\infty}}{d\bar{x}} + \frac{\mathrm{Re}_{\infty}}{R_a}\frac{dR_a}{d\bar{x}} = \mathrm{Re}_L\left[\Psi_M\Psi_t\Psi_f\frac{c_{f_0}}{2} - (1+H_{\mathrm{crit}})f_{\mathrm{crit}}\bar{\delta}^*\right]. \tag{7-2-44}$$

Linearizing the right-hand side of the equation, we get

$$\frac{d\,\mathrm{Re}^{**}_{\infty}}{d\bar{x}} + \mathrm{Re}^{**}_{\infty}\left[\frac{(1+H_{\mathrm{crit}})}{w_e}\frac{dw_e}{d\bar{x}} + \frac{1}{R_a}\frac{dR_a}{d\bar{x}}\right] = \mathrm{Re}_L\Psi_{Mt}\frac{c_{f_0}}{2}. \tag{7-2-45}$$

Taking H_{crit} = const on the first approximation, we get

$$\mathrm{Re}^{**}_{\infty} = \frac{m+1}{U^{1+H_{\mathrm{crit}}}R_a}\left[\frac{1+m}{2}B\mathrm{Re}_{\infty}\int_{\bar{x}_0}^{\bar{x}}(\Psi_t\Psi_M)_{\infty} \times\left(\frac{\mu_w}{\mu_{\infty}}\right)^m U^{1+(1+m)H_{\mathrm{crit}}}R_a^{1+m}(1-U^2)^{\frac{1}{k-1}}d\bar{x} + C\right]^{\frac{1}{m+1}} \tag{7-2-46}$$

For gas flow in a nozzle, the velocity at the outer edge of the boundary layer can be determined in the first approximation from a one-dimensional model. In this case the continuity equation (7-2-43) can be written as /140

$$U(1-U^2)^{\frac{1}{k-1}} = \left(\frac{k-1}{k+1}\right)^{0.5}\left(\frac{2}{k+1}\right)^{\frac{1}{k-1}}\frac{F_{\mathrm{crit}}}{F}, \tag{7-2-47}$$

where F_{crit} is the nozzle throat area.

Moreover, for accelerated streams the shape parameter H can be determined by formula (4-2-8). Consequently,

$$\mathrm{Re}^{**}_{\infty} = \frac{1}{U^{1+H}}\left\{\frac{1+m}{2}B\mathrm{Re}_{\infty}\bar{D}^{-(1+m)}\int_{\bar{x}_1}^{\bar{x}}(\Psi_t\Psi_M)_{\infty} \times\left(\frac{\mu_w}{\mu_{\infty}}\right)^m U^{(1+m)H}\bar{D}^{m-1}d\bar{x} + C\right\}^{\frac{1}{m+1}}, \tag{7-2-48}$$

where $\bar{D} = D/D_{crit}$.

The local drag coefficients are found by formula (7-2-8). Using Eq. (7-2-48) it is not difficult also to determine the velocity coefficient, which takes into account the

effect of the boundary layer on the flow parameters in the outlet section of the nozzle, since $\varphi = U_{av}/U_a = 1 - 2\left(\frac{\delta^{**}}{R}\right)$.

The integral energy relation for a two-dimensional boundary layer at an impermeable wall in the absence of internal heat sources can be written conveniently as

$$\frac{d\,\mathrm{Re}^{**}_{T00}}{d\bar{x}} + \frac{\mathrm{Re}^{**}_{T00}}{\Delta i_\Sigma}\frac{d\,(\Delta i_\Sigma)}{d\bar{x}} = \mathrm{Re}_L\,\mathrm{St}_\Sigma. \tag{7-2-49}$$

Using (2-6-4) and the invariancy of the heat transfer law under change of boundary conditions, we have

$$\mathrm{Re}^{**}_{T00} = \frac{1}{\Delta i_\Sigma}\left\{\frac{1+m}{2\mathrm{Pr}^n} B\,\mathrm{Re}_{00}\int_{\bar{x}_1}^{\bar{x}} \Psi_\infty \left(\frac{\mu_w}{\mu_{00}}\right)^m U\,(1-U^2)^{\frac{1}{k-1}} \times \Delta i_\Sigma^{(1+m)}\,d\bar{x} + (\mathrm{Re}^{**}_{T00}\Delta i_\Sigma)^{1+m}_{\bar{x}=\bar{x}_1}\right\}^{\frac{1}{1+m}} \tag{7-2-50}$$

Accordingly, for an axisymmetric boundary layer /141

$$\mathrm{Re}^{**}_{T00} = \frac{1}{\Delta i_\Sigma \bar{D}}\left\{\frac{1+m}{2\mathrm{Pr}^n} B\,\mathrm{Re}_{00}\int_{\bar{x}_1}^{\bar{x}} \Psi_\infty \left(\frac{\mu_w}{\mu_{00}}\right)^m U\,(1-U^2)^{\frac{1}{k-1}} \times \Delta i_\Sigma^{1+m}\bar{D}^{1+m}\,d\bar{x} + (\mathrm{Re}^{**}_{T00}\Delta i_\Sigma \bar{D})^{1+m}_{\bar{x}=\bar{x}_1}\right\}^{\frac{1}{m+1}}. \tag{7-2-51}$$

For the case of gas flow in a supersonic nozzle with allowance for Eq. (7-2-47) we get

$$\mathrm{Re}^{**}_{T00} = \frac{1}{\Delta i_\Sigma \bar{D}}\left\{\frac{1+m}{2\,\mathrm{Pr}^n} B\,\mathrm{Re}_{00}\int_{\bar{x}_1}^{\bar{x}} \Psi_\infty \left(\frac{\mu_w}{\mu_{00}}\right)^m \bar{D}^{m-1}\Delta i_\Sigma^{1+m}\,d\bar{x} + (\mathrm{Re}^{**}_{T00}\Delta i_\Sigma \bar{D})^{1+m}_{\bar{x}=\bar{x}_1}\right\}^{\frac{1}{m+1}}. \tag{7-2-52}$$

The local values of the Stanton number and the magnitude of the specific heat fluxes are determined by the formulas

$$\mathrm{St}_\Sigma = \Psi_S \frac{B}{2\,\mathrm{Re}^{**n}_{T00}\,\mathrm{Pr}^n}\left(\frac{\mu_w}{\mu_{00}}\right)^m; \tag{7-2-53}$$

$$q_w = \mathrm{St}_\Sigma \rho_0 w_0 \Delta i_\Sigma; \tag{7-2-54}$$

Ψ_S is determined by formula (7-1-19) or by the approximation formula (7-1-25).

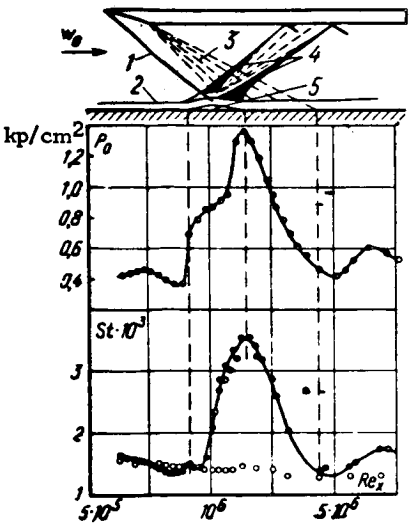

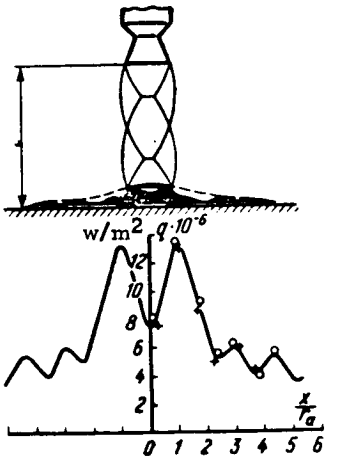

FIG. 7.9. Distribution of pressure and Stanton number on a flat surface in the zone of shock interaction with a turbulent boundary layer. $M_0 = 2.51$; $v_0 = 572$ m/sec; $\rho_0 = 0.11$ kg · sec^2/m^4 = 0.41 kp/cm^2; 1—incident shock; 2—boundary layer; 3—rarefaction wave; 4—shock system; 5—separation zone. Experimental points: ●—15° wedge; o—boundary layer without shock.

FIG. 7.10. Heat flux distribution for interaction of a supersonic jet with a flat surface. $M_0 = 2.27$ in the Mach number at the nozzle exit; $n = P_c/P_a = 0.8$ in the off-design factor; $\bar{l} = l/d_c = 3$; $\alpha = 90°$; $k = 1.14$.

It must be kept in mind that when compression shocks occur in a supersonic stream, the shock has a substantial effect on the intensity of the heat transfer.

Shown in Fig. 7.9 are the results of measuring the local heat-transfer coefficients in the zone of shock interaction with a turbulent boundary layer, done by Yu. V. Baryshev [7]. As can be seen from this figure, the shock can increase the heat transfer coefficient by a factor of 2.5.

Analogous results are obtained for interaction of a supersonic jet with a flat surface. Presented in Fig. 7.10 are the experimental results of I. K. Ermolaev and V. A. Fadeev [27].

For the subsonic gas flow region, $\Delta i_\tau = C_p \Delta T$, $U \ll 1$ and Eqs. (7-2-50) and (7-2-51) change to /142

$$\mathrm{Re}^{**}_T = \frac{1}{\Delta T}\left\{\frac{1+m}{2\mathrm{Pr}^n} B\,\mathrm{Re}_{x_1} \int_{\bar{x}_1}^{\bar{x}} \Psi_\infty \left(\frac{\mu_w}{\mu_0}\right)^m u_0 \Delta T^{1+m} d\bar{x} + (\mathrm{Re}^{**}_T \Delta T)^{1+m}_{\bar{x}=\bar{x}_1}\right\}^{\frac{1}{m+1}} \qquad (7\text{-}2\text{-}55)$$

Accordingly, for an axisymmetric flow

$$\mathrm{Re}^{**}_{T}=\frac{1}{\Delta\bar{T}\bar{D}}\left\{\frac{1+m}{2\mathrm{Pr}^{n}}B\,\mathrm{Re}_{0}\int_{\bar{x}_1}^{\bar{x}}\Psi_{\infty}\left(\frac{\mu_w}{\mu_0}\right)^{m}\bar{w}_0\Delta T^{1+m}\bar{D}^{1+m}dx+(\mathrm{Re}^{**}_{T}\Delta T\bar{D})^{1+m}_{\bar{x}=\bar{x}_1}\right\}^{\frac{1}{m+1}}. \quad (7\text{-}2\text{-}56)$$

For flow around a plate with a constant wall temperature and turbulent boundary layer generation at the leading edge of the plate, we get from Eq. (7-2-49) /143

$$\mathrm{Re}^{**}_{T_w}=\left[\frac{1+m}{2\mathrm{Pr}^{n}}B\Psi_{S\infty}\mathrm{Re}_{x_w}\right]^{\frac{1}{m+1}}; \quad (7\text{-}2\text{-}57)$$

$$\mathrm{St}_x=\frac{B^{\frac{1}{m+1}}\Psi_{S\infty}}{2\,\mathrm{Pr}^{n}\left(\frac{1+m}{2\,\mathrm{Pr}^{n}}B\right)^{\frac{m}{m+1}}}\mathrm{Re}_{x_w}^{-\frac{m}{m+1}}. \quad (7\text{-}2\text{-}58)$$

When m = 0.25 and B = 0.0256

$$\mathrm{St}_x=0{,}0288\,(\Psi_S)^{0.8}\mathrm{Re}_{x_w}^{-0.2}\mathrm{Pr}^{-0.8}, \quad (7\text{-}2\text{-}59)$$

where Ψ_S is determined by formula (7-1-19) or (7-1-25).

For flow around a blunt-nosed body with a constant surface temperature we have

$$\mathrm{Re}^{**}_{T_w}=\left[\frac{1+m}{2\,\mathrm{Pr}^{n}}B\,\mathrm{Re}_{01w}\Psi_{S_\infty}\frac{C\bar{x}^2}{2}\right]^{\frac{1}{m+1}}; \quad (7\text{-}2\text{-}60)$$

$$\mathrm{St}_x=\frac{B}{2\,\mathrm{Pr}^{0.75}}\frac{\Psi_S^{\frac{1}{m+1}}}{\left[\frac{1+m}{2\,\mathrm{Pr}^{0.75}}B\frac{C}{2}\bar{x}^2\,\mathrm{Re}_{01w}\right]^{\frac{m}{m+1}}}. \quad (7\text{-}2\text{-}61)$$

In particular, for the case of transverse flow around a plate with m = 0.25, B = 0.256, n = 0.75, c = 1.0,

$$St=0{,}0375\Psi_S^{0.8}(\mathrm{Re}_{01w})^{-0.2}\bar{x}^{-0.4}\mathrm{Pr}^{-0.8}. \quad (7\text{-}2\text{-}62)$$

Whenever the specific heat flux distribution is prescribed the energy equation can be reduced to the form

$$\frac{d\,(\mathrm{Re}^{**}_{T\infty}\Delta i_x)}{d\bar{x}}=\frac{1}{\mathrm{Pr}_{\infty}}\frac{q_{wx}L}{\lambda_{\infty}}. \quad (7\text{-}2\text{-}63)$$

/144

For the boundary conditions $\mathrm{Re}^{**}_{T_{00}}=0$ at $\bar{x}=0$ we have

$$Re^{**}_{T\infty} = St_x Re_{L\infty} \frac{\int_0^{\bar{x}} q_{w\bar{x}} d\bar{x}}{q_{w\bar{x}}} \qquad (7\text{-}2\text{-}64)$$

When the heat-transfer law is conservative to the heat load distribution we get

$$St_x = \left(\frac{B\Psi_S}{2\,Pr^n}\right)^{\frac{1}{m+1}} \left(\frac{\mu_w}{\mu_\infty}\right)^{\frac{m}{m+1}} \left[Re_{L\infty} \frac{\int_0^{\bar{x}} q_{w\bar{x}}\, d\bar{x}}{q_{w\bar{x}}}\right]^{-\frac{m}{m+1}} \qquad (7\text{-}2\text{-}65)$$

In the case q_w = const and $Re^{**}_T = 0$ at $\bar{x} = 0$ we have

$$Re^{**}_T = StRe_x \qquad (7\text{-}2\text{-}66)$$

and

$$St^{**} = A^{\frac{1}{m+1}} Re_x^{-\frac{m}{m+1}}. \qquad (7\text{-}2\text{-}67)$$

Taking B/2 = 0.0128 and m = 0.25, we get from Eq. (7-2-67) an equation which was derived earlier for the case of flow around a flat plate. Thus, from the condition of heat-transfer law conservative to a change in velocity around an immersed body it follows that for any laws of velocity variation and for a constant thermal stress the equation for a flat plate will hold if the local values of the free-stream parameters are introduced into the Re_x. It is easy to demonstrate that this conclusion can also be applied to the more general case of an arbitrary heat-load distribution.

7.3. Conservative Properties of the Heat-Transfer Law to Changes in Wall Boundary Conditions

In Chapter 6 it was shown that the heat-transfer law is more conservative to changes in the longitudinal pressure gradient than the frictional drag law, and for practical thermal boundary-layer calculations the effect of the longitudinal pressure gradient on the heat-transfer law can be disregarded.

An analogous result is also obtained when the heat-transfer law is affected by changes in the thermal conditions on the heat-transfer surface (i.e. in the laws of variation of wall temperature or thermal stress). Given in [72] are the results of an experimental investigation of the effect of changes in the boundary conditions on heat-transfer laws in the case of flow around a flat plate. /145

A diagram of the experimental section is shown in Fig. 7.11 and the laws of distribution of T_w and q_w over the length of the plate in Fig. 7.12. The experimental data were processed by the method of local simulation [70] in the form of the relation $St_0 = f(Pe^{**}_T)$, where $Pe^{**}_T = Re^{**}_T Pr$;

$$\left.\begin{aligned} \mathrm{St}_0 = \frac{q_w}{\gamma_0 w_0 C_p (T_w - T_0)}\,;\quad \delta^{**}_T = \frac{\int_0^x q_w\,dx}{\gamma_0 w_0 C_p (T_w - T_0)}\,; \\ \mathrm{Pe}^{**}_T = \frac{w_0 \delta^{**}_T}{a}. \end{aligned}\right\} \qquad (7\text{-}3\text{-}1)$$

The results of processing the experimental data are presented in Fig. 7.13 as can be seen from the graph. All the experimental points, except those of the last two modes, fit, in general, relation (2-6-4), regardless of the form of the boundary conditions.

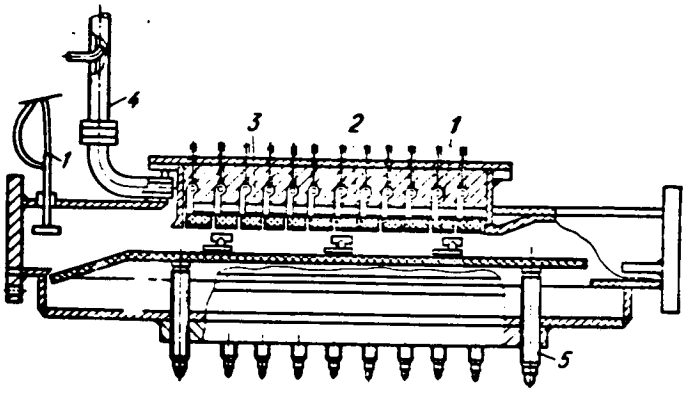

FIG. 7.11. Diagram of the experimental section for investigation of the conservatism of the heat-transfer law to variation of the boundary conditions: 1—Prandtl tube; 2—flexible band; 3—calorimeters; 4—ejector for boundary layer suction; 5—band adjustment values.

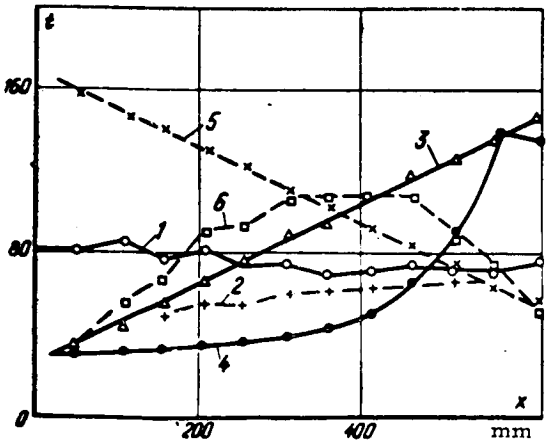

FIG. 7.12

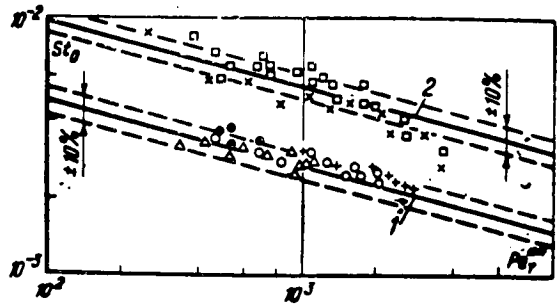

FIG. 7.13

FIG. 7.12. Variation in wall temperature, °C, over the length of a plate for various boundary conditions [72]: 1—ΔT = const; 2—q_w = const; 3—$\Delta T = b + d_0\bar{x}$; 4—$q_w = q_0 \exp(k\bar{x})$; 5—$\Delta T = b - d_0 x$; 6—$q_w = q_0 \sin(\pi\bar{x})$.

FIG. 7.13. Heat-transfer law for various boundary conditions [72]. The quantity $St_0 \cdot A$ is plotted on the ordinate axis: 1—A = 1; 2—A = 2; o—ΔT = const; Δ - $\Delta T = b + d_0 x$; ●-$q_w = q_0 \exp(k\bar{x})$; + -q_0 = const; x - $\Delta T = b - d_0 x$; □—$q_w = q_0 \sin(\pi\bar{x})$.

The graph reveals that the experimental points are clearly stratified as a function of the boundary conditions and are in satisfactory agreement with the corresponding analytical relations obtained by integrating Eq. (7-2-49) for given boundary conditions. The integral in Eq. (7-2-49) for a given law of wall temperature variation has the form, taking (2-6-4) into account, /147

$$\mathrm{Re}^{**}_{T} = \frac{1}{\Delta T}\left[\frac{(1+m)}{2\mathrm{Pr}^{0.75}} B\,\mathrm{Re}_{L}\int_{0}^{\bar{x}} \Delta T^{1+m}\,d\bar{x}\right]^{\frac{1}{1+m}} \qquad (7\text{-}3\text{-}2)$$

and, accordingly, for a given heat stress distribution

$$\mathrm{Re}^{**}_{T} = \left[\frac{B}{2\,\mathrm{Pr}^{0.75}}\,\mathrm{Re}_{L}\,\frac{1}{q_{w}}\int_{0}^{\bar{x}} q_{cT}\,d\bar{x}\right]^{\frac{1}{1+m}}. \qquad (7\text{-}3\text{-}3)$$

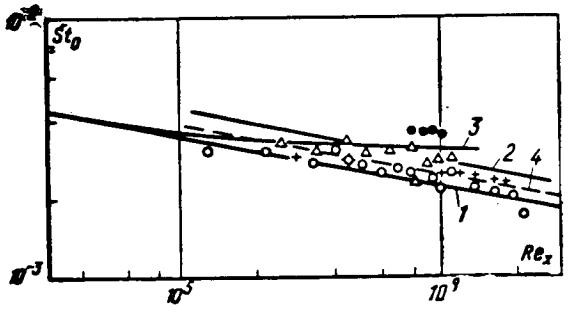

FIG. 7.14. Dependence of St_0 on Re_x for various boundary conditions: 1—formula (7-3-4); 2—formula (7-3-5); 3—formula (7-3-7); 4—formula (7-3-6); o—ΔT = const, Δ - $\Delta T = b + d_0\bar{x}$; ●—$T_w = q_0 \exp(k\bar{x})$; + -$q_w$ = const.

From Eqs. (2-6-4), (7-3-2) and (7-3-3) we get:

a) for the case ΔT = const

$$St_0 = \frac{0.0288}{\mathrm{Re}_x^{0.2}\,\mathrm{Pr}^{0.6}}; \qquad (7\text{-}3\text{-}4)$$

b) for the case $\Delta T = d_0 x$

$$St_0 = \frac{0.0338}{\mathrm{Re}_x^{0.2}\,\mathrm{Pr}^{0.6}}; \qquad (7\text{-}3\text{-}5)$$

c) for the case q_w = const

$$St_0 = \frac{0.0306}{\mathrm{Re}_x^{0.2}\,\mathrm{Pr}^{0.6}}; \qquad (7\text{-}3\text{-}6)$$

d) for the case $q_w = q_0 \exp(k\bar{x})$ /148

$$St_0 = \frac{0.0306(k\bar{x})^{0.2}}{\mathrm{Re}_x^{0.2}\,\mathrm{Pr}^{0.6}}\left(\frac{\exp k\bar{x}}{\exp k\bar{x} - 1}\right)^{0.2}; \qquad (7\text{-}3\text{-}7$$

e) for the case $q_w = q_0 \sin\left(\frac{\pi}{b} x\right)$

$$St_x = \frac{0{,}0306\left(\frac{\pi\bar{x}}{b}\right)^{0.2}}{Re_x^{0.2}\,Pr^{0.6}}\left[\frac{\sin\left(\frac{\pi\bar{x}}{b}\right)}{1-\cos\left(\frac{\pi\bar{x}}{b}\right)}\right]^{0.2}. \qquad (7\text{-}3\text{-}8)$$

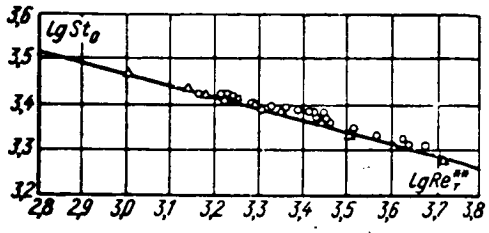

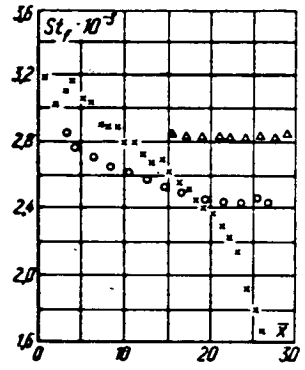

FIG. 7.15. Heat-transfer law for the initial section of the pipe; curve calculated by (2-6-4): the points are from [150]; Δ - $q_w = q_0 \sin\left(\frac{\pi}{6}\bar{x}\right)$; □ - $q_w = q_0 \exp(a\bar{x})$; o - q_w = const.

FIG. 7.16. Distribution of the local values of the Stanton number over the pipelength is the expiments of Hall and Price [150]. St_f - Stanton number determined from the wall temperature gradient and the mean mass temperature; Δ - $q_w = q_0 \exp(ax)$; x - $q_w = q_0 \sin\left(\frac{\pi}{6}x\right)$; o - q_w = const.

The results of an analogous processing of the experimental data of Hall and Price [150] which were obtained for three different heat-supply laws, are given in Fig. 7.15. The initial data for the distribution of local heat-transfer coefficients over the pipe length are shown in Fig. 7.16. The experiments were carried out with a developed dynamic boundary layer at the pipe inlet and with relatively small temperature drops. In such a case the variation of the gas parameter over the pipe length can be disregarded and formulas (7-3-6), (7-3-7), (7-3-8) can be used. As is evident from Fig. 7.15, the experiments of Hall and Price are in good agreement with heat-transfer law (2-6-4) for all the boundary conditions investigated.

A comparison of the experimental data with (7-3-6)-(7-3-8) is given in Fig. 7.17. It is interesting to note that in the experiments of Hall and Price the thermal and dynamic boundary layers did not develop simultaneously, but the computational results obtained assuming a consecutive heat-transfer law are in satisfactory agreement /149 with experiment. This conclusion receives further confirmation by comparing the

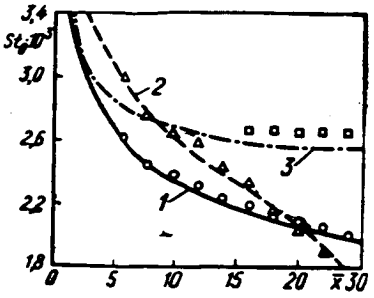

FIG. 7.17. Distribution of the local values of the Stanton number over the length of the initial section of the pipe. 1—calculated by (7-3-6); 2—by (7-3-8); 3—by (7-3-7); the experiments of Hall and Price [150]: o—q_w = const; Δ—$q_w = q_0 \sin\left(\frac{\pi}{6}\bar{x}\right)$; □—$q_w = q_0 \exp(a\bar{x})$.

results of calculating the heat transfer by the proposed method with the experiments of Eichhorn, Eckert and Anderson [136], in which measurements were made of local heat fluxes for flow of an air stream past a flat plate. The plate had an initial heat-insulated section of length x_0 and a subsequent linear variation in wall temperature over the length:

$$\Delta T = \frac{d(\Delta T)}{dx}(x - x_0). \tag{7-3-9}$$

The heat-transfer law for the laminar boundary layer can be written as

$$St_0 = \frac{0.22}{Re_T^{\infty} Pr^{4/3}}. \tag{7-3-10}$$

Then the solution of Eq. (7-2-49), taking (7-3-10) and (2-6-4) into account, can be represented as follows: /150

a) for a laminar boundary layer

$$\frac{q_w}{Pr^{1/3}\lambda\frac{d(\Delta T)}{dx}\cdot 0.332\sqrt{Re_x}} = \sqrt{3}\sqrt{1-\frac{x_0}{x}}; \tag{7-3-11}$$

b) for a turbulent boundary layer

$$\frac{q_w}{Pr^{1/3}\lambda\frac{d(\Delta T)}{dx}\cdot 0.0296\,Re_x^{0.8}} = 1.18\left(1-\frac{x_0}{x}\right)^{0.8}. \tag{7-3-12}$$

Given in Fig. 7.18 is a comparison of the experiments of [136] with formulas (7-3-11) and (7-3-12). Also plotted in this graph are curves calculated for an isothermal plate. It can be deduced that in this case also the assumption of heat-transfer laws stable to a change in the boundary conditions is fully applicable.

The results are in agreement with an analysis of the conservative properties of a turbulent boundary layer made by V. M. Ievlev [30, 31]. According to Ievlev, the relative error in St_0 stemming from disregard of the boundary condition effect on the heat-transfer law is defined by the inequality /151

$$\frac{\Delta St}{St_0} < 0.1\left[\frac{Re^{**}_T}{St_0 Re_L}\frac{d(\Delta T)}{dx}\right] \tag{7-3-13}$$

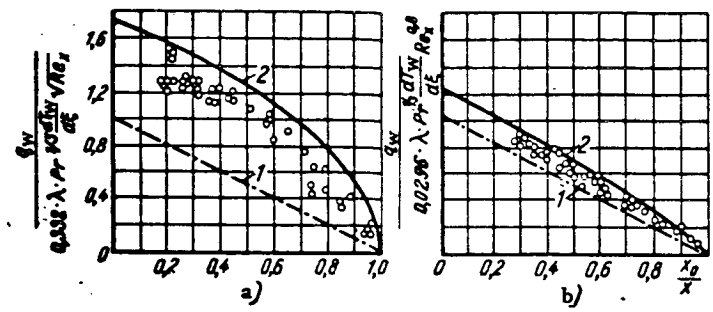

FIG. 7.18. Effect of wall temperature variation over the plate length on heat released. a—laminar boundary layer: 1—calculated by the dimensionless formula for an isothermal surface; 2—calculated by (7-3-11); b—turbulent boundary layer: calculated by the dimensionless formula for an isothermal surface; 2—calculated by (7-3-12). The points are the experiments of [136].

For the boundary conditions $q_w = q_0 \exp(k\bar{x})$ we get

$$\frac{\Delta St}{St_0} < 0{,}1 \frac{\exp(k\bar{x}) - 1}{\exp(k\bar{x})}$$

or

$$\frac{\Delta St}{St_0} < 0{,}1,$$

since $k > 0$, $0 < \bar{x} < 1$.

An analogous result is obtained also for $\Delta T = b + d_0\bar{x}$. In this case

$$\frac{Re^{**}_T}{St_0 Re_L \Delta T} \frac{d(\Delta T)}{d\bar{x}} = 0{,}55 \left[1 - \left(\frac{b}{d_0\bar{x} + b}\right)^{2.25}\right] \qquad (7\text{-}3\text{-}14)$$

and

$$\frac{\Delta St}{St_0} < 0{,}055.$$

But the error in determining St_0 increases if the boundary conditions correspond to a decrease in wall temperature or heat flow over the plate length. In particular, for the case $\Delta T = b - d_0\bar{x}$, we get

$$\frac{Re^{**}_T}{St_0 Re_L \Delta T} \frac{d(\Delta T)}{d\bar{x}} = 0{,}55 \left[\left(\frac{b}{b - d_0\bar{x}}\right)^{2.25} - 1\right], \qquad (7\text{-}3\text{-}15)$$

and, since $\left(\frac{b}{b - d_0\bar{x}}\right) > 1$ we find $\Delta St/St_0 \geq 0.055$.

This conclusion is supported by the experiments in Fig. 7.13. The methods of calculating a turbulent boundary layer for similar conditions are presented in Chapter 9.

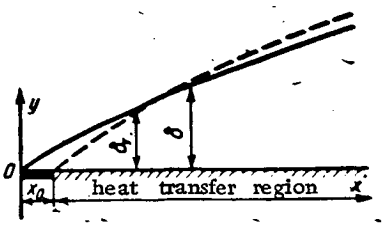

FIG. 7.19. Plate with initial heat-insulated section (Pr = 0.72).

In some cases the dynamic and thermal boundary layer do not develop simultaneously, even when Pr = 1, $\delta \neq \delta_T$. Let us examine flow over one plate with an initial heat-insulated section (Fig. 7.19) of length x_0, /152 at the station $x = x_0$ heat begins to be exchanged between the plate and the gas. The thermal boundary layer forming in the initial section is submerged in the dynamic layer. Setting Pr = 1, $\rho = \rho_0$, $\beta_T = 0$, $l_T = l$, $\bar{q} = \bar{q}_0$ and $\delta > \delta_T$, we reduce Eq. (2-1-12) to the form

$$q_0 \mathrm{St} = l^2 \frac{\partial \omega}{\partial y} \frac{\partial \vartheta}{\partial y}. \tag{7-3-16}$$

On the other hand, for these conditions it follows from (1-3-6) that

$$l \frac{\partial \omega}{\partial y} = \sqrt{\frac{c_{f0}}{2} \tilde{\tau}_0}. \tag{7-3-17}$$

From these equations, taking $\tilde{\tau}_0 \approx \tilde{q}_0$ and integrating, we get

$$\frac{2\,\mathrm{St}}{c_{f0}} (\omega_T - \omega_{10}) = 1 - \vartheta_{10}. \tag{7-3-18}$$

Taking (2-3-10) into account,

$$\omega_T = \left(\frac{\delta_T}{\delta}\right)^n. \tag{7-3-19}$$

The dimensionless temperature difference at the boundary of the viscous sublayer, assuming that $\tilde{q}_0$ is constant in this region, is

$$\vartheta_{10} = \mathrm{St}\,\mathrm{Pr}\,\eta_{T0} \sqrt{\frac{2}{c_{f0}}} \tag{7-3-20}$$

or

$$\vartheta_{10} = \frac{2\mathrm{St}}{c_{f0}} \mathrm{Pr}\,\omega_{10}. \tag{7-3-21}$$

Substituting this value of ϑ_{10} into (7-3-18), we find that when Pr = 1

$$\frac{2\mathrm{St}}{c_{f0}} = \frac{1}{\omega_T}. \tag{7-3-22}$$

Let us assume in the first approximation that the conservative properties of the heat-transfer law can be used to determine Re^{**}_T. Then, for n = 1/7 and Pr = 1, by integrating the equations

$$\frac{d\,\mathrm{Re}^{**}_T}{d\mathrm{Re}_x} = \frac{0{,}0128}{\mathrm{Re}^{**0{,}25}_T}, \tag{7-3-23}$$

$$\frac{d\mathrm{Re}^{**}}{d\,\mathrm{Re}_x} = \frac{0{,}0128}{\mathrm{Re}^{**0{,}25}} \qquad (7\text{-}3\text{-}24)$$

from x_0 to x in the first case and from x = 0 to x in the second and assuming in the first approximation that $\delta^{**}/\delta \approx \delta^{**}_T/\delta_T$, we get

$$\frac{\delta_T}{\delta} = \left(\frac{x - x_0}{x}\right)^{0{,}8}. \qquad (7\text{-}3\text{-}25)$$

Accordingly,

$$\frac{2\mathrm{St}}{c_{f0}} = \left(\frac{x}{x - x_0}\right)^{0{,}111}. \qquad (7\text{-}3\text{-}26)$$

Given in Fig. 7.20 is a comparison of the experimental data of Reynolds, Kays and Kline [199] with (7-3-26). As can be seen from the graph, the first approximation yields completely satisfactory results. Taking into account Eq. (7-3-26) and the assumption $\mathrm{Re}^{**}_T = (\delta_T/\delta)\,\mathrm{Re}^{**}$, we get a correction to the heat-transfer law in the first approximation: /153

$$\mathrm{St} = \frac{0{,}0128}{\mathrm{Re}_T^{**0{,}25}} \left(\frac{x - x_0}{x}\right)^{0{,}889} \qquad (7\text{-}3\text{-}27)$$

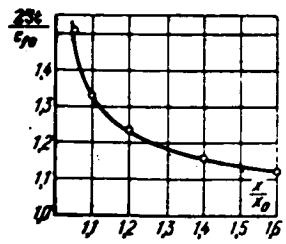

FIG. 7.20. Heat released to a plate with an initial heat-insulated section. The curve was calculated by (7-3-26); the points represent the experiments of [199].

or

$$\frac{\mathrm{St}}{\mathrm{St}_0} = \left(\frac{x - x_0}{x}\right)^{0{,}889}, \qquad (7\text{-}3\text{-}28)$$

where

$$\mathrm{St}_0 = \frac{0{,}0128}{\mathrm{Re}_T^{**0{,}25}}.$$

The second approximation does not add much to the accuracy of this result.

The results of calculating the ratio $\mathrm{St}/\mathrm{St}_0$ by (7-3-28) are presented in Table 7.3.

Introducing the correction into the Prandtl number, it is convenient to write (7-3-26) as

$$\mathrm{St} = \frac{0{,}0288}{\mathrm{Re}_\Delta^{0{,}2}\mathrm{Pr}^{0{,}6}} \left(\frac{x - x_0}{x}\right)^{0{,}889} \qquad (7\text{-}3\text{-}29)$$

Table 3. Data of calculation by (7-3-28)

x/x_0	1,0	1,10	1,25	1,50	1,75	2	3	∞
St/St_0	0	0,81	0,87	0,91	0,93	0,94	0,95	1,0

or

$$Nu_\Delta = 0{,}0288 Re_\Delta^{0,8} Pr^{0,4} \left(\frac{x - x_0}{x}\right)^{0,889}, \qquad (7\text{-}3\text{-}30)$$

where

/154

$$Re_\Delta = \frac{w_0 (x - x_0)}{\nu}; \quad Nu_\Delta = \frac{\alpha (x - x_0)}{\lambda}.$$

Thus, for $x/x_0 > 1.7$, it can be assumed, with an error not exceeding 8%, that

$$Nu_\Delta = 0{,}0288 Re_\Delta^{0,8} Pr^{0,4}. \qquad (7\text{-}3\text{-}31)$$

But if as the characteristic dimension in Eq. (7-3-31) we take the total plate length, the error with $x/x_0 \approx 1.7$ will be about 30%. For the average value of the Nusselt number we get from (7-3-31)

$$\overline{Nu}_\Delta = 0{,}037 Re_\Delta^{0,8} Pr^{0,4}. \qquad (7\text{-}3\text{-}32)$$

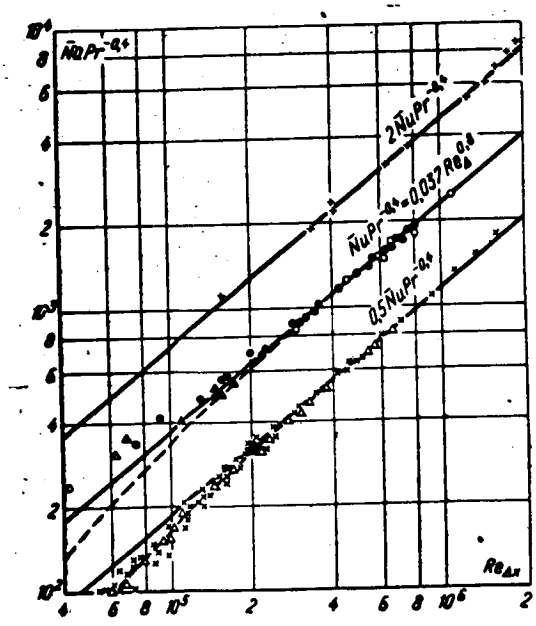

FIG. 7.21. Comparison of the experimental data on heat transfer to a plate with (7-3-32). The dashed lines represent calculation of the initial laminar section.

Formula (7-3-32) was proposed by M. A. Mikheev [74] on the basis of a generalization of the experimental data on heat transfer with an advance heat-insulated section. The results of this analysis are presented in Fig. 7.21.

7.4. Friction and Heat Transfer for Gas Flow in the Initial Section of a Cylindrical Pipe with Impermeable Walls

/155

In the inlet section of a pipe the boundary layer develops as in external flow past a plate until the boundary layers, increasing on opposite walls, intersect. Therefore, in order to calculate the processes of heat and mass transfer and of friction in the inlet portion of a pipe we can use all the methods presented above for calculation of a turbulent boundary layer. The difference between this "inner" problem and outer flow consists in the fact that the gas velocity at the outer edge of the boundary layer is not a given parameter, but one being sought. To determine this velocity in the inner problem, however, we have an additional relation, the equation of constant mass flow over the length of the pipe.

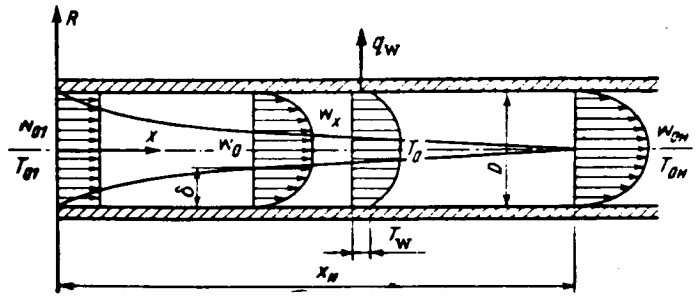

FIG. 7.22. Diagram of fluid flow in the initial portion of a cylindrical pipe (Pr ≈ 1).

Consider a flow of gas in the initial section of a cylindrical pipe (Fig. 7.22). The distribution of velocities and temperatures at the pipe inlet is taken to be uniform in cross section. We shall assume that the dynamics and thermal turbulent boundary layers grow simultaneously from the initial section of the pipe downstream.

The continuity equation is written as

$$\rho_{01}\omega_{01} = 2\int_0^{R_0} \rho w R\, dR = \text{const}, \qquad (7\text{-}4\text{-}1)$$

where ρ_{01} and ω_{01} are the density and velocity of the gas in the initial section of the pipe.

For a cylindrical pipe

$$\delta^* = \int_0^{\delta} \left(1 - \frac{\rho w}{\rho_0 \omega_0}\right)\left(1 - \frac{y}{R_0}\right) dy. \qquad (7\text{-}4\text{-}2)$$

Then the continuity equation is written as

/156

$$\rho_{01}\omega_{01} = \rho_0\omega_0\left(1 - 2\frac{\delta^*}{R_0}\right), \tag{7-4-3}$$

where ρ_0 and ω_0 are the density and velocity of the gas in the flow core at section x.

Taking into account the dependence of the gas density on the dimensionless velocity

$$\frac{\rho_0}{\rho_{00}} = (1 - U^2)^{\frac{1}{k-1}} \tag{7-4-4}$$

we have

$$2\frac{\delta^*}{R_0} = 1 - \frac{U_1}{U}\left(\frac{1 - U_1^2}{1 - U^2}\right)^{\frac{1}{k-1}}. \tag{7-4-5}$$

Introducing the shape parameter H, we get

$$\mathrm{Re}^{**}_{00} = \frac{\mathrm{Re}_{00}}{4H}\left[U(1 - U^2)^{\frac{1}{k-1}} - U_1(1 - U_1^2)^{\frac{1}{k-1}}\right], \tag{7-4-6}$$

where $\mathrm{Re}_{00} = \rho_{00}\omega_{\max}D/\mu_{00}$; $\mathrm{Re}^{**}_{00} = \rho_0\omega_0\delta^{**}/\mu_{00}$.

The momentum equation is written in the form

$$\frac{d\mathrm{Re}^{**}_{00}}{d\bar{x}} + \frac{\mathrm{Re}^{**}_{00}dU}{Ud\bar{x}}(1 + H) = U(1 - U^2)^{\frac{1}{k-1}} \times \omega_{00}\frac{B}{2}\left(\frac{\mu_w}{\mu_{00}}\right)^m \frac{1}{\mathrm{Re}^{**m}_{00}}. \tag{7-4-7}$$

For the supersonic gas velocity region at the pipe inlet the flow will always be divergent, but at small values of M the value of the shape parameter f will not be greatly different from zero. As can be seen from Fig. 4.6, the shape parameter

$$H' = \frac{1}{\delta^{**}}\int_0^{\delta}\left(1 - \frac{\omega_x}{\omega_0}\right)\frac{\rho}{\rho_0}dy \tag{7-4-8}$$

is much less dependent on the nonisothermicity parameters than the shape parameter H. The shape parameters H and H' are interrelated as follows:

$$H = \frac{1}{1 - U^2}\left(U^2 + H' - \frac{\Delta T}{T_{00}}H'_T\frac{\mathrm{Re}^{**}_{T\infty}}{\mathrm{Re}^{**}_{00}}\right),$$

where

$$H'_T = \frac{1}{\delta^{**}_T}\int_0^{\delta_T}(1 - \theta)\frac{\rho}{\rho_0}dy. \tag{7-4-9}$$

Then /157

$$H = \frac{1}{1 - U^2}\left[U^2 + 1.3\left(1 - \frac{T^*_w - T_w}{T_{00}}\right)\right]; \tag{7-4-10}$$

$$\mathrm{Re}^{**}_{00}=\frac{\mathrm{Re}_{00}\left[(1-U^2)^{\frac{1}{k-1}}U-(1-U_1^2)^{\frac{1}{k-1}}U_1\right](1-U^2)}{4\left[U^2+1{,}3\left(1-\frac{T^*_w-T_w}{T_{00}}\right)\right]} \tag{7-4-11}$$

and the momentum equation is rewritten as

$$\frac{d\,\mathrm{Re}^{**}_{00}}{d\bar{x}}+\frac{\mathrm{Re}^{**}_{00}}{U(1-U^2)}\left[1+1{,}3\left(1-\frac{T^*_w-T_w}{T_{00}}\right)\right]\frac{dU}{d\bar{x}}$$
$$=\frac{B}{2}\Psi_\infty\left(\frac{\mu_w}{\mu_{00}}\right)^m\frac{1}{\mathrm{Re}^{**m}_{00}}U(1-U^2)^{\frac{1}{k-1}}\mathrm{Re}_{00}. \tag{7-4-12}$$

Substituting Re^{**}_{00} from (7-4-11) into this equation, we get

$$\left[\frac{U(1-U^2)^{\frac{1}{k-1}}-U_1(1-U_1^2)^{\frac{1}{k-1}}}{1{,}69\left(1-\frac{T^*_w-T_w}{T_{00}}\right)}\right]^m\left\{\left[1{,}3\left(1-\frac{T^*_w-T_w}{T_{00}}\right)\right.\right.$$
$$\left.+U^2\right]\left[(1-U^2)^{\frac{1}{k-1}}-\frac{2k}{k-1}U^2(1-U^2)^{\frac{1}{k-1}}+2UU_1\right.$$
$$\times(1-U_1^2)^{\frac{1}{k-1}}\Big]-\left[(1-U^2)^{\frac{k}{k-1}}U-(1-U^2)U_1(1-U_1^2)^{\frac{1}{k-1}}\right] \tag{7-4-13}$$
$$\left.\times 2U\right\}U+\frac{\left[U(1-U^2)^{\frac{1}{k-1}}-U_1(1-U_1^2)^{\frac{1}{k-1}}\right]^{1+m}(1-U^2)^m}{U\left[1{,}3\left(1-\frac{T^*_w-T_w}{T_{00}}\right)+U^2\right]^{1+m}}$$
$$\times\left[1-1{,}3\left(1-\frac{T^*_w-T_w}{T^*_{00}}\right)\right]dU=2B\Psi_\infty$$
$$\times\left(\frac{4\mu_w}{\mu_{00}\mathrm{Re}_{00}}\right)^m U(1-U^2)^{\frac{1}{k-1}}d\bar{x}.$$

In solving (7-4-7) we can set

$$\frac{\mathrm{Re}^{**}_{T00}}{\mathrm{Re}^{**}_{00}}H'_T=H_T=H_0=1{,}3.$$

With a specified law of wall temperature variation and velocities and stagnation parameters at the duct inlet, it is possible to determine the law of variation of the dimensionless velocity U over the length of the pipe from Eq. (7-4-13). The local values of Re^{**}_{00} are calculated by (7-4-6). The local values of the friction coefficients are determined by the formula /158

$$c_f=\Psi\frac{B}{\mathrm{Re}^{**m}}\left(\frac{\mu_w}{\mu_{00}}\right)^m, \tag{7-4-14}$$

where Ψ is taken from (7-1-19) or (7-1-25).

The static pressure distribution over the length of the pipe is found from the formula

$$\frac{P_0}{P_{00}} = (1 - U^2)^{\frac{k}{k-1}}, \tag{7-4-15}$$

where P_{00} is the stagnation pressure in the flow core, which remains constant in the initial portion of the pipe.

It should be noted that the proposed calculation method is valid only for the conditions of shockless entry of gas into the pipe. The thermal boundary layer is calculated analogously.

The energy equation has the form

$$\frac{d\,\mathrm{Re}^{**}_{T00}}{d\bar{x}} + \frac{\mathrm{Re}^{**}_{T00}}{\Delta i}\frac{d(\Delta i)}{d\bar{x}} = \mathrm{Re}_{00} U (1 - U^2)^{\frac{1}{k-1}} \times \frac{B}{2(\mathrm{Re}^{**}_{T00})^m \mathrm{Pr}^n}\left(\frac{\mu_w}{\mu_{00}}\right)^m \Psi_{S\infty}. \tag{7-4-16}$$

The integral of Eq. (7-4-16) is

$$\mathrm{Re}^{**}_{T00} = \frac{1}{\Delta i}\left[\frac{B(m+1)}{2\,\mathrm{Pr}^n}\mathrm{Re}_{00}\int_0^{\bar{x}} U (1 - U^2)^{\frac{1}{k-1}} \times \left(\frac{\mu_w}{\mu_{00}}\right)^m \Psi_{S\infty}\Delta i^{m+1} d\bar{x}\right]^{\frac{1}{m+1}}. \tag{7-4-17}$$

Substituting into (7-4-17) the dependence of U on $\bar{x}$ obtained above for a given law of variation of Δi over x, we determine the local values of $\mathrm{Re}^{**}_{T_{00}}$ and the local values of the Stanton number by (7-2-53).

It should be kept in view that all the formulas are valid only for the initial section of the pipe. At the end of this section the boundary layers intersect, i.e. the boundary-layer thickness becomes equal to the radius of the pipe. From Eq. (7-4-5) it follows that the following equality should be satisfied at the end of the initial reaction:

$$\frac{U_{in}(1 - U_{in}^2)^{\frac{1}{k-1}}}{U_1 (1 - U_1^2)^{\frac{1}{k-1}}} = \left(1 - 2\frac{\delta^{**}}{R_0} H\right)^{-1}, \tag{7-4-18}$$

/159

where U_{in} is the dimensionless velocity in the core at the end of the initial section.

Substituting δ^{**}/R_0 and H as functions of ψ^* and $\Delta\psi$ into (7-4-18) and taking relation (7-2-37) into account, we get an equation in U_{in}. Substituting this value of U_{in} into the integral of (7-4-13), we find the length of the initial section $\bar{x}_{in}$.

For the region of subsonic gas flow and constant wall temperature, a solution can be obtained in analytic form. In this case, $U^2 << 1$ and Eq. (7-4-13) reduces to the form

$$[(1+1{,}3\psi)(1+m)+1]\int_1^{\tilde{w}_0}\frac{(\bar{w}_0-1)^m}{\bar{w}_0}d\bar{w}_0-(1+1{,}3\psi)\times\frac{(\bar{w}_0-1)^{1+m}}{\bar{w}_0}=2B\Psi_\infty\left(\frac{4}{\mathrm{Re}_{01}}\frac{\mu_w}{\mu_{a0}}\right)^m(1+1{,}3\psi)\,x. \tag{7-4-19}$$

Setting m = 0.25, B = 0.0258, taking Eq. (7-1-23) into account, we get ($\tilde{w}_0 = w_0/w_{01}$)

$$[(1+1{,}3\psi)\,1{,}25+1]\left[4(\bar{w}_0-1)^{0{,}25}-\ln\frac{(\bar{w}_0-1)^{0{,}5}+\sqrt{2}(\bar{w}_0-1)^{0{,}25}+1}{(\bar{w}_0-1)^{0{,}5}-\sqrt{2}(\bar{w}_0-1)^{0{,}25}+1}-\sqrt{2}\,\mathrm{arctg}\frac{\sqrt{2}(\bar{w}_0-1)^{0{,}25}}{1-(\bar{w}_0-1)^{0{,}5}}\right]-(1+1{,}3\psi)\frac{(\bar{w}_0-1)^{1{,}25}}{\bar{w}_0}=\frac{0{,}4\psi^{1{,}25}x}{(\sqrt{\psi}+1)^2\,\mathrm{Re}_{0w}^{0{,}25}}. \tag{7-4-20}$$

Accordingly, Eq. (7-4-10) reduces to the form

$$H=\psi H_0=1{,}3\psi \tag{7-4-21}$$

and Eq. (7-4-11) to the form

$$\mathrm{Re}^{**}=\frac{\mathrm{Re}_0(\bar{w}_0-1)}{5{,}2\psi}. \tag{7-4-22}$$

The local frictional drag coefficients are defined by the formula

$$c_f=\Psi\frac{0{,}0256}{\mathrm{Re}^{**m}}, \tag{7-4-23}$$

where Ψ is calculated by (7-1-21) or (7-1-23).

The length of the initial section is determined from (7-4-18), which, for the conditions under study here, is written as /160

$$\bar{w}_{in}=\left(1-2\frac{\delta^{**}}{R_0}H\right)^{-1} \tag{7-4-24}$$

or, taking (7-4-21) into account,

$$\bar{w}_{in}=\left(1-2{,}6\frac{\delta^{**}}{R_0}\psi\right)^{-1}. \tag{7-4-25}$$

From Eqs. (7-4-20) and (7-4-25) we get the dependence of the length of the initial section on the gas parameters at the pipe inlet and on the nonisothermicity parameter ψ:

$$\bar{z}_{in} = \frac{Re_{0w}^{0.25}}{\psi 0{,}0725 H^{1.25}} \left\{ \left[(1+H)\frac{5}{4} + 1 \right] \left[4(\bar{w}_{in}-1)^{0.25} \right.\right.$$
$$- \frac{1}{\sqrt{2}} \ln \frac{(\bar{w}_{in}-1)^{0.5} + \sqrt{2}(\bar{w}_{in}-1)^{0.25} + 1}{(\bar{w}_{in}-1)^{0.5} - \sqrt{2}(\bar{w}_{in}-1)^{0.25} + 1} \qquad (7\text{-}4\text{-}26)$$
$$\left.\left. - \sqrt{2} \operatorname{arctg} \frac{\sqrt{2}(\bar{w}_{in}-1)^{0.25}}{1-(\bar{w}_{in}-1)^{0.5}} \right] - (1+H)\frac{(\bar{w}_{in}-1)^{1.25}}{w_*} \right\}.$$

The results of solving this system of equations are approximated quite well by the following simple formula:

$$\frac{\bar{z}_{in}}{Re_0^{0.25}} = \frac{0{,}8\psi + 0.55}{\psi^{0.25}}, \qquad (7\text{-}4\text{-}27)$$

where

$$Re_* = \frac{4G}{\pi D \mu_*}; \quad \frac{\mu}{\mu_*} \approx \left(\frac{T}{T_*}\right)^k.$$

For the case $\psi = 1$

$$\bar{z}_{in} = 1{,}35\, Re_0^{0.25}. \qquad (7\text{-}4\text{-}28)$$

The question of experimental determination of the length of the initial section is as yet insufficiently clear. Thus, in experimental work [4, 151] the length of the initial section was determined from the change in local Nusselt number and local heat-transfer coefficient over the length of a pipe. The pipe cross section where these data exceeded their asymptotic values by a certain value (5% or 1%) was taken as the origin of stabilized flow. Such a method cannot yield satisfactory results, since it does not take into account the particular features of boundary layer interaction with the flow core; as a result, the heat-transfer coefficient in the initial section may first decrease, and then increase again [151]. Compiled in Table 7.4 are the results of some investigations to determine the length of the initial section. From this table it can be seen that even for a quasi-isothermal gas flow ($\Delta T \to 0$) great discrepancies exist between the data of the various researchers. /161

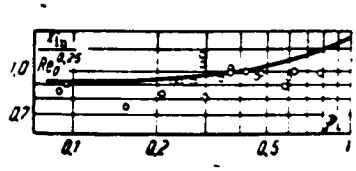

FIG. 7.23.

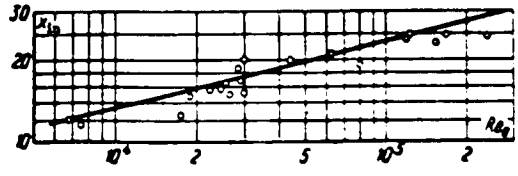

FIG. 7.24.

FIG. 7.23. Effect of cooling on the length of the initial section of the pipe. Curve calculated by (7-4-27); the points represent the experiments of [67].

FIG. 7.24. Effect of the Reynolds number on the length of the initial section. Curve calculated by (7-4-27); the points represent the experiments of [67].

Table 7.4. Determination of the length of the initial section

Liquid	Range of Re	$\bar{x}_н$	Method*	Experimental conditions	Source
Water	$1.7\cdot10^4$—$9\cdot10^4$	10—15	A_1	q_w=const	[151]
Air	$2.7\cdot10^4$	12	A_1	T_w=const	[151]
Air, CO_2	$5\cdot10^4$—$2.5\cdot10^5$	11—27	A_1	q_w=const	[171]
Water	10^4—10^5	40—20	A_1	T_w=const	[4]
Water	$4.9\cdot10^4$—$6.5\cdot10^4$	14—20	A_2		[189]**
Air	$3\cdot10^3$—$4.2\cdot10^3$	16—17	A_3		[6]***
Air	$6.9\cdot10^3$—$2.4\cdot10^5$	7.9—22	A_4	T_w=const	Author's data

*Methods of determination: A_1 - from the change of the local heat-transfer coefficient; A_2 - from the change of the local pressure gradient; A_3 - from the results of comparing the stagnation enthalpy and the velocity, as calculated for the initial and main sections; A_4 - from the change in enthalpy on the axis of the pipe.

**The length of hydrodynamic stabilization was determined. The data were taken from an analysis of the graph in Fig. 7 from [189].

***Determined were the lengths of thermal and hydrodynamic stabilization.

Given in Figs. 7.23 and 7.24 is a comparison of formula (7-4-27) (for k = 0.64) with the experiments of A. I. Leont'ev, B. P. Mironov and A. V. Fafurin [67]. Measured in these experiments was the length of the initial thermal section; for the case ψ = const and Pr ≈ 1 it is equal to the length of the dynamic initial section.

The length of the thermal initial section was determined by the following method. /162 The energy balance equation for a pipe segment of length x can be written as

$$\rho_{01} w_{01} i_{01} R_0^2 = 2\int_0^x q_w R_e\, dx + \int_0^{R_e} 2\rho w i R\, dR. \qquad (7\text{-}4\text{-}29)$$

For the conditions being considered here we can take $\delta^{**}_T = \delta^{**}$; then the following equality can be written for the main section of the pipe:

$$\rho_e w_e = \frac{\rho_{01} w_{01}}{1 - 2H\dfrac{\delta^{**}}{R_e}}. \qquad (7\text{-}4\text{-}30)$$

Then, taking Eqs. (7-4-21) and (7-4-29) into account, we get

$$\frac{i_{01} - i_w}{i_e - i_w} = \frac{1 - N}{1 - S}, \qquad (7\text{-}4\text{-}31)$$

where

$$N = \frac{1}{\dfrac{R_e}{2\delta^{**}} - H_e\psi}; \quad S = \frac{1}{G(i_{01} - i_w)}\sum_1^n Q_{wi}.$$

Here Q_{wi} is the quantity of heat absorbed by the i — calorimeter; b is the mass gas flow through the pipe.

In the initial section, $i_0 = i_{01}$, by definition, and the condition $(i_{01} - i_w)/(i_0 - i_w) = 1$ must be fulfilled; accordingly

$$N = S. \tag{7-4-32}$$

The experimental data were processed on a computer. The pipe cross-section for which equality (7-4-32) was fulfilled with an accuracy of ±1% was taken to be the end of the initial thermal section. As can be seen from Figs. 7.21 and 7.22, the proposed calculation method is in satisfactory agreement with the experimental data. From an analysis of the results obtained it can be deduced that the length of the initial section increases substantially with increasing Reynolds number at the pipe inlet.

Pipe cooling has a relatively lesser effect on the length of the stabilization section. In the 1 to 0.08 range of ψ the length of the initial section decreases by a total of 30%.

The dependence of the parameter $\bar{x}\,\mathrm{Re}_{0w}^{-0.25}$ on w_0 and ψ, as calculated by (7-4-20), is shown in Fig. 7.25. The length of the initial section was determined by (7-4-27). Given in Fig. 7.26 is a comparison of the results of calculating the mass-flow function q(U) by (7-4-20) with the experimental data obtained from a measurement of the static pressure distribution over the pipe length in [67]. As can be seen from the graph, satisfactory agreement is observed between the proposed method of calculation and experiment. From (7-4-17), taking (7-4-20) into account, we get /163

$$\mathrm{Re}^{**}_T = \frac{\mathrm{Re}_0(\bar{w}_0 - 1)}{5.2\psi}\left\{(2 + 1.3\psi) - \frac{1.25 + 1.62\psi}{(\bar{w}_0 - 1)^{1.25}}\right.$$
$$\times\left[4(\bar{w}_0 - 1)^{0.25} - \sqrt{2}\,\mathrm{arctg}\,\frac{\sqrt{2}(\bar{w}_0 - 1)^{0.25}}{1 - (\bar{w}_0 - 1)^{0.5}}\right. \tag{7-4-33}$$
$$\left.\left. - \frac{1}{\sqrt{2}}\ln\frac{(\bar{w}_0 - 1)^{0.5} + \sqrt{2}(\bar{w}_0 - 1)^{0.25} + 1}{(\bar{w}_0 - 1)^{0.5} - \sqrt{2}(\bar{w}_0 - 1)^{0.25} + 1}\right]\right\}^{0.8}.$$

Thus, the following relationship exists between the energy loss thickness and the momentum loss thickness for a gas flow (Pr ≈ 1) in the initial section of a pipe with a constant wall temperature:

$$\frac{\delta^{**}_T}{\delta^{**}} = \left\{(2 + 1{,}3\psi) - \frac{1.25 + 1{,}62\psi}{(\bar{w}_0 - 1)^{1.25}}\left[4(\bar{w}_0 - 1)^{0.25}\right.\right.$$
$$- \frac{1}{\sqrt{2}}\ln\frac{(\bar{w}_0 - 1)^{0.5} + \sqrt{2}(\bar{w}_0 - 1)^{0.25} + 1}{(\bar{w}_0 - 1)^{0.5} - \sqrt{2}(\bar{w}_0 - 1)^{0.25} + 1} \tag{7-4-34}$$
$$\left.\left. - \sqrt{2}\,\mathrm{arctg}\,\frac{\sqrt{2}(\bar{w}_0 - 1)^{0.25}}{1 - (\bar{w}_0 - 1)^{0.5}}\right]\right\}^{0.8}. \qquad /164$$

Shown in Fig. 7.27 is the dependence of $\delta^{**}_T/\delta^{**}$ on the parameters $x\,\mathrm{Re}_{0w}^{-0.25}$ and ψ.

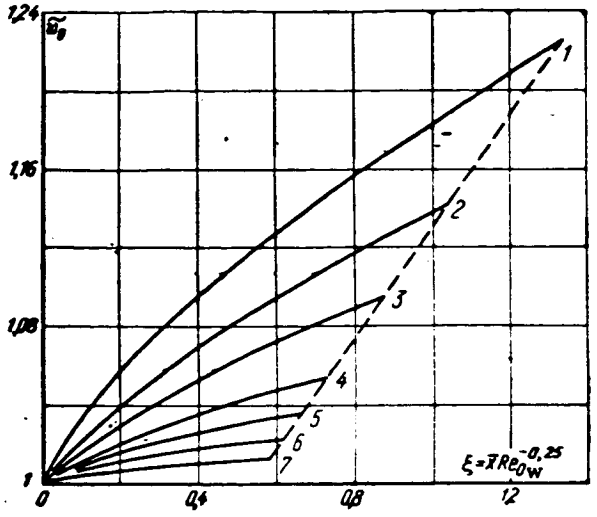

FIG. 7. 25. Effect of wall cooling on the velocity distribution in the flow case over the length of the initial section of the pipe. 1—ψ = 1.0; 2—0.6; 3—0.4; 4—0.2; 5—0.137; 6—0.0875; 7—0.044; the dashed line indicates the length of the initial section according to (7-4-27).

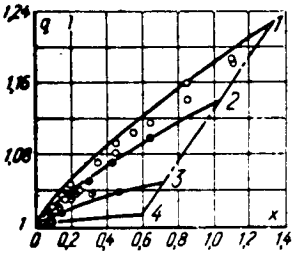

FIG. 7.26.

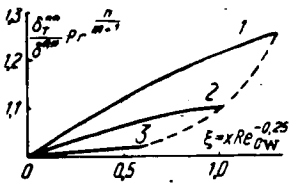

FIG. 7.27.

FIG. 7.26. Comparison of the results of calculating the mass-flow function q(U) with the experiments of [67]: 1—ψ = 1; 2—0.6; 3—0.2; 4—0.044.

FIG. 7.27. Effect of heat transfer on the ratio of $\delta^{**}_T/\delta^{**}$ in the initial section of the pipe: 1—ψ = 1; 2—0.6; 3—0.044.

As can be seen from the graph, we can take $Re^{**}_T \approx Re^{**}$ in the region $\psi < 1$. In view of this fact, a convenient method can be proposed for generalizing the experimental data on heat transfer in the initial section of a pipe [61].

From (7-4-16) it follows that

$$Re^{**}_{T00} = \frac{\int_0^x q_w\, dx}{\mu_{00}\Delta i}. \qquad (7\text{-}4\text{-}35)$$

In addition, we have the relations

$$\mathrm{St} = \frac{q_w D}{\mathrm{Re}_D \mu_{\infty} \Delta i}; \tag{7-4-36}$$

$$\mathrm{Re}_D = U(1-U^2)^{\frac{1}{k-1}} \mathrm{Re}_{\infty}; \tag{7-4-37}$$

$$\frac{P}{P_{\infty}} = (1-U^2)^{\frac{k}{k-1}}. \tag{7-4-38}$$

Thus, by measuring the static pressure distribution over the pipe length, the wall temperature, and the heat flux, the experimental dependence of St on Re^{**}_T can be constructed by (7-4-35)-(7-4-38). If the static pressures are not measured in the experiments, then, taking the equality $\mathrm{Re}^{**}_T \approx \mathrm{Re}^{**}$ into account, the Stanton number can be determined by the formula (for the region M << 1)

$$\mathrm{St} \approx \frac{q_w D}{(\mathrm{Re}_{D1} + 5{,}24\,\mathrm{Re}^{**}_{T(1)})\,\mu_{\infty} \Delta i}. \tag{7-4-39}$$

Presented in Fig. 7.28 are the results of an analysis, by this method, of the experimental data of B. S. Petukhov [85], V. L. Lel'chuk and B. V. Dedyakin [36], I. A. Kozhinov, S. I. Kosterin, A. I. Leont'ev and V. K. Fedorov [54]. All the data have been reduced to thermal insulation conditions by the formula $\mathrm{St}_0 - \mathrm{St}/\Psi_*$.

A mean line drawn through all the experimental points is described by the formula /165

$$\mathrm{St}_0 = \frac{0{,}014}{\mathrm{Re}_T^{**0{,}25}\,\mathrm{Pr}^{0{,}75}}, \tag{7-4-40}$$

which coincides with the relation

$$\mathrm{St}_0 = \frac{c_{f0}}{2\,\mathrm{Pr}^{0{,}75}} \tag{7-4-41}$$

for $c_{fo}/2$ calculated by (1-10-3). The result confirms that the laws of heat transfer and friction are common to the inner and outer problems of aerodynamics.

Shown in Fig. 7.29 are the results of processing, by this method, the experimental data on heat transfer for pipes, nozzles, plates and missile nose cones. These experiments cover a broad range of M and $\Delta\psi$. Despite the considerable scatter of the experimental points, they all fit around a line corresponding to (7-4-41).

It should be noted that in generalizing the experimental data on heat transfer in the initial section of a pipe it is necessary to devote serious attention to the pipe inlet conditions. The results given in Fig. 7.28 of generalizing experimental data by the proposed method indicate that the inlet conditions have an appreciable affect on the law of heat transfer in the initial section of the pipe, but the method outlined below for calculating a thermal boundary layer remains valid for these conditions also, except that the coefficients B and m are changed [61].

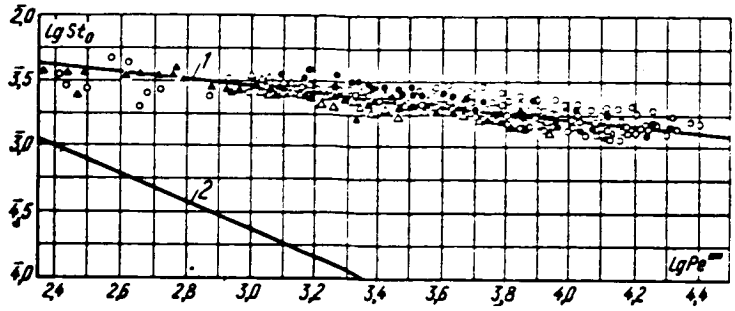

FIG. 7.28. Results of generalizing the experimental data on heat transfer in the initial section of a cylindrical pipe: 1—turbulent layer $St_0=\frac{0,0143}{Pe^{**0,25}Pr^{0,5}}$; 2—laminar layer $St_0=\frac{0,22}{Pe^{**}Pr^{1,3}}$; ●—experiments of B. V. Dedyakin and V. L. Lel'chuk [26]; ▲—experiments of B. S. Petukhov [85]; ○—experiments of I. A. Kozhinov, S. I. Kosterin, A. I. Leont'ev and V. K. Fedorov [51]; △—experiments of A. I. Leont'ev, B. P. Mironov and A. V. Fafurin [65].

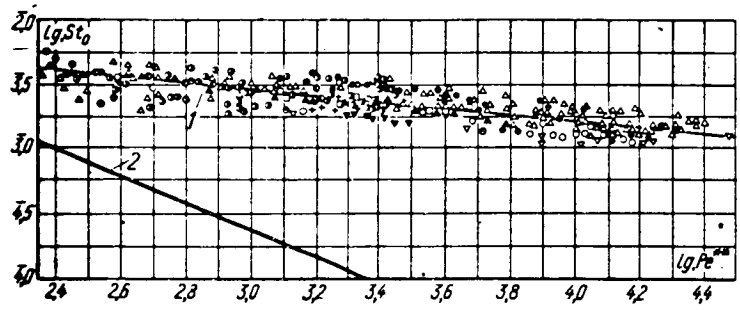

FIG. 7.29. Results of generalizing experimental data on heat transfer in a turbulent boundary layer of compressed gas. 1—turbulent conditions $St_0=\frac{0,0143}{Pe^{**0,25}Pr^{0,5}}$; 2—laminar conditions $St_0=\frac{0,22}{Pe^{**}Pr^{1/3}}$; experimental data: △—V. K. Fedorov (pipe); ◓—Pappas (plate): ▽—Fischer and Noris (V-2 nose cone); ▼—Eber (cone); ◐—B. S. Petukhov (plate); ⊓—Bradfield (cone); ◑—A. I. Leont'ev and B. P. Mironov (pipe): ▲—B. S. Petukhov (pipe); +—Fallis (plate); ●—V. L. Lel'chuk and B. V. Dedyakin (pipe); ○—B. A. Sveshnikov (pipe).

The equation of a thermal boundary layer for the initial section of a pipe ($M << 1$) can be written conveniently in the form /166

$$\frac{d\,Pe^{**}}{d\bar{x}}+Pe^{**}\frac{d}{d\bar{x}}[\ln(1-\psi)]=St\,Pe_D, \qquad (7\text{-}4\text{-}42)$$

where

$$\mathrm{Pe}^{**} = w_0 \delta^{**}_T / a_0; \quad \mathrm{Pe}_D = w_0 D / a_0.$$

Taking into account Eqs. (7-4-3) and (7-4-5) we have

$$\frac{d\,\mathrm{Pe}^{**}}{d\bar{x}} + \mathrm{Pe}^{**} \frac{d}{d\bar{x}} [\ln (1-\psi)] = \mathrm{St}_0 \Psi_t (\mathrm{Pe}_{D1} + 5{,}2\psi\,\mathrm{Pe}^{**}), \tag{7-4-43}$$

where

$$\mathrm{Pe}_{D1} = w_{01} D / a_0.$$

For the case ψ = const

$$\frac{d\,\mathrm{Pe}^{**}}{d\bar{x}} = \frac{B (\mathrm{Pe}_{D1} + 5{,}2\psi\,\mathrm{Pe}^{**})}{2 (\mathrm{Pe}^{**m})\,\mathrm{Pr}^{0.5}} \Psi_t. \tag{7-4-44}$$

Taking m = 0.25, with allowances for (7-4-44) we get

$$\bar{x} = \frac{2\,\mathrm{Pr}^{0.5}}{\left(\frac{2}{\sqrt{\psi}+1}\right)^2 \left(\frac{\mu_W}{\mu_0}\right)^m B} \left\{ \frac{4\,\mathrm{Pe}^{**0.25}}{5{,}2\psi} - \frac{\mathrm{Pe}_{D1}^{0.25}}{\sqrt{2}\,(5{,}2\psi)^{1.25}} \times \left[\ln \frac{\mathrm{Pe}^{**0.5} + \sqrt{2}\left(\frac{\mathrm{Pe}_{D1}\mathrm{Pe}^{**}}{5{,}2\psi}\right)^{0.25} + \left(\frac{\mathrm{Pe}_{D1}}{5{,}2\psi}\right)^{0.5}}{\mathrm{Pe}^{**0.5} - \sqrt{2}\left(\frac{\mathrm{Pe}_{D1}\mathrm{Pe}^{**}}{5{,}2\psi}\right)^{0.25} + \left(\frac{\mathrm{Pe}_{D1}}{5{,}2\psi}\right)^{0.5}} + 2 \operatorname{arctg} \frac{\sqrt{2}\left(\frac{\mathrm{Pe}_{D1}\mathrm{Pe}^{**}}{5{,}2\psi}\right)^{0.25}}{\left(\frac{\mathrm{Pe}_{D1}}{5{,}2\psi}\right)^{0.5} - \mathrm{Pe}^{**0.5}} \right] \right\}. \tag{7-4-45}$$

/167

The local values of Pe** are calculated by (7-4-45) for given gas parameters at the duct inlet and for given wall temperature.

The local values of the Nusselt number are determined by the formula

$$\mathrm{Nu} = \frac{B \left(\frac{2}{\sqrt{\psi}+1}\right)^2 \left(\frac{\mu_W}{\mu_0}\right)^{0.25}}{2\,\mathrm{Pr}^{0.5}\mathrm{Pe}^{**0.25}} (\mathrm{Pe}_{D1} + 5{,}2\psi\,\mathrm{Pe}^{**}). \tag{7-4-46}$$

This method of calculation can also be applied to the case of flow of a dissociating gas in the initial section of a pipe. As shown in [65], the limit frictional drag law for a "frozen" boundary layer of a multi-component dissociating gas is obtained in the form

$$\left.\begin{aligned} \Psi_\infty &= 4 (\sqrt{\psi_a}+1)^{-2}; \quad \psi_a = \frac{\phi_i - \Sigma a_{W\,i}\phi^0}{1 - \Sigma a_{0\,i}\psi_i^0}; \quad \psi_\rho = \frac{\rho_0}{\rho_W}; \\ \phi_i &= \frac{i_W}{i_0}; \quad \phi_i^0 = \frac{i_i^0}{i_0}; \quad i_i = \int_0^T C_p\,dT + i_i^0. \end{aligned}\right\} \tag{7-4-47}$$

Taking the effect of finite Re^{**}_T into account,

$$\psi_i = \frac{(1 - \Sigma a_{i0}\psi_i^0)(2 - \sqrt{\psi})^2 + \psi \Sigma a_{wi}\psi_i^0 - [1 - \Sigma (a_0 - a_w)_i \psi_i^0]}{\Psi (1 - 8{,}2 \sqrt{c_{f0}\psi_\rho \Psi})} \times 8.2 \sqrt{c_f \psi_\rho \Psi}\, \Psi. \tag{7-4-48}$$

Equation (7-4-47) was obtained under the assumption that the density of the gas can be determined by the formula.

$$\frac{\rho}{\rho_0} = \frac{1 - \Sigma a_{i0}\psi_i^0}{\psi_i - \Sigma a_{w\,i}\psi_i^0 + \{1 - \psi_i - \Sigma (a_0 - a_w)_i \psi_i^0\}\omega}. \tag{7-4-49}$$

It is interesting to analyze the effect of gas dissociation on the integral characteristics of the boundary layer. /168

It is well known that the physical displacement thickness is related to the displacement thickness in Dorodnitsyn variables by

$$\delta^* = \delta^*_D - \int_0^{R_0} \left(\frac{\rho}{\rho_0} - 1\right)\left(1 - \frac{y}{R_0}\right) dy. \tag{7-4-50}$$

Taking (7-4-49) into account we get

$$\delta^* = \delta^*_D - \int_0^{R_0} \frac{(i - \Sigma a_i i_i^0) - (i_0 - \Sigma a_{i0} i_i^0)}{i_0 - \Sigma a_{i0} i^0} \left(1 - \frac{y}{R_0}\right) dy \tag{7-4-51}$$

and

$$\delta^* = \delta^*_D \left\{1 - \frac{1}{1 - \Sigma a_{i0}\psi_i^0} i[1 - \psi_i - \Sigma_i (a_0 - a_w)_i \psi_i^0]\right\}, \tag{7-4-52}$$

from which we find

$$H = H_1 \psi_w, \tag{7-4-53}$$

where $H_1 = \delta^*_D/\delta^{**}_D$, and where $\delta^{**}_D = \delta^{**}$.

Shown in Fig. 7.30 are the results of calculating the parameters of an axisymmetric turbulent boundary layer under the assumption that $w = \xi^n (n = 1/7)$ and, using (7-4-49), for the density. As can be seen from the graph, the parameters δ^* and δ^*_D depend greatly on the nonisothermicity and degree of dissociation of the gas, but the shape parameter $H_1 = \delta^*_D/\delta^{**}_D$ remains essentially constant, equaling 1.347. /169 The results of calculating the shape parameter H under the same assumptions and a comparison with (7-4-53) are given in Fig. 7.31. Clearly evident in the graph is the influence of gas dissociation on the shape parameter H.

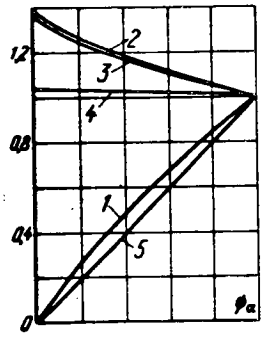

FIG. 7.30.

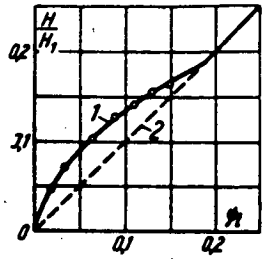

FIG. 7.31.

FIG. 7.30. Effect of nonisothermicity and dissociation on the integral characteristics of a turbulent boundary layer. 1—$\delta^{**}/\delta^{**}_0$; 2—$\delta^{**}/\delta^{**}_0$; 3—$\delta^{**}_D/\delta^{**}_{D_0}$; 4—$H_1/H_{1\,iso}$; 5—$\delta^*/\delta^{**}$.

FIG. 7.31. Effect of air dissociation on the shape parameter H. 1—Calculation by (7-4-53); 2—by (7-4-53) without account of dissociation; the points represent calculation in terms of integral parameters; all calculations made for $T_w = 300°K$.

Thus, for the boundary conditions $\psi_\alpha = \text{const}$ the shape parameter H can be assumed to be constant over the length of the pipe. As a result, Eqs. (7-4-20), (7-4-26), (7-4-27) and (7-4-33)-(7-4-35) can be applied to the case of flow of a dissociated gas, except that ψ_α must be substituted into all the formulas in the place of the parameter ψ.

For the case of a given constant thermal stress over the length of the pipe, we have from (7-4-42)

$$\mathrm{Pe}^{**} = \frac{\mathrm{Nu}_1 \Psi}{1-\psi}, \tag{7-4-54}$$

where $\mathrm{Nu}_1 = q_w D/\lambda_{01} T_{01}$.

In the range of $\psi = 0.5$ to 3.0 the function Ψ can be series expanded and can be limited to the first term; i.e. we can take

$$\Psi_1 = \frac{2}{1+\psi}. \tag{7-4-55}$$

Then,

$$\mathrm{St} = \frac{\mathrm{Nu}_1}{\mathrm{Pe}_D (1-\psi)} = \frac{B}{\mathrm{Pe}^{**0.25} \mathrm{Pr}^{0.5} (1+\psi)}.$$

Moreover, taking into account Eqs. (7-4-3), (7-4-21) and the relation $Re^{**} \approx Re^{**}_T$, we have

$$Pe_D = Pe_{D1} + 5{,}2\psi Pe^{**}. \tag{7-4-56}$$

As a result, we have a system of three equations, (7-4-54)-(7-4-56), with three unknowns, ψ, Pe^{**} and Pe_D.

Solving this system for the independent variable $\bar{x}$, we get

$$\bar{x} = 3{,}36\,Nu_1^{-1}[Nu_1 Pe^{**0{,}25}Pr^{0{,}5} - 0{,}0286Pe_{D1} - 0{,}149Pe^{**} - \sqrt{(0{,}0286Pe_{D1} + 0{,}149Pe^{**} - Nu_1 Pe^{**}Pr^{0{,}5})^2 + 1{,}19Nu_1 Pe^{**1{,}25}Pr^{0{,}5}}]. \tag{7-4-57}$$

Knowing the local values of Pe^{**}, we define from (7-4-54)

$$\psi = 1 + \frac{Nu_1}{Pe^{**}}\bar{x}. \tag{7-4-58}$$

This method of calculating can also be applied to the case of an arbitrary law of thermal stress distribution. In this case it is necessary to use (7-4-42) instead of (7-4-54).

There exists, in principle, no impediment to also applying this method of turbulent boundary-layer calculation in the initial section of a pipe to ducts with cross-sectional area varying with length. The only difference is that in this case we get from the continuity equation not (7-4-6) but /170

$$Re^{**}_{\delta\delta} = \frac{Re_{\delta\delta}}{4H}\left[U(1-U^2)^{\frac{1}{k-1}} - U_1(1-U_1)^{\frac{1}{k-1}}\left(\frac{R_{01}}{R_0}\right)^2\right], \tag{7-4-59}$$

where R_{01} and R_0 are the radii of the inlet and current cross section of the duct.

Hence, the momentum and energy equations must be written in the form of (7-2-45) and (7-2-51). The subsequent deductions remain the same as for a cylindrical duct.

7.5. Friction and Heat Transfer with a Stabilized Gas Flow in a Cylindrical Pipe with Impermeable Walls

Stabilized flow sets in after merging of the boundary layers that arise in the initial section of a pipe; typical of such a flow for isothermal conditions is self-similar distribution of all the parameters over the pipe length. For a stabilized isothermal turbulent flow of incompressible fluid the velocity distribution over the radius of the pipe is described rather well by (1-10-2). The reason for this is that flow in the pipe is convergent with a comparatively small value of the shape parameter f. The pressure drop in the pipe is determined by the formula

$$\frac{dP}{dx} = \zeta\frac{\rho_0\bar{w}^2}{2D}, \tag{7-5-1}$$

where the mean gas velocity is

$$\bar{w} = \frac{1}{R_0^2} \int_0^{R_0} wR\,dR. \qquad (7\text{-}5\text{-}2)$$

Substituting velocity profile (1-10-2), we find

$$\bar{w} = w^*_w \left(1{,}75 + 2{,}5 \ln \frac{w^*_w R_0}{\nu}\right), \qquad (7\text{-}5\text{-}3)$$

where

$$w^*_w = \bar{w} \sqrt{\frac{\zeta}{8}}.$$

From this we get the drag law

$$\frac{1}{\sqrt{\zeta}} = 0{,}88 \left(\ln \mathrm{Re}_D \sqrt{\zeta}\right) - 0{,}8. \qquad (7\text{-}5\text{-}4)$$

In the region $5 \cdot 10^3 < \mathrm{Re}_D < 10^5$ satisfactory results are obtained by the Blasius formula

$$\zeta = \frac{0{,}316}{\mathrm{Re}_D^{0{,}25}}, \qquad (7\text{-}5\text{-}5)$$

where $\mathrm{Re}_D = \bar{w}D/\nu$.

A power-law velocity distribution with n = 1/7 corresponds to (7-5-5). /171

Let us determine the shape parameter f for a stabilized flow of incompressible fluid in a pipe:

$$f = -\frac{\delta}{\tau_w} \frac{dP}{dx} \frac{\delta^{**}}{\delta} \frac{c_f}{2}. \qquad (7\text{-}5\text{-}6)$$

In the stabilized flow region $\delta = R_0$ and $-dP/dx = 2\tau_w/R_0$.

Hence,

$$f = \frac{\delta^{**}}{\delta} c_f. \qquad (7\text{-}5\text{-}7)$$

When n = 1/7

$$f = \frac{0{,}0308}{\mathrm{Re}_D^{0{,}25}}, \qquad (7\text{-}5\text{-}8)$$

that is, $f < 0.003$ when $\mathrm{Re}_D > 10^4$ and $f < 0.002$ when $\mathrm{Re}_D > 10^5$.

Thus, the effect of a longitudinal pressure gradient on the laws of frictional drag and heat transfer for a stabilized flow of incompressible fluid in a pipe can be neglected.

Heat transfer in the region of stabilized gas flow in a pipe with $Re_D > 10^4$, $0.5 < Pr < 1.5$, is determined by the formula

$$Nu_D = 0.023 Re_D^{0.8} Pr^{0.4}, \tag{7-5-9}$$

where

$$Nu_D = \alpha D/\lambda; \quad \alpha = q_w/(\bar{T} - T_w); \quad \bar{T} = \frac{2\pi}{G}\int_0^{R_0} \rho w T R\, dR; \quad Re_D = 4G/\pi D\mu.$$

In the presence of heat transfer, a stabilized or self-similar gas flow does not set in, strictly speaking, in the general case. The coefficients of friction and heat transfer can change over the length of the pipe even after the boundary layers have merged. Therefore, by a "stabilized" gas flow in a pipe we mean the gas flow downstream from the section where both the dynamic and the thermal boundary layers have merged.

The limit laws of frictional drag and heat transfer can also be applied to stabilized gas flow in a pipe, except that then the gas parameters on the axis of the pipe will correspond to the gas parameters at the outer edge of the boundary layer.

Consequently,

$$\left[\frac{\frac{\tau_w}{\rho_0 w_0^2}}{\left(\frac{\tau_w}{\rho_0 w_0^2}\right)_*}\right]_{Re^{**}_{0w}} = \Psi_\infty. \tag{7-5-10}$$

where ρ_0, w_0 are the gas density and velocity on the axis of the pipe; and $Re^{**}_{0w} = \rho_0 w_0 \delta^{**}/\mu_w$ is the Reynolds number over the momentum loss thickness.

/172

From (7-5-10), taking into account (1-11-2), we have

$$\frac{\tau_w}{\rho_0 w_0^2} = \frac{B}{2\,(Re^{**}_{0w})^m}\,\Psi_\infty. \tag{7-5-11}$$

In processing experimental data on friction and heat transfer for a stabilized gas flow in a pipe it is customary to introduce average parameters, which for the gas flow are defined by the following relations:

$$\bar{T} = \frac{2\pi}{G}\int_0^{R_0} \rho w T R\, dR, \tag{7-5-12}$$

$$\bar{w} = \frac{G}{F\bar{\rho}} = \frac{2}{R_0^2}\int_0^{R_0} w R\, dR. \tag{7-5-13}$$

We introduce the dimensionless parameters

$$f_1 = \int_0^1 \frac{\rho w}{\rho_0 w_0} \bar{R}\, d\bar{R}; \tag{7-5-14}$$

$$f_2 = \int_0^1 \frac{\rho w}{\rho_0 w_0} \left(1 - \frac{w}{w_0}\right) \bar{R}\, d\bar{R}; \tag{7-5-15}$$

$$f_3 = \int_0^1 \frac{w}{w_0} \bar{R}\, d\bar{R}. \tag{7-5-16}$$

where

$$\bar{R} = \frac{R}{R_0}.$$

Then

$$\frac{\overline{\rho w}}{\rho_0 w_0} = 2f_1; \tag{7-5-17}$$

$$\frac{\bar{w}}{w_0} = 2f_3; \tag{7-5-18}$$

$$\frac{\delta^{**}}{R_0} = f_2. \tag{7-5-19}$$

Taking (7-5-17), (7-5-18) and (7-5-19) into account, Eq. (7-5-11) can be written in the form

$$\frac{\tau_w}{\rho \bar{w}^2} = \frac{B\Psi_\infty}{2^{1-m}(\bar{\mathrm{Re}}_w)^m} f_2^{-m} f_3^{2-m} \psi^{-m} \frac{f_3'}{f_1}, \tag{7-5-20}$$

where $\bar{\mathrm{Re}}_w = \rho_w \bar{w} D/u_w$.

It can be assumed in the first approximation that non-isothermicity does not have much effect on the velocity profile. Thus, for an ideal gas, taking a power-law distribution of velocities and temperatures over the boundary-layer cross section (n = 1/7), it is possible to obtain the following formulas for the functions f_1, f_2 and f_3 from (7-5-14)-(7-5-16): /173

$$f_1 = 0{,}408\psi^{-0{,}162},\quad f_2 = 0{,}074\psi^{-0{,}318},\quad f_3 = 0{,}408, \tag{7-5-21}$$

where $\psi = T_w/T_0$.

Taking these relations into account, we get from (7-5-20) (for m = 0.25, B/2 = 0.0128),

$$\frac{\tau_w}{\rho \bar{w}^2} = \frac{0{,}00316}{(\bar{\mathrm{Re}}_w)^{0{,}25}} \frac{(\psi^{0{,}318})^{0{,}25}}{\psi^{0{,}25}} \psi^{0{,}163}\Psi_\infty. \tag{7-5-22}$$

Consequently,

$$\left(\frac{c_f}{c_{f0}}\right)_{\overline{Re}_w} \approx \Psi_\infty = \left(\frac{2}{\sqrt{\bar{\psi}}+1}\right)^2. \qquad (7\text{-}5\text{-}23)$$

The following relationship exists between the temperature factors $\zeta = \frac{T_w}{T_0}$ and $\psi = \frac{T_w}{T}$:

$$\psi = \bar{\psi}\frac{f_0}{f_1} = \bar{\psi}^{1.2}. \qquad (7\text{-}5\text{-}24)$$

Then,

$$\left(\frac{\bar{c}_f}{\bar{c}_{f0}}\right)_{\overline{Re}_w} = \left(\frac{2}{\bar{\psi}^{0.6}+1}\right)^2. \qquad (7\text{-}5\text{-}25)$$

From the Reynolds analogy it follows that

$$\left(\frac{St}{St_0}\right)_{\overline{Re}_w} = \left(\frac{\bar{c}_f}{\bar{c}_{f0}}\right)_{\overline{Re}_w} = \left(\frac{2}{\bar{\psi}^{0.6}+1}\right)^2. \qquad (7\text{-}5\text{-}26)$$

Going onto the Nusselt number and the gas parameters at wall temperature, taking (2-6-4) into account, we get

$$Nu_w = 0{,}023\overline{Re}_w^{0.8}Pr_w^{0.4}\bar{\psi}\left(\frac{2}{\bar{\psi}^{0.6}+1}\right)^2 \qquad (7\text{-}5\text{-}27)$$

or, if we take $\Psi_\infty \approx \bar{\psi}^{-0.6}$,

$$Nu_w = 0{,}023\overline{Re}_w^{0.8}Pr_w^{0.4}\bar{\psi}^{0.28}. \qquad (7\text{-}5\text{-}28)$$

It is interesting to note that in this case the effect of the temperature factor on the magnitude of the Nusselt number is less noticeable than on the friction coefficient and is opposite in sign.

If all the gas parameters occurring in the Reynolds and Nusselt numbers are defined with respect to average temperature, we get

$$\overline{Nu} = 0{,}023\overline{Re}^{0.8}\overline{Pr}^{0.4}\bar{\psi}^{-0.27}, \qquad (7\text{-}5\text{-}29)$$

where

/174

$$\overline{Nu} = \alpha D/\bar{\lambda},\ \overline{Re} = \bar{\rho}\bar{w}D/\bar{\mu};\ \lambda_w/\bar{\lambda} = \mu_w/\bar{\mu} = \bar{\psi}^{0.75},$$
$$\overline{Pr} = \bar{\mu}\bar{C}_p/\bar{\lambda};\ (T_w - T_0)/(T_w - \bar{T}) \approx 1.$$

The experimental heat-transfer data given in Fig. 7.32 are from the work of Perkins and Worsoe-Schmidt [194], V. L. Let'chuk and B. V. Delyakin [26] and McEligot [177]; they give a stronger dependence of the Nusselt number on non-isothermicity:

$$\overline{Nu} = 0{,}023\overline{Re}^{0.8}Pr^{0.4}\bar{\psi}^{-0.7}. \qquad (7\text{-}5\text{-}30)$$

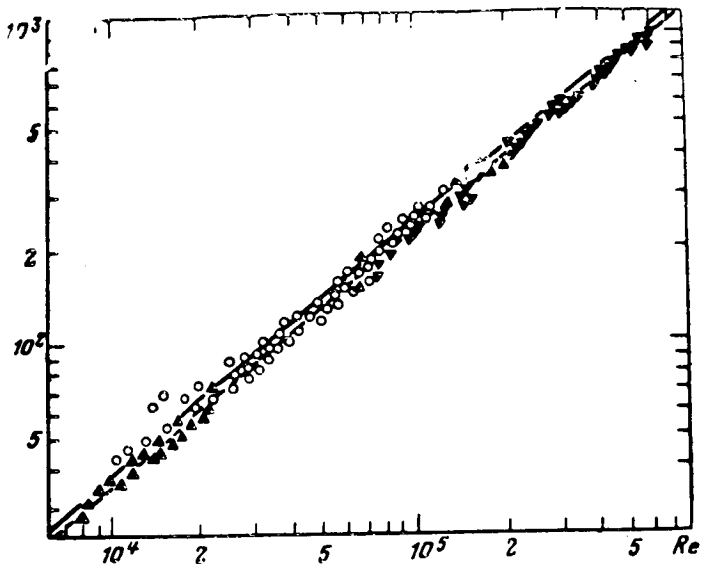

FIG. 7.32. Effect of nonisothermicity on the heat-transfer coefficient for a stabilized gas flow in a cylindrical pipe. The straight line was calculated taking (7-5-30) into account: ▲—[177]; ▼—[26]; ○—[194].

The discrepancy between the experimental and calculated data on heat transfer can be explained by the fact that the experiments were carried out with variable wall temperature and thermal stress over the length of the pipe, leading to infraction of the Reynolds analogy between the friction and heat transfer.

Using the hypothesis of heat-transfer law conservative to change in the boundary conditions, a method can be proposed for calculating the thermal boundary layer in a long cylindrical duct for an arbitrary law of thermal stress distribution over the length of the pipe. In the range of ψ from 1 to 5 we can take with a sufficient level of accuracy /175

$$\Psi_\infty \approx \psi_x^{-0.5}. \qquad (7\text{-}5\text{-}31)$$

where $\psi_x = T_w/T_{0x}$.

It can be shown that when

$$\frac{\mu_{0\infty}}{\mu_{01}} = (T_{0\infty}/T_{01})^{n_1}$$

$$\mathrm{Re}^{**}_T = \frac{\mathrm{Re}_{D1} f_2(\psi_\infty)}{4\left(\frac{T_{0\infty}}{T_{01}}\right)^{n_1} f_1(\psi_\infty)} \qquad (7\text{-}5\text{-}32)$$

where

$$f_2(\psi_\infty) = \int_0^1 \frac{\rho w}{\rho_0 w_0}\left(1 - \frac{T - T_w}{T_0 - T_w}\right)\left(1 - \frac{y}{R_0}\right) d\left(\frac{y}{R_0}\right);$$

$$f_1(\psi_\infty) = \int_0^1 \frac{\rho w}{\rho_0 w_0}\left(1 - \frac{y}{R_0}\right) d\left(\frac{y}{R_0}\right).$$

Taking into account (7-5-32) and (2-6-1), we have

$$\frac{\psi_x^{0.5}}{\psi_x - 1} = \frac{B \cdot 4^m \mathrm{Pr}_{01}^{1-n_1} \mathrm{Re}_{D1}^{1-m}}{2 f_1^{1-m} f_2^m \mathrm{Nu}_1} \left(\frac{T_{0x}}{T_{01}}\right)^{1+n_1 m} \tag{7-5-33}$$

From the heat balance equation we find

$$\frac{T_{0x}}{T_{01}} = \frac{f_1}{f_2}\left(1 + \frac{4\int_0^x q_w\, dx}{\mathrm{Re}_{D1}\mathrm{Pr}_{01}\lambda_{01}T_{01}}\right), \tag{7-5-34}$$

where

$$f_2 = \int_0^1 \frac{w}{w_m}\left(1 - \frac{y}{R_0}\right) d\left(\frac{y}{R_0}\right).$$

Taking Eq. (7-5-33) into account we have

$$\frac{\psi_x^{0.5}}{\psi_x - 1} = \frac{B \cdot 4^m \mathrm{Pr}_0^{1-n_1} \mathrm{Re}_{D1}^{1-m} f_1^{m(1+n_1)}}{2 f_2^m f_3^{1+n_1 m} \mathrm{Nu}_1}\left(1 + \frac{4\int_0^x q_w\, dx}{\mathrm{Re}_{D1}\mathrm{Pr}_{01}\lambda_{01}T_{01}}\right)^{1+n_1 m} \tag{7-5-35}$$

In the general case the function f_1, f_2 and f_3 depend on the nonisothermicity of the stream; the nonisothermicity shows up directly in the temperature factor ψ_x and indirectly in the deformation of the velocity and temperature profiles. It was shown earlier that the velocity profile is slightly deformed by nonisothermicity, and in the first approximation, therefore, we can take $\omega = \omega_0 = \xi^{1/7}$. Then, assuming like velocity and temperature distributions, we get /176

$$f_1 = 0,403\psi_x^{-0,163};\ f_2 = 0,074\psi_x^{-0,318};\ f_3 = 0,408. \tag{7-5-36}$$

When $m = 0.25$ and $n_1 = 0.75$

$$\left(\frac{f_1^{1+n_1}}{f_2}\right)\frac{1}{f_3^{1+n_1 m}} \sim \psi_x^{0,006},$$

that is, the combination of these parameters is essentially independent of the temperature factor.

Then, solving (7-5-35) for ψ_x, we get

$$\psi_x = 1 + \frac{1}{2c^2}(1 + \sqrt{1 + 4c^2}), \tag{7-5-37}$$

where

$$c = \frac{4^m}{2} B \mathrm{Re}_{D1}^{1-m} \mathrm{Pr}_{01}^{1-n_2} \frac{f_1^{m(1+n_1)}}{f_2^m f_3^{1+n_1 m}} \frac{\left(1 + \dfrac{4\int_0^x q_w\,dx}{\mathrm{Re}_{D1}\mathrm{Pr}_{01}\lambda_{01}T_{01}}\right)}{\mathrm{Nu}_1}.$$

Taking (7-5-34) into account, we have

$$\frac{T_w}{T_{01}} = \frac{f_1}{f_3}\left[1 + \frac{1}{2c^2}\left(1 + \sqrt{1+4c^2}\right)\right]\left(1 + \frac{4\int_0^x q_w\,dx}{\mathrm{Re}_{D1}\mathrm{Pr}_{01}\lambda_{01}T_{01}}\right). \qquad (7\text{-}5\text{-}38)$$

According to the work of P. N. Romanenko and N. V. Krylova [99], $B/2 = 0.0075$ and $m = 0.2$ for the stabilized gas flow region in a pipe. Taking $n_1 = n_2 = 0.75$, we get

$$T_w = T_{01}\left(1 + \frac{4\int_0^x q_w\,dx}{\mathrm{Re}_{D1}\mathrm{Pr}_{01}\lambda_{01}T_{01}}\right) \times \left\{1 + \frac{1\,640 q_w D_0^2}{\mathrm{Pr}_{01}^{0,86}\mathrm{Re}_{D1}^{1,6}\lambda_{01}^2 T_{01}^2\left(1 + 4\int_0^x \frac{q_w\,dx}{\mathrm{Pr}_{01}\mathrm{Re}_{D1}\lambda_{01}T_{01}}\right)^{2,3}}\right. \times \left.\left[1 + \sqrt{\frac{\mathrm{Pr}_{01}^{0,72}\mathrm{Re}_{D1}^{1,6}}{820\,\mathrm{Nu}_1^2}\left(1 + \frac{4\int_0^x q_w\,dx}{\mathrm{Re}_{D1}\mathrm{Pr}_{01}\lambda_{01}T_{01}}\right)^{2,3}}\right]\right\}^{0,54} \qquad (7\text{-}5\text{-}39)$$

/177

Given in Fig. 7.33 is a comparison of the results of a calculation by (7-5-39) with the experiments of V. L. Lel'chuk and B. V. Dedyakin [26]. The dashed line shows the calculation of the wall temperature in the initial section by the method outlined above, taking into account the effect of inlet conditions, according to the work of A. I. Leont'ev, and V. K. Fedorov [61].

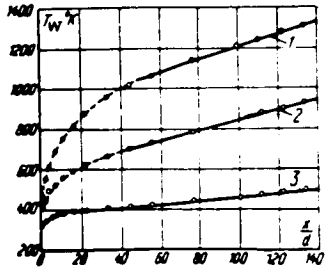

FIG. 7.33. Comparison of the results of wall-temperature calculation with the experiments of V. L. Lel'chuk and B. V. Dedyakin [26]. The solid curves represent calculation by (7-5-39); the broken line curves by formulas for the initial section [61]: 1—experiment No. 35; 2—No. 25; 3—No. 12 [26].

Given in Fig. 7.34 is a comparison of the results of wall temperature calculation by (7-5-39) with the experiments of B. S. Petukhov, V. V. Kirillov, Tsu Tzu-Hsiang and B. N. Maidanik [87]. The experiments were carried out with a considerable variation in thermal stress over the length of the duct (in experiment 13-II, for example, by a factor of 6). As is evident from the graphs, the proposed computational

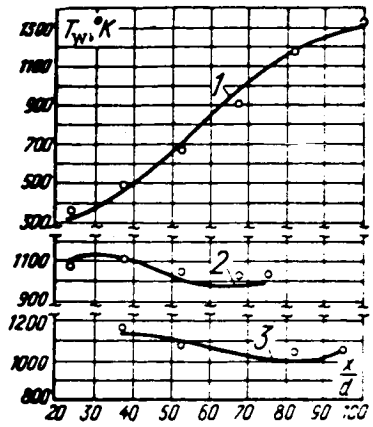

FIG. 7.34. Comparison of the results of wall-temperature calculation with the experiments of B. S. Petukhov et al. [87]. The curves were calculated by (7-5-39): 1—experiment 13-II; 2—6-VIII; 3—10-V.

method yields satisfactory results and takes correct account of the influence of both the thermal stress distribution and the thermal factor on the intensity of heat transfer of the gas in a pipe in the "stabilized" flow region. The method proposed by Ya. M. Visel [8] is applied to the case of the diffusion problem (condensation of vapor from a vapor-gas mixture).

7.6. Turbulent Boundary Layer of Gas in the Duct of an MHD Generator /178

In view of the relatively short lengths of seal MHD generator ducts ($L/D \approx 20$) and of the high Reynolds numbers (Re_L/L up to 10^6 m^{-1}), the boundary layers, which increase at the duct walls, do not intersect, as a rule, and the methods of turbulent boundary-layer calculation outlined in Chapter 7 for the initial section of a duct can be applied to these conditions.

A distinctive feature of an MHD boundary layer in the initial section of a duct is the fact that the unperturbed flow outside the boundary layer is also conductive, and therefore the flow core and the boundary layers are interconnected both electrically and gasdynamically.

In the absence of electric and magnetic fields the static pressure and longitudinal velocity in the flow core are uniquely related by the Bernoulli equation.

In an MHD generator it is necessary to distinguish between boundary layers at the electrode and insulator walls. The insulator wall is usually cooled, and only the outer portion of the boundary layer is electrically conductive and is subjected to the effect of volumetric forces. On the other hand, the temperature of the electrodes is close to that of the gas. The current induced by the flow core flows through the boundary layer, increasing at the electrode walls. The Lorenz force acting on the inner strata of the boundary layer will decelerate the gas and can bring about boundary layer separation from the wall of the electrode.

In ducts with appreciable longitudinal currents, e.g. Hall generators, there are appreciable transverse pressure gradients; as a result, gas flows arise along the insulator walls from one electrode to the other greatly complicating the flow pattern.

It should be kept in mind that the theory developed for a plane flow of conducting gas in transverse magnetic and electric fields cannot be applied directly to an axisymmetric flow, since circular symmetry is not preserved in the presence of a magnetic field.

The presence of additional terms in the energy equation, stemming from Joule heat generation, also complicates the problem appreciably. Therefore, the results presented below were obtained with certain assumptions and are estimative in nature. /179

The following hypotheses were adopted:

1. Considered is a plasma flow in the range of low magnetic Reynolds numbers and Hall parameters. These are the conditions that usually obtain during flow in the ducts of MHD generators.

2. Fluctuations of the electric and magnetic quantities and also the direct effect of the magnetic field on the turbulent pulsations are neglected. Some justification for this approximation, called the gasdynamic approximation, can be found in the papers of V. P. Panchenko [17]. Obviously, this hypothesis will be justified if the Joule heating and the ponderomotive force (in the layer at the insulator wall) are small compared to the heat flux and friction at the wall. At short distances from the electrode and low wall temperatures this hypothesis is not fulfilled, since then diffusion processes, Joule heating and other effects become significant.

3. The longitudinal electric field equals zero. The influence of end and near-electrode effects, which lead to the appearance of a longitudinal magnetic field, is disregarded.

The integral momentum and energy relations for these conditions are written as [see (1-2-1), (1-2-13), (2-4-9), (2-4-13)]

a) for the insulator wall

$$\frac{d\,\mathrm{Re}^{**}}{d\bar{x}} + \mathrm{Re}_L (1+H) f + \mathrm{Re}^{**} \frac{B_z j_y^0}{\rho_0 w_0^2} H_j = \mathrm{Re}_L \frac{c_f}{2}; \tag{7-6-1}$$

$$\frac{d\,\mathrm{Re}^{**}_{i\Sigma}}{d\bar{x}} + \mathrm{Re}^{**}_{i\Sigma} f_{i\Sigma} = \mathrm{Re}_L \mathrm{St}_\Sigma, \tag{7-6-2}$$

where

$$f_{i\Sigma} = \frac{1}{\Delta i_\Sigma} \frac{d(\Delta i_\Sigma)}{d\bar{x}} + \frac{1}{\Delta i_\Sigma} \frac{di^*_0}{d\bar{x}} (H - H_j);$$

$$H_j = \frac{\int_0^{\delta_1} \left(1 - \frac{j}{j_0}\right) dz}{\delta^{**}_1};$$

b) for the electrode wall /180

$$\frac{d\,\mathrm{Re}^{**}}{d\bar{x}} + \mathrm{Re}_L (1+H) f = \mathrm{Re}_L \frac{c_f}{2}; \tag{7-6-3}$$

$$\frac{d\,\mathrm{Re}^{**}_{i\Sigma}}{d\bar{x}} + \mathrm{Re}^{**}_{i\Sigma} f_{i\Sigma} = \mathrm{Re}_L \mathrm{St}_\Sigma, \tag{7-6-4}$$

where

$$f_{i\Sigma} = \frac{1}{\Delta i_\Sigma}\frac{d(\Delta i_\Sigma)}{d\bar{x}} + \frac{1}{\Delta i_\Sigma}\frac{di^*_e}{d\bar{x}}(H - H_E);$$

$$H_E = \frac{\int_0^{\delta_i}\left(1 - \frac{E}{E_e}\right)dy}{\delta^{**}_{i\Sigma}}.$$

Thus, the momentum equation for the turbulent boundary layer at the electrode wall retains the same form it had for nonconducting fluid, except that the velocity gradient in the flow core appearing in the shape parameter f must be defined by the formula

$$\rho_e w_e \frac{dw_e}{dx} = -\frac{dP}{dx} + j_y B_z. \tag{7-6-5}$$

Consequently, with the gasdynamic approximation we have adopted, the dynamic turbulent boundary layer at the electrode walls is calculated by the formulas of Chapter 6.

Important for supersonic MHD generators is the question of the stability of the turbulent boundary layers at the electrode walls. If the reserve of kinetic energy in the boundary layer when the flow core is decelerated proves to be inadequate to overcome the friction, pressure and ponderomotive forces, boundary-layer separation from the wall occurs and a system of compression shock arises.

The section of boundary layer separation from the electrode wall is determined by the formulas of Chapter 6 with allowance for the effect of non-isothermicity and compressibility on the frictional drag law and the critical separation parameters.

After linearizing the integral momentum relation (7-2-6) we get

$$\frac{d\,\mathrm{Re}^{**}_{ee}}{d\bar{x}} + (1 + H_{\mathrm{crit}})\frac{\mathrm{Re}^{**}_{ee}}{w_e}\frac{dw_e}{d\bar{x}} = \Psi_t \Psi_M \left(\frac{\mu_w}{\mu_{ee}}\right)^m \mathrm{Re}_L \frac{B}{2(\mathrm{Re}^{**}_{ee})^m} \tag{7-6-6}$$

After integration we get

/181

$$\mathrm{Re}^{**}_{ee} = \exp\left(-\frac{J}{1+m}\right)\left[(m+1)\frac{B}{2}\mathrm{Re}_{ee}\int_{\bar{x}_e}^{\bar{x}}(\Psi_t\Psi_M)\left(\frac{\mu_w}{\mu_{ee}}\right)^m U(1-U^2)^{\frac{1}{k-1}}\exp(J)\,d\bar{x} + c\right]^{\frac{1}{m+1}} \tag{7-6-7}$$

For the shape parameter H_{crit} we have the expression

$$H_{crit}=2{,}41\psi^*+1{,}38\Delta\psi-0{,}52. \tag{7-6-8}$$

The local values of the friction coefficients are determined by the formula

$$c_f=\Psi_i\Psi_M\Psi_f\frac{B}{(\mathrm{Re}^{**}_{\infty})^m}\left(\frac{\mu_w}{\mu_\infty}\right)^m, \tag{7-6-9}$$

where Ψ_i, Ψ_M and Ψ_f are determined by (7-1-19) and (6-2-14).

The shape parameter f is defined by the relation

$$f=\frac{\mathrm{Re}^{**}_{\infty}}{\mathrm{Re}_{\infty}U^2(1-U^\eta)^{\frac{1}{k-1}}}\frac{dU}{d\bar{x}}. \tag{7-6-10}$$

The parameter f_{crit} is calculated by (6-4-6), (6-4-7) and (6-4-12) or by the graphs in Figs. 6.10 and 6.13. In the section where the shape parameter f reaches the value f_{crit}, the turbulent boundary layer separates from the wall.

To solve the integral energy relations it is necessary to know the value of the electromagnetic shape parameters H_E and H_j.

D. N. Vasil'ev [19] has made an estimate of these parameters, using as a basis a power-law approximation of the velocity distribution and stagnation temperatures over the boundary-layer cross section.

Taking

$$\omega=\vartheta=\xi^n, \tag{7-6-11}$$

with allowance for (2-3-8) we have

$$\frac{j}{j_\delta}=[\psi+(\psi^*-\psi)\xi^n-(\psi^*-1)\xi^{2n}]. \tag{7-6-12}$$

/182

Ohm's law is written in the form

$$E=B\omega-\frac{j}{\sigma_\delta}, \tag{7-6-13}$$

and for the flow core it is written as

$$E_\delta=B\omega_\delta-\frac{j_\delta}{\sigma_\delta}. \tag{7-6-14}$$

Estimates will be made only for the thermal conductivity, when $\sigma=\sigma(P, T)$.

We take

$$\frac{\sigma}{\sigma_\delta}=\left(\frac{P}{P_\delta}\right)^{\nu_1}\left(\frac{T}{T_\delta}\right)^{\nu_2} \tag{7-6-15}$$

In the boundary layer P = const and it can be assumed that

$$\frac{\rho}{\rho_0} \approx \left(\frac{T}{T_0}\right)^{1/\varepsilon} \tag{7-6-16}$$

Taking Eqs. (7-6-12), (7-6-13) and (7-6-16) into account, we have

$$H_j = \frac{(n+1)(2n+1)}{n} \int_0^1 \left[1 - \frac{1}{1-k} \bar{P}^{1/\varepsilon} \{[\psi + (\psi^* - \psi)\xi^n - (\psi^* - 1)\xi^{2n}]^{1/2} (\xi^n - k)\right] d\xi; \tag{7-6-17}$$

$$H_E = \frac{(n+1)(2n+1)}{n} \int_0^1 \left[1 - \frac{\xi^n}{k} - \left(\frac{1-k}{k}\right) \bar{P}^{1/\varepsilon} \{[\psi + (\psi^* - \psi)\xi^n - (\psi^* - 1)\xi^{2n}]\}^{1/2} (\xi^n - k)\right] d\xi. \tag{7-6-18}$$

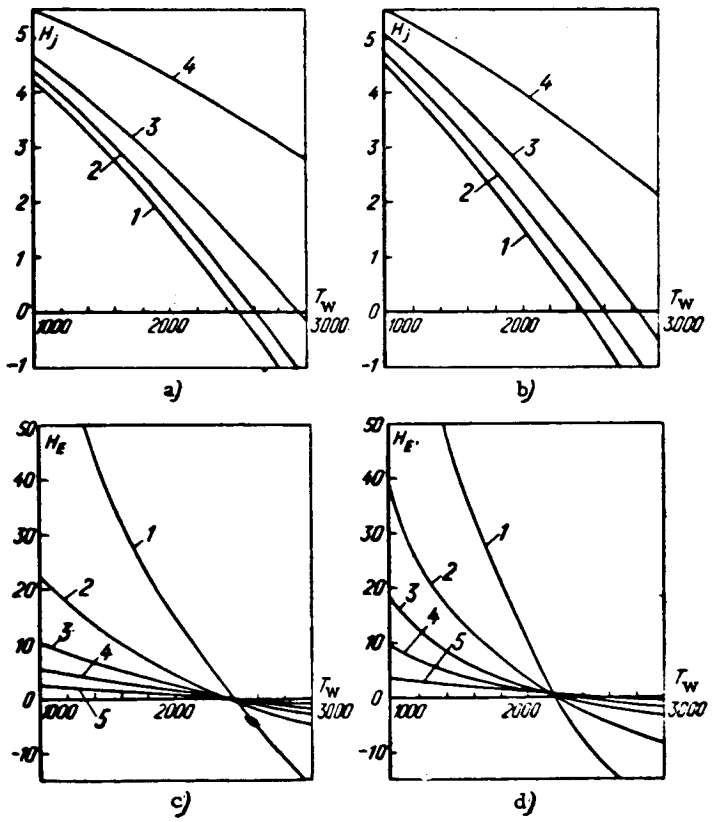

FIG. 7.35. Dependence of the electromagnetic shape parameters H_j and H_E on the non-isothermicity and load factor k. Calculations were made for T_{00} = 3,000 °K and M_0 = 2.5. a, c—n = 1/7; b, d—n = 1/10; 1—k = 0.1; 2—k = 0.3; 3—k = 0.5; 4—k = 0.7; 5—k = 0.9.

From Eqs. (7-6-17) and (7-6-18) it follows that the shape parameters H_j and H_E depend on the three variables ψ, ψ^* and k, where $k = E_0/Bw_0$ is the load factor.

The results of numerical calculation of the parameters H_j and H_E by (7-6-17) and (7-6-18) for $M_0 = 2.5$ ($\psi^* = 1.6$), $T_{00} = 3,000$ °K and various values of n and k are given in Fig. 7.35.

From the graphs it can be seen that the exponent n has a considerable influence on the shape parameters H_j and H_E at wall temperatures below 1,500 °K ($\psi < 0.5$). H_E and H_j decrease with increasing temperature and can become negative at certain values of ψ. Knowing the value of the shape parameters H_E and H_j, it is easy to determine the drop in potential and overflow current at the duct walls /183

$$\Delta\varphi_{\text{пр}} = \delta_{\text{эл}}^{**} H_E; \quad \Delta J = \delta_{\text{ин}}^{**} H_j, \tag{7-6-19}$$

where δ_{el}^{**} and δ_{in}^{**} are the momentum loss thickness at the electrode and insulator walls, respectively.

7.7. Examples of Calculation of a Turbulent Boundary Layer on an Impermeable Surface /184

Example 1. Calculate the friction and heat transfer on the surface of a cone in an air stream with parameters corresponding to an altitude of 10,000 m (P = 198.2 mm Hg, t = 50 °C) for M = 6. The cone apex angle is $2\omega = 20°$. The surface temperature is 600 °C.

The gas parameters behind the shock are determined from the diagram in the book of Yu. A. Kibardin, S. A. Kuznetsov and B. Ya. Shumyatskiy [39]. The angle of shock inclination to the axis of the cone is $\beta_{sh} = 14°$, $w_0/w_\infty = 0.975$; $\rho_0/\rho_\infty = 2$; $T_0/T_\infty = 1.37$; $M_0 = 4.97$. The gas parameters along the surface of the cone are taken to be constant. Then we get $w_0 = 1,750$ m/sec; $\rho_0 = 0.084$ kg · sec^2/m^4; $T_0 = 306$ °K; $u_w = 4.05 \cdot 10^{-6}$ kg · sec/m^2; $u_0 = 1.93 \cdot 10^{-6}$ kg · sec/m^2.

Very important for these conditions is the question of determining the laminar to turbulent boundary layer transition. The existing theoretical investigations of the loss of boundary layer stability, based on the method of small perturbations, can yield only qualitative results. /185

The limits of laminar-to-turbulent transition on the basis of existing experimental data are given in Table 7.5.

The results of calculating the complete stability of the boundary layer and a comparison of experimental data on laminar-to-turbulent boundary layer transitions on the surface of a cone with the results of calculation by van Driest [132] are given in Fig. 7.36.

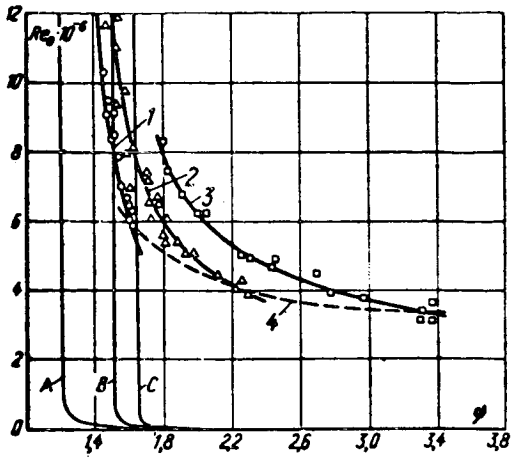

FIG. 7.36. Influence of cooling on the Reynolds transition number on a cone with a 10° angle. A, B, C—boundaries of complete stability; 1—M = 1.9, $Re_0 = 2.13 \cdot 10^7$; 2—M = 2.7, $Re_0 = 2.64 \cdot 10^7$; 3—M = 3.65, $Re_0 = 1.97 \cdot 10^7$; 4—thermally insulated surface; o, △, □ —van Driest's experiments [132].

From this figure it follows that under the conditions considered in the example cone cooling does not ensure complete stabilization of the laminar boundary layer. The boundary of complete stability for $M_0 = 4.97$ corresponds to $\psi = 2.7$. In our case $\psi^* = T_w/T_0 = 2.85$; $\psi^* = T_w/T_0 = 5.15$;

$$\frac{\Delta\psi}{1 + r\frac{k-1}{2}M_0^2} = -0.39. \qquad \text{/186}$$

According to the data of van Driest and Boison (see Table 7.5) cooling of the cone surface to values of

$$\frac{\frac{\Delta\psi}{\psi}}{1 + r\frac{k-1}{2}M_0^2} = -0.38$$

increases $Re_{x\ crit}$ by a factor of about 2.

According to the experiments of Laufer et al. [132], $Re_{x\ crit} \approx 3 \cdot 10^6$ for a heat-insulated cone. Then, for a cooled cone under the conditions being examined we find

$$Re_{x\ crit} \approx 6 \cdot 10^6 \text{ and } x_{crit} \approx 0.08 \text{ m}.$$

The friction and heat transfer in the laminar boundary layer were calculated using the integral momentum and energy relations.

The frictional drag and heat-transfer laws for a laminar boundary layer can be represented as [43]

$$\frac{c_f}{2} = \frac{0.22}{Re^{**}}\psi^{-0.22}(\psi^*)^{-0.08}. \qquad (7\text{-}7\text{-}1)$$

that is,

$$\Psi_l = \psi^{-0.22}(\psi^*)^{-0.08}.$$

Table 7.5. Critical values of the Reynolds

Author	Source	Cone angle deg	M
Laufer, Marte	[132]	5	1,79 2,55 4,5
Lange, Giseler, Lee	J. Aeronaut. Sci., 1953, vol. 20, № 12, p. 718	5	1,9—4,2
Van Driest	J. Aeronaut. Sci., 1957, № 12	10 10 10 10	1,9 2,7 3,65 1,9—3,65
Ross, Sincolair, Czarnecki	NACA TN 3020, TN 3648	10	1,4—2,01
Scherrer	NACA TR 1055, 1951	20	1,5—2,0 1,5—2,0
Van Driest, Boison	J. Aeronaut. Sci., 1955, vol. 22, p. 455	20	
Gazlay	J. Aeronaut. Sci., 1953, vol. 20, № 1	20	4,2
Sack, Diaconis	NACA TR 1055, 1951		3,12

For the case T_w = const /187

$$St = \Psi_l \frac{c_f}{2} \frac{1}{Pr^{2/3}}. \quad (7-7-2)$$

The momentum equation for flow around a cone has the form

$$\frac{d\,Re^{**}}{d\bar{x}} + \frac{Re^{**}}{\bar{x}} = Re_L \frac{c_f}{2}, \quad (7-7-3)$$

where $Re_L = w_0 L/\nu_{w0}$ and $c_f/2$ is the local friction coefficient.

Taking into account Eq. (7-6-1) we have

$$Re^{**} = \sqrt{\Psi_l}\,\frac{0{,}664}{\sqrt{3}}\sqrt{Re_x}; \quad (7-7-4)$$

$$\frac{c_f}{2} = \frac{0{,}574}{\sqrt{Re_x}}\sqrt{\Psi_l}; \quad (7-7-5)$$

$$St = \frac{0{,}574}{\sqrt{Re_x}}\,\frac{\sqrt{\Psi_l}}{Pr^{2/3}}. \quad (7-7-6)$$

number for supersonic flow around a core

$Re_{x\,crit}$	Φ	$\frac{V_x}{w_x}$, %	$\frac{\Delta\phi}{1+\frac{k-1}{2}M^2}$	Comments
$(4,3—3,3)\cdot10^6$ $3\cdot10^6$ $2,7\cdot10^6$		0,6—6 0,6—6 0,6—6		The influence of flow turbulance not discussed
$(3,4—1)\cdot10^6$				
$(12—5)\cdot10^6$ $(12—4)\cdot10^6$ $(8—3,5)\cdot10^6$ $(6—3,5)\cdot10^6$	1,4—1,65 1,5—2,3 1,8—3,4		0	
$(7—8)\cdot10^6$			0	The influence of the Mach number not evident
$4,1\ 10^6$ $3\cdot10^6$			0 0,14	Change in Re_{crit} due to variation of Re_L
$(2,7—5,4)\cdot10^6$			0—(—0,38)	
$4,5\cdot10^6$				
$(3—0,85)\cdot10^6$			20,2—(+0,5)	

In the laminar-to-turbulent boundary layer transition region we have

$$Re^{**}_{crit}=\frac{0,664}{\sqrt{3}}\sqrt{\Psi_l}\sqrt{Re_{x\,crit}}=0,383\cdot2,85^{-0,11}\cdot0,515^{-0,04}\times\sqrt{6\cdot10^6}=788$$

and

$$Re^{**}_{crit\,w}=Re^{**}_{crit}\frac{\mu_0}{\mu_w}=700;$$

$$Re^{**}_{T\,crit}=\frac{Re^{**}}{Pr^{2/3}}=993,\ Re^{*}_{T\,crit\,w}=830; \tag{7-7-7}$$

$$c_{f\,crit}=\frac{1,15\sqrt{\Psi_l}}{\sqrt{Re_{x\,crit}}}=\frac{1,15\,(1,19)^{-1}}{\sqrt{6\cdot10^6}}=3,94\cdot10^{-4} \tag{7-7-8}$$

The local frictional drag coefficient is

$$c_f=\frac{1,15\psi^{-0,11}\psi^{-0,04}}{\sqrt{\frac{w_0\rho_0}{\mu_0}x}}=\frac{1,105\cdot10^{-4}}{\sqrt{x}}. \tag{7-7-9}$$

The local heat-transfer coefficient is

$$\alpha = \frac{c_f}{2\,\mathrm{Pr}^{2/3}}\,\gamma_\infty c_{p0}\,w_0 = \frac{86.7}{\sqrt{x}}. \qquad (7\text{-}7\text{-}10)$$

For a turbulent boundary layer it is convenient to define the Reynolds number in terms of the viscosity with respect to wall temperature $\mathrm{Re}^{**}_w = (\rho_0 w_0 \delta^{**})/u_w$.

Considering the equality of the momentum loss thickness at the point of transition from a laminar to a turbulent layer, the integral of the momentum equation for a turbulent boundary layer is written as /190

$$\mathrm{Re}^{**}_w = C^{\frac{1}{m+1}}\left[\mathrm{Re}_{xw} - \frac{1}{\mathrm{Re}^{m+1}_{xw}}\left(\mathrm{Re}^{2+m}_{x1w} - \frac{\mathrm{Re}_w \mathrm{Re}^{**1+m}_{cr}}{C}\right)\right]^{\frac{1}{m+1}}. \qquad (7\text{-}7\text{-}11)$$

Hence, for the local friction drag coefficient we have

$$c_f = \Psi_\infty B C^{-\frac{m}{1+m}}\left\{\mathrm{Re}_x - \frac{1}{\mathrm{Re}^{m+1}_x}\left[\mathrm{Re}^{2+m}_{x1} - \frac{\mathrm{Re}^{1+m}_{x1}(\mathrm{Re}^{**}_{cr})^{1+m}}{C}\right]\right\}^{-\frac{m}{m+1}}, \qquad (7\text{-}7\text{-}12)$$

where

$$C = \left[\frac{1+m}{2(2+m)} B \Psi_\infty\right].$$

For the heat transfer we get

$$\mathrm{St} = \Psi_{x\infty}\frac{B}{2}\frac{C^{-\frac{m}{1+m}}}{(\mathrm{Pr}^{0,75})^{1+m}}\left[\mathrm{Re}_x - \frac{1}{\mathrm{Re}^{1+m}_x}\left(\mathrm{Re}^{2+m}_{x1} - \frac{\mathrm{Re}^{1+m}_{x1}\mathrm{Re}^{**1+m}_{T1}\mathrm{Pr}^{0,75}}{C}\right)\right]^{-\frac{m}{m+1}}. \qquad (7\text{-}7\text{-}13)$$

The results of turbulent boundary-layer calculations by formulas (7-6-12) and (7-6-13) are compiled in Table 7.6.

Given in Fig. 7.37 are the results of calculating the frictional-drag and heat-transfer coefficients for the conditions being examined. /191

Example 2. For the conditions of the Viking-10 [35] rocket, calculate the heat transfer on the surface of the rocket cone of angle $2\omega = 25°$ at a distance of 0.66 m

Table 7.6. Table for calculation of example 1

No. of the formula in the text	Formulas and calculation	Comments
(4-1-2)	$\Psi_t = \Psi_S = \frac{1}{\psi^* - 1}\left[\arcsin\frac{2(\psi^* - 1) + \Delta\psi}{\sqrt{4(\psi^* - 1)(\psi^* + \Delta\psi) + \Delta\psi^2}} - \right.$ $\left. - \arcsin\frac{\Delta\psi}{\sqrt{4(\psi^* - 1)(\psi^* + \Delta\psi) + \Delta\psi^2}}\right]^2 = \frac{1}{5{,}15 - 1} \times$ $\times\left[\arcsin\frac{2(5{,}15 - 1) - 2{,}3}{\sqrt{4(5{,}15 - 1)(5{,}15 - 2{,}3) + 2{,}3^2}} - \right.$ $\left. - \arcsin\frac{-2{,}3}{\sqrt{4(5{,}15 - 1)(5{,}15 - 2{,}3) + 2{,}3^2}}\right]^2 = 0{,}311;$ $n = \frac{1}{7}; \quad m = 0{,}25; \quad B = 0{,}0232;$ $T_{aw} = T_0\left(1 + \frac{k-1}{2}M_0^2\right) = 306\left(1 + \frac{1{,}4-1}{2}4{,}97^2\right) = 1\,820\ ^\circ\text{K}.$	The limit frictional drag and heat-transfer law is the same for coves and plates
(7-2-12)	$c_f = \Psi_t B C^{-\frac{m}{1+m}}\left[\mathrm{Re}_x - \frac{1}{\mathrm{Re}_x^{1+m}}\left(\mathrm{Re}_{x1}^{2+m} - \frac{\mathrm{Re}_{x1}^{1+m}(\mathrm{Re}^{**}_1)^{1+m}}{C}\right)\right]^{\frac{1}{1+m}} =$ $= \Psi_t B\left[\frac{1+m}{2(2+m)}B\Psi_t\right]^{-\frac{m}{m+1}}\left\{\frac{w_0\rho_0}{\mu_w}x - \frac{1}{\left(\frac{w_0\rho_0}{\mu_w}x\right)^{1+m}} \times\right.$ $\left.\times\left[\left(\frac{w_0\rho_0 x_1}{\mu_w}\right)^{1+m} - \frac{\left(\frac{w_0\rho_0}{\mu_w}x_1\right)^{1+m}\mathrm{Re}^{**1+m}_1}{\frac{1+m}{2(2+m)}B\Psi_t}\right]\right\}^{-\frac{m}{1+m}} =$ $= \frac{0{,}823\cdot 10^{-3}}{(x - 2{,}8\cdot 10^{-3}x^{-1{,}25})^{0{,}2}}$	$x_1 = x_{crit} = 0.08$; Re^{**}_1 from calculation of a laminar boundary layer
(7-2-53)	$\mathrm{St} = \Psi_S\frac{B}{2}\frac{\left[\frac{1+m}{2(2+m)}B\Psi_S\right]^{-\frac{m}{m+1}}}{\mathrm{Pr}^{0,75}}\left\{\frac{w_0\rho_0}{\mu_w}x - \right.$ $\left. - \frac{1}{\left(\frac{w_0\rho_0}{\mu_w}x\right)^{1+m}}\left[\left(\frac{w_0\rho_0}{\mu_w}x_1\right)^{2+m} - \frac{\left(\frac{w_0\rho_0}{\mu_w}x_1\right)^{1+m}}{\frac{1+m}{2(2+m)}B} \times\right.\right.$ $\left.\left. \times\frac{(\mathrm{Re}^{**}_{T1})^{1+m}\mathrm{Pr}^{0,75}}{\Psi_t}\right]\right\}^{-\frac{m}{1+m}} = \frac{0{,}575\cdot 10^{-3}}{(x - 2{,}8\cdot 10^{-3}x^{-1{,}25})^{0{,}2}};$ $\alpha = \mathrm{St}C_p\gamma_0 w_0 = \frac{0{,}575\cdot 10^{-3}}{(x - 2{,}8\cdot 10^{-3}x^{-1{,}25})^{0{,}2}}0{,}24\cdot 0{,}084\cdot 9{,}81\cdot 1\,770\cdot 3\,600 =$ $= \frac{716}{(x - 2{,}8\cdot 10^{-3}x^{-1{,}25})^{0{,}2}}.$	$\mathrm{Re}^{**}_{T1} = \mathrm{Re}^{**}_{T\,crit}$ from calculation of a laminar boundary layer

Table 7.7. Initial data for example 2

τ, sec	H, m	V, m/sec	P_0, mm hg	T_0, °K	ρ_0, kg·sec/m³	M_0	t_w, °C
60	13 200	455	119,8	216,5	$2,62 \cdot 10^{-2}$	1,64	24
70	19 000	660	48	216,5	$1,05 \cdot 10^{-2}$	2,23	52
75	22 500	800	27,6	216,5	$0,605 \cdot 10^{-2}$	2,7	80
80	26 500	925	14	216,5	$0,307 \cdot 10^{-2}$	3,12	111,5
85	32 200	1 100	7,2	216,5	$0,157 \cdot 10^{-2}$	3,72	138

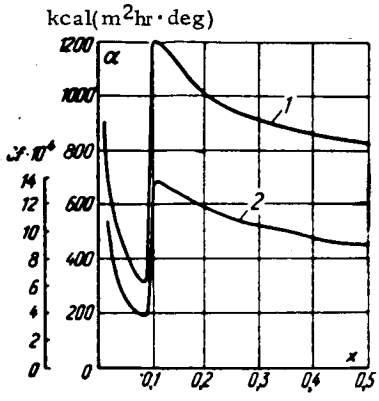

FIG. 7.37. Results of calculating frictional drag and heat transfer on a 10° cone for $M_0 = 6.0$. 1—a; 2—c_f.

from the cone apex and behind a turbulence generator at this same station. The initial data for the calculation are given in Table 7.7.

According to the data of Table 7.5 it follows that the boundary layer at the point of calculation should remain laminar in the flight time under study. A turbulence generator mounted just ahead of the calculation cross section ($x = x_1 = 0.64$) should make the laminar boundary layer turbulent.

We shall assume that the boundary layer downstream of the turbulence generator has become completely turbulent and that the values of Re^{**} just before and just behind the turbulence generator are the same. The calculation is performed by the method outlined above. The calculation results are given in Table 7.8 and in Fig. 7.38.

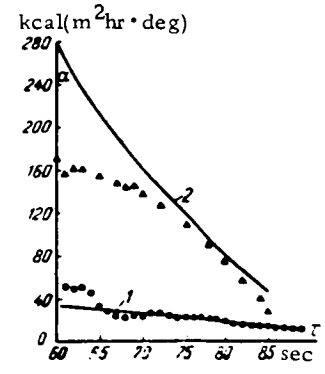

FIG. 7.38. Comparison of the results of calculating example 2 with the experimental data of Snodgrass [222]: 1—laminar boundary layer; 2—turbulent boundary layer; ▲—experimental values of α behind a turbulence generator; ●—value of α for a laminar boundary layer.

Table 7.8. Table for calculation of example 2

Formulas and Calculations	τ, sec				
	60	70	75	80	85
Laminar Boundary Layer					
$St = \frac{0,574}{\sqrt{Re_x}} \frac{\sqrt{\Psi_S}}{Pr^{3/2}}$	0,003288	0,000372	0,000415	0,000535	0,00065
$\alpha = St\, C_{p0}\, T_0 \omega_0 \cdot 3600$, kcal/(m^2 hr · deg)	34,9	27,3	23,7	21,2	16,5
$Re^{**}_{T1} = Re^{**}_1/Pr^{3/2} = \frac{0,363}{Pr^{3/2}} \psi - 0,11\psi^* - 0,04\sqrt{Re_x}$	1100	845	727	560	452
Turbulent Boundary Layer					
$\Psi_S = \frac{1}{\psi^* - 1} \left[\arcsin \frac{2(\psi^* - 1) + \Delta\psi}{\sqrt{4(\psi^* - 1)(\psi^* + \Delta\psi) + \Delta\psi^2}} - \right.$ $\left. - \arcsin \frac{\Delta\psi}{\sqrt{4(\psi^* - 1)(\psi^* + \Delta\psi) + \Delta\psi^2}} \right]^2$	0,834	0,7	0,728	0,694	0,585
$St = \Psi_S \frac{B}{2} \frac{C^{-\frac{m}{1+m}}}{(Pr^{0,75})^{\frac{1}{1+m}}} \left[Re_x - \frac{1}{Re_x^{\frac{1}{1+m}}} \left(Re_{x1}^{2+m} - \right. \right.$	0,00224	0,00219	0,00222	0,00226	0,00204
$\left. \left. - \frac{Re_{x1}^{1+m} Re_{T1}^{**1+m} Pr^{0,75}}{C} \right) \right]^{\frac{m}{1+m}}$; $m = 0,25$; $B = 0,0252$	274	162	126	81,5	49,3
$\alpha = St\, C_{p0} T_0 \omega_0 \cdot 3600$, kcal/(m^2 hr · deg)					

Example 3. Calculate the distribution of specific heat load over the length of the nozzle of a liquid-fuel rocket engine. The initial data for the calculation are as follows:

pressure in the precombustion chamber: P = 6, 8, 14 kp/cm^2;
characteristic velocity: 1617, 1653 m/sec;
nozzle wall temperature: 478 °K
recovery factor: r = 0.9;
propellant: hydrazine (N_2H_4) and nitrogen tetroxide N_2O_4 in the ratio 1:1;
adiabatic index: k = 1.22;
gas constant of the combustion products: R = 44.49.

The geometrical dimensions of the nozzle are shown in Figs. 7.39 and 7.40.

The combustion products of hydrazine in nitrogen tetroxide consist of a mixture of nitrogen, hydrogen and water vapor. The weight concentrations of these gases (for $m_{ox}/m_{fuel} = 1$) an $C_{N_2} = 0.59$, $C_{H_2} = 0.019$, and $C_{H_2O} = 0.391$. The rest of the initial data are given in Table 7.9. /193

The stagnation temperature of the gas is related to the characteristic velocity as

$$T_{00} = \frac{(c^*)^2 [\beta \cdot \chi(k)]^2}{gR}, \qquad (7\text{-}7\text{-}14)$$

where /195

$$\chi(k) = \sqrt{\frac{2k}{k+1}} \Big/ \left(\frac{k+1}{2}\right)^{\frac{1}{k-1}};$$

β is the mass flow coefficient, k = 1.22 and R = 44.49 kg · m/deg.

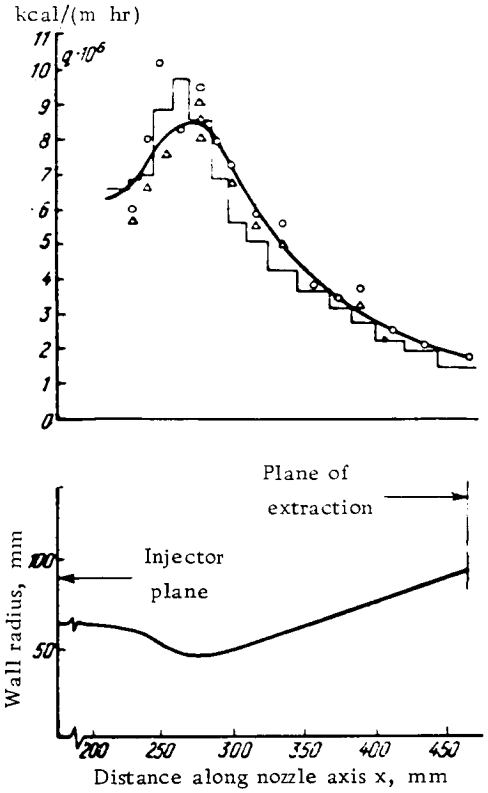

FIG. 7.39.

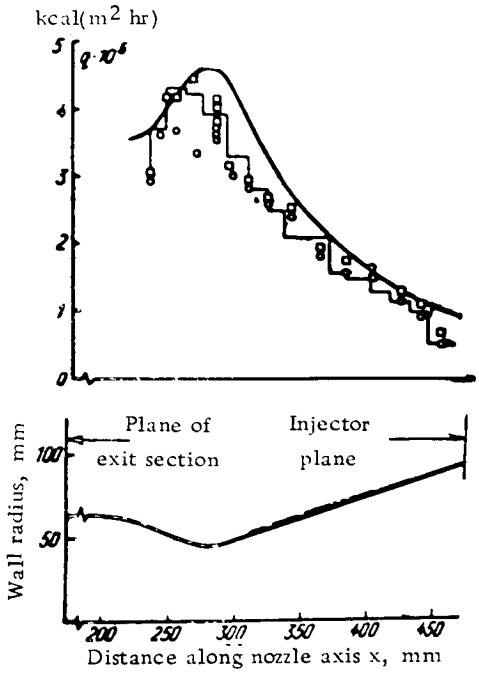

FIG. 7.40.

FIG. 7.39. Comparison of the results of calculating heat transfer on a nozzle with the experiments of [247]. P_{00} = 6.82 kp/cm^2. The curve was calculated by (7-6-16) and (7-6-17); o, Δ —measurements of q_w from the temperature drop in the wall; broken line—results of measuring q_w by the calorimetric method.

FIG. 7.40. Comparison of the results of calculating heat transfer in a nozzle with the experiments of [247]. P_{00} = 14.06 kp/cm^2. The curve was calculated by (7-6-16) and (7-6-17); o, □ —measurements of q_w from the temperature drop in the wall; broken line—measurements of q_w by the calorimetric method.

Table 7.9. Initial data for example 3

T, °C	1 000	1 200	1 400	1 600	1 800	2 000
C_p, kcal/(kg·deg)	0,473	0,49	0,505	0,517	0,527	0,536
$\mu \cdot 10^{-6}$, kg·sec/m^2	3,86	4,25	4,6	4,96	5,3	5,56

Then, $T_{00} = 2,820.7$ °K for $c^* = 1,617$ m/sec and $T_{00} = 2,940$ °K for $c^* = 1,653$ m/sec.

The computational formula for the heat transfer coefficient has the form

$$\alpha = \frac{B}{2} C_{p0}\, 3600 \gamma_0 w_0\, \mathrm{Pr}^{-0,75} \Psi_\infty \left(\frac{R}{R_{crit}}\right)^m \times \left[\frac{B(1+m)\gamma_{crit} w_{cr}}{2\,\mathrm{Pr}^{0,75} g \mu_{00}} \int_0^x \Psi_\infty \left(\frac{R}{R_{crit}}\right)^{1-m} dx\right]^{-\frac{m}{m+1}} \qquad (7\text{-}7\text{-}15)$$

Taking $m = 0.25$, $B = 0.0252$ and $\mathrm{Pr}^{0.75} = 0.846$ we have

$$\alpha = C_{p0}\gamma_0 w_0 53,6 \Psi_\infty \left(\frac{R}{R_{crit}}\right)^{0,25} \times \left[0,0186\, \frac{\gamma_{cr} w_{cr}}{g \mu_{00}} \int_0^x \Psi_\infty \left(\frac{R}{R_{crit}}\right)^{-0,75} dx\right]^{-0,2}. \qquad (7\text{-}7\text{-}16)$$

The magnitude of the specific heat fluxes is determined by the formula

$$q_w = \alpha(T_w - T^*_w). \qquad (7\text{-}7\text{-}17)$$

The calculation results are given in Table 7.10 and are shown in Figs. 7.39 and 7.40. Given in the same graphs are the results of the experiments of Whitte and Harper [247], which were obtained with an engine under the same conditions for which

Table 7.10. Table for calculation of example 3

x, m	$Re^{**}_{T(1)}$	$Re^{**}_{T(2)}$	Ψ_T	$\frac{R_{cr}}{R}$	$\left(\frac{R_{cr}}{R}\right)^{-0,75}$	$\Delta T_{(1)}$	$\Delta T_{(2)}$	$T_0 w_{0(1)}$	$T_0 w_{0(2)}$	$C_{p0(1)}$, kcal/kg·deg	$C_{p0(2)}$, kcal/kg·deg	$q \cdot 10^{-6}_{(1)}$, kcal/m²·hr	$q \cdot 10^{-6}_{(2)}$, kcal/m²·hr	$Re^{**}_{(1)}$
0,213	9 850	17 500	2	0,782	0,831	2342	2462	252	508	0,554	0,556	3,52	6,33	8 700
0,229	10 900	19 350	1,96	0,809	0,858	2340	2460	271	548	0,552	0,554	3,64	6,60	9 780
0,241	12 650	22 450	1,94	0,877	0,903	2330	2450	317	642	0,550	0,552	3,96	7,36	11 300
0,254	14 700	26 100	1,92	0,938	0,955	2320	2430	354	738	0,549	0,550	4,21	8,02	13 150
0,266	16 400	29 100	1,90	0,987	0,991	2310	2420	401	810	0,548	0,550	4,56	8,44	14 650
0,279	17 300	30 700	1,88	1,00	1,00	2300	2410	414	835	0,548	0,548	4,55	8,41	15 350
0,292	17 000	30 200	1,82	0,987	0,99	2290	2405	401	810	0,542	0,545	4,26	7,91	15 500
0,305	16 100	28 600	1,80	0,937	0,952	2280	2400	362	732	0,540	0,542	3,81	7,06	14 900
0,317	14 820	26 300	1,75	0,885	0,910	2270	2395	322	649	0,535	0,537	3,35	6,15	13 150
0,330	13 400	23 850	1,68	0,833	0,872	2270	2390	286	579	0,530	0,532	2,87	5,39	12 000
0,356	11 800	20 900	1,64	0,749	0,803	2260	2380	232	466	0,525	0,527	2,33	4,28	10 400
0,361	10 130	17 950	1,54	0,677	0,746	2250	2370	189	374	0,517	0,520	1,82	3,30	9 500
0,406	8 950	16 500	1,50	0,618	0,695	2240	2360	158	319	0,510	0,512	1,49	2,73	7 500
0,432	8 080	14 400	1,46	0,569	0,654	2230	2350	133	269	0,507	0,510	1,235	2,31	7 180
0,457	7 320	13 000	1,42	0,527	0,617	2230	2350	115	232	0,502	0,505	1,06	1,97	6 440
0,465	7 040	12 550	1,40	0,514	0,607	2225	2340	109	221	0,500	0,503	0,995	1,85	6 320

the calculation was made. The heat flux was measured by two methods, balance and non-stationary. As can be seen from the graphs, the proposed calculation method is in satisfactory agreement with the experiments.

Example 4. Calculate the changes in momentum loss thickness and shape parameter H for a supersonic turbulent boundary layer in the diffusor region. The initial data for the calculation are as follows:

T_{00} = 338 °K; diffusor wall thermally insulated;

P_{00} = 1 kp/cm^2;

δ^{**}_0 = 0.406 mm (at $\bar{x}$ = 0).

The variation of the Mach number over the diffuser length is given in the following table:

$\bar{x} = x/L$	0	0,2	0,4	0,6	0,8	1,0
M	3,01	2,76	2,49	2,17	1,93	1,79

The geometrical dimensions of the diffusor are shown in Fig. 7.41. /198

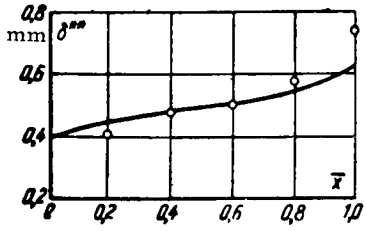

FIG. 7.41

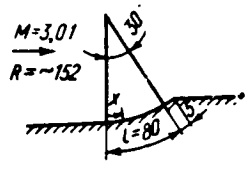

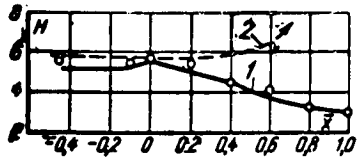

FIG. 7.42

FIG. 7.41. Variation of δ^{**} over the length of a supersonic diffusor. The curve is theoretical; the points represent the experiments of [178].

FIG. 7.42. Change of the shape parameter H over diffusor length: 1—calculated by the proposed method; 2—calculated in [198]; the points represent the experiments of [178].

The results of calculating a turbulent boundary layer by the proposed method for the conditions under study are presented in Table 7.11 and in Figs. 7.41 and 7.42. Shown in these same graphs are the experimental results of McLafferty and Barber [178]. As can be seen from the graphs, the proposed computational method is in satisfactory agreement with the experiments.

Table 7.11. Computational results for example 4 /197

$\bar{x}$	M	w, m/sec	ψ°	H_{cr}	Ψ	B	C	$\int_0^{\bar{x}} A d\bar{x} \cdot 10^3$	Re^{**}	δ^{**}, mm	$\frac{dw}{d\bar{x}}$, sec^{-1}	$-f \cdot 10^3$	$-f_{cr} \cdot 10^3$	$\frac{f}{f_{cr}}$	$\bar{H}$	H
0	3,01	668	2,64	5,82	0,5	1	1	0	1 050	0,406	1 310	0,8	1,02	0,785	0,975	5,66
0,2	2,76	644	2,37	5,19	0,54	1,34	0,69	0,616	1 460	0,455	1 750	1,13	1,31	0,86	0,98	5,08
0,4	2,49	616	2,12	4,59	0,58	1,78	0,485	1,21	2 020	0,490	2 390	1,66	1,68	0,985	0,999	4,59
0,6	2,17	577	1,85	3,94	0,63	2,32	0,349	1,83	2 690	0,496	2 180	1,8	2,4	0,75	0,96	3,78
0,8	1,93	542	1,67	3,50	0,68	2,98	0,255	2,46	3 580	0,546	1 500	1,65	2,88	0,574	0,94	3,29
1,0	1,79	518	1,577	3,27	0,73	3,8	0,189	3,05	4 670	0,63	1 500	1,97	3,28	0,6	0,941	3,07
—0,4	3,01	668	2,64	5,82							0	0		0	0,89	5,2

Remarks:

$$B = \frac{1}{\exp \int (1 + H_{cr}) \frac{dw_0}{w_0}}. \qquad C = \exp (1 + m) \int (1 + H_{cr}) \frac{dw_0}{w_0}. \qquad A = \Psi \left(\frac{\mu_0}{\mu_\infty}\right)^m \frac{\rho_0}{\rho_\infty} \frac{w'_0}{w'_\infty} C.$$

CHAPTER 8
TURBULENT BOUNDARY LAYER OF GAS ON A PERMEABLE SURFACE

/198

8.1. Comparison of the Limiting Relative Laws of Friction, Heat-and Mass Transfer on a Permeable Plate with Experiment

It is well known that when gas is injected at the surface of a body the stability of the laminar boundary layer decreases. It can be assumed that in a turbulent boundary layer the contribution of viscous friction forces to the total drag decreases with increasing intensity of injection. This fact reduces the influence of the Reynolds number on the relative laws of friction and heat transfer and should favor the applicability of the limiting laws of friction and heat transfer for practical calculations in the range of finite Reynolds numbers. In order to compare the experimental data with the limit formulas let us obtain the relative frictional-drag and heat-transfer coefficients for the condition Re_x = idem.

/199

The integral momentum relation for a plane turbulent boundary layer of incompressible fluid on a permeable plate can be written in the form of (1-2-11):

$$\frac{d\,\mathrm{Re}^{**}}{d\,\mathrm{Re}_x} = (\Psi + b)\frac{c_{f_0}}{2}, \tag{8-1-1}$$

where, as usual, $\mathrm{Re}^{**} = \omega_0\delta^{**}/\nu$; $\mathrm{Re}_x = \omega_0 x/\nu$.

Let us examine two canonical cases: b = const and j_w = const. We shall assume that the turbulent boundary layer develops off the leading edge of the plate, i.e. for x = 0, δ = 0. Then, taking $c_{f_0} = B(\mathrm{Re}^{**})^{-m}$, for the case b = const we have

$$\mathrm{Re}^{**} = \left[\frac{B}{2}(1+m)(\Psi+b)\,\mathrm{Re}_x\right]^{\frac{1}{1+m}}. \tag{8-1-2}$$

We define the friction coefficient for standard conditions by the formula

$$\frac{c_{f_{0x}}}{2} = \frac{B_1}{\mathrm{Re}_x^{m_1}}, \tag{8-1-3}$$

where

$$m_1 = \frac{m}{1+m};\quad B_1 = \left(\frac{B}{2}\right)^{\frac{m_1}{m}}(1+m)^{-m_1}.$$

When m = 0.25 and B/2 = 0.0128, we have $c_{f_{0x}}/2 = 0.0296\,\mathrm{Re}_x^{-0.2}$.

We introduce the relative friction coefficient and the permeability parameter in the form

$$\left.\begin{aligned}\Psi_x &= \left(\frac{c_f}{c_{f_0}}\right)_{\mathrm{Re}_x};\\ b_x &= \frac{2}{c_{f_{0x}}}\bar{j}_w.\end{aligned}\right\} \tag{8-1-4}$$

The quantity Ψ_x is the ratio of the friction coefficient on a permeable plate to the friction coefficient on an impermeable plate for equal values of Re_x.

From Eqs. (8-1-2) and (8-1-4) it follows that /200

$$\left.\begin{aligned} c_{fox} &= c_{f_0}(\Psi+b)^{m_1},\ b_x = \frac{b}{(\Psi+b)^m};\\ \Psi_x &= \frac{\Psi}{(\Psi+b)^{m_1}},\ b_{\text{crit}x} = b_{\text{crit}}^{1-m_1}. \end{aligned}\right\} \quad (8\text{-}1\text{-}5)$$

Let us recall that $\Psi = \left(\frac{c_f}{c_{f_0}}\right)_{Re^{**}}$, $b = \zeta_w \frac{2}{c_{f_0}}$. When $b = b_{crit}$, we have $\Psi_x = \Psi = 0$.

From Eqs. (8-1-5)

$$\Psi_x = \left(1 - \frac{b}{4}\right)^2 \frac{b_x}{b}, \quad (8\text{-}1\text{-}6)$$

consequently, $\Psi_x \longrightarrow b_x$ when $b \longrightarrow 4$; that is, in this case

$$j_w = -\frac{c_f}{2} \quad (8\text{-}1\text{-}7)$$

and

$$\tau_w = \rho(-w_w)w_0. \quad (8\text{-}1\text{-}8)$$

Thus, there exists a limit solution for suction of a turbulent layer, as is known [100], an analogous result is also obtained for a laminar boundary layer (the case of an asymptotic solution). As follows from (8-1-1), in this case Re^{**} = const and δ^{**} = const.

When m = 0.25

$$\left.\begin{aligned} \Psi_{x\infty} &= \frac{(1-0{,}25b)^2}{(1+0{,}25b)^{0{,}4}};\\ b_x &= \frac{b}{(1+0{,}25b)^{0{,}4}};\\ b_{x\text{crit}} &= 3{,}0 \end{aligned}\right\} \quad (8\text{-}1\text{-}9)$$

and the flow being examined exists in the region

$$-4 < b < +4 \text{ and } -\infty < b_x < +3{,}0.$$

For the conditions j_w = const and the boundary conditions $\delta^{**} = 0$ at x = 0 for m = 0.25, we get from the momentum relation

/201

$$\mathrm{Re}_x = \int_0^{\mathrm{Re}^{**}} \frac{\frac{B}{2}\,\mathrm{Re}^{**1/4}\,d\,\mathrm{Re}^{**}}{\left(\frac{B}{2}+\frac{1}{4}\bar{j}_w\mathrm{Re}^{**1/4}\right)^2}$$

$$= \frac{16}{3\bar{j}_w\beta^3(1+\beta\mathrm{Re}^{**1/4})}\{\beta^3\mathrm{Re}^{**} - 2\beta^3(\mathrm{Re}^{**})^{3/4} + 6\beta^3(\mathrm{Re}^{**})^{1/2} + 12\beta(\mathrm{Re}^{**})^{1/4} - 12[1 + \beta(\mathrm{Re}^{**})^{1/4}]\ln[1+\beta(\mathrm{Re}^{**})^{1/4}]\}. \quad (8\text{-}1\text{-}10)$$

where

$$\beta = \bar{j}_w/2B.$$

Expanding the logarithms from this formula into a series and limiting ourselves to the first five terms, we get

$$\mathrm{Re}^{**} = \left[\frac{B}{8}(1+\beta\mathrm{Re}^{**1/4})\,\mathrm{Re}_x\right]^{4/5}. \quad (8\text{-}1\text{-}11)$$

Consequently,

$$\left.\begin{aligned} \Psi_{x\infty} &= \frac{(1-0.25b)^2}{(1+0.25b)^{0.2}};\\ b_x &= \frac{b}{(1+0.25b)^{0.2}};\\ b_{x\,\mathrm{crit}} &= 3{,}5. \end{aligned}\right\} \quad (8\text{-}1\text{-}12)$$

The asymptotic solution for these boundary conditions also yield

$$\tau_w = -\rho w_{c\tau} w_0.$$

In the region of existence of a flow with j_w = const

$$-4 < b < 4 \text{ and } -\infty < b_x < +3{,}5.$$

When c_{f_0} = const (e.g., flow over a rough surface), the conditions b = const and j_w = const become identical and the functions Ψ and Ψ_x coincide.

Given in Fig. 8.1 is a comparison of the results of calculating the frictional drag laws by formulas (8-1-9) and (8-1-12). As can be seen from the graph, the difference between the formulas is not great.

The triple Reynolds analogy should be satisfied fro these conditions; that is,

$$\Psi_\infty = \Psi_{S\infty} = \Psi_{D\infty}, \quad (8\text{-}1\text{-}13)$$

where, as will be shown below, the conditions T_w = const and c_w = const correspond to the conditions b_T = const and b_D = const.

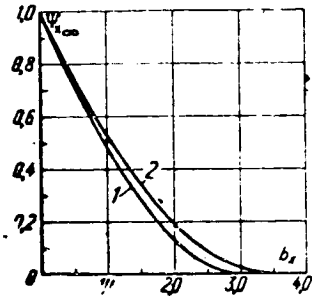

FIG. 8.1. Comparison of the relative friction coefficients on a permeable plate for the case b = const (1) and j_w = const (2). 1—calculated by (8-1-9); 2—calculated by (8-1-12).

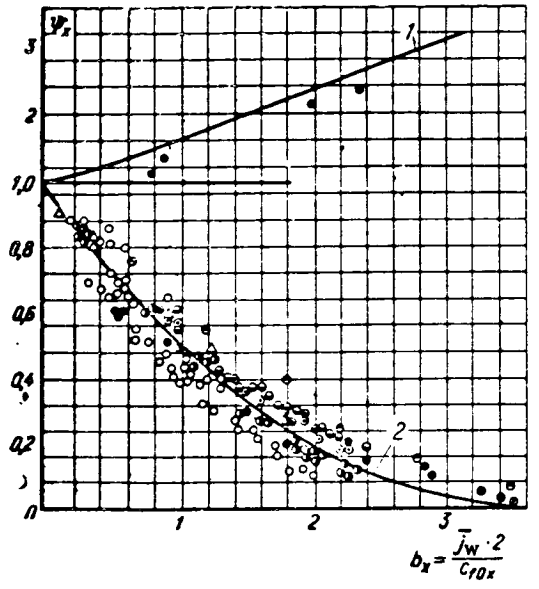

FIG. 8.2. Influence of gas injection on the turbulent friction coefficient on a permeable plate: 1—gas suction, calculated by (8-1-12) for b < 0; 2—gas injection, calculated by (8-1-12) for b > 0; ○—[148]; △—[191]; ◑—[90]; ●—[181]; ◓—[49]; ◒, ⊙—[156].

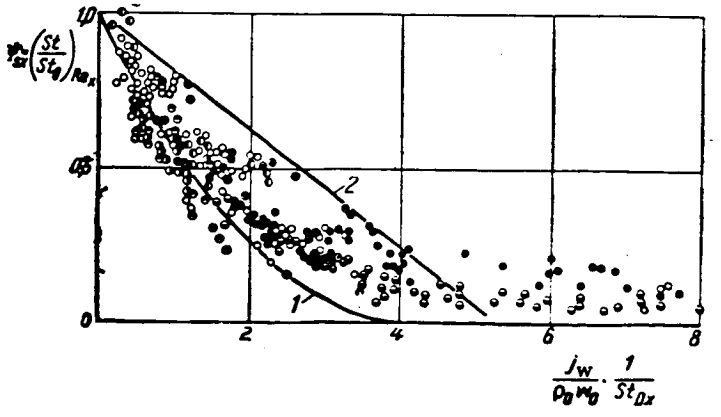

FIG. 8.3. Influence of gas injection on the coefficient of heat transfer on a permeable plate. 1—calculated by (8-1-12); 2—calculated the empirical formula of [83]; ○—[180]; ◐—[141]; ◑—[90]; ⊙—[125]; ◓—[238]; ●—[96]; ◒—[145].

The existing experimental data from measurement of friction on a permeable plate are compared in Fig. 8.2 with the limit formulas (8-1-12). The agreement between the limit frictional drag law and the experimental data obtained for finite Reynolds numbers can be considered as completely satisfactory, although the great scatter of the experimental points, especially at high injection intensities, should be noted. From our viewpoint, the most reliable data of Kendall [135], Dershin [135] and Mickley (as processed by Leadon) [169] are located somewhat above the limit relation. /202 /203

The limit law of heat transfer is compared in Fig. 8.3 with experimental data on a permeable plate for the subsonic velocity range with injection of a homogeneous gas. As can be seen from the graph, the experimental data on heat transfer exhibit substantially greater dispersion than those on friction, especially in the region of intense injection. From our viewpoint, the most reliable results, obtained by Kays et al. [182], are located somewhat above the limit relation, which may be explained by the influence of the finite Reynolds number.

8.2. Critical Injection Parameters

Three regions can be defined for gas injection through a permeable surface, depending on the intensity of injection, as follows:

1. The friction coefficient $c_f/2$ in the momentum equation is commensurate with the relative injection j_w. In this case the basic assumptions of boundary layer theory remain in force, but a simple self-similar solution cannot be obtained because the equation contains the friction coefficient. /204

2. Relative injection is considerably greater than the friction coefficient ($j_w \geqslant c_f/2$, but the momentum of the injected gas mass is much lower than that of the main gas flow. In this case the fundamental assumptions of boundary-layer theory remain in force, and a simple relationship between δ^{**} and j_w is obtained from the momentum equation:

$$\delta^{**} = \bar{j}_w x. \tag{8-2-1}$$

3. The momentum fluxes of the injected gas and main flow are commensurate. In this case the assumptions of boundary-layer theory are unsuitable.

An approximate estimate can be made of the region of variation of the transverse mass flow, where the basic assumptions of boundary-layer theory remain valid.

Reducing the Navier-Stokes equations to dimensionless form and considering that

$$w'_y \sim \frac{w_w}{\bar{w}_e} = f,$$

during gas injection, we get

$$w'_x \frac{\partial w'_x}{\partial x'} + w'_y \frac{\partial w'_x}{\partial y'} = -\frac{\partial P'}{\partial x'} + \frac{1}{\mathrm{Re}}\left(\frac{\partial^2 w'_x}{\partial x'^2} + \frac{\partial^2 w'_x}{\partial y'^2}\right); \tag{8-2-2}$$

$$w'_x \frac{\partial w'_y}{\partial x'} + w'_y \frac{\partial w'_y}{\partial y'} = -\frac{\partial P'}{\partial y'} + \frac{1}{\mathrm{Re}}\left(\frac{\partial^2 w_y}{\partial x'^2} + \frac{\partial^2 w'_y}{\partial y'^2}\right). \tag{8-2-3}$$

Thus, the principal consumption of boundary-layer theory (that is, $\partial P/\partial y = 0$) remain valid if $f \sim \delta'$, that is, $w_{yw}/w_o \sim \delta/L$. Since $\delta/L \approx 0.37/Re_x^{0.2}$, the domain f applicability of the methods f boundary-layer theory, according to the estimates, is bounded by the maximum value of the permeability parameter $b_x \approx 12$.

One of the interesting results of the asymptotic turbulent boundary-layer theory under development is that the boundary layer separates from the wall at certain injection intensities, defined by the critical injection parameter. In particular, the critical injection parameter is $b_{crit} = 4$ for injection of a homogeneous gas into a subsonic stream under quasi-isothermal conditions. In this cross section the friction coefficient equals zero, the wall temperature equals the temperature of the injected gas and the concentration of injected gas at the wall is 100%. /205

Taking these ideas into account, a qualitative picture of turbulent boundary layer development over a permeable plate at a constant mass flow rate of injected gas can be given in the form of the diagram illustrated in Fig. 8.4.

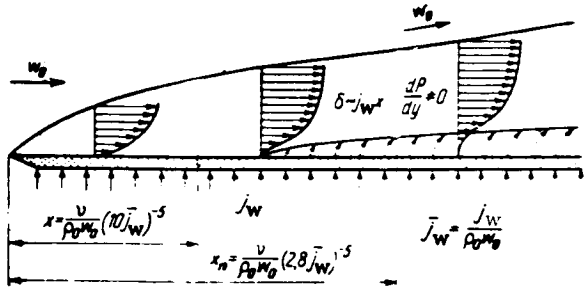

FIG. 8.4. Diagram of boundary-layer development along a permeable plate.

Up to the section $x = x_{crit}$ we are dealing with the first region. At the section $x = x_{crit}$ the boundary layer is displaced from the wall. In accordance with the limit formulas (8-1-12)

$$Re_{x\,crit} \approx [10\bar{j}_w]^{-5}. \qquad (8\text{-}2\text{-}4)$$

In the region $x > x_{crit}$ the boundary layer is separated from the wall; here Eq. (8-2-1) becomes valid. When $x > x_{trans}$, the boundary-layer equations are inexact, and to get a rigorous result it is necessary to solve the complete system of Navier-Stokes (or Reynolds) equations. The value of x_{trans} can be obtained from the estimates made above:

$$Re_{x\,trans} \approx [2{,}8\bar{j}_w]^{-5} \qquad (8\text{-}2\text{-}5)$$

Given in Table 8.1 are basic data on experimental studies in which the critical injection parameters were measured.

As can be seen from Table 8.1, the experimental values of the critical injection parameters, determined by various methods, are sufficiently close to the theoretical limit values. Considering the complexity of determining the critical injection parameter and the law experimental accuracy, the agreement between theory and experiment /207

Table 8.1. Composite table of the papers in which critical injection parameters were measured

Author	Measurement method	b_{crit}	Experimental Conditions	Source
Hacker (U.S.), 1956	From the indications of a Preston tube	3.5-4.0	Flat plate	Jet Propulsion, 1956, 26, No. 9
Hacker (U.S.), 1958	From an interferogram velocity profiles	8.0-15	Flat plate	An ASME publication; Paper No. 58-A-249
A.I. Leont'ev, B.P. Mironov, P.P. Lugovskoy, 1966	Interaction for acid medium with an alkali one	5.0-5.4	Two-dimensional duct	Inzh-fiz Zh., 1966, X, No. 4
Baker (England), 1967	From the indications of a Preston tube and velocity profiles	3.5-4.0	Axisymmetric wall jet; rough, permeable plate	Thesis, Univ. of London, Jan. 1967
Rosenbaum and Margolis (U.S.), 1967	From measurements of pressure fluctuations at this wall	4.0	Flat plate	Phys. Fluids, 1967, 10, No. 6
S.A. Druzhinin, et al., (1968)	From measurements of turbulent fluctuations and boundary layer displacement thickness	5.0-6.0	Flat plate. Injection of various gases (air, Freon, helium)	Teplo- i massoperenos, "Energiya" Press, 1968
V.P. Motulevich, et al.,	From interferograms in monochromatic light	—	Plate in a two-dimensional duct	ENIN (Power Institute) 1969 80 .

must be considered as better than satisfactory. It is interesting to note that the velocity measurements made in [49] in the boundary-layer displacement region have demonstrated convincingly that the longitudinal velocity component near the wall equals zero, in agreement with the adopted scheme.

An interferogram of the turbulent boundary layer on a permeable plate from the paper of V. P. Motulevich [80] was given in Fig. 1.5. A comparison of that interferogram with Fig. 8.4 also supports the scheme adopted for turbulent boundary-layer development in the egion of intense injection.

From an analysis of Table 8.1 it follows that the experimental values of the critical injection parameters obtained by direct optical methods [149, 63] are greater than the theoretical limit values obtained for infinitely large Reynolds numbers. /208

Interesting results from measurements of wall pressure fluctuations for a displaced boundary layer on a permeable surface are given in the paper of Rosenbaum and Margolis [201].

Shown in Fig. 8.5 are the results of measurement of the rm wall pressure fluctuations at various injection intensities. As can be seen from the graph, the wall pressure fluctuations increase with increasing injection and at certain injection rates a maximum is observed, explained by the authors as blow-off of the boundary layer from the wall. The broken line in Fig. 8.5 corresponds to a calculation for $b_{crit} = 4$; it passes

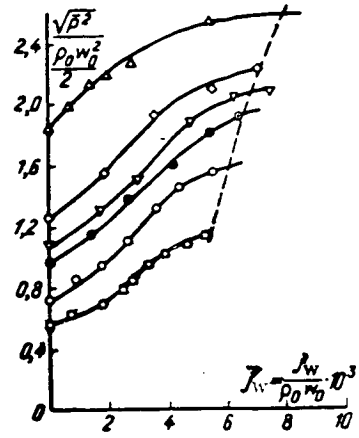

FIG. 8.5. Dependence of the rms pressure fluctuations on a plate on the injection intensity according to the data of [201]. The dashed-line curve was calculated from the boundary-layer displacement condition (b = 4.0); the points represent the experiment of [201].

Symbol	△	◇	▽	⊙	○	□
Velocity w_0, m/sec	15,2	23	26,6	30,5	45	61

approximately through the pressure-fluctuation maxima; this is an additional quantitative confirmation of the theory being proposed.

Using the method applied in Chapter 9, let us taken into account the influence of a finite Reynolds number on the critical permeability parameters.

In the immediate vicinity of the wall the horizontal velocity component $w_x \approx 0$, and the equation of motion for the viscous sublayer can be written as

$$\mu \frac{\partial^2 w_x}{\partial y^2} = j_1 \frac{\partial w_x}{\partial y}. \qquad (8\text{-}2\text{-}6)$$

In integrating we find that

$$\omega = \frac{\Psi}{b}\left[\exp\left(\frac{j_{01} y}{\mu}\right) - 1\right]. \qquad (8\text{-}2\text{-}7)$$

in the region $0<\xi<\xi_1$ on a permeable plate.

When $j_w = 0$, we get the usual linear velocity distribution. At the point of boundary-layer break-away, $\Psi=0$ and $j_w = b_{crit}\sqrt{c_{fo}}/2$, the quantity b_{crit} having a finite value. Consequently, $\omega \approx 0$ at the point of boundary-layer separation near the wall. This means that a layer in which the longitudinal velocity component $w_x \approx 0$ replaces the viscous sublayer at the point of turbulent boundary-layer separation near the permeable surface.

Taking $l(\xi) = 0{,}4\xi\sqrt{\bar{\tau}_0}$ for the turbulent part of the boundary layer and taking into account (1-3-6) and (5-1-2) we get /209

$$0{,}4\xi\frac{d\omega}{d\xi} - \sqrt{\frac{\rho_e}{\rho}\left(\frac{c_f}{2} + \bar{j}_{w''}\right)} = 0. \qquad (8\text{-}2\text{-}8)$$

Setting $c_f = 0$ and $\omega_1 = 0$ at the point of boundary-layer separation, we get

$$\int_0^{\omega} \frac{d\omega}{\sqrt{\frac{\rho_e}{\rho}\omega}} = 2{,}5\sqrt{\bar{j}_{w\,crit}}\ln\frac{\xi}{\xi_{crit}}. \qquad (8\text{-}2\text{-}9)$$

When $\xi = 1$ we have $\omega = 1$ and

$$\xi_{crit} = \exp\left(-0{,}4\sqrt{\frac{b_{crit\infty}}{b_{crit}c_{fe}}}\right). \qquad (8\text{-}2\text{-}10)$$

Accordingly,

$$\int_0^{\omega} \frac{d\omega}{\sqrt{\frac{\rho_e}{\rho}\omega}} = \sqrt{b_{crit\infty}} + 2{,}5\sqrt{B_{crit}\frac{c_{fe}}{2}}\ln\xi. \qquad (8\text{-}2\text{-}11)$$

Since $\omega_1 = 0$ at the point of separation,

$$\frac{b_{crit\infty}}{b_{crit}} = Z^2. \qquad (8\text{-}2\text{-}12)$$

On the other hand

$$b_{crit} = \left(\frac{1}{Z}\int_0^1 \sqrt{\frac{1+2\xi}{\frac{\rho_e}{\rho}\omega}}\,d\omega\right)^2. \qquad (8\text{-}2\text{-}13)$$

In the first approximation the quantity Z can be defined as

$$Z = 1 - 11{,}6\sqrt{\Psi_\infty\frac{c_f}{2}}. \qquad (8\text{-}2\text{-}14)$$

The results of calculating b_{crit} by (8-2-13), with account taken of (5-2-5) and (8-2-14), are presented in Table 8.2.

The calculation results are sufficiently well approximated by the formula /210

$$b_{crit} \approx b_{crit\infty}\left[1 + \frac{0{,}83}{(Re^{**})^{0{,}14}}\right]. \qquad (8\text{-}2\text{-}15)$$

Table 8.2. Values of the critical permeability parameter in the range of finite Reynolds numbers

Re^{**}	$2\cdot10^3$	10^4	10^6	∞
b_{crit}	5,18	4,92	4,48	4,0
b'_{crit} for $b = const$	3,74	3,57	3,35	3,0

The results of calculating b_{crit} by (8-2-13) for a boundary layer of variable density, defined by (5-5-13), at subsonic velocities are compiled in Table 8.3.

Table 8.3. Values of b_{crit} for a plate submerged in a supersonic, non-isothermal gas stream

Φ	Re^{**}			
	$2\cdot10^3$	10^4	10^6	∞
0,25	11,6	11	10	9,25
0.5	7,96	7,54	6,87	6,21
1	5,18	4,92	4,48	4,00
2	3,23	3,06	2,79	2,47
4	1,92	1,83	1,67	1,46

As follows from the graph in Fig. 8.6, the critical injection parameter in the range of finite Reynolds numbers for injection of foreign gases under non-isothermal conditions can be determined by (8-2-15), while the effect of variable density is taken into account in $b_{crit\infty}$ by formulas (5-3-5) and (5-3-6). In this case /211

$$\frac{b_{crit}}{b_{crit\bullet}} = \frac{b_{crit\infty}}{crit0\infty} = \frac{1}{4}\frac{1}{1-\psi_1}\left(\ln\frac{1+\sqrt{1-\psi_1}}{1-\sqrt{1-\psi_1}}\right)^2, \qquad (8\text{-}2\text{-}16)$$

for $\psi_1 < 1$ and

$$\frac{b_{crit}}{b_{crit\bullet}} = \frac{1}{4}\frac{1}{\psi_1-1}\left(\arccos\frac{2-\psi_1}{\psi_1}\right)^2, \qquad (8\text{-}2\text{-}17)$$

for $\psi_1 > 1$, where $\psi_1 = \rho_0/\rho_w$; b_{crit} is defined by (8-2-15).

With allowance for the approximating formulas we find

$$\frac{b_{crit}}{b_{crit\bullet}} = \frac{3}{1+2\psi_1}. \qquad (8\text{-}2\text{-}18)$$

In particular, for injection of a foreign gas under non-isothermal conditions we get $\psi_1 = \bar{R}$ and

$$\frac{b_{crit}}{b_{crit}} = \frac{3}{1+2\bar{R}}. \qquad (8\text{-}2\text{-}19)$$

Formula (8-2-19) is compared in Fig. 8.7 with the experiments of [75].

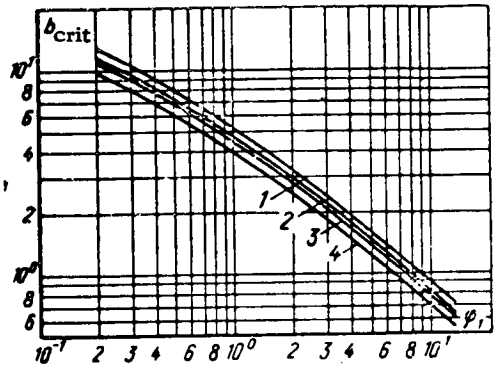

Fig. 8.6

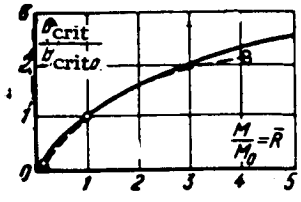

Fig. 8.7

FIG. 8.6. Influence of non-isothermicity and Re^{**} on the critical injection parameter. 1—$Re^{**} = 2 \cdot 10^4$; 2—10^5; 3—10^6; 4—∞.

FIG. 8.7. Effect of the molecular weight of the injected gas on the critical injection parameter. Curve calculated by (8-2-19); the points represent the experiments of [75].

8.3. Taking into Account the Influence of a Finite Reynolds Number on the Laws of Frictional Drag and Heat Transfer on a Permeable Surface

In Chapter 7 it was demonstrated that a formula of the form

$$\overline{\Psi} = (1-b)^2, \qquad (8\text{-}3\text{-}1)$$

where

$$\overline{\Psi} = \Psi/\Psi_i\Psi_e\Psi_M, \quad b = b'/b_{crit}$$

is universal.

Considering the relatively weak effect of a finite Reynolds number on the relative law of frictional drag, we retain formula (8-3-1) also for the region of finite Reynolds numbers and will take into account the effect of the numbers only on b_{crit} (by (8-2-15)). /212

Final conclusions as to the valdity of this supposition can be drawn after comparing the proposed formula with experiment. It is well known that gas injection reduces the critical values of the Reynolds number. If we take a minimum value of $Re^{**}_{crit} = 10^3$, we find that $b_{crit} \approx 5.3$. Then,

$$\Psi = (1-0{,}189b)^2; \qquad (8\text{-}3\text{-}2)$$

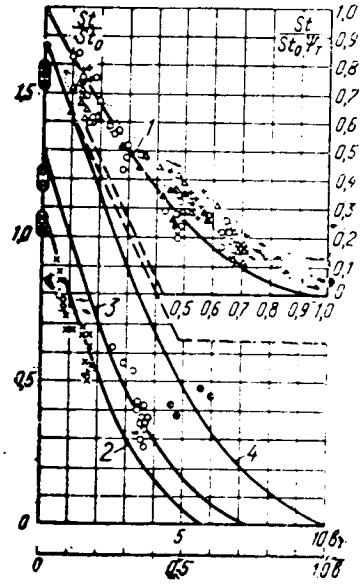

Fig. 8.8

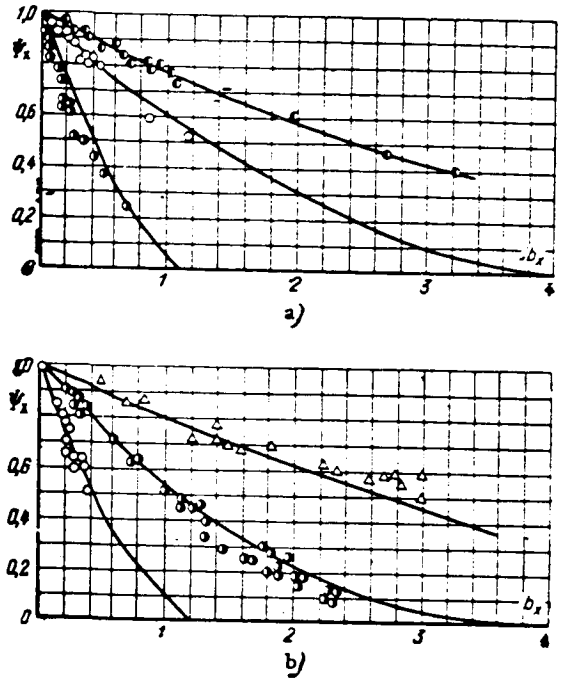

Fig. 8.9

FIG. 8.8. Effect of injection and non-isothermicity on heat transfer in the initial section of a pipe. Coordinates $\frac{St}{St_w \Psi_t} = f(\bar{b})$. 1—calculation by (8-3-1), (8-2-16) and (8-2-17). The experimental data are from [68]: inlet variant I: o—air-air; $\psi_1 = 0.47$-0.8. Inlet variant II: △—air-air, $\psi_1 = 0.47$-0.8; ▲—air-air, $\psi_1 = 0.3$-0.42; +—helium-air. The region bounded by dashed lines is the experiments of [182] (air-air). Coordinate $\frac{St}{St_0} = f(b)$. 2, 3, 4—calculation by (8-3-1) and (8-2-16) for $\psi_1 = 0.8$, 0.6, 0.3, respectively. Experimental data from [68]: x—$\psi_1 = 0.7$-0.8, $\psi_1 = 0.56$-0.6; ii—$\psi_1 = 0.3$; the points in the ovals are experiments with $b = 0$.

FIG. 8.9. Effect of injection of a foreign gas in the frictional drag coefficient. a—experiments of Pappas and Okuno [191]: ◑—helium-air; ◐—freon 12-air; o—air-air ($M_0 = 0.3$; $m = 0.153$); b—experiments of P. N. Romanenko and V. N. Kharchenko [90]: o—helium-air; ◑—air-air; Δ—freon 12-air; the curves were calculated by (8-3-1) and (8-2-15).

$$b_{crit\,x} = 4{,}5, \quad \Psi_x = \frac{(1-0.19b)^2}{(1+0.25b)^{0.2}}. \tag{8-3-3}$$

Given in Fig. 8.8 is a comparison of (8-3-1) with the experiments of [68], in which ata were obtained in heat transfer in the initial section of a porous pipe under relaively strong non-isothermal conditions (up to $\psi_1 = 0.3$). The effect of non-isothermicty on St was determined by (8-2-16), and the function Ψ_t appearing in Ψ_1 was calcuated by (4-1-5). The number St_0 was defined by /213

$$St_0 = \frac{0.0128}{(Re^{**}_{iw})^m Pr^{0.75}},$$

where $Re^{**}_{iw} = \rho_0 w_0 \delta_i^{**}/u_w$.

As can be seen from the graph, the proposed calculation method yields satisfactory results even for an appreciably non-isothermal turbulent boundary layer on a permeable surface. It is interesting to note that the influence of non-isothermicity on the relative laws of frictional drag and heat transfer on a permeable surface is considerably greater than on an impermeable surface.

The experimental data of P. N. Romanenko and V. N. Kharchenko [90], Pappas and Okuno [191] from measurements of friction during the injection of foreign gases are compared with (8-3-1) in Fig. 8.9. An analogous comparison is made in Fig. 8.10 with the data on heat transfer obtained in a paper of Tewfik, Ekker and Shatladen [237]. /214

Given in Fig. 8.11 is a comparison of the results of a measurement by Jonsson and Scott of the helium concentration on a permeable surface with formula (5-5-7).

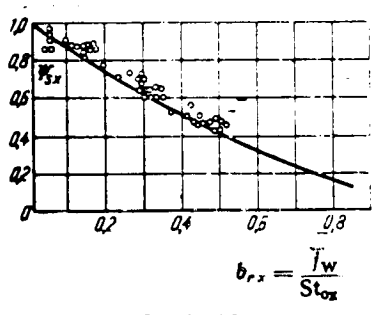

FIG. 8.10.

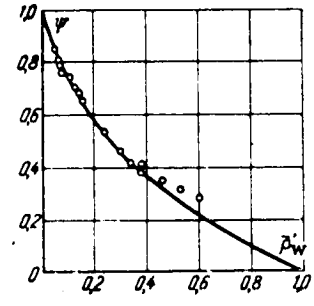

FIG. 8.11.

FIG. 8.10. Influence of injection of helium on the heat-transfer law. Curve calculated by (8-3-1) and (8-2-16) for $Re^{**} = 10^4$; the points represent the experiments of [237].

FIG. 8.11. Relationship between the relative friction coefficient and the concentration of injected gas (helium) at a wall. Curve calculated by (5-5-7); the points represent the experiment of Jonsson and Scott [158].

Pore cooling is widely used in the supersonic gas flow region. The limit laws of frictional drag and heat transfer for this region, as shown in Chapter 6, can be approximated by

$$\Psi = \bar{\Psi}_t \Psi_M \Psi_b, \qquad (8\text{-}3\text{-}4)$$

where

$$\overline{\Psi}_t=\left(\frac{2}{\sqrt{\bar{\psi}}+1}\right)^2;\quad \Psi_M=\left(\frac{\operatorname{arctg} M\sqrt{r\frac{k-1}{2}}}{M\sqrt{r\frac{k-1}{2}}}\right)^2;$$

$$\Psi_b=\left(1-\frac{b}{b_{\text{crit}}}\right)^2;\quad \Psi=(c_f/c_{f0})_{Re^{**}_w};\quad Re^{**}_w \qquad /215$$

$$=\rho_e w_e \delta^{**}/\mu_w,\quad \bar{\psi}=T_w/T^*_w.$$

The values of the critical permeability parameter are approximated by

$$b_{\text{crit}}=b_{\text{crit0}}\Psi_M, \qquad (8\text{-}3\text{-}5)$$

where b_{crit} is defined by (5-3-5) and (5-3-6).

It should be noted that the frictional drag coefficient $c_{fo}/2$ occurring in the permeability parameters is also defined by Re_w^{**}. For the condition of flow over a flat plate being considered here Eq. (8-3-4) is applicable for the laws of both heat and mass transfer.

In calculations of heat-transfer processes in a supersonic flow on a permeable plate there arises the question of the effect of injection on the recovery factor. Fig. 8.12 gives the not too numerous experimental data in this region, processed in the form of the dependence of r/r_0 on $b_M = j_w \frac{2}{c_{fM}}$, where $c_{fM}/2$ is the frictional drag coefficient in the absence of injection, but with allowance for the effect of compressibility. A substantial decrease of the recovery factor with increasing injection intensity can be noted. This factor may be of great significance in generalizing the experimental data on heat transfer in a supersonic stream in the region of relatively small temperature drops. The heat-transfer coefficient, defined as $\alpha_{00} = q_w/(T_{00}-T_w)$, may differ by several factors from the heat-transfer coefficient $\alpha = q_w/(T^*_w-T_w)$. In analogy with a subsonic flow, the second definition of the heat-transfer coefficient is more convenient, since it satisfies the condition for $T_w \to T^*_w$, $q_w \to 0$. /216

The experimental data on heat transfer of B. P. Mironov, M. I. Smirnov and N. I. Yarygin [76] are compared with (8-3-4) in Fig. 8.13. The experiments were carried out for a longitudinal flow over a porous cylinder with $M_0 \approx 3.0$ in a rather broad range of variation of the injection parameter. First data were obtained in the recovery factor (see Fig. 8.12), which were used in determining the heat-transfer coefficients.* Good agreement can be noted between the experimental results and (8-3-4). /217

In calculating a turbulent boundary layer of compressible gas on a permeable surface allowance should be made for the appearance of an oblique shock at the leading edge of the plate in view of the increase in displacement thickness and flow deflection.

*Shown in this graph are the experimental data of Leadon and Scott.

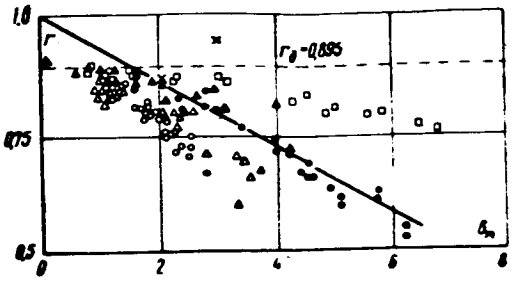

FIG. 8.12. Influence of gas injection on the recovery factor. ●—experiments of Yu. V. Baryshev [7] (M = 2.5); Δ—experiments of B. P. Mironov, N. I. Yarygin [76] (M = 2.06, 3.05, 4); x—Pappas and Okuno [192] (M = 4.7); □—Bartle and Leadon [169] (M = 3.2); ▲—Leadon and Scott [168] (M = 3.0); o—Rubesin [206] (M = 2.7). —— —calculation by the formula [7]

$$r = 1 - 2\frac{1+b_1}{b_1}\frac{2(1+b_1^2)}{b_1^2(2-\mathrm{Pr}_T)}\left[1 - \frac{(1+b_1)^{\mathrm{Pr}_T-2}}{(2-\mathrm{Pr}_T)^2}\right].$$

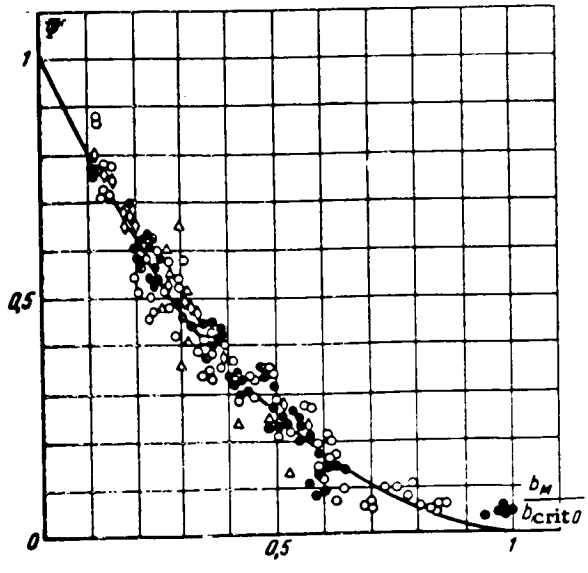

FIG. 8.13. Effect of injection and compressibility on heat transfer for longitudinal flow over a cylinder. Curve calculated by (8-3-4). The points represent the experiments of B. P. Mironov, M. I. Smirnov and N. I. Yarygin [76].

Symbol	◇	△	○	●
Mach number	≤1	2,05	3,05	4,0

Shown in Fig. 8.14 is a shadow photograph obtained by Yu. V. Baryshev of a boundary layer on a plate with an initial porous section in a supersonic flow. The

FIG. 8.14. Turbulent boundary layer of compressible gas on a permeable surface (shadow photograph). $M_0 = 2.25$; $j_w/\rho_{01} w_{01} = 0.032$; $\rho_{01} w_{01}$ - mass gas flow behind the shock; the white line shows the position of the shock calculated by (8-3-7).

shock intensity and therefore the parameters at the outer edge of the boundary layer can be determined using the formulas of gas dynamics for flow past a wedge.

The angle of flow deviation can be determined in the first approximation from the boundary layer displacement thickness on the plate.

The value of the shape parameter H is calculated by the formula (for $\psi < 1$)

$$H = [2{,}41\psi^* + 1{,}38\Delta\psi - 0{,}52][1 + 0{,}05b]. \qquad (8\text{-}3\text{-}6)$$

The flow is deflected appreciably under strong injection; in the first approximation, therefore, we can write /218

$$\operatorname{tg}\omega = \frac{d\delta^{**}}{dx} = H\frac{d\delta^{**}}{dx} = H\bar{j}_w. \qquad (8\text{-}3\text{-}7)$$

where ω is the angle of flow deviation.

Using gas-dynamic functions [39], the shock intensity and the gas parameters behind the shock are determined by the method of successive approximation.

The position of the shock, calculated by the proposed method, is shown in Fig. 8.14. Satisfactory agreement between calculation and experiment is noted.

8.4. Solution of the Equations of Momentum and Energy on a Permeable Surface of Weak Curvature

The integral momentum relation for a plane turbulent boundary layer on a permeable surface can be written conveniently in the following form:

$$\frac{d\,\mathrm{Re}^{**}_{\infty}}{d\bar{x}} + (1+H)\frac{\mathrm{Re}^{**}_{\infty}}{w_\bullet}\frac{dw_\bullet}{d\bar{x}} = \mathrm{Re}_L\frac{c_{f0}}{2}(\Psi + b), \qquad (8\text{-}4\text{-}1)$$

where $\mathrm{Re}^{**}_{\infty} = \rho_0 w_0 \delta^{**}/\mu_{\infty}$; $H = \delta^*/\delta^{**}$; $\mathrm{Re}_L = \rho_0 w_0 L/\mu_{\infty}$; $\Psi = (c_f/c_{f0})_{\mathrm{Re}^{**}}$; $b = \bar{j}_w (2/c_{f0})$.

The dependence of the shape parameter H on the non-isothermicity and injection is determined by the formula

$$H = \frac{\psi_i \psi_g}{\psi_{C_P}} (1 + 0{,}05b) H_0, \tag{8-4-2}$$

where $\psi_i = i_w/i_0$; $\psi_{C_P} = C_{Pw}/C_{P0}$; $\psi_g = M_0/M_w$; $H_0 = 1{,}347$.

For a constant value of the permeability parameter and for constant surface temperature of the body we get from (8-4-1)

$$\mathrm{Re}^{**}_w = \bar{w}_0^{-s} \left[\frac{1+m}{2} B \mathrm{Re}_{0w} (\Psi + b) \int_{\bar{x}_0}^{\bar{x}} \bar{w}_0^{1+(1+m)s} d\bar{x} + (\mathrm{Re}^{**}_w \bar{w}_0^s)_{\bar{x}_0}^{1+m} \right]^{\frac{1}{1+m}}, \tag{8-4-3}$$

where $\mathrm{Re}^{**}_w = \rho_0 w_0 \delta^{**}/\mu_w$; $\mathrm{Re}_w = \rho_0 w_{01} L/\mu_w$; $\bar{w}_0 = w_0/w_{01}$; $\varkappa = 1 + H$; $\bar{x} = x/L$; Ψ is determined by (8-3-4). The local friction coefficients are found by the formula /219

$$\frac{c_f}{2} = \Psi_\infty \frac{B}{2\mathrm{Re}_w^{**m}}. \tag{8-4-4}$$

For an axisymmetric boundary layer we have

$$\mathrm{Re}^{**}_w = \frac{1}{\bar{w}_0^s} \left[\frac{1+m}{2} B \mathrm{Re}_{0w} \bar{D}^{-(1+m)} (\Psi + b) \times \int_{\bar{x}_0}^{\bar{x}} \bar{w}_0^{1+(1+m)s} \bar{D}^{m+1} d\bar{x} + (\mathrm{Re}^{**}_w \bar{w}_0^s \bar{D})_{\bar{x}=\bar{x}_0}^{1+m} \right]^{\frac{1}{1+m}}. \tag{8-4-5}$$

For a flow without a gradient $dw_0/d\bar{x} = 0$ and Eqs. (8-4-3) and (8-4-4) reduce to Eqs. (8-1-5). A solution is obtained for Eq. (8-4-1) for critical injection conditions. In this case

$$\mathrm{Re}^{**}_w = \bar{w}_0^{-s} \left[\frac{1+m}{2} B \mathrm{Re}_{0w} b_{\mathrm{crit}} \int_{\bar{x}_0}^{\bar{x}} \bar{w}_0^{1+(1+m)s} d\bar{x} + (\mathrm{Re}^{**}_w \bar{w}_0^s)_{\bar{x}_0}^{1+m} \right]^{\frac{1}{1+m}}, \tag{8-4-6}$$

where b_{crit} is determined by (8-3-5). The corresponding law of distribution of injected gas that gives rise to boundary layer separation is found from the formula

$$j_w = \rho_0 w_0 \frac{c_{f0}}{2} b_{\mathrm{crit}} = \rho_0 w_0 \frac{B b_{\mathrm{crit}}}{2\mathrm{Re}_w^{**m}}. \tag{8-4-7}$$

The other limit solution corresponds to the case of gas suction from the surface according to the law

$$j_w = -\frac{c_f}{2}. \tag{8-4-8}$$

Then, from Eq. (8-4-1) we get

$$\frac{d\,\mathrm{Re}^{**}_{w}}{d\bar{x}} + (1+H)\frac{\mathrm{Re}_{w}}{\bar{w}_{e}}\frac{d\bar{w}_{0}}{d\bar{x}} = 0. \tag{8-4-9}$$

Hence, taking H = const in the first approximation, we have /220

$$\frac{\mathrm{Re}^{**}_{w}}{\mathrm{Re}^{**}_{w1}} = \left(\frac{\bar{w}_{0}}{\bar{w}_{01}}\right)^{1+H}. \tag{8-4-10}$$

From Eq. (8-4-8) it follows that

$$\bar{b}b_{\mathrm{crit}} = -\Psi = -\Psi_{1}\Psi_{M}(1-\bar{b})^{2}, \tag{8-4-11}$$

and therefore

$$\bar{b} = \frac{2+b_{\mathrm{crit}}}{2} \pm \sqrt{\frac{2+b_{\mathrm{crit}}}{2} - 1}. \tag{8-4-12}$$

Thus, knowing the dependence of Re^{**}_{w} and b on x, we get the law of gas suction from the surface corresponding to the self-similar solution:

$$j_{w} = \rho_{0}w_{0}b\frac{B}{2(\mathrm{Re}^{**}_{w})^{m}}. \tag{8-4-13}$$

A second approximation can be introduced using the dependence of the shape parameter H on the injection parameter b. A solution to the problem can be obtained in more complicated form for the case of a given transverse mass flow distribution over the surface of the body.

As the first approximation we can use the solution for a given distribution of the permeability parameter b = f(x), with $c_{fo}/2$ being determined from the integral momentum relation for an impermeable wall (7-2-11).

Then,

$$b = \bar{j}_{w}\frac{2}{c_{f0}} = f(\bar{x}) \tag{8-4-14}$$

and from Eq. (8-4-1) we get

$$\mathrm{Re}^{**}_{w} = e^{-\int (1+H)\frac{d}{d\bar{x}}\ln\bar{w}_{0}}\left[\frac{1+m}{2}B\,\mathrm{Re}_{0w}\int_{\bar{x}_{0}}^{\bar{x}}(\Psi_{\infty}+b)^{(1+m)}\right.$$
$$\left.\times e^{\int (1+H)\frac{d}{d\bar{x}}\ln\bar{w}_{0}}\bar{w}_{0}\,d\bar{x} + C\right]^{\frac{1}{m+1}}. \tag{8-4-15}$$

The local friction coefficients are found by formula (8-4-4). The second approximation is obtained after substituting Re^{**}_{w} from (8-4-15) into (8-4-14).

For the inner axisymmetric problem of gas flow in a nozzle, taking Eq. (7-2-47) into account, we have /221

$$\mathrm{Re}^{**}_{w}=\frac{1}{U^{2}}\left\{\frac{1+m}{2}B\mathrm{Re}_{00}\bar{D}^{-(1+m)}\int_{\bar{x}_{0}}^{\bar{x}}(\Psi_{\infty}+b)\times U^{(1+m)H}\bar{D}^{m-1}\,d\bar{x}+C\right\}^{\frac{1}{m+1}}. \tag{8-4-16}$$

The dimensionless velocity U is linked to the duct geometry by the formula

$$U(1-U^{2})^{\frac{1}{k-1}}=\left(\frac{k-1}{k+1}\right)^{0.5}\left(\frac{2}{k+1}\right)^{\frac{1}{k-1}}\frac{F_{\mathrm{crit}}}{F}. \tag{8-4-17}$$

The energy equation of a two-dimensional boundary layer on a permeable surface can be written conveniently in the following form:

$$\frac{d\,\mathrm{Re}^{**}_{i}}{d\bar{x}}+\frac{\mathrm{Re}^{**}_{i}}{\Delta i}\frac{d(\Delta i)}{d\bar{x}}=\mathrm{Re}_{L}\mathrm{St}_{0}(\Psi_{S}+b_{i}), \tag{8-4-18}$$

where

$$\mathrm{Re}^{**}_{i}=\rho_{0}\omega_{0}\delta^{**}/\mu^{*};\ \mathrm{Re}_{L}=\rho_{0}\omega_{0}L/\mu^{*};$$

$$\Delta i=i^{*}_{w}-i_{w};\ \bar{x}=x/L;\ \Psi_{S}=(\mathrm{St}/\mathrm{St}_{0})_{\mathrm{Re}^{**}_{i}};\ b_{i}=\bar{j}_{w}/\mathrm{St}_{0}.$$

Let us consider the thermal energy balance on a permeable surface. From Fig. 8.15 it follows that

$$\Psi_{S}=b_{i}\frac{K}{\sigma}, \tag{8-4-19}$$

where $K=\frac{(i_{cr}-i')}{(i^{*}_{cr}-i_{cr})}$ is the generalized phase transition criterion introduced in [43]; $\sigma=1-\frac{q_{R}+q_{cond}}{\alpha(i^{*}_{cr}-i_{cr})}$; q_{R} is the radiative heat flux; and q_{cond} is the conductive heat flux.

For the case $q_{R}=q_{cond}=0$ we have

$$\frac{d\,\mathrm{Re}^{**}_{i}}{d\bar{x}}+\frac{\mathrm{Re}^{**}_{i}}{\Delta i}\frac{d(\Delta i)}{d\bar{x}}=\mathrm{Re}_{L}\mathrm{St}_{0}b_{i}(1+K). \tag{8-4-20}$$

Solving Eqs. (8-3-1) and (8-4-19) for the thermal permeability parameter we get /222

$$b_{i}=b_{i\,\mathrm{crit}}-\frac{Kb_{i\,\mathrm{cri}}}{2\Psi_{i}\Psi_{M}}\left(\sqrt{\frac{4\Psi_{i}\Psi_{M}}{Kb_{i\,\mathrm{crit}}}+1}-1\right). \tag{8-4-21}$$

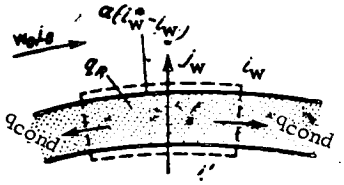

FIG. 8.15. Thermal energy balance in a permeable surface.

The values of b_i and K are determined as functions of $\bar{x}$ from Eqs. (8-4-19) and (8-4-21) for known functions i_w, i' and known parameters at the outer edge of the boundary layer. The integral of the energy equation is written as

$$\mathrm{Re}^{**}_i = \frac{1}{\Delta i}\left\{\frac{1+m}{2\mathrm{Pr}^{*,75}} B \mathrm{Re}_{0L} \int_{\bar{x}_0}^{\bar{x}} U(1-U^2)^{\frac{1}{K-1}} b_i \times (1+K)\Delta i^{1+m} d\bar{x} + (\mathrm{Re}^{**}_i \Delta i)^{1+m}_{\bar{x}_0}\right\}^{\frac{1}{1+m}}. \quad (8\text{-}4\text{-}22)$$

In calculations of porous cooling the mass flow of coolant gas is usually the desired variable; it is defined by the formula

$$j_w = \rho_0 w_0 \mathrm{St}_0 b_i, \quad (8\text{-}4\text{-}23)$$

where

$$\mathrm{St}_0 = \frac{B\,\mathrm{Pr}^{-*,75}}{2\,\mathrm{Re}^{**m}_{i\,w}}; \quad \mathrm{Re}^{**}_{i\,w} = \mathrm{Re}^{**}_i \left(\frac{\mu_w}{\mu^*}\right).$$

For the subsonic gas flow region, with constant T_w and T and the boundary condition $\mathrm{Re}^{**}_T = 0$ at $\bar{x} = 0$, we have

$$\mathrm{Re}^{**}_{T\,w} = \left\{\frac{1+m}{2\,\mathrm{Pr}^{*,75}} B b_T (1+K)\,\mathrm{Re}_{0\,w} \int_0^{\bar{x}} \bar{w}_0\, d\bar{x}\right\}^{\frac{1}{m+1}}. \quad (8\text{-}4\text{-}24)$$

Taking (8-4-23) into account we get

/223

$$\left(\frac{\mathrm{St}}{\mathrm{St}_{0\infty}}\right)_{\mathrm{Re}_\infty} = \frac{\Psi_T\left(1-\frac{b_T}{b_{T\,\mathrm{crit}}}\right)^2}{\left[\Psi_T\left(1-\frac{b_T}{b_{T\mathrm{crit}}}\right)^2 + b_T\right]^{\frac{m}{m+1}}}, \quad (8\text{-}4\text{-}25)$$

where St_{0x} are the local values of the Stanton number on an impermeable surface for the same Re_x and an analogous law of velocity variation at the outer edge of the boundary layer over the length, with T_w = const.

We have the following relationship between St_0, the Stanton number calculated from the actual value of Re^{**}_T, but without allowance for the effect of transverse mass flow, and St_{0x}:

$$\left(\frac{St_0}{St_{0x}}\right)=\frac{b_{Tx}}{b_T}=\frac{1}{\left[\Psi_T\left(1-\frac{b_T}{b_{T\,crit}}\right)^3+b_T\right]^{\frac{m}{m+1}}} \tag{8-4-26}$$

and

$$b_{Tx}=\frac{b_T}{\left[\Psi_T\left(1-\frac{b_T}{b_{T\,crit}}\right)^3+b_T\right]^{\frac{m}{m+1}}}. \tag{8-4-27}$$

To determine the mass distribution of injected gas over the surface of the body, we get from Eqs. (8-4-26) and (8-4-24)

$$j_w=\rho_0 w_0\frac{\frac{B}{2}b_T}{\{b_T(1+K)\}^{\frac{m}{m+1}}\left[\frac{B(m+1)}{2\,Pr^{0.75}}Re_{01}\int_0^{\bar{x}}\bar{w}_0\,d\bar{x}\right]^{\frac{m}{m+1}}}. \tag{8-4-28}$$

Taking B/2 = 0.0128, m = 0.25 and Pr = 0.72, we have

$$j_w=\rho_0 w_0\frac{b_T^{0.8}}{(1+K)^{0.2}}\frac{1}{Re_{01}^{0.2}\left[\int_0^{\bar{x}}\bar{w}_0\,d\bar{x}\right]^{0.2}}. \tag{8-4-29}$$

For flow over the forward portion of blunt-nosed bodies the law of velocity variation at the outer edge of the boundary layer is close to the linear law: /224

$$\bar{w}_0=C\bar{x}, \tag{8-4-30}$$

where the value of the constant C depends on the shape of the body in the flow.

For this case we get from Eq. (8-4-28)

$$j_w=\frac{\rho_{01}w_{01}C\frac{B}{2}b_T^{\frac{1}{m+1}}\bar{x}^{0.8}}{(1+K)^{\frac{m}{m+1}}\left[\frac{B(m+1)}{2\,Pr^{0.75}}\frac{Re_{01}C}{2}\right]^{\frac{m}{m+1}}}. \tag{8-4-31}$$

For B/2 = 0.0128, m = 0.25 and Pr = 0.72 we have

$$j_w=\frac{\rho_{01}w_{01}b_T^{0.8}\bar{x}^{0.8}C^{0.8}}{(1+K)^{0.2}Re_{01}^{0.2}}. \tag{8-4-32}$$

In conformity with the Reynolds analogy, formulas (8-1-9) and (8-1-12) remain valid for the case of longitudinal flow around a flat plate. From Eq. (8-4-21) it follows that the case b_T = const corresponds to the case of T_w = const being considered.

From Eq. (8-4-29) we have

$$j_w = \rho_0 w_0 \frac{b_T^{0.8}}{(1+K)^{0.2}} \frac{\bar{x}^{-0.2}}{\mathrm{Re}_{01}^{0.2}}. \tag{8-4-33}$$

From Eqs. (8-4-32) and (8-4-33) it follows that to maintain constant emperature of a plate in a longitudinal flow, the mass flow rate of the injected gas must decrease in inverse proportion to $\bar{x}^{0.2}$, while in a transverse flow it must increase in proportion to $\bar{x}^{0.6}$.

In the case of a given mass flow of coolant gas the thermal boundary layer equation can be written as

$$\frac{d(\mathrm{Re}^{**}_T \Delta i)}{d\bar{x}} = \mathrm{Re}^*_L \left(\frac{i^*_w - i'}{i^*_w - i_w} \right), \tag{8-4-34}$$

where $\mathrm{Re}^*_L = j_{cr} L/\mu^*$ and i' is the enthalpy of the injected gas.

For the region of subsonic velocities and constant physical parameters /225

$$\frac{d(\mathrm{Re}^{**}_T \Delta T)}{d\bar{x}} = \mathrm{Re}^*_L (1+K). \tag{8-4-35}$$

The integral of Eq. (8-4-35) under the boundary condition $\mathrm{Re}^{**}_T = 0$ at $\bar{x} = 0$, is

$$\mathrm{Re}^{**}_T \Delta T = (T_0 - T') \mathrm{Re}_{L1} \int_0^{\bar{x}} \bar{j}_{w1} \, d\bar{x} \tag{8-4-36}$$

or

$$K+1 = \frac{\mathrm{Re}^{**}_T}{\mathrm{Re}_{L1} \int_0^{\bar{x}} \bar{j}_{w1} d\bar{x}}, \tag{8-4-37}$$

where $\mathrm{Re}_{L1} = \rho_{01} w_0 L/\mu^*$, $\bar{j}_w = j_w/\rho_{01} w_{01}$, and $\rho_{01} w_{01}$ is the specific mass flow in the section $\bar{x} = 0$.

On the other hand, it follows from Eq. (8-4-19) that

$$K = \frac{\Psi_t \left(1 - \frac{b_T}{b_{T\,\mathrm{crit}}}\right)^2}{b_T}. \tag{8-4-38}$$

From Eqs. (8-4-37) and (8-4-38) it follows that

$$\mathrm{Re}^{**}_T = \left[\Psi_t\left(1-\frac{b_T}{b_{T\,\mathrm{crit}}}\right)^2 + b_T\right]\frac{\mathrm{Re}_{L1}}{b_T}\int_0^{\bar{x}} \bar{j}_{w1}\, d\bar{x}. \qquad (8\text{-}4\text{-}39)$$

Thus, the dependence of the number $\mathrm{Re}^{**}_T = f(x)$ in the case of a given mass flow of coolant gas is obtained directly from the energy equation (8-4-34) and the equation of heat balance on the surface (8-4-38). The local values of the Stanton number are determined by the formula

$$\mathrm{St} = \frac{B\Psi_t\left(1-\frac{b_T}{b_{T\,\mathrm{crit}}}\right)^2}{2\,\mathrm{Pr}^{0,75}\left\{\left[\Psi_t\left(1-\frac{b_T}{b_{T\,\mathrm{crit}}}\right)^2 + b_T\right]\frac{\mathrm{Re}_{L1}}{b_T}\int_0^{\bar{x}} \bar{j}_w\, d\bar{x}\right\}^m}. \qquad (8\text{-}4\text{-}40)$$

Strictly speaking, Eq. (8-4-40) is valid for the boundary conditions $b_T = \mathrm{const}$, /226 but, in analogy with the law of heat transfer on a permeable plate, it can be assumed that heat transfer law (8-4-40) is conservative to variation in the mass flow rate of the injected gas over the length of the plate.

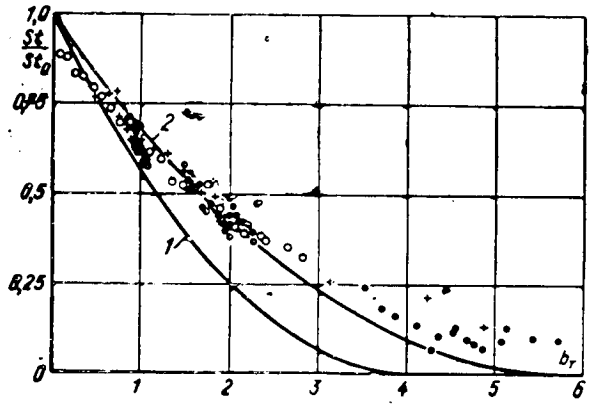

FIG. 8.16. Effect of various gas injection laws on the heat-transfer law. 1—calculated by (5-2-1); 2—calculated by (8-3-1) for $\mathrm{Re}^{**}_T = 100$. The points represent the experiments of Whitten, Moffett and Kays [244].

Symbols	Boundary conditions	Range of Re^{**}_T
o	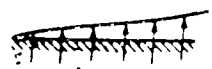	$1.7\cdot10^3$—$80\cdot10^3$
+		$1\cdot10^3$—$128\cdot10^3$
●		$2\cdot10^3$—$70\cdot10^3$

The results of an experimental check of this hypothesis are given in Fig. 8.16. The experimental points in the figure, taken from [244], correspond to different laws of mass flow distribution of injected gas over the length. As can be seen from the figure, the experimental data confirm that the heat-transfer law is conservative to variation of the boundary conditions and are in satisfactory agreement with formula (8-4-40). Equations (8-4-39) and (8-4-40) are solved for T_w by the method of successive approximation. /227

For the case j_w = const we have

$$\mathrm{Re}^{**}{}_T' = \left\{\frac{B}{2\,\mathrm{Pr}^{*,75}}\,\mathrm{Re}_x\left[\Psi_t\left(1-\frac{b_T}{b_{T\,\mathrm{crit}}}\right)^2+b_T\right]\right\}^{\frac{1}{m+1}} \qquad (8\text{-}4\text{-}41)$$

and

$$\mathrm{St} = \frac{\frac{B}{2}\,\Psi_t\left(1-\frac{b_T}{b_{T\,\mathrm{crit}}}\right)^2}{\left\{\frac{B}{2\,\mathrm{Pr}^{*,75}}\,\mathrm{Re}_x\left[\Psi_t\left(1-\frac{b_T}{b_{T\,\mathrm{crit}}}\right)^2+b_T\right]\right\}^{\frac{m}{m+1}}\mathrm{Pr}^{*,75}}. \qquad (8\text{-}4\text{-}42)$$

From Eqs. (7-2-67) and (8-4-42) it follows that

$$\left(\frac{\mathrm{St}}{\mathrm{St}^*_{0x}}\right)_{\mathrm{Re}_x} = \frac{\Psi_t\left(1-\frac{b_T}{b_{T\,\mathrm{crit}}}\right)^2}{\left[\Psi_t\left(1-\frac{b_T}{b_{T\,\mathrm{crit}}}\right)^2+b_T\right]^{\frac{m}{m+1}}}, \qquad (8\text{-}4\text{-}43)$$

where St^*_{0x} is the Stanton number on an impermeable surface for the same value of Re_x and the same law of variation in mass velocity over length at the outer edge of the boundary layer.

Comparing (8-4-43) and (8-4-25) we have

$$\left(\frac{\mathrm{St}}{\mathrm{St}^*_{0x}}\right)_{\mathrm{Re}_x} = \left(\frac{\mathrm{St}}{\mathrm{St}_{ex\,w}}\right)_{\mathrm{Re}_x} \qquad (8\text{-}4\text{-}44)$$

for arbitrary but like velocity distributions at the outer edge of the boundary layer.

Accordingly,

$$b_{Tx} = \frac{b_T}{\left[\Psi_t\left(1-\frac{b_T}{b_{T\,\mathrm{crit}}}\right)^2+b_T\right]^{\frac{m}{m+1}}}. \qquad (8\text{-}4\text{-}45)$$

For quasi-isothermal conditions ($\Psi_t \approx 1.0$; $b_{T\mathrm{crit}} = 4.0$), the sequence of wall-temperature calculation is as follows: /228

1. We determine St_{0x}^{**} from Eq. (7-2-67) for given Re_x.

2. We determine $b_{Tx} = \frac{j_w}{\rho_0 w_0} \frac{1}{St_{0x}}$.

3. We calculate b_T from Eq. (8-4-45) and St from Eq. (8-4-43).

4. We determine the value of the Kutateladze number:

$$K = \frac{\rho_e w_e}{j_w} St \quad \text{or} \quad K = \Psi_b / b_T$$

and the dependence of the wall temperature on $\bar{x}$:

$$T_w = \frac{KT_e + T'}{1 + K}. \tag{8-4-46}$$

In the case j_w = const, it follows from Eqs. (8-4-21), (8-4-36) and (8-4-38) for the region $M_0 > 1$ that

$$\left\{ b_{crit} - \frac{Kb_{crit}^2}{2\Psi_t \Psi_M} \left[\sqrt{\frac{4\Psi_t \Psi_M}{Kb_{crit}} + 1} - 1 \right] \right\} (K+1)^{-0,25} = \frac{(Re_{0L}\bar{x})^{0,25} Pr^{0,75} \bar{j}_w^{1,25}}{0,0128 \bar{w}_e}. \tag{8-4-47}$$

In this equation the left-hand side represents a certain function F, dependent only on the enthalpy ratio

$$\psi_i = i_w / i_0, \quad \psi' = i' / i_0, \quad K = (\psi_i - \psi') / (1 - \psi_i)$$

and M_0.

The results of calculating the function F by Eq. (8-4-47) are presented in Figs. 8.17 and 8.18. This auxiliary graph makes it much easier to calculate the temperature of a porous wall for constant mass flow of injected gas and arbitrary law of velocity variation at the outer edge of the boundary layer. With a known $w_0 = f(\bar{x})$ for a given j_w the right-hand side of the equation is a known function of $\bar{x}$. Then the desired wall temperature is determined in Fig. 8.15 from a given value of ψ' and M_0.

In the more general case, the problem is solved by the method of successive approximation, taking into account the effect of non-isothermicity of the chemical reactions and the inhomogeneity of the injected gas on Ψ_t and b_{Tcrit}. /230

The proposed method of calculating a thermal turbulent boundary layer is not difficult to apply to the case of an axisymmetric boundary layer. In this case the integral energy relation is written in the form

$$\frac{d\,Re_t^{**}}{d\bar{x}} + \frac{Re_t^{**}}{\Delta i} \frac{d(\Delta i)}{d\bar{x}} + \frac{1}{R_e} \frac{dR_e}{d\bar{x}} \Bigg\} = Re_L St_0 b_i (1 + K). \tag{8-4-48}$$

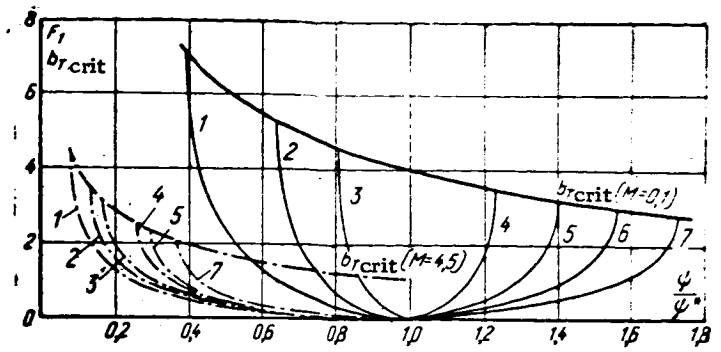

FIG. 8.17. Dependence of the function F and of b_{Tcrit} on non-isothermicity and compressibility; $d = i'/i^{**}_w$. 1—d = 0.392; 2—d = 0.64; 3—d = 0.812; 4—d = 1.23; 5—d = 1.4; 6—d = 1.56; 7—d = 1.73.

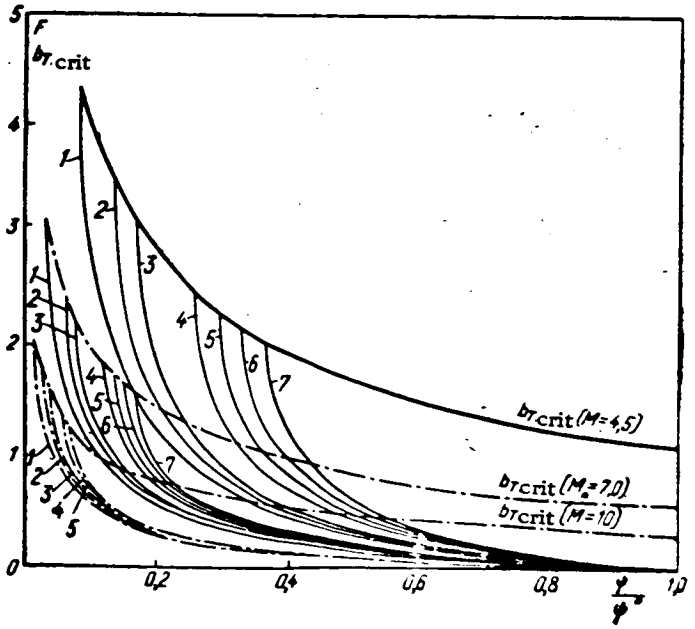

FIG. 8.18. Dependence of the function F and of b_{crit} on non-isothermicity and compressibility in the porous wall cooling region. $d = i'/i^{**}_w$; 1—d = 0.392; 2—d = 0.64; 3—d = 0.812; 4—d = 1.23; 5—d = 1.4; 6—d = 1.56; 7—d = 1.73.

The rest of the reasoning is as before. For the internal problem (gas flow in a nozzle with porous walls) it is convenient to make use of continuity equation (8-4-17). Then the integral of Eq. (8-4-48) is written as

$$\mathrm{Re}^{**}_i = \frac{1}{\Delta i}\left\{\frac{1+m}{2\,\mathrm{Pr}^{0,75}}\left(\frac{K-1}{K+1}\right)^{0,5}\left(\frac{2}{K+1}\right)^{\frac{1}{K-1}}\bar{D}^{-(1+m)}\right.$$

$$\left.\times\int_{\bar{x}_0}^{\bar{x}} b_i(1+K)\,\Delta i^{1-m}\bar{D}^{m-1}\,d\bar{x} + (\mathrm{Re}^{**}_i\Delta i\bar{D})^{1+m}\right\}^{\frac{1}{1+m}}. \qquad (8\text{-}4\text{-}49)$$

With a given geometry of the nozzle flow section and a given variation of the parameters Δi_1, b_i and K with respect to $\bar{x}$, the local values of Re_i^{**} are determined from Eq. (8-4-49) and the mass flow distribution of the injected gas by (8-4-23).

This method of calculation is based on the assumption that the heat-transfer law is conservative to a longitudinal pressure gradient. But, as shown in the paper of Baylay and Turner [104], this method can also be applied to the case of appreciable longitudinal gradients if the effect of the pressure gradient on the critical permeability parameter is taken into account in the heat-transfer law. For the case of flow around the porous blade for gas turbine, according to [104],

$$\frac{b_{\mathrm{crit}}}{b_{\mathrm{crit}_0}} = \left(1 - \frac{1}{w_0}\frac{dw_0}{d\bar{x}}\right)^{-2}, \qquad (8\text{-}4\text{-}50)$$

when $\bar{x} = x/L$ and L is the blade chord.

It should be noted that formula (8-4-50) is in satisfactory agreement with the theoretical formula (6-5-17). /231

The results of processing the experiments of Baylay and Turner on the local heat-transfer coefficients on the blade of a gas turbine with pore cooling [104] are given in Fig. 8.19.

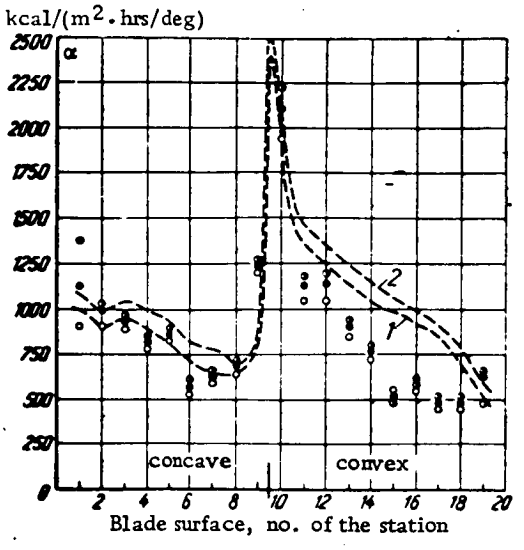

FIG. 8.19. Distribution of heat transfer coefficients over the surface of a porous blade of a gas turbine. The curves were calculated by the proposed method: 1—ψ = 0.376; 2—ψ = 0.437; the experiments of Baylay and Turner [104]: ◑—ψ = 0.485; ●—ψ = 0.437; o—ψ = 0.376.

The agreement between theory and experiment for a concave blade surface, considering the exceptional complexity of the experiment, must be assessed as being good. The deviation of the experimental data from the calculated curve on the convex blade surface can be explained by the laminarizing effect of the longitudinal pressure gradient, which is disregarded in the proposed theory.

8.5. Turbulent Boundary Layer on a Permeable Surface in the Presence of Chemical Reactions

/232

The method outlined in Section 8.4 for calculating a turbulent boundary layer can be applied to the case when chemical reaction takes place in the flow and on the surface of a body.

The integral energy relation in this case has the form

$$\frac{d\,\mathrm{Re}^{**}_{i\Sigma}}{d\bar{x}} + \mathrm{Re}^{**}_{i\Sigma}\frac{d\,(\Delta i_\Sigma)}{(\Delta i_\Sigma)\,d\bar{x}} = \mathrm{Re}_L \mathrm{St}_0 \Psi\,(1 + b_{i_1}), \tag{8-5-1}$$

where

$$\mathrm{St}_0\Psi = \mathrm{St}_\Sigma = q_w/\rho_0 w_0 \Delta i_\Sigma;\ \Delta i_\Sigma = i^*_{\Sigma w} - i_{\Sigma w};$$

$i^*_{\Sigma w}$ is the total equilibrium enthalpy at the wall; $i_{\Sigma w}$ is the total enthalpy at the wall;

$$b_{i_1} = f_w \frac{1}{\mathrm{St}_\Sigma}. \tag{8-5-2}$$

In many practical cases it is possible to neglect thermal diffusion, pressure diffusion and diffusion thermal conductivity. Then,

$$q_{w\Sigma} = -\frac{\lambda}{C_P}\left[\frac{\partial i^*_\Sigma}{\partial y} - \sum_{i=1}^{n} i_i \frac{\partial c_i}{\partial y} + \frac{\rho D_{12} C_P}{\lambda}\sum_{i=1}^{n} i_i \frac{\partial c_i}{\partial y}\right]_w, \tag{8-5-3}$$

where

$$i^*_\Sigma = i_\Sigma + r\,(w_\infty^2/2);\ i_\Sigma = \sum_{i=1}^{n} c_i i_i;$$

$$i_i = \int_0^T C_p\,dT + i_i^0;$$

i_i^0 is the heat of formation of the i-th component; and

$$\mathrm{Re}^{**}_i = \rho_0 w_0 \delta^{**}_{i\Sigma}/\mu^*,\ \delta^{**}_{i\Sigma}$$

$$= \int_0^1 \frac{\rho w}{\rho_0 w_0}\left(1 - \frac{i^*_\Sigma - i_{\Sigma w}}{i^*_{\Sigma\,ст} - i_{\Sigma w}}\right)\left(1 - \frac{y}{R_0}\right)dy.$$

For the subsonic gas flow region $i^*_\Sigma = i_\Sigma$ and $i^*_{\Sigma w} = i_{\Sigma 0}$.

Let us examine the case of a "frozen" boundary layer, when all the chemical reactions take place on the surface and the intensity of burn-up of the material is governed by the process of oxidizer diffusion through the boundary layer to the surface of the body. /233

For these conditions, taking the total enthalpy distribution and the reduced oxidizer concentrations over the boundary-layer cross section to be similar,

$$\frac{i^*_{\Sigma} - i_{\Sigma w}}{i^*_{\Sigma w} - i_{\Sigma w}} = \frac{c_i^0 - (c_i^0)_w}{(c_i^0)_e - (c_{i_2}^0)_w} \qquad (8\text{-}5\text{-}4)$$

and taking into account the mass balance of the surface, (5-5-6), for

$$\mathrm{Le} = \rho D C_p / \lambda \approx 1,$$

we get

$$b_{i_1} = \frac{(c_i^0)_e - (c_i^0)_w}{(c_i^0)_w}. \qquad (8\text{-}5\text{-}5)$$

Here c_i^0 is the reduced concentration of the i-th chemical element, for which the heat-transfer surface is impermeable, regardless of the chemical compound containing it.

Accordingly, for the injected component we have

$$b_{i_1} = \frac{c_w^0(C)}{1 - c_w^0(C)}. \qquad (8\text{-}5\text{-}6)$$

For example, let us consider the case of chemical erosion of carbon in a flow of a mixture of gases, the combustion products of an organic fuel. The energy balance at the heat-transfer surface, neglecting radiation heat transfer, has the form

$$q_{w\Sigma} = q_w + j_w i'_{\Sigma w} - j_w i''_{\Sigma w}, \qquad (8\text{-}5\text{-}7)$$

where

$$i'_{\Sigma w} - i''_{\Sigma w} = i^0_{\Sigma};$$

here $i'_{\Sigma w}$ is the total gas enthalpy near the surface, $i_{\Sigma w}$ is the total enthalpy of the material in the solid state, and i^0_{Σ} is the total heat of reaction.

The gas mixture acting on the carbon surface has a complex composition, in the general case. The chemical erosion of the carbon under these conditions is promoted by a complex of oxidative reduction reactions in the surface of the body. The following can be considered to be the most probable reactions up to $T_w \approx 4,000°$ K: /234

$$\left.\begin{array}{l} O+C\rightarrow CO; \\ \frac{1}{2}O_2+C\rightarrow CO; \\ OH+C\rightarrow CO+H; \\ NO+C\rightarrow CO+N; \\ H_2O+C\rightarrow CO+H_2; \\ CO_2+C\rightarrow 2CO. \end{array}\right\} \qquad (8\text{-}5\text{-}8)$$

The total heat of reaction is defined by the formula

$$i_w^0=\frac{Q_p}{M_w};\ Q_p=\sum_{i=1}^{n}(n_iQ_i)_1-\sum_{i=1}^{n}(n_iQ_i)_2. \qquad (8\text{-}5\text{-}9)$$

where Q_p is the total thermal effect of all the reactions taking place on the surface, and n is the number of moles of one product or other participating in the reaction.

After relatively simple transformations of Eq. (8-5-7), taking (8-5-8) into account, we get

$$i_{\Sigma w}=i_{\Sigma 0}+b_{i_1}i_\Sigma^0+\frac{q_w}{q_{\Sigma w}}(i_{\Sigma w}-i_{\Sigma 0}). \qquad (8\text{-}5\text{-}10)$$

The parameter b_{i_1} is defined from (8-5-5), allowing for the fact that

$$(c_i^0)_0=\sum_{j=1}^{p}\frac{m_i}{M_j}(c_j)_0, \qquad (8\text{-}5\text{-}11)$$

where m_i/M_j is the molar fraction of the i-th element, and p is the number of chemical compounds containing the i-th element.

For example, the reduced concentration $(c_0^0)_0$ of oxygen in the free stream for a complex gas composition is

$$c_0^0(O)=c_0(O_2)+\frac{16}{17}c_0(OH)+\frac{16}{18}c_0(H_2O)+\frac{16}{30}c_0(NO)+\frac{16}{44}c_0(CO_2)+\ldots \qquad (8\text{-}5\text{-}12)$$ /235

Here $c_0(O_2)$, $c_0(OH)$, $c_0(H_2O)$, etc. are the weight fractions of the chemically active, oxygen-containing compounds in the free stream.

From Eqs. (8-5-5) and (8-5-11) it follows that

$$b_{i_1}=\frac{1}{\frac{16}{28}c_w(CO)}\left(\sum_{j=1}^{p}\frac{m_0}{M_j}\left[(c_j)_0-\frac{16}{18}c_w(CO)\right]\right). \qquad (8\text{-}5\text{-}13)$$

On the other hand, from Eq. (8-5-6) we can get

$$c_w(CO) = \frac{16}{28}\frac{b_{i_1}}{1+b_{i_1}}, \tag{8-5-14}$$

and therefore

$$b_{i_1} = \frac{3}{4}\left[\sum_{j=1}^{p}\frac{m_0}{M_j}(c_j)_0\right] \tag{8-5-15}$$

Here m_0 is the weight fraction of the chemically action oxygen and M_j is the molecular weight of the j-th component containing oxygen.

In the first approximation we take $q_w = 0$ in Eq. (8-5-10) and find $i_{\Sigma w}$ and T_w. Then, by solving the problem of thermal conductivity of a semi-bounded body with a shifting outer edge and given T_w, we determine q_w and, by Eq. (8-5-10), we find $i_{\Sigma w}$ in the second approximation, which is usually sufficient for the case of burn-up of thermally insulated coatings. In more complex cases it is necessary to solve the conjugate problem.

Determining $i_{\Sigma w}$, we find Ψ_s from Eq. (5-5-17) and carry out the integration of Eq. (8-5-1). For the case $i_{\Sigma w} = \text{const}$ we have

$$Re^{**}_{\Sigma w} = \left\{\frac{1+m}{2\,Pr^{0,75}}B\Psi_s(1+b_{i_1})\,Re_{0w}\int_0^{\bar{x}}\bar{u}_0^{\,m}\,d\bar{x}\right\}^{\frac{1}{m+1}}. \tag{8-5-16}$$

The quantity of burned material is determined by the formula

$$j_w = \rho_0 w_0 b_{i_1} St_0 \Psi_s, \tag{8-5-17}$$

where /236

$$St_0 = \frac{B}{2Pr^{0,75}(Re^{**}_{\Sigma w})^m}$$

For the case of gas flow in a nozzle the integral of (8-5-1) can be written conveniently in the form

$$Re^{**}_{\Sigma w} = \frac{1}{\bar{D}}\left[\frac{B(1+m)}{2\,Pr^{0,75}}\Psi_s(1+b_{i_1})\right.$$
$$\left.\times Re_0\int_0^{\bar{x}}(\bar{D})^{-0,75}\,d\bar{x}\right]^{0,8}, \tag{8-5-18}$$

where $\bar{D} = D/D_{crit}$, D_{crit} is the diameter of the nozzle throat section, $R_* = \frac{4G}{\pi g u_w D_{crit}}$, and b is the mass gas flow through the nozzle.

Various heat-resistant coatings are an effective means of protecting the surface of a body from high heat fluxes. These coatings are usually porous carbonized layers

filled with material with a high yield of volatiles (based on phenol resins). Some coatings give off up to 70% (by weight) of gaseous materials when they decompose. The intense crossflow of gas on the surface of the body reduces the heat flux and, therefore, the burning rate of the carbon base. We write the heat flux reaching the wall as

$$q_w = q_{w1} + q_{w2}, \tag{8-5-19}$$

where q_{w1} is the heat that goes to heat the carbon residue and q_{w2} is the heat that goes to heat the gases to wall temperature (here too is the convenient place to put the heat of conversion of the decomposition products, i_Σ^p, which goes to evaporate the water evolved during decomposition of the resins, the additional decomposition of the heavy hydrocarbon, etc.).

Thus,

$$q_{w2} = j_{w2}[i_{w2} + i_\Sigma^p - i']. \tag{8-5-20}$$

Then the thermal energy balance on the surface is written as

$$q_{wt} = j_{w1} i_\Sigma^0 + j_{w2}[i_{w2} + i_\Sigma^p - i'] + q_{w1}, \tag{8-5-21}$$

where i' is the heat content of the material at a temperature corresponding to the onset of destruction of the coating material. After appropriate transformations we have /237

$$i_{\Sigma w} = i_{\Sigma 0} + b'_{i1} i_\Sigma^0 + b''_{i1}[i_{w2} + i_\Sigma^p - i'] + \frac{q_{w1}}{q_{w\Sigma}}(i_{\Sigma w} - i_{\Sigma 0}). \tag{8-5-22}$$

The permeability parameter b'_{i1} is governed only by the chemical erosion and is found by formula (8-5-15).

The permeability parameter b''_{i1} depends on the yield of volatile substance, i.e. it is the thermophysical characteristic of the material.

The total permeability parameter, which takes into account the effect of the crossflow of material on the heat transfer and is contained in the integral energy relation, is

$$b_{i1} = b'_{i1} + b''_{i1}. \tag{8-5-23}$$

The heat content at the wall i_w is determined, as before, by the method of successive approximation. After solving the problem of nonstationary thermal conductivity with a shifting outer boundary at temperature T_w, we find the rate of heating of the material, the quantity of gas evolved (j_{w2}) and q_{w1}. Then we determine T_w in the second approximation. The further sequence of calculation is similar to the preceding case. The rate of burn-up of the carbon base is

$$j_{w1} = b'_{i1}\rho_0 w_e \mathrm{St}_\Sigma. \tag{8-5-24}$$

Since St_{Σ} is defined with allowance for the effect of the overall crossflow of material, i.e. $b_{i_1} = b'_{i_1} + b''_{i_1}$, formula (8-5-24) shows a substantial decrease in burn-up of the graphite base with increasing yield of volatiles (that is, b''_{i_1}).

A comparison of the experimental data of Bartlet and Denison on the burn-up of a graphite duct [126] with the results of the proposed computational method is given in Figs. 8.20 and 8.21. As can be seen from the comparison, this method takes quite good account of the effect of such factors as pressure, temperature and concentration of the oxidizer in the gas flow on the graphite erosion rate.

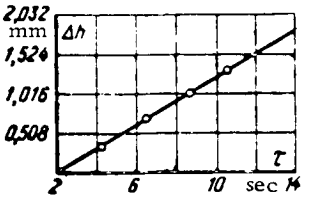

Fig. 8.20

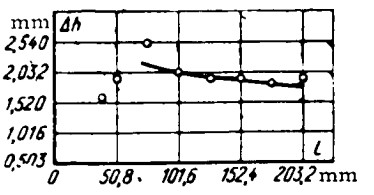

Fig. 8.21

FIG. 8.20. Dependence of the burn-up of a graphite duct on time. The curve was calculated by the method proposed here; the points represent the experiments of Bartlet and Denison [126].

FIG. 8.21. Burn-up of a graphite duct over the length. The curve was calculated by the method proposed here; the points represent the experiments of Bartlet and Denison [126].

Since the duct was relatively short, all the calculations were made as for a flat plate. /238

In Fig. 8.22 the results of experiments of E. P. Volchkov, E. G. Zaulichnyy, A. I. Leont'ev and E. I. Sinaiko [14] on the burn-up of a graphite duct are compared with the proposed computational method. Shown in the graph is the change in thickness of the burned layer over the length of the duct. Curve 1 corresponds to calculation by the Reynolds analogy without accounting for the effect of non-isothermicity and crossflow of material by the formula

$$j_w = \rho_0 \omega_0 b_{i_1} St_0, \qquad (8\text{-}5\text{-}25)$$

where $St_0 = 0{,}029\,Re_x^{-0,2} Pr^{-0,6}$; $b_{i_1} = 3/4\,(\tilde{K}_0)_0$ for the diffusion region, and $b_{i_1} = 0{,}173$ for $(\tilde{K}_0)_0 = 0{,}231$.

Curves 2 and 3 correspond to calculation by the proposed method, on the basis of this method we get for the conditions being examined

$$St_x = 0{,}029 Re_x^{-0,2} \bar{Pr}^{-0,6} \Psi^{0,8} (1 + b_{i_1})^{-0,8} \left(\frac{\mu_w}{\mu_0}\right)^{0,2} \qquad (8\text{-}5\text{-}26)$$

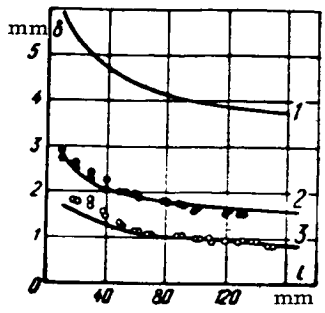

FIG. 8.22. Burn-up of a graphite duct over the length 1—calculation by Reynolds analogy without allowing for the effect of nonisothermicity and crossflow of material on the heat-transfer coefficient; 2, 3—calculation by the proposed method; experiments of [14]: ●—$\gamma_0 w_0$ = 362 kg/(m^2 · sec); τ = 63 sec; o—$\gamma_0 w_0$ = 67 kg/(m^2 · sec); τ = 144 sec.

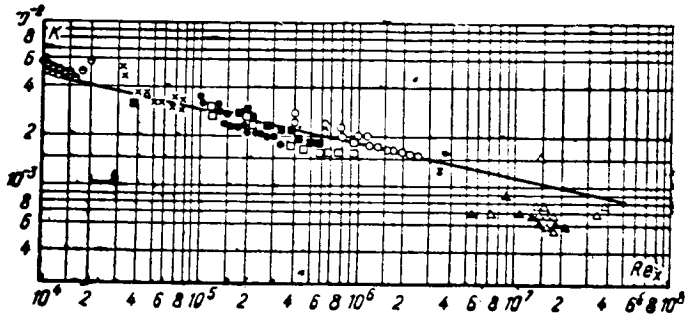

FIG. 8.23. Generalized data on mass transfer during the burn-up of a graphite surface. Curve calculated by (8-5-27).

Experiments of 14							Experiments of [126]	
Symbols	◓	×	●	⊐	■	○	△	▲
kg/m^2 · sec	3,89	10,5	36,6	198,5	67,2	362		
τ, sec	1 271	500	420	73	144	63		

or

$$K = \frac{St_x Pr^{0.6}(1 + b_{(1)})}{\Psi^{0.8}\left(\frac{\mu_w}{\mu_0}\right)^{0.2}} = 0{,}029 Re_x^{-0.2} \qquad (8\text{-}5\text{-}27)$$

As follows from Fig. 8.22, non-isothermicity and crossflow of material exert an appreciable influence on the rate of burn-up of the graphite surface, and this effect is taken into good account by the proposed computational method. /239

All the experimental data of [14] and [26] are compared with formula (8-5-27) in Fig. 8.23. Satisfactory agreement between theory and experiment can be noted. As was demonstrated earlier, the relative law of heat transfer for the conditions being examined can be written as

$$\Psi_s = \Psi_l \Psi_b. \qquad (8\text{-}5\text{-}28)$$

where

$$\Psi_i=\left(\frac{2}{\sqrt{\Psi_i}+1}\right)^2;\ \Psi_b\left(1-\frac{b_i}{b_{i\text{crit}}}\right)^2;$$

$$\Psi_i=\frac{i_w}{i_0}.$$

/240

The calculations show that for the experimental conditions of [14] and [126] the effect of crossflow of material on Ψ lies in the limits of 12%, that is, essentially within the limits of experimental accuracy. Non-isothermicity has the principal effect on Ψ_s and, accordingly, on j_w; for the conditions of the experiments being examined the non-isothermicity ($\Psi_i \approx 9{,}0$) reduces the heat-transfer coefficient by a factor of about 2.5, and it is not permissible to disregard this effect in engineering calculation.

8.6. Turbulent Boundary Layer in the Initial Section of a Pipe under Non-isothermal and Injection Conditions

A crossflow of material at the pipe walls can have an appreciable effect on the gas parameters in the flow case in the initial section of a pipe. This effect can be taken into account by simultaneous solution of the momentum, energy and continuity equations.

Let us consider the case of subsonic gas flow velocities at the entrance to a cylindrical duct with a uniform distribution of all the parameters in the initial section of the duct. We shall assume that the turbulent boundary layer forms from the initial section downstream. A diagram of this problem is shown in Fig. 8.24.

/241

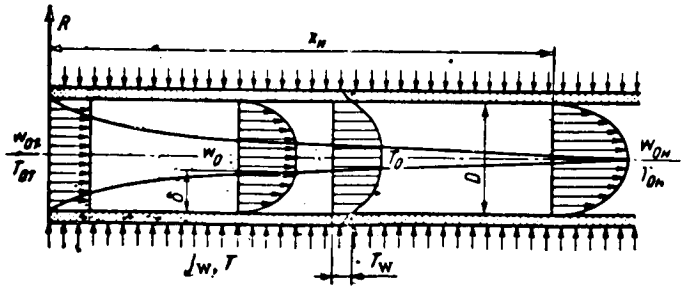

FIG. 8.24. Diagram of boundary-layer development in the initial section of a porous pipe.

In the general case the mass flow distribution of the injected gas over the pipe length and the initial parameters of the cooling gas are prescribed. It is required to determine the distribution of static pressure, friction and heat-transfer coefficients, the wall temperature, the concentration of injected gas at the wall and the length of the initial section.

The continuity equation for these conditions is written in the form

$$4H\overline{\mathrm{Re}}^{**}=\bar{w}_0-1-4\int_0^{\bar{x}}\frac{j_w}{\rho_0 w_{01}}\mathrm{Re}_{D1}^m d\left(\frac{x}{\mathrm{Re}_{D1}^m}\right), \qquad (8\text{-}6\text{-}1)$$

where

$$\overline{\mathrm{Re}}^{**}=\rho_0 w_0 \delta^{**}/\mu_*\,\mathrm{Re}_{D1};\ \mathrm{Re}_{D1}=\rho_0 w_{01} D/\mu_*;$$

$$\bar{w}_0=w_0/w_{01};\ H=\delta^*/\delta^{**};\ \bar{x}=x/D;$$

ρ_{01}, w_{01} are the density and velocity in the initial section and u_* is the characteristic viscosity, which is constant over the length.

The integral momentum relation can be written conveniently in the following form:

$$\frac{d\overline{\mathrm{Re}}^{**}}{d\tilde{x}} + (1+H)\frac{\overline{\mathrm{Re}}^{**}}{\bar{w}_0}\frac{d\bar{w}_0}{d\tilde{x}} = \bar{w}_0\frac{B}{2}(\overline{\mathrm{Re}}^{**})^m(\Psi+b), \tag{8-6-2}$$

where

$$\tilde{x} = x/\mathrm{Re}_{D1}^m; \quad b = \frac{j_w}{\rho_0 w_0}\mathrm{Re}_{D1}^m\frac{2}{B}\overline{\mathrm{Re}}^{**m}.$$

The function Ψ is defined by formulas (5-3-2) and (5-3-3), and the function H by (5-3-12). The considerable non-linearity of Eq. (8-6-2) does not permit obtaining an analytic solution in the general formulation. But for some particular cases the solution reduces to simple quadratures.

For the case b = const and i_w = const, we get from Eqs. (8-6-1) and (8-6-2)

$$\frac{\tilde{x}}{\mathrm{Re}_{D1}^m} = \frac{2(\Psi+b)^m}{B\{4[b(2+H)+H(\Psi+b)]\}^{1+m}} \times \int_1^{\bar{w}_0}\left[(2+H)\frac{(\bar{w}_0^{a+1}-1)^m}{\bar{w}_0^{am+1}} - (1+H-a)\frac{(\bar{w}_0^{a+1}-1)^m}{\bar{w}_0^{a(m+1)+2}}\right]d\bar{w}_0 \tag{8-6-3}$$

/242

and

$$\mathrm{Re}^{**} = \frac{\Psi+b}{4[b(2+H)+H(\Psi+b)]}\frac{\bar{w}_0^{a+1}-1}{\bar{w}_0^a}, \tag{8-6-4}$$

where

$$a = \frac{(1+H)b}{b+H(\Psi+b)}.$$

For b = 0 and m = 0.25 we get formulas (7-4-20) and (7-4-22) for a pipe with impermeable walls.

Let us determine the length of the initial section from the condition that the boundary-layer thickness in the initial section becomes equal to the pipe radius. Then,

$$\mathrm{Re}_H^{**} = \frac{1}{2}\bar{w}_{0H}\frac{\delta^{**}}{r_0}. \tag{8-6-5}$$

Simultaneous solution of Eqs. (8-6-3) and (8-6-5) yields /243

$$\bar{w}_{0H}=\left\{\frac{\Psi+b}{\Psi+b-2\frac{\delta}{r_0}[b(2+H)+H(\Psi+b)]}\right\}^{\frac{1}{1+s}} \qquad (8\text{-}6\text{-}6)$$

The result of calculating the dimensionless velocity distribution ($\bar{w}_0 = w_0/w_{01}$), according to the literature, are given in Fig. 8.25 for three values of the permeability parameter and for the injection of various gases. As can be seen from the graph, injection of a heavier gas has a lesser effect on the velocity in the potential flow core, in that the length of the initial section (for identical permeability parameters) decreases.

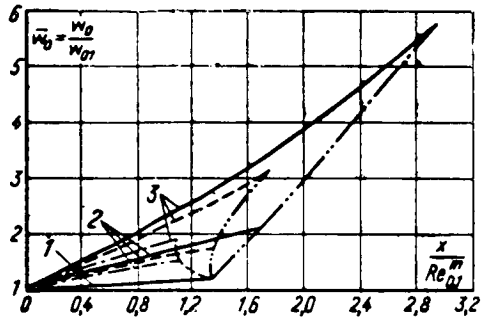

FIG. 8.25. Velocity distribution in the potential flow core over the pipe length for various injection gases. Calculations by (8-6-3) and (8-6-6). —— air-air; - - - CO_2-air; — · — Freon-air; — ·· — boundary of the initial section according to (8-6-6); 1—b = 0; 2— b = 2; 3—b = 4.

With increasing injection of a homogeneous gas, the length of the stabilization section increases. Thus, e.g., with critical injection of air into air under quasi-isothermal conditions and like values of Re_{D_1}, the length of the stabilization section increases by a factor greater than 2 compared to that for a pipe with impermeable walls. This factor can be of great importance in processing experimental data in the initial section of a porous pipe.

To evaluate this effect we can make use of Fig. 8.26, where results are given of a calculation, by the proposed method, of the velocity w_0 for injection of a homogeneous gas under quasi-isothermal conditions at various values of b.

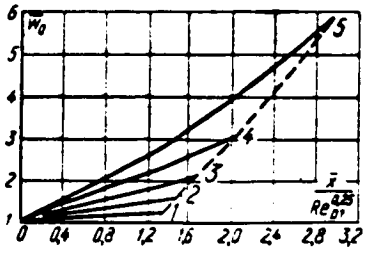

FIG. 8.26. Variation of the dimensionless velocity over the length of a pipe for injection of a homogeneous gas (the case b = const). —— calculation by (8-6-3); - - - boundary of the initial section according to (8-6-6): 1—b = 0, 2—b = 1; 3—b = 2; 4—b = 3; 5—b = 4.

Let us consider the other extreme case of constant mass flow of injected gas over the pipe length, corresponding to the condition

$$j_w/\rho_{01}w_{01}=\text{const}.$$

In this case system of Eqs. (8-6-1) and (8-6-2) reduces to the form

$$\frac{d\overline{\mathrm{Re}}^{**}}{d\bar{x}}=\frac{1+4\,kbH_0\,\overline{\mathrm{Re}}^{**}\bar{w}_0^{-1}-(1+H)\,4b\,(\Psi+b)^{-1}\,\dfrac{\mathrm{Re}^{**}}{\bar{w}_0}}{4kmbH_0+4H+4b\,(\Psi+b)^{-1}}; \qquad (8\text{-}6\text{-}7)$$

/244

$$\frac{\bar{x}}{\mathrm{Re}_{D1}^{m}}=(\bar{w}_0-1-4H\,\overline{\mathrm{Re}}^{**})\,(4\bar{j}_w\,\mathrm{Re}_{D1}^{m})^{-1}, \qquad (8\text{-}6\text{-}8)$$

where $\bar{j}_w=j_w/\rho_{01}w_{01}$; $b=\bar{j}_w\,\mathrm{Re}_{D1}^{m}\,\overline{\mathrm{Re}}^{**m}/\bar{w}_0$.

The relationship between $\bar{w}_0$ and Re^{**} can be found by numerical solution of Eq. (8-6-7). The results of calculations by Eqs. (8-6-7) and (8-6-8) for injection of a homogeneous gas under quasi-isothermal conditions are shown in Fig. 8.27. In Fig. 8.28 the results of measuring the velocity in the flow core given in [71] are compared with the proposed computational method. As can be seen from the graph, the agreement between theory and experiment is satisfactory.

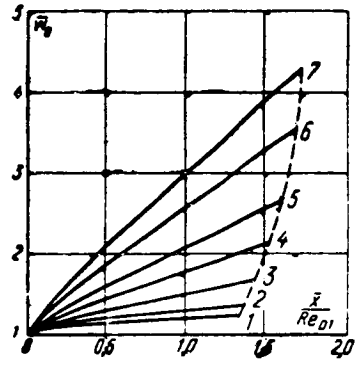

FIG. 8.27. Variation of the dimensionless velocity over the pipe length for injection of a homogeneous gas (the case $j_w=\dfrac{j_w}{\rho_0 w_0}=\text{const}$). —— calculation by (8-6-7) and (8-6-8); - - - boundary of the initial section.

No. of the curve	1	2	3	4	5	6	7
$\bar{I}_{w1}\mathrm{Re}_{D1}^{m}$	0	0,02	0,06	0,1	0,15	0,23	0,296

/245

For a duct with an impermeable end face ($\rho_{01}w_{01}=0$), the momentum equation can be written conveniently in the form

$$\frac{d\,\mathrm{Re}^{**}}{d\bar{x}}+(1+H)\,\frac{\mathrm{Re}^{**}}{\mathrm{Re}_D}\,\frac{d\,\mathrm{Re}_D}{d\bar{x}}=\mathrm{Re}_D\,\frac{B}{2}\,\frac{\Psi+b}{\mathrm{Re}^{**m}}. \qquad (8\text{-}6\text{-}9)$$

For the case b = const, continuity equation (8-6-1) has the form

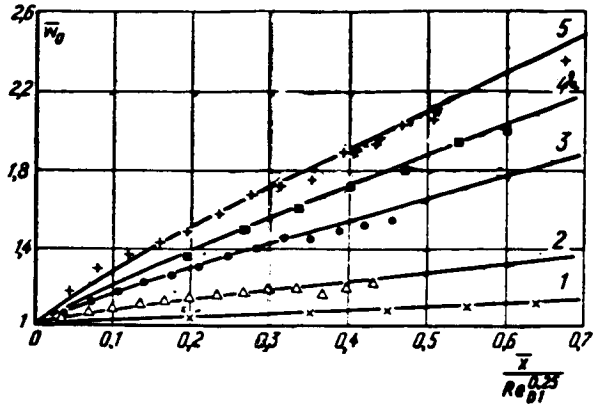

FIG. 8.28. Variation of the dimensionless velocity on the axis of a pipe with permeable walls. Curves calculated by (8-6-7) and (8-6-8); the points represent the experiments of [71].

No. of the curve	1	2	3	4	5
$T_{w1}\mathrm{Re}_{D1}^{0,25}$	0	0,0853	0,174	0,229	0,296

$$4H\,\mathrm{Re}^{**} = \mathrm{Re}_D - 4\int_0^{\bar{x}} \mathrm{Re}_w\,d\bar{x}, \tag{8-6-10}$$

where $\mathrm{Re}_D = \rho_0 w_0 D/\mu_*$; $\mathrm{Re}_w = j_w D/\mu_*$.

Accordingly,

$$b = \frac{2}{B}\frac{\mathrm{Re}_w}{\mathrm{Re}_D}\mathrm{Re}^{**m}. \tag{8-6-11}$$

Equation (8-6-9), with (8-6-11) taken into account, is written as

$$\frac{d\,\mathrm{Re}^{**}}{d\,\mathrm{Re}_D} + (1+H)\frac{\mathrm{Re}^{**}}{\mathrm{Re}_D} = \frac{\Psi+b}{b}\mathrm{Re}_w\frac{d\bar{x}}{d\,\mathrm{Re}_D}. \tag{8-6-12}$$

Differentiating Eq. (8-6-10) we get /246

$$\mathrm{Re}_w\frac{d\bar{x}}{d\,\mathrm{Re}_D} = \frac{1}{4} - H\frac{d\,\mathrm{Re}^{**}}{d\,\mathrm{Re}_D}. \tag{8-6-13}$$

Substituting this relation into Eq. (8-6-12) we get

$$\left\{1+H\frac{\Psi+b}{b}\right\}\frac{d\,\mathrm{Re}^{**}}{d\,\mathrm{Re}_D} + (1+H)\frac{\mathrm{Re}^{**}}{\mathrm{Re}_D} - \frac{\Psi+b}{4b} = 0. \tag{8-6-14}$$

The integral of Eq. (8-6-14) for the boundary conditions $Re^{**} = 0$ with $Re_D = 0$ has the form

$$Re^{**} = cRe_D, \tag{8-6-15}$$

where

$$c = \frac{\Psi + b}{4\{b(2+H) + H(\Psi + b)\}}.$$

Substituting (8-6-15) into (8-6-13) and (8-6-10) we obtain

$$Re_D^m = d \cdot x, \tag{8-6-16}$$

where

$$d = \frac{B}{2}\frac{m}{2+H}\frac{[\{4[b(2+H) + H(\Psi + b)]\}^{m+1}}{(\Psi + b)^m}$$

and

$$Re_w = \frac{B}{2} b \frac{Re_D}{Re^{**m}} = D\bar{x}^{\frac{1-m}{m}}, \tag{8-6-17}$$

where

$$D = \frac{b}{\Psi + b}\left(\frac{m}{2+H}\right)^{\frac{1-m}{m}}\left(\frac{B}{2}\right)^{\frac{1}{m}}\{4[b(2+H) + H(\Psi + b)]\}^{\frac{1}{m}}.$$

Thus, when m = 0.25, the mass gas flow through the permeable wall under the condition b = const increases over the length of the pipe proportionally to $\bar{x}^3$. Since $b = b_1\Psi$ and Ψ is a single-valued function of b_1 [see (5-3-2), (5-3-3) and (5-5-7)], formulas (8-6-15), (8-6-16) and (8-6-17) can also be applied to the conditions b_1 = const.

As was shown in Chapter 5, these conditions are met when chemical erosion of the wall material in the diffusion section occurs.

For a duct with an impermeable end face in the case j_w = const we have from Eq. (8-6-10)

$$4H Re^{**} = Re_D - 4Re_w\bar{x};$$

from it we get

/247

$$\bar{x} = \frac{Re_D - 4H\,Re^{**}}{4Re_w}. \tag{8-6-18}$$

Substituting dx/dRe_D from (8-6-18) into Eq. (8-6-13) and considering that $H = H_0(1 + kb)$, after transformations we get

$$\frac{dRe^{**}}{dRe_D} = \frac{1 + \left[4H_0kb - (1+H)\frac{4b}{\Psi + b}\right]\frac{Re^{**}}{Re_D}}{4H + 4H_0kmb + \frac{4b}{\Psi + b}}. \tag{8-6-19}$$

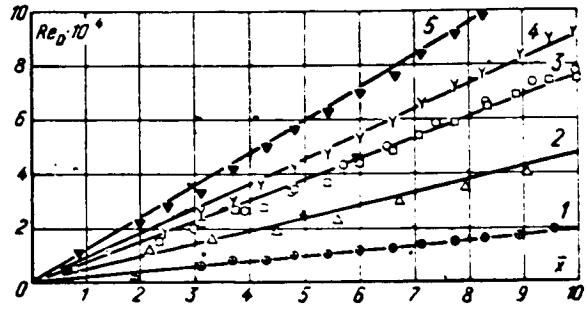

FIG. 8.29. Variation of the dimensionless velocity on the axis of a pipe with porous walls and on impermeable end face. Curves calculated by (8-6-18) and (8-6-19); the points represent the experiments of [71].

No. of the curve	1	2	3	4	5
$Re_w = \frac{l_w D}{\mu}$	300	788	1 290	1 533	1 948

For the permeability parameter b we have the formula

$$b = \frac{2}{B} \frac{Re_w}{Re_D} Re^{**m}. \qquad (8\text{-}6\text{-}20)$$

Nonlinear Eq. (8-6-19) can be integrated numerically, taking (8-6-20) and (8-6-18) into account. Using relation (8-6-18), it is possible to get the variation of Re_D and Re^{**} over the length of the pipe.

The results of a numerical calculation of the variation of $Re_D = \frac{\rho_0 w_0 D}{u_0}$ carried out on an M-20 computer by the Range-Kutta method (for B = 0.0128, k = 0.05 and m = 0.25) are compared in Fig. 8.29 with the experiments of A. I. Leont'ev, A. V. Fafurin and N. V. Nikitin [71]. /248

The energy equation (8-4-18), taking (8-4-19) into account, can be written conveniently as

$$Re^{**}_i = \int_0^{\bar{x}} \left(\frac{1-\psi'}{1-\psi_i}\right)^{\bar{j}} Re_{D1}^m \, d\left(\frac{\bar{x}}{Re_{D1}^m}\right), \qquad (8\text{-}6\text{-}21)$$

where $\psi' = i'/i_0$, and i' is the critical enthalpy of the injected gas.

For a given law of distribution of the injected gas over the length of the pipe, the local values of Re^{**}_i can be determined from (8-6-21).

Let us consider the case b_i = const, which corresponds to the condition i_w = const. From (8-6-21) it follows that:

$$\int_0^{\mathrm{Re}^{**}_i} \mathrm{Re}_i^{\infty m}\, d\,\mathrm{Re}^{**}_i = \frac{1-\phi'}{1-\phi_i}\frac{B}{2} \times b\,\mathrm{Pr}^n \int_0^{\frac{x}{\mathrm{Re}^m_{D1}}} \bar{w}_0\, d\left(\frac{x}{\mathrm{Re}^m_{D1}}\right). \tag{8-6-22}$$

Taking (8-6-2) into account, we get

$$\mathrm{Re}^{**}_i = \frac{\Psi + b}{4\,[(2+H)\,b + H(\Psi+b)]\,\mathrm{Pr}^{0,6}} \times \left\{\left(\frac{1-\phi'}{1-\phi_i}\right) b\left(\frac{m+1}{\Psi+b}\right)\int_1^{\bar{w}_0}\left[(2+H)\frac{(w_0^{a+1}-1)^m}{\bar{w}_0^{a(m+1)-1}} - (1+H-a)\frac{(\bar{w}_0^{a+1}-1)^m}{\bar{w}_0^{a(m+1)+1}}\right] d\bar{w}_0\right\}^{\frac{1}{1+m}}. \tag{8-6-23}$$

An analytic solution of this problem can be obtained if we set $\mathrm{Re}^{**} = \mathrm{Re}^{**}_i$ in the continuity equation. Then,

$$\mathrm{Re}_D = 4H\,\mathrm{Re}^{**}_i + \mathrm{Re}_{D1}(1+4G), \tag{8-6-24}$$

where $G = \int_0^{\bar{x}} \frac{j_w}{\rho_{01} w_{01}}\, dx$. Consequently, $j_w/\rho_{01} w_{01} = dG/dx$. /249

The energy equation can be written in the form

$$\frac{d\,\mathrm{Re}^{**}_i}{dx} = \frac{\Psi + b}{b_i}\mathrm{Re}_{D1}\frac{dG}{dx}. \tag{8-6-25}$$

Integrating, we get

$$\mathrm{Re}^{**}_i = \frac{\Psi + b_i}{b_i}\mathrm{Re}_{D1} G. \tag{8-6-26}$$

Taking m = 0.25, B/2 = 0.0128, Pr ≈ 1.0 and allowing for (8-6-24) we get

$$\frac{AG^{0,25}\,dG}{BG+1} = dx, \tag{8-6-27}$$

where

$$A = \frac{\mathrm{Re}_{D1}\frac{\Psi+b_i}{b_i}}{0{,}0128 b_i};\quad B = 4H\frac{\Psi+b_i}{b_i} + 4.$$

The integral of Eq. (8-6-27) is

$$x=\frac{4A}{B}\left\{G^{0,25}-\frac{\sqrt[4]{\frac{1}{B}}}{4\sqrt{2}}\right.$$

$$\times\left[\ln\frac{G^{0,5}+\sqrt[4]{\frac{1}{B}}G^{0,25}\sqrt{2}+\sqrt{\frac{1}{B}}}{G^{0,5}-\sqrt[4]{\frac{1}{B}}G^{0,25}\sqrt{2}+\sqrt{\frac{1}{B}}}\right. \tag{8-6-28}$$

$$\left.\left.+2\operatorname{arctg}\frac{\sqrt[4]{\frac{1}{B}}\sqrt{2}G^{0,25}}{\sqrt{\frac{1}{B}}-G^{0,5}}\right]\right\}.$$

The law of distribution of injection over the length is found from Eq. (8-6-27):

$$\frac{j_w}{\rho_{01}w_{01}}=\frac{1+BG}{AG^{0,25}}. \tag{8-6-29}$$

For the case $j_w/\rho_{01}w_{01}$ = const it follows from (8-6-21) that /250

$$\overline{\mathrm{Re}}^{**}_i=\frac{1-\psi'}{1-\psi_i}(\tilde{j}_i\,\mathrm{Re}^m_{D1})\left(\frac{x}{\mathrm{Re}^m_{D1}}\right) \tag{8-6-30}$$

or, introducing the dimensionless enthalpy,

$$\theta_0=\frac{i_0-i_w}{i_0-i'} \tag{8-6-31}$$

and

$$\mathrm{Re}^{**}_i=\overline{\mathrm{Re}}^{**}_i\mathrm{Re}_{D1};\qquad \mathrm{Re}^{**}_i=\tilde{j}_i\,\mathrm{Re}_{D1}x\frac{1}{\theta_0}. \tag{8-6-32}$$

The continuity equation can be written in the form

$$\mathrm{Re}_D=4H\,\mathrm{Re}^{**}_i+\mathrm{Re}_{D1}(1+4\tilde{j}_i x), \tag{8-6-33}$$

where we have set $\mathrm{Re}^{**}\approx\mathrm{Re}^{**}_i$. Then, from Eqs. (8-6-32) and (8-6-33) we get

$$\left[\tilde{j}_i\,\mathrm{Re}_{D1}\frac{1}{\theta_0}x\right]^{0,25}=\frac{0,0128b_i}{\mathrm{Pr}^{0,75}}\left[\frac{4H}{\theta_0}+\left(\frac{1}{\tilde{j}_i}+4x\right)\right]. \tag{8-6-34}$$

Taking Eq. (8-4-21) into account we get the equation

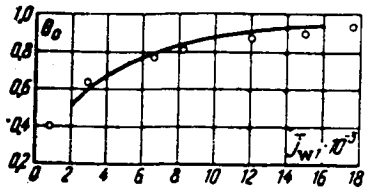

FIG. 8.30. Effect of injection on the temperature of a porous wall. Curve calculated by (8-6-35); points represent the experiments of [252].

$$\left[\bar{j}_1 \mathrm{Re}_{D1}\frac{x}{\theta_0}\right]^{0.25} = \frac{0{,}0128}{\mathrm{Pr}^{0.75}}\left[4\frac{H}{\theta_0}+\left(\frac{1}{\bar{j}_1}+4x\right)\right] \times\left\{b_{i\,\mathrm{crit}}-\frac{k}{2\Psi_t}\,b_{i\,\mathrm{crit}}\left(\sqrt{\frac{4\Psi_t}{kb_{i\,\mathrm{crit}}}+1}-1\right)\right\}, \qquad (8\text{-}6\text{-}35)$$

where $k=\frac{1}{\theta_0}-1$.

For known Ψ and $b_{i\,\mathrm{crit}}$ as a function of ψ_i we get an equation in the desired parameter θ_0. The equation is solved graphically or by the method of successive approximation. /251

The results of calculating the mean wall temperature of a porous pipe by the proposed method are compared in Fig. 8.30 with the experiments of Yuan and Barazotti [252]. It is simpler to calculate by the graphs of Figs. 8.14 and 8.25.

8.7. Gas Flow in a Long Pipe with Porous Walls

Formula (5-2-1) can be used to calculate hydrodynamics and heat transfer for a gas flow in long pipes. In this case, a one-dimensional model of the gas flow can be used to obtain preliminary results, and the influence of the crossflow of material at the walls of the pipe will be taken into account directly in the momentum equation and indirectly by the laws of friction and heat transfer.

As an example let us consider a flow of gas with constant physical properties in a long cylindrical pipe with gas sucked through the walls at a constant rate. A diagram of this problem is shown in Fig. 8.31.

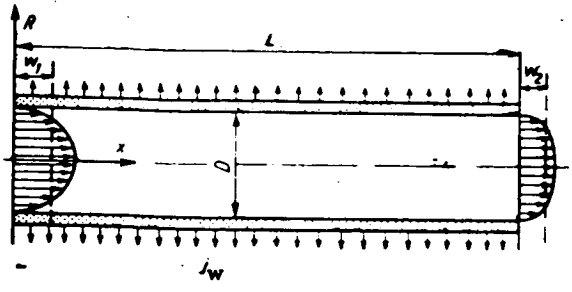

FIG. 8.31. Diagram of gas flow in a pipe with permeable walls.

The momentum equation for a one-dimensional model is written as

$$\frac{dP}{dx}=\frac{4}{D}\rho\bar{u}^2\frac{c_{f0}}{2}[2xb-\Psi], \qquad (8\text{-}7\text{-}1)$$

where $a=\frac{\pi D^2}{4}\frac{\int_0^{R_0} w^2 2\pi R\,dR}{\left[\int_0^{R_0} w 2\pi R\,dR\right]^2}$ is the nonuniformity coefficient, which in what follows will be taken equal to 1, $b=\frac{m}{\bar{w}\frac{c_{f0}}{2}}$ is the permeability parameter, and is the mean flow velocity.

From the continuity equation it follows that

$$m=\left(1-\frac{\bar{w}_2}{\bar{w}_1}\right)\frac{w_1 D}{4L}, \tag{8-7-2}$$

where $\bar{w}_2$ is the gas velocity at the exit from the pipe.

Consequently,

$$b=\frac{r}{(1-r\bar{x})\bar{x}_1}, \tag{8-7-3}$$

where

$$r=1-\frac{\bar{w}_2}{\bar{w}_1};\quad \bar{x}=\frac{4x}{D}\frac{c_{f0}}{2};\quad \bar{x}_1=\frac{4Lc_{f0}}{D2}.$$

Taking (5-2-6) and (8-7-3) into account, Eq. (8-7-1) can be written as

$$\frac{dP}{d\bar{x}}=4l\rho\bar{w}_1^2\frac{c_{f0}}{2}[1{,}5z(1-r\bar{x})-0{,}0625z^2-(1-r\bar{x})^2], \tag{8-7-4}$$

where $z=r/\bar{x}$, $\bar{l}=x/D$.

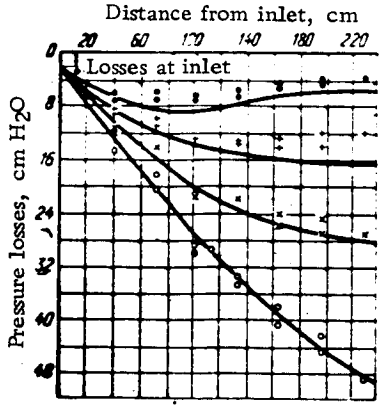

FIG. 8.32. Pressure variation over the length of a pipe with permeable walls for various suction intensities. Curves calculated by (8-7-5); the points correspond to the experiments of Wallis [242]: o—w_2/w_1 = 0.68; ×—0.45; +—0.231; ●—0.

After integrating we get

$$\frac{P-P_0}{\varepsilon_1 \rho \bar{w}_1^2} = x(1{,}5z - 0{,}0625z^2 - 1) + x^2 r(1 - 0{,}75z) - \frac{r^2 x^3}{3}. \tag{8-7-5}$$

The results of calculating by Eq. (8-7-5) are compared in Fig. 8.32 with the experiments of Wallis [242]. As follows from Fig. 8.32, the proposed calculation method to more complex compressed gas-flow conditions in a long porous pipe with considerable non-isothermicity. In this case it is necessary to take into account the effect of compressibility and non-isothermicity on the function Ψ in accordance with the formulas of (5-4-6). The problem is solved by the methods of numerical or graphic integration.

CHAPTER 9
EFFECTIVENESS OF GAS SCREENS

9.1. Effectiveness of a Gas Screen at a Flat Wall under Quasi-Isothermal Conditions

/253

The method of heat shielding with gas screens is widely used in modern engineering practice. Arrangements of basic gas screen design variations are illustrated in Fig. 9.1. Other combinations of these variations are also possible. For example, film cooling, which is widely used in liquid-fuel rocket engines, is combined with the usual wall cooling. The flow-through section of a solid-fuel rocket engine is usually made in sectional form with different thermal-isolation coverings, and in this case the gas screen is dispersed over the surface by the lateral flux of matter.

/254

The basic parameter defining the intensity of the heat transfer in the presence of a gas screen is the so-called gas-screen effectiveness

$$\theta = \frac{i_0 - i_w}{i_0 - i_{w1}}, \qquad (9\text{-}1\text{-}1)$$

where i_0 is the total enthalpy of the undisturbed flow, i_w the enthalpy at the thermally-insulated wall, and i_{w1} is the enthalpy at the wall in the initial section.

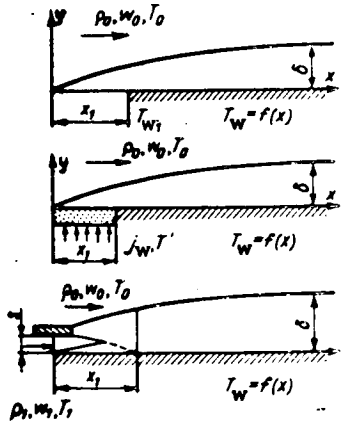

FIG. 9.1. Diagrams of principal versions of the gas screen.

Thus the effectiveness of the gas screen determines the temperature of the thermally-insulated wall with a screen. As will be shown later, this parameter is also needed for calculations of heat transfer if a screen is present.

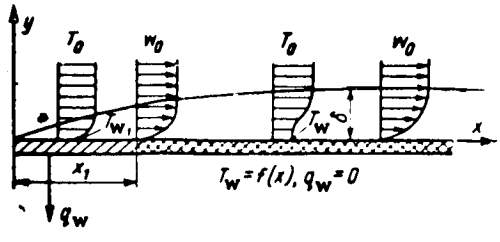

FIG. 9.2. Diagram of a thermal screen.

Consider a longitudinal flow of an incompressible fluid with constant physical properties around a flat, thermally-insulated plate (Fig. 9.2). A section of length x, is cooled, and the temperature of the wall in section x, is T_{w1}. In the region $x>x_1$ the wall is thermally-insulated and the wall temperature varies along the plate, approaching the temperature of the incoming flow. Radiative heat exchange will be ignored. /255

The energy equation for the region $x>x_1$ is written as

$$\frac{d\,\mathrm{Re}^{**}_T}{d\bar{x}}+\frac{\mathrm{Re}^{**}_T}{\Delta T}\frac{d(\Delta T)}{d\bar{x}}=0. \tag{9-1-2}$$

Integrating from $\bar{x}$, to $\bar{x}$ we obtain

$$\mathrm{Re}^{**}_T\Delta T=\mathrm{Re}^{**}_{T1}\Delta T_1. \tag{9-1-3}$$

We introduce the thermal screen effectiveness parameter and find

$$\theta=\frac{\Delta T}{\Delta T_1}=\frac{\mathrm{Re}^{**}_{T1}}{\mathrm{Re}^{**}_T}; \tag{9-1-4}$$

where $\mathrm{Re}^{**}_{T_1}$ is Reynolds number in section x_1.

It is obvious that Eq. (9-1-4) will also be valid for a more general case, if the total enthalpy is introduced in place of the temperature. In the section $x<x_1$, with Pr = 1, the conditions

$$\delta_T\approx\delta;\ \delta^{**}_T\approx\delta^{**}. \tag{9-1-5}$$

are satisfied.

In the region $x>x_1$ the similarity of the dynamic- and thermal boundary layers breaks down, since the boundary conditions at the surface of the plate are changed. For the heat-insulated portion we can write

$$\left.\begin{aligned}&\text{with } y=0\quad q=0,\ \frac{\partial T}{\partial y}=0;\\&\text{with } y=\delta_T\quad q=0,\ \frac{\partial T}{\partial y}=0.\end{aligned}\right\} \tag{9-1-6}$$

Temperature equalization occurs within the boundary layer only because of turbulent mixing and the intake of gas from the outer flow. In this case the most intense mixing takes place near the wall, where the derivative $\partial w_x/\partial y$ is maximum. As a result, the temperature profile is distorted in such a way that the region with $\partial T/\partial y\approx 0$ grows continuously--i.e. the range with $T\approx T_w$ increases. Simultaneously the temperature in the boundary layer approaches T_0, due to the leakage of gas from the outer flow, i.e. with /256

$$x\longrightarrow\infty\quad T\longrightarrow T_w\longrightarrow T_0. \tag{9-1-7}$$

The energy-loss thickness, with constant physical properties, is defined by the formula

$$\bar{\delta}^{**}_T = \int_0^1 \omega \left(1 - \frac{T - T_w}{T_e - T_w}\right) d\bar{\xi}_T.$$

With $x \to \infty$, condition (9-1-7) corresponds to the limiting value of the energy-loss thickness

$$\bar{\delta}^{**}_T = \int_0^1 \omega \, d\bar{\xi}_T. \qquad (9\text{-}1\text{-}8)$$

This maximum possible energy-loss thickness corresponds to that temperature distribution with which the gas temperature in the main part of the boundary layer is close to the wall temperature.

Adopting $\omega = \omega_0 = \xi^{1/7}$ for the conditions being considered, we have, for the region $x < x_1$

$$\bar{\delta}^{**}_T \approx \bar{\delta}^{**} = 0{,}097.$$

At the boundary layer separation point, due to the action of the longitudinal pressure gradient, n = 1/2, but $n_T \approx 1/7$, and then $\bar{\delta}^{**}_T = 0{,}097$ and $\bar{\delta}^{**} = 0{,}16$.

The limits of the quantity $\bar{\delta}^{**}_T$, according to (9-1-8), are

$$\left.\begin{aligned} &\text{with } f = 0 \quad \bar{\delta}^{**}_{T\max} = 0{,}875; \\ &\text{with } f = f_{sp} \quad \bar{\delta}^{**}_{T\max} = 0{,}7. \end{aligned}\right\} \qquad (9\text{-}1\text{-}9)$$

Thus, with any pressure gradient, the relative energy-loss thickness on an impermeable, thermally-insulated surface with $x \to \infty$ becomes close to unity. This result is confirmed qualitatively by the measurements presented in the paper by Nichiwaki, Hirata and Tsuchida [187].

According to these measurements $\delta^{**}_{T\max}/\delta^{**}_{T0} = 6$, and the limiting value of this ratio is 9. /257

For the thermal screen depicted in Fig. 9.2, for a fluid with constant physical parameters and Pr ~ 1, we can assume that $\delta_T \approx \delta$ over the entire length of the plate; since with $x > x_1$ the "scouring" of the thermal boundary layer should be limited to a region where $\partial w_x/\partial y \neq 0$, i.e. the thickness of the dynamic boundary layer.

Then Eq. (9-1-4) is written in the form

$$\theta = \frac{\delta^{**}_1}{\beta \delta^{**}}, \qquad (9\text{-}1\text{-}10)$$

where $\beta = \delta^{**}_T/\delta^{**}$ is a coefficient accounting for the deformation of the temperature field.

With $x \to x_1$, $\beta \to 1$, and with $x \to \infty$, $\beta \to \beta_{max}$.

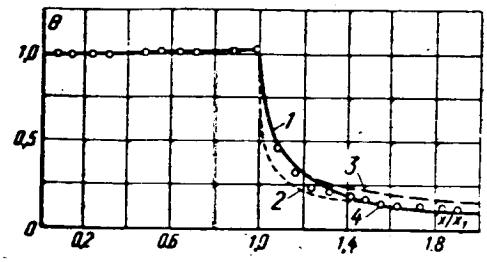

FIG. 9.3. Effectiveness of a thermal gas screen. 1—calculated from (9-1-14); 2—computed as per Seban [214]; 3—computed as per Rubesin [205]; 4—test data of Reynolds et al [199].

In the region $x > x_1$, with quasi-siothermal conditions, the dynamic boundary layer is developed independently of the thermal boundary layer. From the integral momentum ratio we have

$$\frac{\delta^{**}_1}{\delta^{**}} = \left(\frac{x_1}{x}\right)^{0.8}. \qquad (9\text{-}1\text{-}11)$$

Accordingly, with $x \to \infty$

$$\theta \to \frac{1}{\beta_{max}} \left(\frac{x_1}{x}\right)^{0.8}. \qquad (9\text{-}1\text{-}12)$$

Taking into account the momentum equation and the conditions $Re^{**}_{T_1} = Re^{**}_1$ and $\beta = 1$, with $x = x_1$ we obtain /254

$$\theta \approx \left(1 + \beta^{1.25}_{max} \frac{x - x_1}{x_1}\right)^{-0.8}. \qquad (9\text{-}1\text{-}13)$$

According to (9-1-8), for the conditions being considered, $\beta_{max} = 9$, and then

$$\theta \approx \left(1 + 15{,}6 \frac{x - x_1}{x_1}\right)^{-0.8}. \qquad (9\text{-}1\text{-}14)$$

Figure 9.3 presents a comparison of the calculations made with (9-1-14) and the test results of Reynolds, Kays and Kline [199].

As can be seen from the diagram, theory and experiment are in good agreement.

Formula (9-1-10), extended to the flow of a compressible gas, and taking Eq. (7-2-14) for Re^{**} into account, reduces to

$$\theta = \left[1 + \frac{B}{2}(1+m)\beta^{m+1}_{max} \int_{\bar{x}_1}^{\bar{x}} \frac{\Psi\, Re_L \left(\frac{\mu_w}{\mu_\infty}\right)^m d\bar{x}}{(Re^{**}_{T1})^{m+1}}\right]^{-\frac{1}{m+1}}, \qquad (9\text{-}1\text{-}15)$$

where

$$\Psi = \left[\frac{2 \operatorname{arctg} M_\infty \sqrt{0.5r(K-1)}}{(\sqrt{\bar{\psi}} + 1) M_\infty \sqrt{0.5r(K-1)}}\right]^2;$$
$$\bar{\psi} = T_w / T^*_w; \qquad (9\text{-}1\text{-}16)$$

$$\beta_{max}=\left(\int_0^1 \frac{\rho}{\rho_0}\omega\, d\xi\right)\left(\int_0^1 \frac{\rho}{\rho_0}\omega(1-\omega)\, d\xi\right)^{-1}. \qquad (9\text{-}1\text{-}17)$$

To estimate the influence of compressibility on β_{max}, we take $\rho/\rho_0=\psi^*-(\psi^*-1)\ \omega^2$ and $\omega=\xi^{1/7}$. The computed values of β_{max}, with these relationships taken into account, are given in Table 9.1.

Table 9.1. Values of β_{max} as a function of M

M	0	1	2	3	4	5
β_{max}	9	9,2	9,8	10,4	11,5	12

Thus the compressibility of the gas does not significantly affect β_{max}. Consequently, in view of the fact that /259

$$Re^{**}_{T1}=\left[\frac{B}{2}(m+1)\,\Psi_1\,Re_{x_1}\left(\frac{\mu_w}{\mu_\infty}\right)_1^m\right]^{\frac{1}{m+1}},$$

we have from (9-1-15)

$$\theta=\left[1+\beta_{max}^{1.25}\frac{x-x_1}{x_1}\right]^{-0.8}. \qquad (9\text{-}1\text{-}18)$$

This formula is derived on the assumption that the parameter $\bar{\psi}=T_{w1}/T^*_w$, i.e., with maximum possible influence of non-isothermicity. Thus the effect of gas compressibility on the effectiveness of the gas screen, with the assumptions adopted, appears in the coefficient β_{max}.

With $x\to\infty$, $T_w \to T_w$. $\Psi/\Psi_1 \to \left(\frac{\sqrt{\bar{\psi}_1}+1}{4}\right)^2$

Consequently

$$\theta|_{\bar{x}\to\infty}\to\left[1+\beta_{max}^{1.25}\left(\frac{\sqrt{\bar{\psi}_1}+1}{4}\right)^2 \times\int_{\bar{x}_1}^{\bar{x}}\left(\frac{\mu_w}{\mu_{w1}}\right)^m d\bar{x}\right]^{-0.8}.$$

Taking $(u_w/u_{w1})^m \approx 1$, we have

$$\theta=\left[1+\beta_{max}^{1.25}\left(\frac{\sqrt{\bar{\psi}_1}+1}{4}\right)^2\frac{\bar{x}-\bar{x}_1}{\bar{x}_1}\right]^{-0.8}.$$

Thus the effectiveness of the screen grows as the intensity of cooling of the initial section of the plate is increased.

For an axisymmetric boundary layer, we have from the energy equation:

$$\theta = \frac{D_1}{D} \frac{\mathrm{Re}^{**}_{T1}}{\mathrm{Re}^{**}_{T}} . \tag{9-1-19}$$

In particular for flow around a cone

(a) With M = 0, $\beta_{max} = 9$,

$$\theta = \frac{x_0}{x}\left[1 + 15{,}6\left(\frac{x - x_0}{x_0}\right)\right]^{-0{,}9}; \tag{9-1-20}$$

(b) With M = 3.5, $\beta_{max} = 10.9$ /260

$$\theta = \frac{x_0}{x}\left[1 + 19{,}7\left(\frac{x - x_0}{x_0}\right)\right]^{-0{,}9}. \tag{9-1-21}$$

Figure 9.4 presents a comparison of the results as computed from (9-1-20) and (9-1-21) with the experimental data of F. H. Durgin [135]. The proposed method of computing the gas-screen effectiveness can be extended to the case of an arbitrary law of change in velocity at the outer limit of the boundary layer. From Eq. (9-1-4), taking (7-2-52) into account, we have, in the general case:

$$\theta_\Sigma = \left\{1 + \frac{\beta_{max}^{l+m}}{\theta_\Sigma^{l+m}} \frac{\int_{\bar{x}_1}^{\bar{x}} \Psi_\infty \left(\frac{\mu_w}{\mu_\infty}\right)^m U(1-U^2)^{\frac{1}{K-1}} \theta_\Sigma^{l+m} d\bar{x}}{\mathrm{Re}_{00}^m \left[\int_0^{\bar{x}_1} \Psi_\infty \left(\frac{\mu_w}{\mu_\infty}\right)^m U(1-U^2)^{\frac{1}{K-1}} d\bar{x}\right]^{m+1}}\right\}^{-\frac{1}{m+1}} \tag{9-1-22}$$

and for the case of gas flow in a supersonic nozzle; /261

$$\theta_\Sigma = \left\{1 + \frac{\beta_{max}^{l+m}}{\theta_\Sigma^{l+m}} \frac{1}{\mathrm{Re}_{00}^m D^{m+1}} \times \frac{\int_{\bar{x}_1}^{\bar{x}} \Psi_\infty \left(\frac{\mu_w}{\mu_\infty}\right)^m D^{m+1} \theta_\Sigma^{m+1} d\bar{x}}{\left[\int_0^{\bar{x}_1} \Psi_\infty \left(\frac{\mu_w}{\mu_\infty}\right)^m d\bar{x}\right]^{m+1}}\right\}^{-\frac{1}{m+1}} \tag{9-1-23}$$

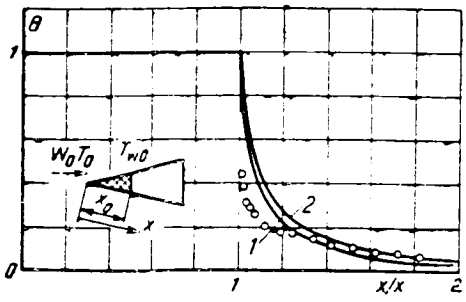

FIG. 9.4. Effectiveness of thermal screen at the surface of a cone in a supersonic flow. 1—Calculated from (9-1-21); 2—calculated from (9-1-20); Points—tests of F. H. Durgin [135].

where

$$\theta_\Sigma = \frac{i^*_w - i_{w\Sigma}}{i^*_w - i_{w1}};$$

$i_{w\Sigma}$ is the total enthalpy of the gas at the thermally-insulated wall; i_{w1} is the total enthalpy of the gas at the cooled wall in the section $\bar{x}_1$.

The parameter $\bar{\psi} = i_{w\Sigma}/i^*_w$ appearing in Ψ_∞ is related to the screen effectiveness by the formula

$$\bar{\psi} = 1 - \theta(1 - \bar{\psi}_1). \qquad (9\text{-}1\text{-}24)$$

Equations (9-1-22) and (9-1-23) are solved for iii by successive approximations. The magnitude of the coefficient β_{max} can be taken from Table 9.1 (first approximation).

9.2. Gas Screen Created by Injection of Gas Through a Porous Section

Let us derive the formula for the effectiveness of the gas screen created by injection of gas through a permeable section of length x_1 (Fig. 9.5). Equation (8-4-20) is written in the form

$$\frac{d(\mathrm{Re}^{**}_{i1})}{d\bar{x}} = \mathrm{Re}_w (i^*_w - i').$$

From this, for the case i_w = const, we have

/262

$$\mathrm{Re}^{**}_{i1} = \mathrm{Re}_{w1}(1 + K_1), \qquad (9\text{-}2\text{-}1)$$

where

$$\mathrm{Re}_{w1} = \frac{1}{\mu_\infty}\int_0^{x_1} j_w dx;$$

$$K_1 = \frac{i_{w1} - i'}{i^*_w - i_{w1}}.$$

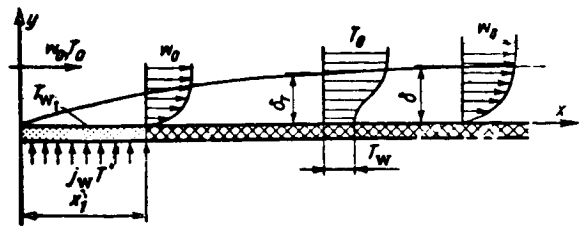

FIG. 9.5. Diagram of gas screen with a porous section.

For the case M << 1 and C_p = const.

$$K_1 = \frac{T_{w_1} - T'}{T_0 - T_{w_1}}.$$

Since $\theta = \frac{1 + K_1}{1 + K}$, we have from (9-1-4)

$$K + 1 = (K_1 + 1)\frac{Re^{**}_T}{Re^{**}_{T_1}}, \qquad (9\text{-}2\text{-}2)$$

or, in view of (9-2-1):

$$K + 1 = \frac{Re^{**}_T}{Re^{**}_{w_1}}. \qquad (9\text{-}2\text{-}3)$$

In the region $0 < x < x_1$, $Re^{**}_T \approx Re^{**}$, and in the region $x > x_1$, $Re^{**}_T = \beta Re^{**}$.

From the momentum equation we have

$$Re^{**} = \left[(1 + m)\frac{B}{2} Re_{\Delta x} + Re_1^{**1+m}\right]^{\frac{1}{m+1}}, \qquad (9\text{-}2\text{-}4)$$

where

$$Re_{\Delta x} = \frac{w_0}{\nu}(x - x_1).$$

With $x \to \infty$, $Re_{\Delta x} \approx Re_x >> Re^{**}_1$, and /263

$$K + 1 \to \frac{\beta_{max}}{Re_{w_1}}\left[(1 + m)\frac{B}{2} Re_x\right]^{\frac{1}{m+1}}. \qquad (9\text{-}2\text{-}5)$$

Taking n = 1/7, B/2 = 0.0128, m = 0.25 and β_{max} = 9, we obtain the limiting formula

$$K + 1 \to 0{,}33\frac{Re_x^{0,8}}{Re_{w_1}}. \qquad (9\text{-}2\text{-}6)$$

For the entire region from x_1 to ∞, we have

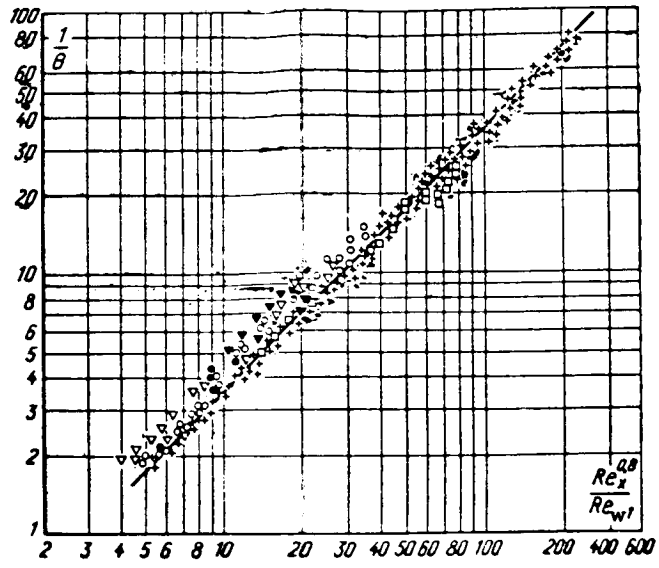

FIG. 9.6. Effectiveness of the gas screen with a a porous section. Straight line—calculated from from (9-2-6); ▽, ○, ●, □—test data of Nichiwaki et al [187]; +—data from V. P. Komarov [51].

$$\theta=\left[1+\frac{0.25\,\mathrm{Re}_{\Delta x}}{\mathrm{Re}_{w}^{1.25}(1+K_1)^{1.25}}\right]^{-0.8} \tag{9-2-7}$$

Figure 9.6 presents a comparison between the calculations using (9-2-6) and the data of Nichiwaki, Hirata and Tsuchida [187] and V. P. Komarov [51]; Fig. 9.7 is a comparison with the data of Goldstein et al [144].

For a flow of compressible gas, taking (9-1-15) into account, we have /264

$$\theta_\Sigma=\left\{1+\frac{\beta_{\max}^{1+m}}{(1+K_1)^{m+1}\theta_\Sigma^{1+m}}\frac{B(1+m)\,\mathrm{Re}_{\infty}}{2\mathrm{Pr}^{0.75}\mathrm{Re}_{w}^{m+1}}\times\int_{\bar{x}_1}^{\bar{x}}\Psi_\infty\left(\frac{\mu_w}{\mu_\infty}\right)^m U(1-U^2)^{\frac{1}{K-1}}\theta_\Sigma^{1+m}d\bar{x}\right\}^{-\frac{1}{m+1}} \tag{9-2-8}$$

For the gas flow in a supersonic nozzle

$$\theta_\Sigma=\left\{1+\frac{\beta_{\max}^{1+m}}{\theta_\Sigma^{1+m}(1+K_1)^{m+1}}\frac{B(1+m)}{2\,\mathrm{Pr}^{0.75}}\frac{\mathrm{Re}_{\infty}}{\mathrm{Re}_{w1}^{m+1}D^{m+1}}\times\int_{\bar{x}_1}^{\bar{x}}\Psi_\infty\left(\frac{\mu_w}{\mu_\infty}\right)^m D^{m-1}\theta_\Sigma^{m+1}d\bar{x}\right\}^{-\frac{1}{m+1}} \tag{9-2-9}$$

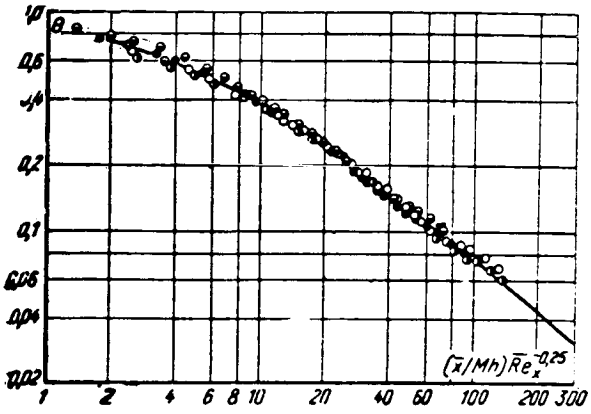

FIG. 9.7. Gas screen effectiveness with a porous section. Curve—calculated from (9-2-7); experimental points—from the paper by Goldstein et al [144].

Equations (9-2-8) and (9-2-9) are solved for θ_z by successive approximations. For a preliminary estimate we can use the formula /265

$$\theta_z \approx \left\{1 + \frac{0,25\,\mathrm{Re}_{00}\Psi_{tool}\left(\frac{\mu_{w1}}{\mu_{00}}\right)^{0,25}\int\limits_{\bar{x}_1}^{\bar{x}}\Psi_M U\,(1-U^2)^{-\frac{1}{K-1}}\,d\bar{x}}{(1+K_1)^{1,25}\,\mathrm{Re}_{w1}^{1,25}}\right\}^{-3,5} \qquad (9\text{-}2\text{-}10)$$

and for the supersonic nozzle

$$\theta_z \approx \left\{1 + \frac{0,25\,\mathrm{Re}_{00}\Psi_{tool}\left(\frac{\mu_{w1}}{\mu_{00}}\right)^{0,25}}{(1+K)^{0,25}\,\mathrm{Re}_{w1}^{1,25}\bar{D}^{1,25}}\int\limits_{\bar{x}_0}^{\bar{x}}\Psi_M\,(\bar{D})^{m-1}\,d\bar{x}\right\}^{-0,8}. \qquad (9\text{-}2\text{-}11)$$

For the flow around a flat plate we have

$$\theta = \left\{1 + \Psi_t\Psi_M\frac{0,25\mathrm{Re}_{\Delta x}}{[(1+K_1)\,\mathrm{Re}_{w1}]^{1,25}}\left(\frac{\mu_{w1}}{\mu_{00}}\right)^{0,25}\right\}^{-0,8}, \qquad (9\text{-}2\text{-}12)$$

where $\mathrm{Re}_{\Delta x} = \frac{\rho_0 w_0 (x - x_1)}{\mu_{00}}$; $\Psi_{t_1} = \left(\frac{2}{\sqrt{\bar{\Psi}_1} + 1}\right)^2$;

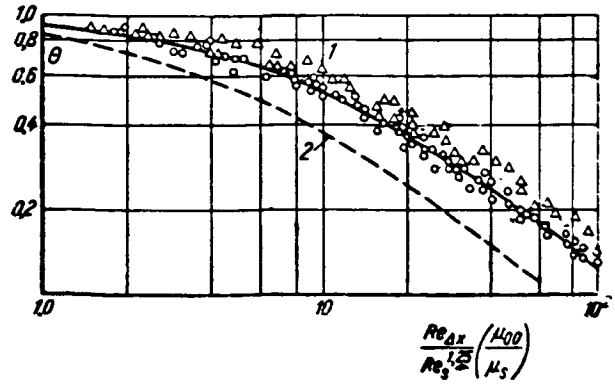

FIG. 9.8. Effectiveness of a gas screen with supersonic flow. 1—Calculated from (9-2-13) for M = 2.9; 2—calculated from (9-2-7) (M → 0); test points from the paper by Goldstein et al [256].

$$\Psi_M = \left[\frac{\operatorname{arctg} M_0 \sqrt{r \frac{k-1}{2}}}{M_0 \sqrt{r \frac{k-1}{2}}} \right]^2.$$

Figure 9.8 gives a comparison between formula (9-2-12) and the data of Goldstein et al [256]. The tests were made with $T_{w1}/T_w^* \approx 1.0$. Then formula (9-2-12) is conveniently written as

$$\theta = \left\{ 1 + 0{,}25 \frac{\Psi_M \mathrm{Re}_{\Delta x}}{[(1+K_1)\,\mathrm{Re}_s]^{1{,}25}} \left(\frac{\mu_{0s}}{\mu_s} \right)^{0{,}25} \right\}^{-0{,}8}, \qquad (9\text{-}2\text{-}13)$$

where $\mathrm{Re}_s = jwx_1/u_s$, u_s is the coefficient of dynamic viscosity of the injected gas at T'.

As is evident from the figure, the experiments and relationship (9-2-13) are in good agreement. It is interesting to note that the screen effectiveness improves considerably with an increase in M-number.

9.3. Gas Screen Created by the Injection of Cooled Gas Through a Slot

The gas is injected through a slot of height s with velocity w_1 at temperature T_1 (Fig. 9.9). The physical properties of the main and injected gases are taken to be alike and constant.

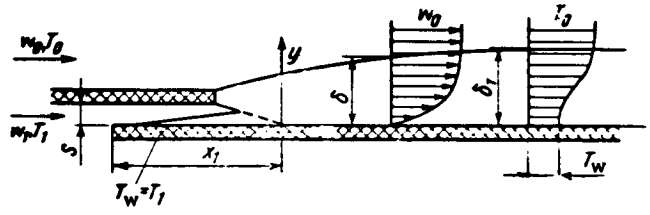

FIG. 9.9. Diagram of a slot gas-screen.

In the section $0 < x < x_1$ the plate is washed only by the injected gas, and the plate temperature is equal to the temperature of the injected gas, i.e. $T_w = T_{w1} = T_2$. Boundary layer heating due to the mixing of the main and injected flows begins to set in with the section $x \approx x_1$.

With $x \to \infty$ the dynamic boundary layer no longer depends on conditions in section x_1, and with n = 1/7

$$\delta^{**}_{x\to\infty} = 0{,}036 x\, \mathrm{Re}_x^{-0{,}2}. \qquad (9\text{-}3\text{-}1)$$

We can write the following balance relationships for the x_1-section:

$$\int_0^h C_p \rho w T dy = C_{p1}\rho_1 w_1 T_1 s + C_{p0}\rho_0 w_0 T_0 (h - s); \qquad (9\text{-}3\text{-}2)$$

$$\int_0^h \rho w\, dy = \rho_1 w_1 s + \rho_0 w_0 (h - s). \tag{9-3-3}$$

For the conditions being considered ($\rho_1 = \rho_0, C_{p1} = C_{p0}$), we have /267

$$\delta^{**}_{T1} = \frac{w_1}{w_0} s. \tag{9-3-4}$$

Substituting (9-3-4) and (9-3-1) into (9-1-10), we obtain

$$\theta_{x\to\infty} \to \frac{27.8}{\beta} \mathrm{Re}_s^{0.2} \left(\frac{w_1 s}{w_0 x}\right)^{0.8}. \tag{9-3-5}$$

where $\mathrm{Re}_s = w_1 s / \nu_s$.

With $\beta_{max} = 9$ we have

$$\theta_{x\to\infty} \to 3.1\, \mathrm{Re}_s^{0.2} \left(\frac{w_1 s}{w_0 x}\right)^{0.8} \tag{9-3-6}$$

For the region $x_1 < x < \infty$ we find:

$$\theta \approx \left[1 + 0{,}25\, \mathrm{Re}_s^{-0.25} \frac{w_0 (x - x_1)}{w_1 s}\right]^{-0.8}. \tag{9-3-7}$$

$\theta = 1$ in the region $0 < x < x_1$.

Using the known relationships for a free turbulent jet [1], to a first approximation we can take, for $w_1 < w_0$

$$\frac{x_1}{s} \approx \left(0.107 + 0.037 \frac{w_1}{w_0}\right)^{-1} \frac{w_0 + w_1}{w_0 - w_1}. \tag{9-3-8}$$

In some instances the section x_1 can be neglected--i.e. we can get $x - x_1 \approx x$, and thereby create some margin for the gas screen effectiveness. Then we obtain a simple computational formula

$$\theta = \left(1 + 0{,}25 \mathrm{Re}_s^{-0.25} \frac{w_0 x}{w_1 s}\right)^{-0.8}. \tag{9-3-9}$$

A comparison of the gas-screen effectiveness computed from (9-3-6) with the tests /268 of Papell and Trout [193], Hartnett, Birkebak and Eckert [152] and Seban [214, 215] is given in Fig. 9.10.

The proposed method can be extended to a flow of compressible gas along a flat wall. In this case $\mathrm{Re}^{**}_{T\infty} = \frac{\rho_0 w_0 s}{\mu_{0\infty}}$ and

$$\theta \approx \left[1 + 0.016 \frac{\Psi_\infty \mathrm{Re}_{\Delta x}}{(\mathrm{Re}^{**}_{T\infty})^{1.25}}\right]^{-0.8}, \tag{9-3-10}$$

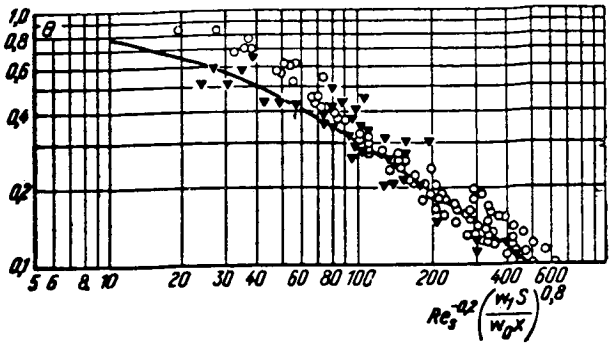

FIG. 9.10. Effectiveness of a slot gas-screen. Curve—computed from (9-3-6); o—tests of Papell and Trout [193]; ▼—tests by Sevan [214, 215].

where Ψ_∞ is found from (4-1-2). For the general case of flow over a curvilinear surface we have

$$\theta \approx \left[1 + \frac{0.016\beta^{1,25}\Psi_{t_1}\left(\frac{\mu_{w1}}{\mu_\infty}\right)^{0,25} \mathrm{Re}_\infty \int_{\bar{x}_1}^{\bar{x}} \Psi_M U (1-U^2)^{\frac{1}{K-1}} d\bar{x}}{(\mathrm{Re}_{\infty\infty})^{1,25}}\right]^{-0,8} \qquad (9\text{-}3\text{-}11)$$

and for the gas flow in a supersonic nozzle:

$$\theta \approx \left[1 + \frac{0.016\beta^{1,25}\Psi_{t_1}\left(\frac{\mu_{w1}}{\mu_\infty}\right)^{0,2} \mathrm{Re}_\infty}{(\mathrm{Re}_{\infty\infty})^{1,25}\bar{D}^{1,25}} \int_{\bar{x}_1}^{\bar{x}} \Psi_M (\bar{D})^{m-1} d\bar{x}\right]^{-0,8} \qquad (9\text{-}3\text{-}12)$$

It should be noted that all formulas obtained for the gas-screen effectiveness can also be extended to the injection of a foreign gas. In this case the gas-screen effectiveness is defined by way of the enthalpy of the gas /269

$$\theta_i = \frac{i_0 - i^*_w}{i_0 - i_{w1}}. \qquad (9\text{-}3\text{-}13)$$

With Sc = 1 similarity should exist between the distributions of enthalpy and total concentration of the injected gas, and hence

$$\theta_i = \frac{i_0 - i^*_w}{i_0 - i_{w1}} = \frac{c_0 - c^*_w}{c_0 - c_{w1}}. \qquad (9\text{-}3\text{-}14)$$

From this

$$c^*_w = c_0 - \theta_i (c_0 - c_{w1}), \qquad (9\text{-}3\text{-}15)$$

where c^*_w is the concentration of the injected component at the thermally-insultated wall; c_{w1} is the concentration of the injected component at the wall in section x_1.

The specific heat of a binary mixture of gases at the wall can be expressed as

$$C^*_{pw} = C_{ps} c^*_w + C_{p0}(1 - c^*_w) = C_{p0} + (C_{ps} - C_{p0}) c^*_w. \qquad (9\text{-}3\text{-}16)$$

From (9-3-13) we have

$$\theta_i = \frac{C_{p0}T_0 - C^*_{pw}T^*_w}{C_{p0}T_0 - C_{pw1}T_{w1}}. \qquad (9\text{-}3\text{-}17)$$

From this, taking (9-3-16) into account, we have

$$\theta_t = \frac{T_0 - T^*_w}{T_0 - T_{w1}} = \frac{\theta_i (C_{p0}T_0 - C_{pw1}T_{w1}) - (C_{pw1} - C_{p0}) T_0 c^*_w}{[C_{p0} + (C_{pw1} - C_{p0}) c^*_w] (T_0 - T_{w1})}. \qquad (9\text{-}3\text{-}18)$$

In the case of injection of a foreign gas through a tangential slot, $c_0 = 0$, $c_{w1} = 1$, $T_{w1} = T_s$, $C_{pw1} = C_{ps}$, and from (9-3-18) we have

$$\theta_t = \frac{\theta_i C_{ps}}{\theta_i (C_{ps} - C_{p0}) + C_{p0}}. \qquad (9\text{-}3\text{-}19)$$

The integral energy relationship (2-4-7) for the region $x > x_1$, where $q_w = 0$, is written as ($q_v = 0$, $j_w = 0$)

$$\frac{d\,(\mathrm{Re}^{**}_{i1}\Delta i)}{dx} = 0. \qquad (9\text{-}3\text{-}20)$$

From this /270

$$\theta_i = \frac{\mathrm{Re}^{**}_{i1}}{\mathrm{Re}^{**}_{i}} = \beta \frac{\mathrm{Re}^{**}_{1}}{\mathrm{Re}^{**}}, \qquad (9\text{-}3\text{-}21)$$

in which case $\theta_i = \frac{i^*_{we} - i^*_w}{i^*_{we} - i_{w1}}$; $\mathrm{Re}^{**} = \frac{\rho_0 w_0 \delta^{**}}{\mu_{we}}$; $\mathrm{Re}^{**}_{i_1} = \frac{\rho_0 w_0 \delta^{**}_{i_1}}{\mu_{we}}$; $\frac{i^*_{we}}{i_0} = 1 + r\frac{k-1}{2}M_0^2$; i^*_w is the enthalpy of the gas at a thermally-insulated wall.

Taking into account Eq. (7-2-15), we obtain a formula for the gas-screen effectiveness in the general case:

$$\theta_i = \left[1 + \frac{B}{2}(1+m)\beta^{m+1}\frac{\mathrm{Re}_L}{(\mathrm{Re}^{**}_{i1})^{m+1}}\int_{\bar{x}_1}^{\bar{x}} \Psi \left(\frac{\mu_w}{\mu_{we}}\right)^{0,25} d\bar{x}\right]^{-0,8}, \qquad (9\text{-}3\text{-}22)$$

where

$$\Psi = \left[\frac{2\,\mathrm{arctg}\, M_0\sqrt{0,5r(k-1)}}{(\sqrt{\bar{\psi}}+1)\,M_0\sqrt{0,5r(k-1)}}\right]^2,$$

in which

$$\bar{\psi} = i_w / i^*_w.$$

The parameter Re^{**}_{i1} is established as a function of the mode of setting up the gas screen:

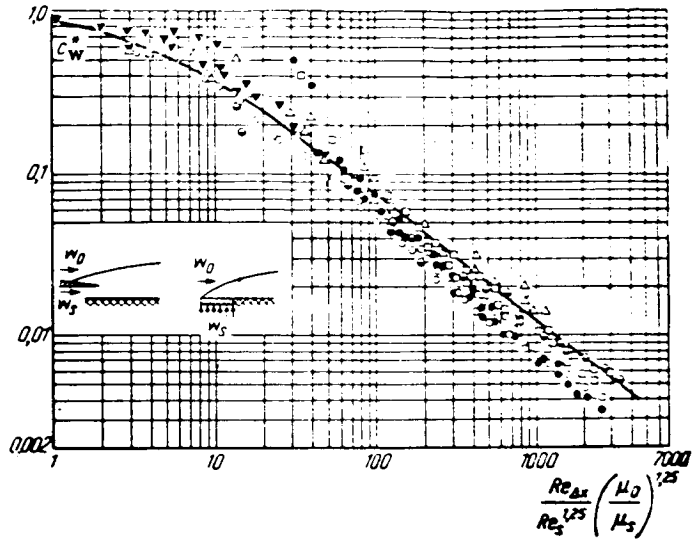

FIG. 9.11. Screen effectiveness with injection of a foreign gas. Curve—computed from formula (9-3-15) with $\Psi = 1$.

Symbol	Injected gas	Reference	Type of screen
●	Helium	[15]	Porous section
□	Helium	[143]	
⊙	Helium	[15]	Slot
△	Helium		
◒	Hydrogen		
▼	Freon-12	[257]	

(a) cooled portion

$$\mathrm{Re}^{**}_{i_1} = \left[\frac{B}{2}(m+1)\,\Psi_1\left(\frac{\mu_{w1}}{\mu_{\infty}}\right)^{0,25}\mathrm{Re}_{x_1}\right]^{0,8}; \tag{9-3-23}$$

(b) porous section

$$\mathrm{Re}^{**}_{i_1} = \mathrm{Re}_{w1}\,(1+K_1); \tag{9-3-24}$$

(c) injection of gas through slot

$$\mathrm{Re}^{**}_{i_1} = \frac{\rho_s w_s s}{\mu_{\infty}}. \tag{9-3-25}$$

For the subsonic gas-flow region, Eq. (9-3-22), for $\beta = 9$, is written as

$$\theta_i = \left[1 + 0{,}25\,\frac{\mathrm{Re}_l}{(\mathrm{Re}^{**}_{i1})^{1,25}}\int_{\bar{x}_0}^{\bar{x}}\Psi\left(\frac{\mu_w}{\mu_e}\right)^{0,25}d\bar{x}\right]^{-0,8}. \tag{9-3-26}$$

An accurate solution of the problem can be had by the method of successive approximations, since the function Ψ depends on Θ_i. In addition, we must obtain an expression for the function Ψ in the presence of a gas-screen, which will be done in Section 9.7. /271

However, for practical calculations we can take, as a first approximation, $\Psi = \Psi_1$, and obtain the limiting value of gas-screen effectiveness under the conditions being considered.

Figure 9.11 presents a comparison between formula (9-3-15) and the test data of E. P. Volchkov and E. I. Sinaiko [15], Goldstein et al [143] and Burus and Stollery [257], in which the concentration of injected gas was changed at the wall with different methods of setting up the gas screen. The curve corresponds to the calculation of Θ_i from Eq. (9-3-26), assuming $\Psi \approx 1$. As can be seen from the diagram, satisfactory agreement exists between computed and experimental data. Better correlation can be attained if the deviation of Ψ from 1 is taken into account in (9-3-26). /272

9.4. Multi-Slot Injection of Cooling Gas

In many cases of practical importance, a mult-gas screen must be used. Possible arrangements of multi-slot- and grating-injection are shown in Fig. 9.12.

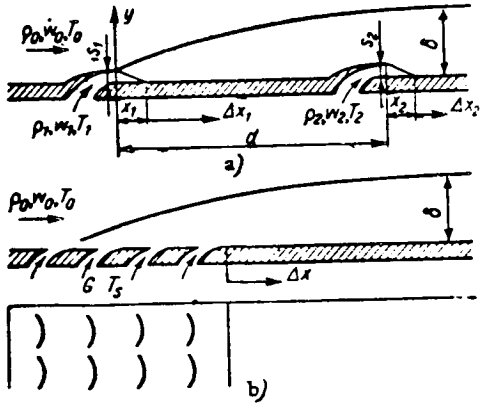

FIG. 9.12. Diagrams of multi-slot (a) and grating (b) cooling.

Consider a uniform turbulent boundary layer of gas with constant physical properties in a given temperature interval. Cooling gas is injected through a series of slots of width S_1, S_2, ... S_n, corresponding to temperatures of T_1, T_2, ..., T_n and velocities w_1, w_2, ..., w_n. Each slot has a zone x_1, x_2, ..., x_n, within which the wall temperature does not change and is equal to the injected gas temperature. Heat is not transferred through the wall, and its temperature is an unknown quantity that varies with the coordinate x. The wall temperature beyond the first slot can be found from (9-3-7). The problem is to find the wall temperature beyond the following slots. /273

The energy-loss thickness in the section of the second slot is:

$$\delta^{**}_{T2} = m_2 S_2 + \frac{T_0 - T^*_{w2}}{T_0 - T_2} (\delta^{**}_T)_2, \qquad (9\text{-}4\text{-}1)$$

where $m_2 = \rho_2 w_2 / \rho_0 w_0$;

$$(\delta^{**}_T)_2 = \int_{S_2}^{\infty} \frac{\rho w}{\rho_0 w_0} \left(\frac{T_0 - T}{T_0 - T^*_{w2}} \right) dy$$

is the energy-loss thickness in the section above the second slot. From the energy equation:

$$\frac{T_0 - T_{w2}}{T_0 - T_1} = \frac{\delta^{**}_{T1}}{(\delta^{**}_T)_2}, \tag{9-4-2}$$

where $\delta_{T1} = m_1 s_1$ is the energy-loss thickness in the section of the first slot.

With (9-4-2), we have from (9-4-1):

$$\delta^{**}_{T2} = m_2 s_2 + \frac{T_0 - T_1}{T_0 - T_2} \delta^{**}_{T1} = m_2 s_2 + \frac{T_0 - T_1}{T_0 - T_2} m_1 s_1. \tag{9-4-3}$$

Hence

$$\delta^{**}_{Tn} = m_n s_n + \frac{T_0 - T_{n-1}}{T_0 - T_n} \delta^{**}_{Tn-1} \tag{9-4-4}$$

or

$$\begin{aligned} \delta^{**}_{Tn} &= m_n s_n + \frac{T_0 - T_{n-1}}{T_0 - T_n} m_{n-1} s_{n-1} \\ &+ \frac{T_0 - T_{n-2}}{T_0 - T_n} m_{n-2} s_{n-2} + \dots + \frac{T_0 - T_1}{T_0 - T_n} m_1 s_1. \end{aligned} \tag{9-4-5}$$

From the integral momentum relationship (for m = 0.25 and B/2 = 0.0128) we have

$$\Delta = \frac{\delta^{**}}{\delta^{**}_1} = [1 + 0{,}016 \chi^{1.25}]^{0.8}, \tag{9-4-6}$$

where $\chi = x / \delta^{**}_1 \, \mathrm{Re}_x^{0.2}$.

A comparison between (9-4-6) and the tests of Hartnett, Eckert and Birkebak [152] and Seban and Back [216] is given in Fig. 9.13.

The momentum-loss thickness in the section above the second slot is /274

$$(\delta^{**}_0)_2 = \left[\delta_1^{**1.25} + 0{,}016 \left(\frac{d}{\mathrm{Re}_d^{0.2}} \right)^{1.25} \right]^{0.8}, \tag{9-4-7}$$

and the total momentum-loss thickness is

$$\delta^{**}_2 = m_2 s_2 \left(1 - \frac{w_2}{w_0} \right) + (\delta^{**}_0)_2. \tag{9-4-8}$$

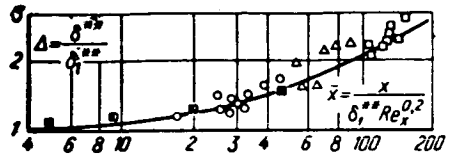

FIG. 9.13. Change in momentum-loss thickness over the length of a plate with multi-slot injection. Curve—calculated from (9-4-6); •—data from Hartnett et al [152]; o. △. □—data from Seban and Back [216].

Hence

$$\delta^{**}_n = m_n s_n\left(1 - \frac{w_n}{w_0}\right) + (\delta^{**}_0)_n. \qquad (9\text{-}4\text{-}9)$$

A first approximate analysis of the effectiveness of thermal shielding can be taken as

$$\delta^{**}_n = m_1 s_1\left(1 - \frac{w_1}{w_0}\right) + m_2 s_2\left(1 - \frac{w_2}{w_0}\right) + \ldots$$
$$\ldots + m_n s_n\left(1 - \frac{w_n}{w_0}\right). \qquad (9\text{-}4\text{-}10)$$

In this case the gas-screen effectiveness with multi-slot injection is calculated from the formula for a single slot. The difference consists only in the determination of the initial parameters of the boundary layer, which are calculated in the cross section of the n-th slot, taking into account the injection of coolant through all preceding slots in accordance with (9-4-4) and (9-4-10).

In particular, for the power-law profile with n = 1/7 we obtain

$$\theta = \left[\left(\frac{\mathrm{Re}^{**}_{Tx}}{\mathrm{Re}_{T\Delta x}}\right)^{0.25}\left(\frac{\mathrm{Re}^{**}_{\Delta x}}{\mathrm{Re}^{**}_{x}}\right)^{0.101} - 1\right]^{0.8}\left(\frac{\mathrm{Re}^{**}_{Tn}}{\mathrm{Re}^{**}_{Tx}}\right)^{0.2}, \qquad (9\text{-}4\text{-}11)$$

where /275

$$\mathrm{Re}^{**}_{Tx} = [\mathrm{Re}^{**1.25}_{Tn} + 0{,}016\,\mathrm{Re}_{\Delta xn}]^{0.8};$$
$$\mathrm{Re}^{**}_{x} = [\mathrm{Re}^{**1.25}_{n} + 0{,}016\,\mathrm{Re}_{\Delta xn}]^{0.8};$$
$$\mathrm{Re}_{T\Delta x} = [0{,}016\,\mathrm{Re}_{\Delta xn}]^{0.8} = \mathrm{Re}^{**}_{\Delta x}.$$

For the case

$$w_0 = w_1 = \ldots = w_n;$$
$$T_0 = T_1 = \ldots = T_n;$$
$$s_1 = s_2 = \ldots = s_n$$

we have

$$\delta^{**}_{Tn} = nms;\ \delta^{**}_n = nms\left(1 - \frac{w_0}{w_0}\right). \qquad (9\text{-}4\text{-}12)$$

Equality (9-4-11) reduces to

$$\theta = \frac{1}{(1 + 0{,}016K)^{0.16}}\left\{(1 + 62{,}5K^{-1})^{0.2}\left[1 + 62{,}5\left(1 - \frac{w_s}{w_0}\right)^{3.25}K^{-1}\right]^{-0.056} - 1\right\}^{0.8}, \qquad (9\text{-}4\text{-}13)$$

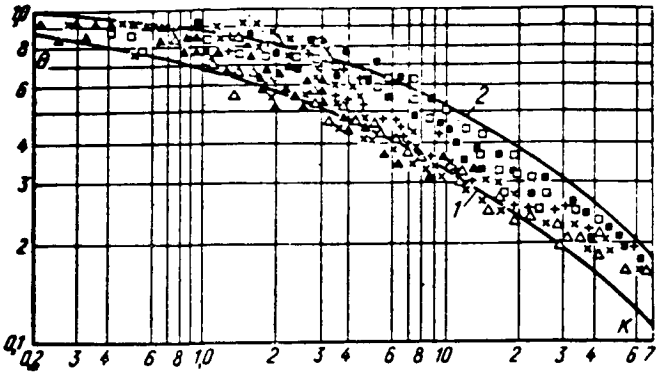

FIG. 9.14. Generalization of test data on the effectiveness of the gas-screen with multi-slot injection. 1—calculated from (9-4-14); 2—computed from (9-4-15); that data points with $0 < w_s/w_0 < 1.33$ from the paper by Chin et al [144]; number of slots: □—1; ○—2, +—3; △—4; ×—5; ▲—6.

where

$$\theta = \frac{T - T^*_{cr}}{T_0 - T_s};$$

$$K = \frac{Re_{\Delta xn}}{Re_{Tn}^{**1.25}} = \frac{Re_{\Delta xn}}{Re_{ns}^{1.25}};$$

$$Re_{ns} = \frac{\rho_0 x_n n S}{\mu_0}.$$

Equation (9-4-13), as shown by E. P. Volchkov [15], can be satisfactorily approximated by the formula

$$\theta = \left[\left(1 + \frac{62.5}{K + 0.143}\right)^{0.125} - 1\right]^{0.8} (1 - 0.016K)^{-0.16} \qquad (9\text{-}4\text{-}14)$$

with $w_s/w_0 \ll 1$ and

$$\theta = \left[\left(1 + \frac{62.5}{K + 2}\right)^{0.2} - 1\right]^{0.8} (1 + 0.016K)^{-0.16} \qquad (9\text{-}4\text{-}15)$$

with $w_s/w_0 \approx 1$.

Figure 9.14 presents a comparison between the experimental data of Chin, Skiwen and Burgraff [114] and the computed results using (9-4-14) and (9-4-15). Those modes were used in the analysis for which the energy-loss thickness due to the injection somewhat exceeded the initial energy-loss thickness due to wall cooling up to the first slot. Reference [114] also contains measurements of the gas-screen effectiveness with the injection of a coolant through a grid-like panel (see Fig. 9.15). /276

Under these conditions the parameter K is found from the formula /277

$$K^* = \left(\frac{\mu_0}{G}\right)^{1.25} Re_{\Delta x}, \qquad (9\text{-}4\text{-}16)$$

where G is the flow-rate of coolant per unit width of surface.

As can be seen from Fig. 9.16, the calculated curves encompass the entire range of experimental points, even in such a complex situation.

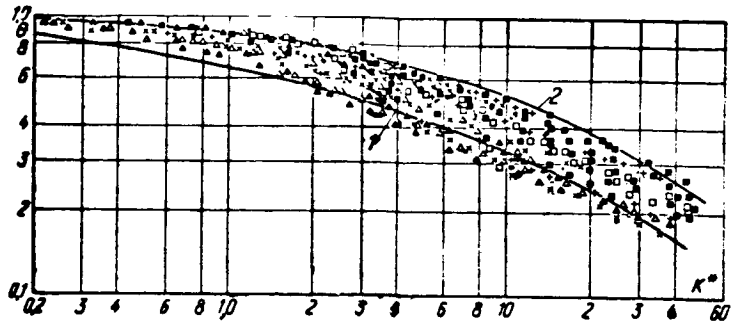

FIG. 9.15. Effectiveness of gas-screen with the injection of a coolant through a tangential grid. 1—calculated from (9-4-14); 2—calculated from (9-4-15); Points- test data from Chin et al [114]; number of rows of slots: □ —2; • —4; + —6; △—8; × —10; ▲—20.

9.5. Effectiveness of Gas-Screen at a Rough Wall

In a paper by E. P. Volchkov and V. Ya. Levchenko [12] it was shown that the proposed method of calculating the gas screen can be successfully extended to a rough surface. In this case, formula (9-3-9) is written as

$$\theta = \left[1 + 0{,}25A\frac{\mathrm{Re}_{\Delta x}}{\mathrm{Re}_{s}^{1.25}}\right]^{-0{,}8}; \qquad (9\text{-}5\text{-}1)$$

$$A = 1 + \frac{4\Delta x\Delta}{(1+m^2)(\Delta x + 2\Delta)^2}, \qquad (9\text{-}5\text{-}2)$$

where Δ is the roughness height.

Figure 9.16 presents a comparison between the test data of E. P. Volchkov and V. Ya. Levchenko [12] and formula (9-5-1). The tests were made on a tubular surface in the range $0.23 < m < 1.0$ and various slot heights ($2 < s < 13$ mm).

In the case of a fine-grain surface, for the region in which the coefficient of friction can be assumed to be constant, we have

$$\delta^{**} = \left(\frac{C_{f\text{т}}}{2}\right)x. \qquad (9\text{-}5\text{-}3)$$

Substituting (9-5-3) into (9-1-4), we obtain

$$\theta \sim \left[1 + 4{,}5C_{\text{г}}\left(\frac{x}{ms}\right)\right]^{-1}. \qquad (9\text{-}5\text{-}4)$$

Strictly speaking, the coefficient of friction on a rough plate varies over the length, since the boundary layer thickness changes. If we use Schlichting's formula /278

$$C_{\text{г}} = \left[2{,}87 + 1{,}58\lg\left(\frac{x}{\Delta}\right)\right]^{-2{,}5}, \qquad (9\text{-}5\text{-}5)$$

we find

$$\delta^{**} = \int_0^x 0{,}5\left[2{,}87 + 1{,}58\lg\left(\frac{x}{\Delta}\right)\right]^{-2{,}5} dx. \qquad (9\text{-}5\text{-}6)$$

Hence

$$\theta = \frac{mS}{4{,}5\int_0^x \left[2.87 + 1.58\lg\left(\frac{x}{\Delta}\right)\right]^{-2{,}5} dx}. \qquad (9\text{-}5\text{-}7)$$

Comparison of formulas (9-3-10) and (9-5-7) shows that the effectiveness of the gas screen is less on a rough surface than on a smooth wall.

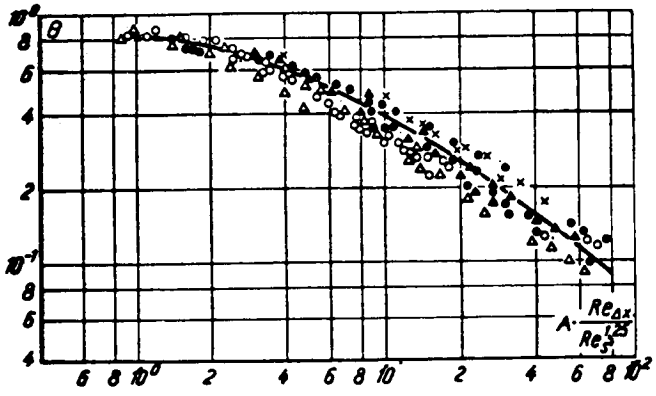

FIG. 9.16. Gas screen effectiveness at a rough surface. Curve—calculated from (9-5-1): Points—tests of E. P. Volchkov and V. Ya. Levchenko [12]; height of roughness in all tests Δ = 13 mm; height of slot, mm: o—13, Δ—10, ▲—6.5, ●—3.5, ×—2.

9.6. Convective Heat Transfer with a Gas Screen

Usually the gas screen is used in conjunction with surface cooling and one must be able to determine the local coefficients of heat transfer for these conditions. The integral energy relationship for the region $x > x_1$ can be written as

/279

$$\frac{d}{dx}\left[(T_w - T^*_w)\,\delta^*_T + (T^*_w - T_0)\,\delta^{**}_{T1}\right] = \frac{q_w}{\rho C_{p0} w_0}, \qquad (9\text{-}6\text{-}1)$$

where

$$\delta^{**}_T = \int_0^\delta \frac{\rho w}{\rho_0 w_0}\left(\frac{T - T'}{T_w - T^*_w}\right) dy;$$

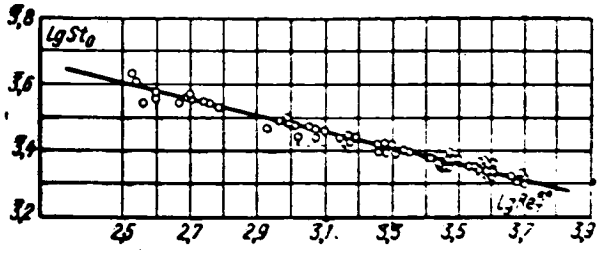

FIG. 9.17. Law of heat transfer in the presence of a gas screen. Line—calculated from (9-6-6); Points—tests of V. P. Komarov [51] with Re_T and St_0 established from (9-6-2) and (9-6-5).

$$\delta^{**}_{T1} = \int_0^{\delta} \frac{\rho w}{\rho_0 w_0} \left(\frac{T' - T_0}{T^*_w - T_0} \right) dy. \tag{9-6-2}$$

Here T' is the temperature at a given point at the boundary layer at the thermally-insulated surface; T_w is the temperature of the surface.

In accordance with Eq. (9-1-2)

$$\frac{d}{dx}[(T^*_w - T_0)\delta^{**}_{T1}] = 0. \tag{9-6-3}$$

Hence

$$\frac{dRe^{**}_T}{d\bar{x}} + \frac{Re^{**}_T}{\Delta T^*} \frac{d(\Delta T^*)}{d\bar{x}} = Re_L St_0. \tag{9-6-4}$$

where

$$St_0 = \frac{q_{ст}}{gC_{p0}\rho_0 w_0 \Delta T^*}; \quad \Delta T^* = T_w - T^*_w. \tag{9-6-5}$$

Thus the integral energy relations for the heat-transfer surface, with a gas screen, keeps its usual form if $\Delta T^* = T_w - T^*_w$ is substituted in place of ΔT.

We assume that the law of heat transfer in the form (2-6-4) is also valid for the conditions being considered, if δ^{**}_T is defined by (9-6-2) and St_0 by (9-6-5), i.e. /280

$$St_0 = \frac{B}{2} Re_T^{**-m} Pr^{-n}. \tag{9-6-6}$$

Figure 9.17 shows a comparison of (9-6-6) with the test data of V. P. Komarov [51].

Figure 9.18 gives the distribution of temperature over the boundary layer cross section at a plate, with a step input of heat, as obtained by E. P. Volchkov [15]. The ratio of the heat fluxes at the first and second steps came to $0.3 \leq q_{w1}/q_{w2} \leq 7.0$. As can be seen from the diagram, the temperature profile in coordinates $\frac{T - T'}{T_w - T^*_w} = f\left(\frac{y}{\delta^{**}_T}\right)$ is in agreement with the usual power-law relationship. /281

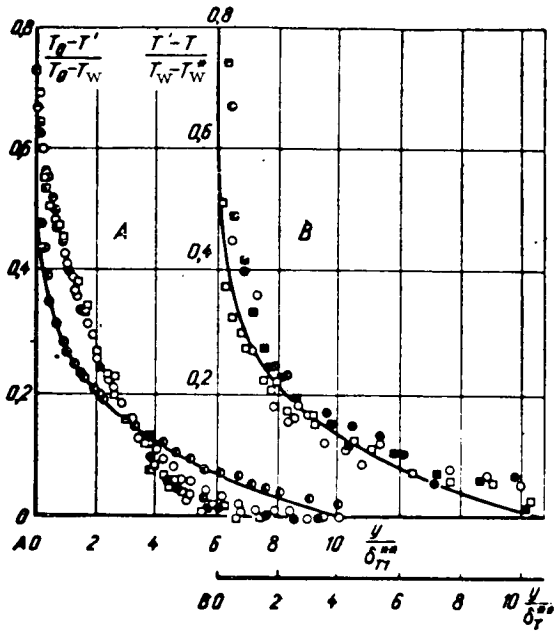

FIG. 9.18. Distribution of temperature over the cross section of the turbulent boundary layer with a step supply of heat.

—— power-law $\frac{T_0-T}{T_0-T_w}=1-0{,}715(y/\delta^{**}_T)^{1/7}$; A—treatment in variables $\frac{T_0-T'}{T_0-T_w}=f(y/\delta^{**}_T)$;

B—treatment in variables $\frac{T'-T}{T^*_w-T_w}=f(y/\delta^{**}_T)$;

Points—test date of E. P. Volchkov [15].

Symbols	◐	○	●	■	□
	q_w = const	$q_{w1}/q_{w2}=6$			
x/x_0		0,1	0,23	0,57	0,77

Figure 9.19 shows a comparison of the results of calculation using (9-6-6) with the tests of E. P. Volchkov [15]. In Fig. 9.19a the test data were generalized in the usual way, and here, with $q_{w1}/q_{w2}>1$ the test points deviated considerably from the calculations made with (9-6-6). On introducing the equilibrium wall temperature, all of the test points fit relationship (9-6-6) (see Fig. 9.18b). /282

Figure 9.20 illustrates the test data of E. P. Volchkov and V. Ya. Levchenko [12] on heat-transfer at a rough surface with a gas screen, as processed similarly. As can be seen, the introduction of the "equilibrium" temperature allows generalizing the heat-transfer data at a rough surface as well. It should be noted that without a gas screen, at this same surface, the authors obtained the formula

$$Nu_x=2{,}6\cdot 10^{-3}Re_x, \qquad (9\text{-}6\text{-}7)$$

which is correct beginning with $x/\Delta>6$.

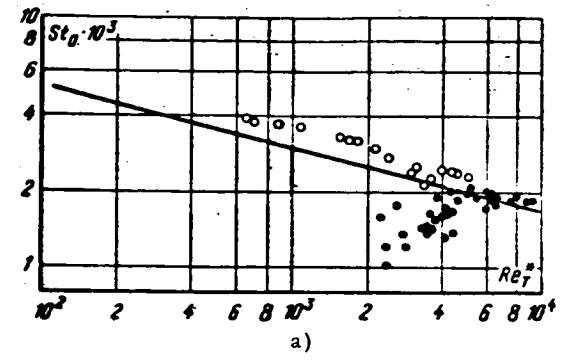

a)

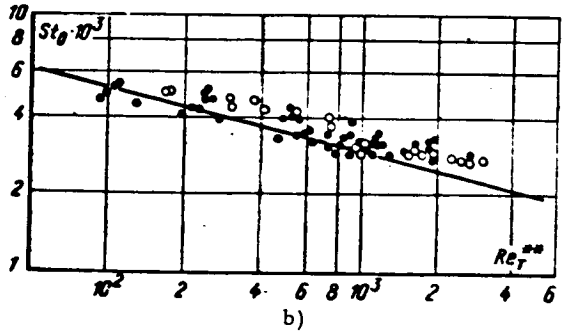

b)

FIG. 9.19. Law of heat transfer with a step input of heat. Straight line—calculated from (9-6-6); points— tests of E. P. Volchkov [15]; o—$0.3 < q_{w1}/q_{w2} < 1$; ●—$3.1 < q_{w1}/q_{w2} < 6.7$; a—computed with $\Delta T = T_w T_0$ and δ^{**}_T according to (2-4-3); b—computed with $\Delta T = T_w - T_w$ and δ^{**}_T according to (9-6-2).

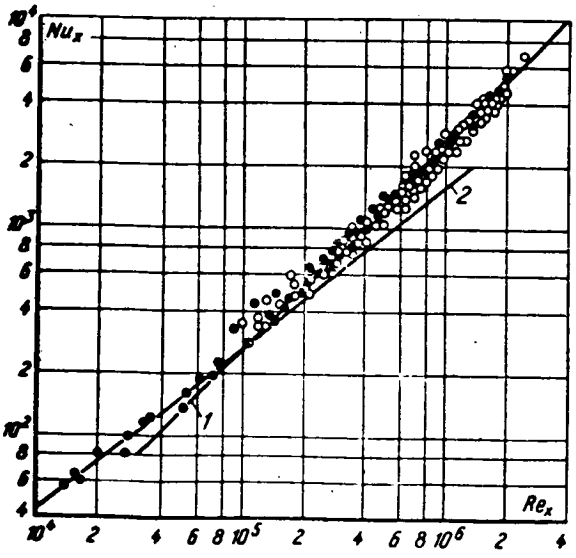

FIG. 9.20. Heat transfer at a rough surface with a gas screen. 1—calculated from $Nu_x = 2.6 \times 10^{-3} Re_x^{0.8}$; Points—data from E. P. Volchkov and V. Ya. Levchenko [12]; ●—without screen; o—with screen ($w_s/w_0 < 1$).

The integral of the energy Eq. (9-6-4), with (9-6-6) taken into account, has the form /283

$$\mathrm{Re}^{**}_T = \frac{1}{\left[\theta - \frac{T_e - T_w}{T_e - T_{w1}}\right]} \left\{ \frac{(m+1)B}{2\mathrm{Pr}^{0.75}} \right. \times \mathrm{Re}_L \int_{\bar{x}_1}^{\bar{x}} \left[\theta - \frac{T_e - T_w}{T_e - T_{w1}}\right]^{m+1} d\bar{x} + (\mathrm{Re}^{**}_T)^{m+1}_{\bar{x}=\bar{x}_1} \left. \right\}^{\frac{1}{m+1}}. \quad (9\text{-}6\text{-}8)$$

Taking into account Eqs. (9-1-14), (9-2-7), (9-2-10), we find Re^{**}_T from (9-6-8) and the local values of St from (9-6-6).

9.7. Effectiveness of the Gas Screen and Heat Transfer on Chemically Reacting Surfaces with Tangential Injection of an Inert Gas into the Boundary Layer

As has been shown in Chapter 8 in the calculations of heat- and mass-transfer processes on chemically reacting surfaces, the non-isothermicity exerts a substantial effect on the coefficients of friction, heat- and mass transfer. It was demonstrated in Section 9.6 that the power-law profile of the dimensionless temperatures is preserved with the introduction of the equilibrium temperature under quasi-isothermal conditions. It may be assumed that the relationship

$$1-\vartheta \approx \frac{i-i'}{i^*_w-i_w}, \tag{9-7-1}$$

will continue to hold under even substantially non-isothermal conditions. Here i is the total enthalpy of the gas at a given point, i' is the total enthalpy of the gas at the given point with the development of a gas screen around the thermally-insulated wall ($q_w = 0$).

With barrier cooling of the wall, when $\partial i/\partial y)_w = 0$, a most intense turbulent mixing takes place in the near-wall region, where the velocity derivative is maximum. Therefore enthalpy profile distortions take place in such a way that the region in which $(\partial i/\partial y) = 0$ grows as the boundary layer develops.

Thus as $x \to \infty$, $i' \to i^*_{cT}$ and in this region equation (9-7-1) takes the form /284

$$\vartheta = \frac{i-i_w}{i^*_w-i_w} = \omega. \tag{9-7-2}$$

With this relationship, the expression for $q_{\Sigma T}$ from (2-1-12) reduces to the usual form

$$\int_0^1 \sqrt{\frac{\tilde{\rho}}{\Psi}\frac{\tilde{q}_0}{\tilde{q}}}\,d\vartheta = -\int_0^1 \sqrt{\frac{\mathrm{St}_0\tilde{q}_0}{\beta_T}}\frac{d\xi}{l}. \tag{9-7-3}$$

It should be remembered that the Stanton number appearing in Ψ is defined as

$$\mathrm{St} = \frac{q_{cT}}{\rho_0 w_0 (i^*_w - i_w)},$$

where i^*_w is the enthalpy of the gas or a thermally-insulated wall with a screen present.

As $Re \to \infty$, $\beta_T \to 1$ and we have

$$\int_0^1 \sqrt{\frac{\tilde{\rho}}{\Psi}\frac{\tilde{q}_0}{\tilde{q}}}\,d\vartheta = \int_0^1 \sqrt{\mathrm{St}_0\tilde{q}_0}\frac{d\xi}{l_0} = Z. \tag{9-7-4}$$

The right-hand side describes the "standard" boundary layer and represents a constant Z, independent of perturbing factors. For "standard" conditions $\Psi = 1$, $\tilde{q} = \tilde{q}_0$, $\tilde{\rho} = 1$ and Z = 1.

Thus the limiting law of heat transfer for the non-isothermal boundary layer of a compressible gas, with a gas screen, on a permeable surface, has the form

$$\Psi_{Re_l^{**} \to \infty} = \left(\int_0^1 \sqrt{\frac{\tilde{q}_0}{\tilde{q}} \frac{\rho}{\rho_0}} \, d\vartheta \right)^2. \qquad (9\text{-}7\text{-}5)$$

The approximation of the heat flux profile over the boundary layer cross section, with a gas screen on the permeable surface is retained in the form

$$\frac{\tilde{q}}{\tilde{q}_0} = 1 + b^*_1 \vartheta, \qquad (9\text{-}7\text{-}6)$$

where $b_1^* = j_w/\rho_0 wSt$ is the wall permeability parameter in the presence of a gas screen; here j_w is the transverse flux of matter at the wall. The gas density is related to the parameter ϑ by the known relationship (for M < 1) /285

$$\frac{\rho}{\rho_0} = \frac{M^*_w}{M_0} \frac{T_0}{T^*_w} \frac{[\psi_2 + (1 - \psi_2)\vartheta]}{[\psi_1 + (1 - \psi_1)\vartheta][\psi_3 + (1 - \psi_3)\vartheta]}, \qquad (9\text{-}7\text{-}7)$$

where

$$\psi_1 = \frac{i_w}{i^*_w}; \quad \psi_2 = \frac{C_{pw}}{C^*_{pw}}; \quad \psi_3 = \frac{M^*_w}{M_w}.$$

For gases of like valency

$$\frac{\rho}{\rho_0} = \frac{M^*_w}{M_0} \frac{T_0}{T^*_w} \frac{1}{\psi_1 + (1 - \psi_1)\vartheta}. \qquad (9\text{-}7\text{-}8)$$

Here M_w^* and T_w^* are the molecular weight and the temperature of the gas mixture at the wall in the absence of heat- and mass-transfer ($q_w = 0$ and $j_w = 0$).

Substituting (9-7-6) and (9-7-8) into Eq. (9-7-5), we obtain the limiting laws of heat transfer for a reacting wall in the presence of a gas screen:

(a) With $\psi_1 < 1$

$$\Psi = \frac{M^*_w}{M_0} \frac{T_0}{T^*_w} \frac{4}{b_1 (1 - \psi_1)} \left[\ln \frac{\sqrt{(1 - \psi_1)(1 + b^*_1)} + \sqrt{b^*_1}}{\sqrt{1 - \psi_1} + \sqrt{b_1 \psi_1}} \right]^2; \qquad (9\text{-}7\text{-}9)$$

$$b_{crit} = \frac{M^*_w}{M_0} \frac{T_0}{T^*_w} \frac{1}{1 - \psi_1} \left[\ln \frac{1 + \sqrt{1 - \psi_1}}{1 - \sqrt{1 - \psi_1}} \right]^2; \qquad (9\text{-}7\text{-}10)$$

(b) With $\psi_1 > 1$

$$\Psi = \frac{M^*_W}{M_0}\frac{T_0}{T^*_W}\frac{4}{b_1(\psi_1-1)} \times\left[\operatorname{arctg}\sqrt{\frac{(\psi_1-1)(1+b^*_1)}{b^*_1}} - \operatorname{arctg}\sqrt{\frac{\psi_1-1}{b^*_1\psi_1}}\right]^2; \tag{9-7-11}$$

$$b_{crit} = \frac{M^*_W}{M_0}\frac{T_0}{T^*_W}\frac{1}{\psi_1-1}\left(\arccos\frac{2-\psi_1}{\psi_1}\right)^2. \tag{9-7-12}$$

For an impermeable wall:

$$\Psi_t = \frac{M^*_W}{M_0}\frac{T_0}{T^*_W}\left(\frac{2}{\sqrt{\psi_1}+1}\right)^2. \tag{9-7-13}$$

Thus the limiting laws (9-7-9)–(9-7-13) differ from those obtained earlier by the presence of a factor $(M^*_W/M_0)(T_0/T^*_W)$ which also accounts for the effect of the gas screen on the relative laws of heat- and mass transfer and on the boundary layer displacement parameters. The values of the parameters ψ_1, M^*_W/M_0 and T_0/T^*_W are found from the formula derived earlier /286

$$\theta_i = \left[1 + 0{,}25\frac{Re_{\Delta x}}{Re_x^{1,25}}\left(\frac{\mu_0}{\rho_0}\right)^{1,25}\right]^{-0,8}, \tag{9-7-14}$$

where

$$\theta_i = \frac{i_0 - i^*_W}{i_0 - i_0} = \frac{(\tilde{c}_i)_0 - (\tilde{c}_i)^*_{cr}}{(\tilde{c}_i)_0 - (\tilde{c}_i)_0}.$$

With injection of an inert gas through a slot

$$(\tilde{c}_0)^*_W = (\tilde{c}_0)_0(1-\theta_i). \tag{9-7-15}$$

The integral diffusion relationship at a reacting wall, with a gas screen, can be written in analogy with the energy equation in the following form

$$\frac{d(Re^{**}_D\Delta\tilde{c})}{\Delta\tilde{c}d\bar{x}} - \frac{j_W}{\gamma_0 w_0}Re_L = St_D Re_L, \tag{9-7-16}$$

where

$$Re^{**}_D = \frac{\rho_0 w_0 \delta^{**}_D}{\mu_0};$$

$$\delta^{**}_D = \int_0^\delta \frac{\rho w}{\rho_0 w_0}\left[\frac{(\tilde{c}_i)-(\tilde{c}_i)^*}{(\tilde{c}_i)_{cr}-(\tilde{c}_i)^*_W}\right]dy;$$

$$\Delta\tilde{c} = (\tilde{c}_i)_W - (\tilde{c}_i)^*_W;$$

$$\bar{x} = x/L;$$

$$Re_L = \frac{\rho_0 w_0 L}{\mu_0}.$$

Here $\tilde{c}^*_i$ is the concentration of the i-th component at a given point in the boundary layer at a non-reacting wall.

Taking the diffusion equation into account as written for the wall conditions

$$j_{iw} = j_w (\tilde{c}_i)_w - \rho D \left(\frac{\partial \tilde{c}_i}{\partial y}\right)_w. \qquad (9\text{-}7\text{-}17)$$

we obtain

$$St_D = \frac{j_w \left[\frac{j_{iw}}{j_w} - \tilde{c}_{iw}\right]}{\rho_e w_e [\tilde{c}_{iw} - \tilde{c}^*_{iw}]}. \qquad (9\text{-}7\text{-}18)$$

We introduce the diffusion parameter of the permeability /287

$$b^*_i = \frac{j_w}{\gamma_e w_e St_D} = \frac{\tilde{c}_{iw} - \tilde{c}_{iw}}{\frac{j_{iw}}{j_w} - \tilde{c}_{iw}}. \qquad (9\text{-}7\text{-}19)$$

Let us consider the burning of a graphite surface, and, by determining b_1^* in terms of the concentration of carbon $(\tilde{c}_i)^*_w = 0$, $j_{iw} = j_w$, we find

$$b^*_1 = \frac{(\tilde{c}_C)_w}{1 - (\tilde{c}_C)_w} \text{ or } (\tilde{c}_C)_w = \frac{b^*_1}{1 + b^*_1}. \qquad (9\text{-}7\text{-}20)$$

We establish b_1^* through the oxygen concentration $j_{iw} = 0$ and obtain

$$b^*_1 = \frac{(\tilde{c}_e)^*_w}{(\tilde{c}_e)_w} - 1. \qquad (9\text{-}7\text{-}21)$$

For the diffusion combustion region, where the reaction C + O → CO takes place, we have

$$(\tilde{c}_C)_w = \frac{12}{28} (\tilde{c}_{CO})_w; \; (\tilde{c}_O)_w = \frac{16}{28} (\tilde{c}_{CO})_w; \qquad (9\text{-}7\text{-}22)$$

Here $(\tilde{c}_{CO})_w$ is the concentration of CO at the wall.

From Eqs. (9-7-20), (9-7-22), taking (9-7-15) into account, we find the permeability parameter at the burning graphite surface in the presence of an inert gas screen:

$$b^*_1 = \frac{(\tilde{c}_C)_w}{(\tilde{c}_O)_w} (\tilde{c}_O)^*_w = \frac{3}{4} (\tilde{c}_O)_e (1 - \theta_i). \qquad (9\text{-}7\text{-}23)$$

The integral equation of diffusion is conveniently written as

$$\frac{d\mathrm{Re}^{**}_D}{d\bar{x}} + \frac{\mathrm{Re}^{**}_D}{\Delta\bar{c}} \frac{d(\Delta\bar{c})}{d\bar{x}} = St_e \Psi (1 + b^*_1) \mathrm{Re}_L. \qquad (9\text{-}7\text{-}24)$$

In analogy with heat-transfer we find the law of mass transfer as

$$St_e = \frac{B}{2} \mathrm{Re}^{**-m}_D \mathrm{Sc}^{-n} \left(\frac{\mu_w}{\mu_e}\right)^m. \qquad (9\text{-}7\text{-}25)$$

We integrate and find /288

$$\mathrm{Re}^{**}_D = \frac{1}{\Delta\tilde{c}}\left[\frac{B(m+1)}{2\mathrm{Sc}^n}\int_0^x \mathrm{Re}_L\left(\frac{\mu_w}{\mu_e}\right)^m \times \Psi(1+b^*_1)\Delta\tilde{c}^{m+1}dx\right]^{\frac{1}{m+1}}. \tag{9-7-26}$$

The intensity of burning of the graphite surface is defined by the formula

$$j_C = b^*_1 \Psi \frac{B}{2}\mathrm{Re}_D^{**-m}\mathrm{Sc}^{-n}\left(\frac{\mu_w}{\mu_e}\right)^m \gamma_e w_e, \tag{9-7-27}$$

where Ψ is found from (9-7-11).

In the experimental determination of the law of mass transfer the local values of Re^{**}_D are found, in analogy with the thermal layer, from the formula

$$\mathrm{Re}^{**}_D = \frac{(1+b^*_1)\int_0^x j_C\,dx}{\mu_e b^*_1}, \tag{9-7-28}$$

and the Stanton number from

$$\mathrm{St}_D = \frac{j_C}{\gamma_e w_e b^*_1}. \tag{9-7-29}$$

If the change in gas parameters over the length is ignored in Eq. (9-7-26), formula (9-7-27) reduces to

$$\frac{j_C}{\gamma_e w_e} = b^*_1 \mathrm{St} = b^*_1 \cdot 0{,}029\mathrm{Re}_x^{-0.2}\mathrm{Sc}^{-0.6}\Psi^{0.8}\left(\frac{\mu_w}{\mu_e}\right)^{0.2}. \tag{9-7-30}$$

Figure 9.21 shows a comparison of the experimental data of E. P. Volchkov and E. I. Sinaiko [16] on the burning of a graphite surface in an air flow; without screen and with a nitrogen screen, with the computed results using (9-7-30). The agreement of the proposal method of computation with the test data is quite good. As can be seen from the curves, the combustion intensity is considerably reduced with the presence of a screen.

Figure 9.22 shows the generalized test data [16] on the intensity of burning of a graphite surface without a screen and with nitrogen and argon injections. The data were developed in the form of the law of mass transfer, taking into account (9-7-28) and (9-7-29). The computational relationships were set up from the formula /289

$$\mathrm{St}_D = 0{,}0128\,\mathrm{Re}_D^{**-0.25}\mathrm{Sc}^{-0.75}\Psi\left(\frac{\mu_w}{\mu_e}\right)^{0.25} \tag{9-7-31}$$

for $\psi_1 = 7$, 0 and 1.

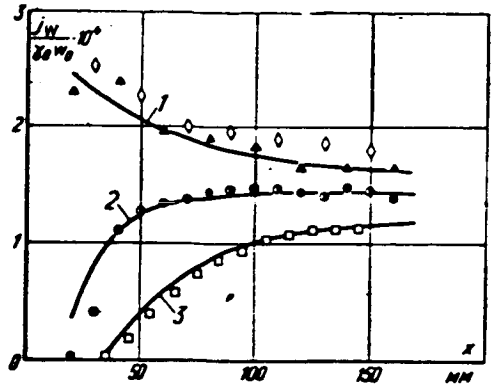

FIG. 9.21. Burning of a graphite duct in an air flow with a nitrogen screen. Curves computed from (9-7-30): 1—for $\psi_1 = 7$; 2—for $\psi_1 = 9$; 3- for $\psi_1 = 10$. Points from the tests of E. P. Volchkov et al [16].

Symbols	Type of graphite	$\rho_0 w_0$, kg/(m^2.sec)	$\rho_e w_e$, kg/m^2.sec	t_w, °C
◇	PPG	168	0	1 620
▲	V-1	156	0	1 600
●	PROG-2400	150	50	1 620
◑	PPG	150	47,1	1 650
□	PPG	150	80,6	1 600

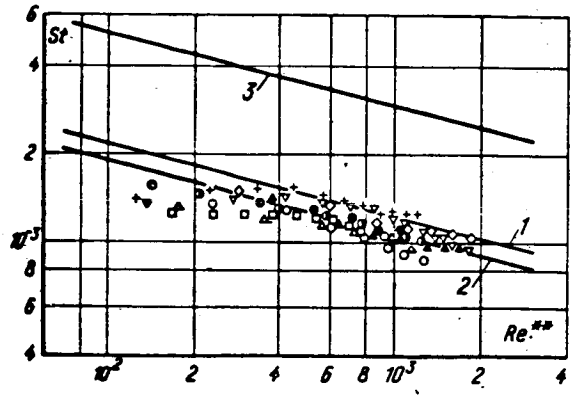

FIG. 9.22. Generalized test data on the burning of a graphite duct with nitrogen and argon screens. Straight line—calculated from (9-7-31): 1—$\psi_1 = 7$; 2—$\psi_1 = 9$; 3—$\psi_1 = 1$: Points—test data of E. P. Volchkov et al [16].

Gas	Nitrogen						Argon		
Symbols	◇	▲	●	◑	□	○	△	▽	+
$\rho_0 w_0$	168	156	150	150	150	210	215	230	175
$\rho_e w_e$	0	0	50	47,1	80,6	59	123	103,8	109,5
T_w°K	1 893	1 873	1 893	1 923	1 873	1 873	1 873	1 795	1 821

As can be seen from Fig. 9.22, the calculations and the test data agree satisfactorily. For the conditions being considered, the non-isothermicity reduces the intensity of mass-transfer by a factor of about 3.

Figure 9.23 represents the test results [16] on the burning of graphite in a flow of air with the injection of helium.

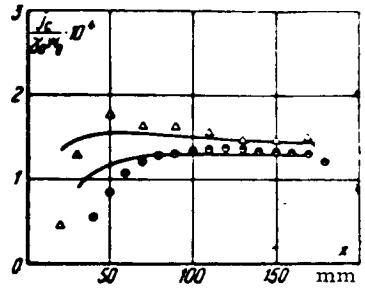

FIG. 9.23. Burning of a graphite duct with a helium screen. Curves—calculated from (9-7-30): Points—tests of E. P. Volchkov et al [16].

Symbols	j_w, kg/(m^2·sec)	j_w, kg/(m^2·sec	T_w, °K
△	143	5,85	1 940
◓	158	11,5	1 950

As the calculations show, under the conditions of the tests by E. P. Volchkov and E. I. Sinaiko the maximum effect of a transverse flow of matter on the law of mass-transfer did not exceed 10%—i.e. within the limits of experimental accuracy. On the other hand, the effect of the non-isothermicity, as already noted, was two orders larger. Taking this circumstance into account we can ignore the effect of a transverse flow of matter on the law of mass transfer, and then $\Psi = \Psi_t = St_D/St_{D0}$. /290

Figure 9.24 shows all of the test data of reference [16] represented as the function

$$\Psi_t = f\left[\sqrt{\frac{M_e}{M^*_w}\frac{T^*_w}{T_e}}\left(\sqrt{\frac{i_w}{i^*_w}}+1\right)\right]. \qquad (9\text{-}7\text{-}32)$$

Here also are presented the test data from the paper by Perkins and Worsoe-Schmidt [194], reworked using the formulas of Chapter 8. As can be seen from the plot, the experimental values and those obtained using the proposed method are in satisfactory agreement.

There is no difficulty in principle in extending the proposed method to a flow of compressible dissociated gas, to the axisymmetric boundary layer, to the internal problem, etc. With the presence of a flame front in the boundary layer, the relative laws of heat- and mass transfer are derived using the formulas of Chapter 4. /292

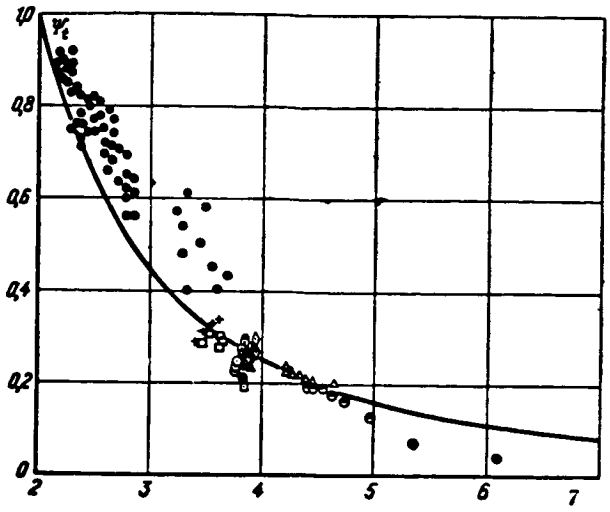

FIG. 9.24. Generalized test data on the burning of a graphite duct with a screen of different gases. The quantity

$$\sqrt{\frac{T^*_w}{T_0}}\ \sqrt{\frac{M_0}{M^*_w}}\ \sqrt{\frac{i_w}{i^*_w}}+1$$

is plotted on the abscissa. Curve—computed from (9-7-13): ●—tests made by Perkins and Worsoe-Schmidt [144]; +, □, ⊙, △, ◓—tests by E. P. Volchkov et al [16].

9.8. Turbulent Wall Jet with $w_s/w_0 \gg 1$

In the preceding sections we have considered the characteristics of a wall jet, essentially with $w_s/w_0 \ll 1$. The effectiveness of a turbulent jet propagating over a flat wall with a stationary ambient gas is a matter of practical interest. A diagram of this problem is shown in Fig. 9.25.

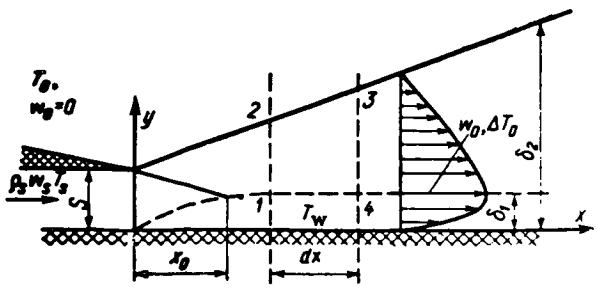

FIG. 9.25. Diagram of a turbulent wall jet.

For a jet element of length dx and thickness δ_2, the momentum equation is

$$\frac{d}{dx}\int_0^{\delta_2}\rho w^2\,dy = -\tau_w \qquad (9\text{-}8\text{-}1)$$

or

$$\frac{d}{dx}\int_0^{\delta_1}\rho w^2\,dy+\frac{d}{dx}\int_{\delta_1}^{\delta_2}\rho w^2\,dy=-\tau_w. \qquad (9\text{-}8\text{-}2)$$

Assuming that the frictional forces at the outer edge of the wall boundary layer are equal to zero (with $y=\delta_1$, $\partial w/\partial x=0$ and $\tau=0$), we can write for the contour 1-2-3-4: /293

$$\frac{d}{dx}\int_{\delta_1}^{\delta_2}\rho w^2\,dy+w_0\frac{d}{dx}\int_0^{\delta_1}\rho w\,dy=0. \qquad (9\text{-}8\text{-}3)$$

Here w_0 is the velocity at the outer edge of the wall boundary layer (with $y=\delta_1$).

Hence, taking (9-8-3) into account, Eq. (9-8-2) takes the form

$$w_0\frac{d}{dx}\int_0^{\delta_1}\rho w\,dy-\frac{d}{dx}\int_0^{\delta_2}\rho w^2\,dy=\tau_w. \qquad (9\text{-}8\text{-}4)$$

We introduce the characteristic thicknesses for the wall boundary layer

$$\delta^*=\int_0^{\delta_1}\left(1-\frac{\rho w}{\rho_0 w_0}\right)dy$$ — displacement thickness;

$$\delta^{**}=\int_0^{\delta_2}\frac{\rho w}{\rho_0 w_0}\left(1-\frac{w}{w_0}\right)dy$$ — momentum loss thickness.

Then Eq. (9-8-4) reduces to

$$\frac{d}{dx}(\rho_0 w_0^2\delta^{**})+\rho_0 w_0(\delta^*-\delta_1)\frac{dw_0}{dx}=\tau_w \qquad (9\text{-}8\text{-}5)$$

or

$$\frac{d\mathrm{Re}^{**}}{dx}+\left(1+\frac{\delta^*}{\delta^{**}}-\frac{\delta_1}{\delta^{**}}\right)\frac{\mathrm{Re}^{**}}{\bar{w}_0}\frac{d\bar{w}_0}{dx}=\frac{c_{f_1}}{2}\mathrm{Re}_s\bar{w}_0, \qquad (9\text{-}8\text{-}6)$$

where

$$\mathrm{Re}^{**}=w_0\delta^{**}/\nu_0;\ x=x/s;\ w_0=\bar{w}_0/w_s;$$
$$c_{f_1}/2=\tau_w/\rho_0 w_0^2;\ \mathrm{Re}_s=w_s s/\nu_0.$$

We must now turn our attention to the circumstance that the parameter $d\bar{w}_0/d\bar{x}$, under the conditions adopted, is not related to the pressure gradient, which is essentially zero in a subsonic submerged jet.

With a power-law distribution of velocity in the wall boundary layer we have ($n=1/7$):

$$\left[1+\frac{\delta^*}{\delta^{**}}-\frac{\delta}{\delta^{**}}\right]=\mathrm{const}=-8. \qquad (9\text{-}8\text{-}7)$$

The law of friction for the boundary layer takes the usual form /294

$$\frac{c_{f_1}}{2}=\frac{B}{2\,(\mathrm{Re}^{**})^m}. \tag{9-8-8}$$

Then

$$\frac{d\mathrm{Re}^{**}}{d\bar{x}}+C_1\frac{\mathrm{Re}^{**}}{u_0}\frac{du_0}{d\bar{x}}=\frac{B}{2\mathrm{Re}^{**m}}\bar{w}_0\mathrm{Re}_s. \tag{9-8-9}$$

Since $\delta_1 << \delta_2$ we can assume that the change in maximum velocity over the length of the plate is the same as that for a free turbulent jet [1]:

$$\bar{w}_0=C_2\bar{x}^{\alpha}=3{,}8\bar{x}^{-0{,}5}. \tag{9-8-10}$$

Integrating, we find

$$\mathrm{Re}^{**}=\left\{\mathrm{Re}_0^{**(m+1)}\left(\frac{x_0}{x}\right)^{C_1\alpha(m+1)}+\frac{B(m+1)\,\mathrm{Re}_S C_2\bar{x}^{1+\alpha}}{2\,[\alpha C_1(m+1)+\alpha+1]}\left[1-\left(\frac{x_0}{x}\right)^{C_1\alpha(m+1)+\alpha+1}\right]\right\}^{\frac{1}{m+1}}. \tag{9-8-11}$$

For $x_0 \to 0$ we have

$$\mathrm{Re}^{**}=\left[\frac{B(m+1)\,\mathrm{Re}_s C_2\bar{x}^{\alpha+1}}{2\alpha C_1(m+1)+\alpha+1}\right]^{\frac{1}{m+1}}. \tag{9-8-12}$$

Taking $B/2 = 0.0128$, $m = 0.25$, $C_2 = 3.8$, $C_1 = -8$, $\alpha = 0.5$, we obtain

$$\frac{c_{f_1}}{2}=\frac{0{,}0315}{\mathrm{Re}_s^{0,2}\bar{x}^{0,1}}. \tag{9-8-13}$$

or

$$c_{f_1}=\frac{0{,}0825}{\left(\frac{w_0 x}{\nu}\right)^{0,2}};\quad \frac{c_{f_2}}{2}=\frac{0{,}457}{\mathrm{Re}_s^{0,2}\bar{x}^{1,1}}=\frac{\tau_w}{\rho_0 w_s^2}. \tag{9-8-14}$$

Figure 9.26 gives a comparison between the tests of Myers et al [185] and the derived formulas. Figure 9.27 shows the same comparison for the test data of Seban and Back [216]. As is evident from the diagrams, the proposed formulas for the dynamic layer of a wall jet are in satisfactory agreement with the test results. Using Reynold's analogy we find the heat-transfer formula: /295

$$\mathrm{St}_x=\frac{\alpha}{\rho_0 w_s C_{p0}}=\frac{0{,}12}{\mathrm{Re}_s^{0,2}\bar{x}^{0,8}\mathrm{Pr}^{0,6}} \tag{9-8-15}$$

or

$$\mathrm{Nu}_x=\frac{\alpha x}{\lambda}=0{,}120\left(\frac{w_s x}{\nu_0}\right)^{0,8}\bar{x}^{-0,4}\mathrm{Pr}^{0,4}. \tag{9-8-16}$$

where $\alpha = q_w/(T_w - T^*_w)$.

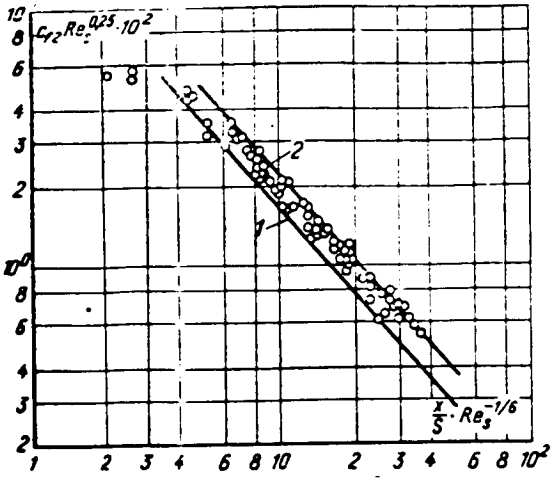

FIG. 9.26. Coefficient of friction in the wall jet. Computed from (9-3-14): 1—$Re_s = 6 \times 10^4$; 2—$Re_s = 7 \times 10^3$. Points from the tests of Myers et al [185].

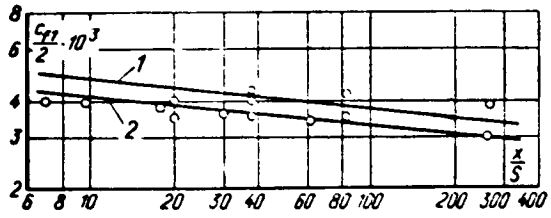

FIG. 9.27. Coefficient of friction in the wall jet. Computed from (9-3-13): 1—$Re_s = 3500$; 2—$Re_s = 7000$. Points from the tests of Seban and Back [216].

/296

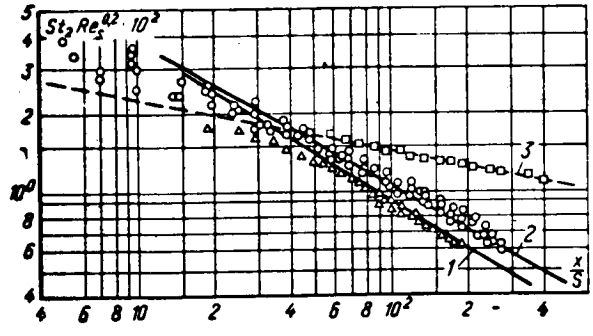

FIG. 9.28. Heat transfer in a wall jet. 1—calculated from (9-8-15) ($w_s/w_0 \to \infty$); 2—calculated from the formula of E. P. Volchkov [15]: $St_s = \frac{0.113}{Re_s^{0.2}\frac{x}{s} - 0.56 Pr^{0.6}}$ ($w_s/w_0 > 3$); 3—calculated from the formula $St_s = 0.0288\, Re_x^{-0.2}\, Pr^{-0.6}$ ($w_s/w_0 = 1$); △, ○, □—tests of Seban and Back [216].

Here T_w is the equilibrium wall temperature, which to a first approximation can be taken equal to the temperature on the axis of a free turbulent jet.

In Fig. 9.28 the test data of Seban and Back [216] are compared with formula (9-8-15). As evident from the diagrams, beginning with x/s = 4 the agreement between theory and experiment is satisfactory.

E. P. Volchkov and P. V. Nikitin have extended this method of computation of the turbulent wall jet to the more complex conditions of the propagation of the jet over a burning graphite surface.

/297

Figure 9.29 is a diagram of this problem with chemical erosion at the wall a transverse flow of matter $j_w = \rho_w w_w$ is created.

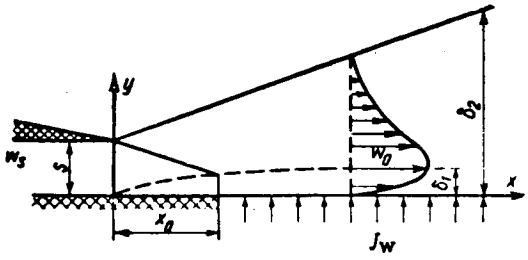

FIG. 9.29. Diagram of wall jet on a permeable surface.

Integrating the equation of motion of the boundary layer along the y-axis from y = 0 to y = δ_1, with boundary conditions

$$\left.\begin{aligned} y=0;\ \tau=\tau_w;\ w_x=0;\ \rho w_y=j_w;\\ y=\delta_1;\ \tau=0;\ w_x=w_0=f(x) \end{aligned}\right\} \tag{9-8-17}$$

and taking into account the equation of continuity, we have

$$\frac{d\mathrm{Re}^{**}}{d\bar{x}}+\left(1+\frac{\delta^*}{\delta^{**}}-\frac{\delta_1}{\delta^{**}}\right)\frac{\mathrm{Re}^{**}}{\bar{w}_0}\frac{d\bar{w}_0}{d\bar{x}}=\frac{c_{f1}}{2}(1+b_1)\,\mathrm{Re}_s\bar{w}_0, \tag{9-8-18}$$

where $b_1=\frac{j_w}{\rho_0 w_0}\frac{2}{c_{f1}}$ is the wall permeability parameter; $\mathrm{Re}^{**}=\rho_0 w_0\delta^{**}/\mu_s$; $\mathrm{Re}_s=\rho_s w_s s/\mu_s$.

We take the law of friction in the wall boundary layer in the form

$$\frac{c_{f1}}{2}=\frac{B}{2}\mathrm{Re}^{**-m}\left(\frac{\mu_w}{\mu_0}\right)^m\Psi. \tag{9-8-19}$$

For subsonic speeds, in the region $\psi_1 > 1$, we have

$$\Psi=\frac{4}{b_1(\psi_1-1)}\left[\operatorname{arctg}\sqrt{\frac{b_1}{(\psi_1-1)(1+b_1)}}-\operatorname{arctg}\sqrt{\frac{b_1\psi_1}{\psi_1-1}}\right]^2, \tag{9-8-20}$$

where $\psi_1 = i_w/i_0$; i_w and i_0 are the total enthalpies of the gas at the wall and at the outer boundary of the wall layer.

If the interaction processes between gas and wall material take place in the diffusion region, the permeability parameter b_1, as shown in Chapter 8, can be expressed in terms of the reduced weight concentrations of the chemical elements entering into the reaction (see 8-5-13). For example, for the interaction of air and carbon in the diffusion regime (with $T_w > 1500°$ K), $b_1 = 0.173$.

It was shown earlier that for isothermal conditions the shape parameter $c_1 = 8$.

Let us estimate the influence of non-isothermicity and the lateral flux of matter on the shape parameter c_1.

Assuming $\omega=\xi^{1/7}$ and taking into account the relationship between density and velocity (for M >> 1) /298

$$\frac{\rho_0}{\rho}=\psi+(1-\psi)\omega, \tag{9-8-21}$$

from the formulas for δ^*/δ_1 and δ^{**}/δ_1, we have

$$\frac{\delta^*}{\delta_1}=1-7\left[\frac{\psi^7}{(1-\psi)^8}\ln\psi+\sum_{\nu=0}^{6}\frac{(-1)^\nu\psi^\nu}{\cdot(7-\nu)(1-\psi)^{\nu+1}}\right]; \tag{9-8-22}$$

$$\frac{\delta^{**}}{\delta_1}=7\left[\frac{\psi^7}{(1-\psi)^8}\ln\psi+\frac{\psi^7}{(1-\psi)^8}+\sum_{\nu=0}^{6}\frac{(-1)^\nu\psi^\nu}{(7-\nu)^2(8-\nu)(1-\psi)^{\nu+1}}\right]. \tag{9-8-23}$$

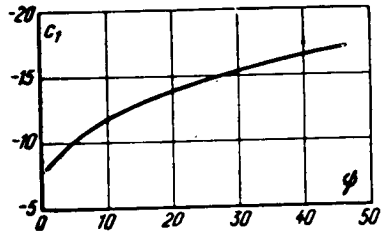

Fig. 9.30

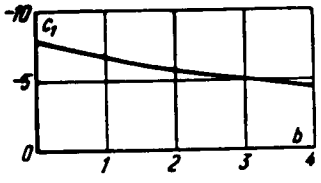

Fig. 9.31

FIG. 9.30. Influence of non-isothermicity on the magnitude of the shape parameter c_1. Curve calculated from (9-8-22) and (9-8-23).

FIG. 9.31. Effect of injection on the shape parameter c_1. Curve calculated from formulas (9-8-25) and (9-8-26).

To estimate the effect of the transverse flow of matter on the shape parameter c_1, we make use of the limiting distributions of velocities, which, for the case ρ = const, take the form (see 5-2-3):

$$\omega=\left(1-\frac{b}{4}\right)\omega_0+\frac{b}{4}\omega_0^2. \tag{9-8-24}$$

Taking $\omega_0=\xi^{1/7}$ we obtain

$$\frac{\delta^*}{\delta_1}=\frac{1}{8}\left(\sqrt{\Psi+b}-\frac{b}{18}\right); \tag{9-8-25}$$

$$\frac{\delta^{**}}{\delta_1}=\frac{1}{8}\left(\sqrt{\Psi+b}-\frac{b}{18}\right)-\frac{1}{36}(\Psi+b)+\frac{1}{240}\sqrt{\Psi+b}-\frac{b^2}{5\,280}. \tag{9-8-26}$$

Figures 9.30 and 9.31 show the dependence of the parameter c_1 on non-isothermicity (with b = 0) and on the injection (with $\psi = 1$). /299

As seen from the plots, the non-isothermicity- and injection-effects on the shape parameter c_1 are quite prominent.

The integral of (9-8-18) is

$$\mathrm{Re}^{**} = \bar{w}_e^{-c_1}\left[\frac{B}{2}(m+1)\,\mathrm{Re}_s\int_{\bar{x}_0}^{\bar{x}}\bar{w}_e^{c_1(m+1)+1}(1+b_1)\times\Psi\left(\frac{\mu_w}{\mu_e}\right)^m d\bar{x} + (\mathrm{Re}^{**}\bar{w}_e^{c_1})_{\bar{x}_0}^{1+m}\right]^{\frac{1}{m+1}}. \tag{9-8-27}$$

With the conditions b_1 = const and Ψ = const, and taking (9-8-10) into account, we have for the region $x \gg x_0$:

$$\mathrm{Re}^{**} = \left\{\frac{B(m+1)\,\mathrm{Re}_s(1+b_1)c_2x^{\alpha+1}\Psi}{2[\alpha c_1(m+1)+\alpha+1]}\left(\frac{\mu_w}{\mu_e}\right)^m\right\}^{\frac{1}{m+1}}. \tag{9-8-28}$$

Making use of the law of friction (9-8-19) and the Reynolds analogy in the form

$$\mathrm{St}_1 = \frac{c_{f1}}{2}\mathrm{Pr}^{-0.6}, \tag{9-8-29}$$

we obtain a formula for computing heat-transfer:

$$\mathrm{St}_1 = \frac{B\Psi[\alpha c_1(m+1)+\alpha+1]^{\frac{m}{m+1}}}{2\left[\frac{B}{2}(m+1)\,\mathrm{Re}_s\Psi(1+b_1)c_2\bar{x}^{\alpha+1}\right]^{\frac{m}{m+1}}\mathrm{Pr}^{0.6}}\left(\frac{\mu_w}{\mu_e}\right)^{\frac{m}{m+1}} \tag{9-8-30}$$

In practical computations it is more convenient to use the number

$$\mathrm{St}_2 = \frac{j_w}{\rho_e w_e b_1} = \mathrm{St}_1\bar{w}_e = c_2\mathrm{St}_1x^{\alpha}. \tag{9-8-31}$$

In the paper by E. P. Volchkov and P. V. Nikitin [15] tests were made in a cylindrical graphite duct with induction heating. A nozzle at the duct input provided an air screen.

The mass-flow of matter at the wall was determined from the intensity of burning of the duct. Preliminary calibration tests showed that in the regimes studied $c_2 = 3.6$ and $\alpha = -0.45$. In addition, the permeability parameter $b = b_1\Psi$ was less than 0.1 in the tests, and its effect on the law of heat-transfer and on the shape parameter c_1 could be neglected. The non-isothermicity factor was the major influence on these parameters; the non-isothermicity was about $\Psi \approx 8.5$ in the tests. /300

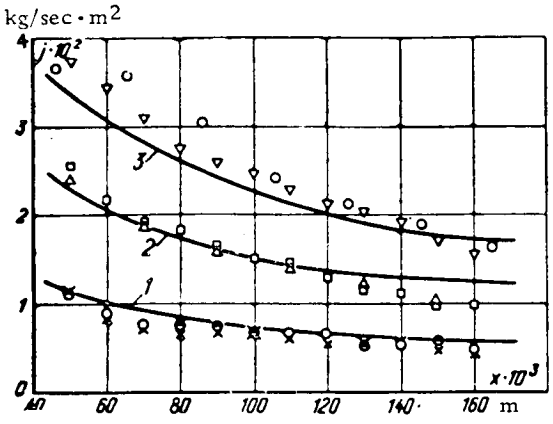

FIG. 9.32. Burning of a graphite duct in an air wall jet. 1, 2, 3—calculated from (9-8-33) for slot velocities of 114, 66 and 26.7 m/sec, respectively. Points from the tests of P. V. Nikitin.

Symbols	○	▽	△	□	◓	×
w_0, m/sec	114	113,4	59,6	72	27,4	26
T_w °K	1 923	1 928	1 938	1 988	1 997	1 959

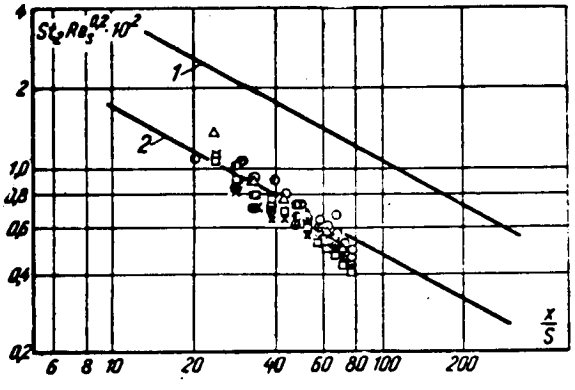

FIG. 9.33. Mass transfer in a wall jet (burning graphite duct). 1—Calculated from (9-8-32) for $\Psi = 1$; 2—calculated from (9-8-32) for $\Psi = 8.5$. Points from the tests by E. P. Volchkov et al.

Symbols	○	△	□	◐	×
$T_0 w_0$, kg/(m²·sec)	135	74,4	88,2	32,3	30,9
T_w, °K	1 923	1 938	1 988	1 997	1 958

In this case we have from Fig. 9.30 that $c_1 = -11$. Then Eq. (9-8-31) reduces to

$$St_0 Re_e^{0.2} = \frac{0.12}{x^{0.08} Pr^{0.6}} \left(\frac{\mu_w}{\mu_e}\right)^{0.8} \Psi^{0.8} \tag{9-8-32}$$

or

$$j_w = \frac{0.12 b_1 \rho_e w_e \Psi^{0.8}}{x^{0.08} Re_e^{0.2} Pr^{0.6}} \left(\frac{\mu_w}{\mu_e}\right)^{0.2}. \tag{9-8-33}$$

A comparison of the calculations of burning intensity of the graphite duct along the length with various injection intensities from (9-8-33) with the tests of E. P. Volchkov and P. V. Nikitin is given in Fig. 9.32. As seen from the plot, there is satisfactory agreement between calculation and experiment.

Figure 9.33 provides a check of formulas (9-8-32) (for $\Psi = 8.5$). But here, for comparison, the curve is calculated for isothermal conditions ($\Psi = 1$). We see that in this case non-isothermicity has a significant effect on mass-transfer, reducing it by a factor of more than two.

APPENDIX

A.1. SUMMARY OF THE PRINCIPAL COMPUTATIONAL FORMULAS

/302.

A.1.1. Flow Past an Impermeable Plate

Standard Conditions

Frictional drag law for isothermal flow:

$$c_{f_0} = \frac{2}{(2{,}5 \ln \mathrm{Re}^{**} + 3{,}8)^2}. \tag{A-1}$$

Heat-transfer law:

$$\mathrm{St}_0 = \frac{2\,\mathrm{Pr}^{-0{,}75}}{(2{,}5 \ln \mathrm{Re}_T^{**} + 3{,}8)^2}. \tag{A-2}$$

Mass-transfer law:

$$\mathrm{St}_{D0} = \frac{2\,\mathrm{Sc}^{-0{,}75}}{(2{,}5 \ln \mathrm{Re}_D^{**} + 3{,}8)^2}. \tag{A-3}$$

Using a power-law approximation:

$$c_{f_0} = B\,\mathrm{Re}^{**-m}; \tag{A-4}$$

$$\mathrm{St}_0 = \frac{B}{2}\,\mathrm{Pr}^{-0{,}75}\mathrm{Re}^{**-m}; \tag{A-5}$$

$$\mathrm{St}_{D0} = \frac{B}{2}\,\mathrm{Sc}^{-0{,}75}\mathrm{Re}_D^{**-m'}. \tag{A-6}$$

where the coefficients B and m are taken from table 1.

For $\mathrm{Re}^{**} < 10^4$, m = 0.25 and B = 0.0256.

For $10^4 < \mathrm{Re}^{**} < 4 \cdot 10^5$, m = 0.182 and B = 0.0148.

The local coefficients of friction, heat- and mass transfer:

$$c_{f_0} = 2\,\mathrm{St}_0\,\mathrm{Pr}^{0{,}75} = 2\,\mathrm{St}_{D0}\,\mathrm{Sc}^{0{,}75}$$

$$= 0{,}0576\,\mathrm{Re}_x^{-0{,}2}\ (\text{for } \mathrm{Re}_x < 10^7); \tag{A-7}$$

$$c_{f_0} = 0{,}0308\,\mathrm{Re}_x^{-0{,}154}\ (\text{for } 10^7 < \mathrm{Re}_x < 10^9). \tag{A-8}$$

The mean coefficients of friction, heat- and mass transfer:

$$\bar{c}_{f_0} = 0{,}072\,\mathrm{Re}_x^{-0{,}2}\ (\text{for } \mathrm{Re}_x < 10^7); \tag{A-9}$$

$$\bar{c}_{f_0} = 0{,}0363\,\mathrm{Re}_x^{-0{,}154}\ (\text{for } 10^7 < \mathrm{Re}_x < 10^9); \tag{A-10}$$

/303

$$\bar{c}_{f_0} = 2\,\overline{\mathrm{St}}_0\,\mathrm{Pr}^{0{,}75} = 2\,\overline{\mathrm{St}}_{D0}\,\mathrm{Sc}^{0{,}75}.$$

Distribution of velocity, temperature and concentration:

$$\omega_0 = 1 + \frac{1}{\chi_0}\sqrt{\frac{c_{f0}}{2}}\ln\xi; \tag{A-11}$$

$$\theta_0 = 1 + \frac{1}{\chi_0}\sqrt{\mathrm{St}_0}\ln\xi_T; \tag{A-12}$$

$$\overline{\Delta c_0} = 1 + \frac{1}{\chi_0}\sqrt{\mathrm{St}_{D0}}\ln\xi_D. \tag{A-13}$$

Effect of Nonisothermicity and Compressibility

Limit Relative Frictional Drag Laws

1. Subsonic velocities:

$$\Psi_\infty = \left(\frac{c_f}{c_{f0}}\right)_{\mathrm{Re}^{**}_w} = \frac{4}{(\sqrt{\psi}+1)^2}. \tag{A-14}$$

2. Supersonic velocities:

$$\Psi_\infty = \left(\frac{c_f}{c_{f0}}\right)_{\mathrm{Re}^{**}_w} = \left(\frac{\arcsin\sqrt{\frac{\psi^*-1}{\psi^*}}}{\psi^*-1}\right)^2 \tag{A-15}$$

or

$$\Psi_\infty = \left(\frac{\operatorname{arctg} M_0\sqrt{r\frac{k-1}{2}}}{M_0\sqrt{r\frac{k-1}{2}}}\right)^2; \tag{A-16}$$

when $\Delta\psi \neq 0$,

$$\Psi_\infty = \frac{1}{\psi^*-1}\left[\arcsin\frac{2(\psi^*-1)+\Delta\psi}{\sqrt{4(\psi^*-1)(\psi^*+\Delta\psi)+(\Delta\psi)^2}} - \arcsin\frac{\Delta\psi}{\sqrt{4(\psi^*-1)(\psi^*+\Delta\psi)+(\Delta\psi)^2}}\right]^2. \tag{A-17}$$

Approximation Formulas

In the general case

$$\Psi_\infty = \left[\frac{2\operatorname{arctg} M_0\sqrt{r\frac{k-1}{2}}}{\left(\sqrt{\frac{T_w}{T^*_w}}+1\right)M_0\sqrt{r\frac{k-1}{2}}}\right]^2. \tag{A-18}$$

For the case r = 0.9, k = 1.4 we have

/304

$$\Psi_\infty = \left[\frac{4{,}7\operatorname{arctg}(0{,}424M_0)}{M_0\left(\sqrt{\frac{T_w}{T^*_w}}+1\right)}\right]^2 \tag{A-19}$$

or

$$\Psi_\infty = \left\{ \frac{1}{4} \left[\left(\frac{T_w}{T_0} \right)^{1/2} + 1 \right]^2 + 0{,}03\, M_0^2 \right\}^{-1}. \tag{A-20}$$

For the power-law approximation of the frictional-drag law under standard conditions we have

$$(\bar{c}_f/\bar{c}_{f0})_{Re_x} = \left(\frac{c_f}{c_{f0}} \right)_{Re_x} = \Psi_\infty^{\frac{1}{1+m}}; \tag{A-21}$$

$$\Psi_\infty = \Psi_{x\infty} = \Psi_{D\infty}; \tag{A-22}$$

$$c_f = 0{,}0576\, Re_{xw}^{-0,2} \Psi_\infty^{0,8} \quad (\text{for } Re_x < 10^7);$$

$$c_f = 0{,}0308\, Re_{xw}^{-0,154} \Psi_\infty^{0,846} \quad (\text{for } 10^7 < Re_x < 10^9),$$

where

$$Re_{xw} = \frac{\rho_0 w_0 x}{\mu_w};$$

$$c_f = 2\, St\, Pr^{0,75} = 2\, St_D\, Sc^{0,75}.$$

Limit Velocity Distributions

1. Subsonic velocities:

$$\omega = \sqrt{\Psi_\infty}\, \omega_0 \left[\sqrt{\psi} + \frac{1 - \sqrt{\psi}}{2}\, \omega_0 \right]; \tag{A-23}$$

$$H = \psi H_0. \tag{A-24}$$

2. Supersonic velocities:

$$\arcsin \frac{2(\psi^* - 1)\,\omega + \Delta\psi}{\sqrt{4\psi(\psi^* - 1) + (\Delta\psi)^2}} = \sqrt{\psi^* - 1}\, \sqrt{\Psi_\infty}\, \omega_0 + \arcsin \frac{\Delta\psi}{\sqrt{4\psi(\psi^* - 1) + (\Delta\psi)^2}}. \tag{A-25}$$

When $\Delta\psi = 0$

$$\omega = \sqrt{\frac{\psi^*}{\psi^* - 1}}\, \sin\left[\sqrt{\psi^* - 1}\, \sqrt{\Psi_\infty}\, \omega_0 \right]; \tag{A-26}$$

$$H = H_0 (1{,}67\psi^* - 0{,}67). \tag{A-27}$$

Effect of Gas Dissociation ("Frozen" Boundary Layer)

Limit frictional-drag law:

$$\Psi_\infty = \Psi_t \Psi_M \Psi_{\alpha_0}, \tag{A-28}$$

where

$$\Psi_t = \left(\frac{2}{\sqrt{\frac{T_w}{T_w^*}} + 1} \right)^2; \quad \Psi_M = \left(\frac{\operatorname{arctg} M_0 \sqrt{r \frac{k-1}{2}}}{M_0 \sqrt{r \frac{k-1}{2}}} \right)^2;$$

$$\Psi_* = \left(\frac{2}{\sqrt{\psi_\alpha}+1}\right)^2; \quad \psi_\alpha = \frac{1+\alpha_w}{1+\alpha_0}.$$

/305

Limit velocity distribution (subsonic velocities, $\psi = 1$):

$$\omega = \sqrt{\Psi}\,\omega_0\left[\omega_0\,\frac{1-\sqrt{\psi_\alpha}}{2}+\sqrt{\psi_\alpha}\right]; \tag{A-29}$$

for the case $\alpha_w = 0$, $\alpha_0 = 1$:

$$\omega = (0{,}17\omega_0 + 0{,}83)\,\omega_0; \tag{A-30}$$

for the case $\alpha_w = 1$; $\alpha_0 = 0$:

$$\omega = \omega_0(1{,}17 - 0{,}17\omega_0). \tag{A-31}$$

Thermal Boundary Layer on a Curvilinear Impermeable Surface

Reynolds Number over the Energy Loss Thickness

1. Two-dimensional boundary layer:

$$\mathrm{Re}^{**}_{T00} = \frac{1}{\Delta i_\Sigma}\left\{\frac{1+m}{2\,\mathrm{Pr}^n}\,B\,\mathrm{Re}_{**}\int_{\bar{x}_1}^{\bar{x}}\Psi_\infty\left(\frac{\mu_w}{\mu_{**}}\right)^m U\,(1 - U^2)^{\frac{1}{k-1}}\,\Delta i_\Sigma^{1+m}\,d\bar{x} + (\mathrm{Re}^{**}_{T00}\,\Delta i_\Sigma)^{1+m}_{\bar{x}=\bar{x}_1}\right\}^{\frac{1}{1+m}}. \tag{A-32}$$

2. Axisymmetric boundary layer is a nozzle:

$$\mathrm{Re}^{**}_{T00} = \frac{1}{\Delta i_\Sigma\,\bar{D}}\left\{\frac{1+m}{2\,\mathrm{Pr}^n}\,B\,\mathrm{Re}_{**}\int_{\bar{x}_1}^{\bar{x}}\Psi_\infty\left(\frac{\mu_w}{\mu_{**}}\right)^m \times \bar{D}^{m-1}\Delta i_\Sigma^{1+m}\,d\bar{x} + (\mathrm{Re}^{**}_{T00}\,\Delta i_\Sigma\bar{D})^{1+m}_{\bar{x}=\bar{x}_1}\right\}^{\frac{1}{m+1}}. \tag{A-33}$$

For the subsonic region:

/306

$$\mathrm{Re}^{**}_{T} = \frac{1}{\Delta T}\left\{\frac{1+m}{2\,\mathrm{Pr}^n}\,B\,\mathrm{Re}_{*1}\int_{\bar{x}_1}^{\bar{x}}\Psi_\infty\left(\frac{\mu_w}{\mu_*}\right)^m \bar{w}_*\,\Delta T^{1+m}\,d\bar{x} + (\mathrm{Re}^{**}_{T}\,\Delta T)^{1+m}_{\bar{x}=\bar{x}_1}\right\}^{\frac{1}{m+1}}. \tag{A-34}$$

For an axisymmetric boundary layer:

$$\mathrm{Re}_T^{**} = \frac{1}{\Delta T \bar{D}} \left\{ \frac{1+m}{2\,\mathrm{Pr}^n} B\,\mathrm{Re}_{01} \int_{\bar{x}_1}^{\bar{x}} \Psi_\infty \left(\frac{\mu_W}{\mu_e}\right)^m \bar{w}_e \Delta T^{1+m} \right.$$

$$\left. \times \bar{D}^{1+m} d\bar{x} + (\mathrm{Re}_T^{**} \Delta T \bar{D})^{\frac{1+m}{\bar{x}=\bar{x}_1}} \right\}^{\frac{1}{m+1}}. \qquad \text{(A-35)}$$

Local values of the Stanton number:

$$\mathrm{St}_x = \Psi_\infty \frac{B}{2\,\mathrm{Pr}^n (\mathrm{Re}_{T\infty}^{**})^m} \left(\frac{\mu_W}{\mu_{e\infty}}\right)^m. \qquad \text{(A-36)}$$

Local heat fluxes:

$$q_{Wx} = \mathrm{St}_x \rho_e w_e \Delta i_x. \qquad \text{(A-37)}$$

Flow Past a Plate with T_W = const

The turbulent boundary layer increases from the leading edge of the plate:

$$\mathrm{St}_x = 0{,}0288\,(\Psi_\infty)^{0.8}\,\mathrm{Re}_{xW}^{-0.2}\mathrm{Pr}^{-0.6}. \qquad \text{(A-38)}$$

For flow over a blunt-nosed body ($\tilde{w}_0 = c\bar{x}$):

$$\mathrm{St} = \frac{B}{2\,\mathrm{Pr}^n} \frac{\Psi_\infty^{\frac{1}{m+1}}}{\left[\frac{1+m}{2\mathrm{Pr}^n} B \frac{c}{2} \bar{x}^2 \mathrm{Re}_{01W}\right]^{\frac{m}{m+1}}}. \qquad \text{(A-39)}$$

For cross flow over a plate (c = 1, m = 0.25, B = 0.0256, n = 0.75):

$$\mathrm{St} = 0{,}0375\Psi_\infty^{0.8}\,\mathrm{Re}_{01W}^{-0.2}\bar{x}^{-0.4}\,\mathrm{Pr}^{-0.6}. \qquad \text{(A-40)}$$

For a given thermal stress distribution:

/307

$$\mathrm{St}_x = \left(\frac{B\Psi_\infty}{2\mathrm{Pr}^n}\right)^{\frac{1}{m+1}} \left(\frac{\mu_W}{\mu_{e\infty}}\right)^{\frac{m}{m+1}} \left[\mathrm{Re}_{L\infty} \frac{\int_0^{\bar{x}} q_{Wx}\, d\bar{x}}{q_{Wx}} \right]^{-\frac{m}{m+1}}. \qquad \text{(A-41)}$$

For the case q_W = const

$$\mathrm{St}_x = 0{,}0288\,(\Psi_\infty)^{0.8}\,\mathrm{Re}_{xW}^{-0.2}\mathrm{Pr}^{-0.6}. \qquad \text{(A-42)}$$

Plate with an initial heat-insulated section:

$$\mathrm{St}=\frac{0.0288}{\mathrm{Re}_{\Delta x}^{0.2}\mathrm{Pr}^{0.6}}\left(\frac{x-x_0}{x}\right)^{0.875}. \tag{A-43}$$

For a diffusion boundary layer it is necessary to replace Δi by Δc, Pr by Sc and St by St_D in Eqs. (A-32)-(A-43).

A.1.2. Flow Past a Permeable Plate

Isothermal Homogeneous Boundary Layer

The limit relative frictional-drag law:

$$\Psi_\infty=\left(1-\frac{b}{4}\right)^2; \tag{A-44}$$

$$b_{\text{crit}\,\infty}=4. \tag{A-45}$$

The limit velocity distribution:

$$\omega=\left(1-\frac{b}{4}\right)\omega_0+\frac{b}{4}\,\omega_0^2; \tag{A-46}$$

$$\omega_{\text{crit}}=\omega_0^2. \tag{A-47}$$

Taking $\omega_0=\xi^n$ we have

$$\tilde{\delta}^{*}_{\infty\,\text{crit}}=\frac{n\left(2n+1+\frac{b}{4}\right)}{(n+1)(2n+1)}; \tag{A-48}$$

$$\tilde{\delta}_{\infty\,\text{av}}=\frac{2n}{2n+1}; \tag{A-49}$$

$$\tilde{\delta}^{**}_{\infty}=\left(1-\frac{b}{4}\right)\frac{1}{n+1}+\left[\frac{b}{4}-\left(1-\frac{b}{4}\right)^2\right]\frac{1}{2n+1} -2\frac{b}{4}\left(1-\frac{b}{4}\right)\frac{1}{3n+1}-\frac{b^2}{16}\,\frac{1}{4n+1}; \tag{A-50}$$

$$\tilde{\delta}^{**}_{\infty\,\text{crit}}=\frac{2n}{(2n+1)(4n+1)}; \tag{A-51}$$

/308

$$H_\infty=\frac{\delta^{*}_{\infty}}{\delta^{**}_{\infty}}=\frac{n\left(2n+1+\frac{b}{4}\right)}{\left(1-\frac{b}{4}\right)(2n+1)+\left[\frac{b}{4}-\left(1-\frac{b}{4}\right)^2\right](n+1) -2\frac{b}{4}\left(1-\frac{b}{4}\right)\frac{(n+1)(2n+1)}{3n+1}-\frac{b^2}{16}\,\frac{(n+1)(2n+1)}{4n+1}}; \tag{A-52}$$

$$H_{\infty\,\text{crit}}=1+4n. \tag{A-53}$$

Uniform gas injection (j_w = const):

$$c_f = 0{,}0576\,\mathrm{Re}_x^{-0,2}\,\frac{(1-0{,}25b)^2}{(1+0{,}25b)^{0,8}}; \tag{A-54}$$

$$b_m = \frac{2j_w}{\rho_e w_e c_{fe}} = \frac{b}{(1+0{,}25b)^{0,8}}; \tag{A-55}$$

$$b_{x\,\mathrm{crit}\,\infty} = 3{,}5. \tag{A-56}$$

Constant permeability parameter (b = const):

$$c_f = 0{,}0576\,\mathrm{Re}_x^{-0,2}\,\frac{(1-0{,}25b)^2}{(1+0{,}25b)^{0,8}}; \tag{A-57}$$

$$b_m = \frac{b}{(1+0{,}25b)^{0,8}}; \tag{A-58}$$

$$b_{x\,\mathrm{crit}\,\infty} = 3{,}5. \tag{A-59}$$

Limit gas suction:

$$\Psi_\infty = -b_m; \tag{A-60}$$

$$j_w = -\frac{c_f}{2}. \tag{A-61}$$

Allowance for a finite Reynolds number:

$$\Psi_\infty = \left(1-\frac{b_*}{b_{\mathrm{crit}}}\right)^2; \tag{A-62}$$

$$b_{\mathrm{crit}} = b_{\mathrm{crit}\,\infty}\left(1+\frac{0{,}83}{(\mathrm{Re}^{**})^{0,86}}\right). \tag{A-63}$$

Turbulent Boundary Layer of Variable Density on a Permeable Plate (Subsonic Velocities)

Limit Relative Laws of Frictional Drag, Heat- and Mass Transfer

1. $\psi_1 < 1$:

$$\Psi_\infty = \frac{4}{(1-\psi_1)b_1}\left[\ln\frac{\sqrt{(1-\psi_1)(1+b_1)}+\sqrt{b_1}}{\sqrt{1-\psi_1}+\sqrt{b_1\psi_1}}\right]^2; \tag{A-64}$$

$$b_{\mathrm{crit}\,\infty} = \frac{1}{1-\psi_1}\left(\ln\frac{1+\sqrt{1-\psi_1}}{1-\sqrt{1-\psi_1}}\right)^2. \tag{A-65}$$ /309

2. $\psi_1 > 1$:

$$\Psi_\infty = \frac{4}{(\psi_1-1)b_1}\left[\operatorname{arctg}\sqrt{\frac{b_1}{(\psi_1-1)(1+b_1)}} - \operatorname{arctg}\sqrt{\frac{b_1\psi_1}{\psi_1-1}}\right]^2; \tag{A-66}$$

$$b_{\text{crit}\,\infty} = \frac{1}{\psi_1 - 1}\left(\arccos\frac{2-\psi_1}{\psi_1}\right)^2. \tag{A-67}$$

Approximation formulas:

$$\Psi_\infty \approx \left[\frac{1}{4}\left\{\psi_1^{1/2} + (1+b_1)^{1/2}\right\}^2 + \frac{1}{6}b_1(\psi_1 - 1)\right]^{-1}; \tag{A-68}$$

$$b_{\text{crit}\,\infty} \approx \frac{4}{\frac{1}{3} + \frac{2}{3}\psi_1}, \tag{A-69}$$

where $\psi_1 = \rho_0/\rho_w$.

Boundary Layer	ψ_1
Homogeneous non-isothermal	$\frac{T_w}{T_0}$
Inhomogeneous isothermal	$1 + \frac{b_1}{1+b_1}(\bar{R} - 1)$
Nonisothermal; mixtures of gases of like latency	$\frac{i_w}{i_0} = \psi\left[1 + \frac{b_1}{1+b_1}(\bar{R} - 1)\right]$

$$\Psi_\infty = \Psi_{b\infty}\left(1 - \frac{b}{b_{\text{crit}\,\infty}}\right)^2, \tag{A-70}$$

where

$$\Psi_{b\infty} = \left(\frac{2}{\sqrt{\psi_1} + 1}\right)^2.$$

Limiting velocity distributions:

for $\psi_1 < 1$

$$\omega = \frac{K^2 - ac}{a(2K + d)}, \tag{A-71}$$

where

$$a = (1-\psi_1)b,\quad d = (1-\psi_1)\Psi_\infty + \psi_1 b;\quad c = \tfrac{1}{2}\Psi_\infty;$$

$$K = \left[\sqrt{a(a+d+c)} + a + \frac{1}{2}d\right]e^{\sqrt{a}(\omega_0 - 1)} - \frac{1}{2}d;$$

for $\psi_1 > 1$:

$$\operatorname{arctg}\sqrt{\frac{(\psi_1 - 1)(1 + b_1\omega)}{\psi_1 + \psi_1(1-\psi_1)\omega}} = \operatorname{arctg}\sqrt{(\psi_1 - 1)(1+b_1)} - \frac{\sqrt{\psi_1 - 1}}{2}\sqrt{\Psi_\infty}(1 - \omega_0). \tag{A-72}$$

/310

For the case of critical injection:

$\psi_1 < 1$

$$\sqrt{\psi_1 + (1-\psi_1)\omega} + \sqrt{(1-\psi_1)\omega} = [1 + \sqrt{1-\psi_1}]\, e^{\frac{\sqrt{1-\psi_1}}{2\pi}\sqrt{b_{\text{crit}\,\infty}}(\omega_0 - 1)}; \tag{A-73}$$

$\psi_1 > 1$

$$\operatorname{arctg}\sqrt{\frac{(\psi_1 - 1)\omega}{\psi_1 + (1-\psi_1)\omega}} = \operatorname{arctg}\sqrt{\psi_1 - 1} - \frac{\sqrt{\psi_1 - 1}}{2}\sqrt{b_{\text{crit}\,\infty}}(1 - \omega_0). \tag{A-74}$$

Shape parameter H:

$$H = H_0\psi_1(1 + 0{,}05b). \tag{A-75}$$

Supersonic Gas Flow along a Permeable Surface (Homogeneous Gas)

In this case

$$\Psi_\infty = \Psi_t \Psi_M \left(1 - \frac{b}{b_{\text{crit}\,\infty}}\right)^2, \tag{A-76}$$

where

$$\Psi_t = \left(\frac{2}{\sqrt{\frac{T_w}{T^*_w}} + 1}\right)^2; \quad \Psi_M = \left(\frac{\operatorname{arctg} M_0 \sqrt{r\frac{k-1}{2}}}{M_0\sqrt{r\frac{k-1}{2}}}\right)^2; \tag{A-77}$$

$$b_{\text{crit}\,\infty} = b_{\text{кр}\psi}\Psi_M;$$

$b_{\text{crit}\ \psi}$ is defined by formulas (A-65), (A-67).

Injection of a Homogeneous Gas of Like Valency ($\overline{R} = \overline{C}$)

In this case

$$\Psi_\infty \approx \left\{\frac{1}{4}\left[\psi^{1/2}\frac{1 + Rb_1}{1 + b_1} + (1 + b_1\psi^*)^{1/2}\right]^2 + \frac{1}{6}(\psi^* - 1) + \frac{b_1}{6}\left[\psi\frac{1 + Rb_1}{1 + b_1} - \psi^*\right]\right\}^{-1}; \tag{A-78}$$

$$b_{\text{crit}\,\infty} \approx \frac{4}{\frac{1}{3}\psi^* + \frac{2}{3}R\psi}. \tag{A-79}$$

Turbulent Boundary Layer of Dissociated Gas on a Permeable Surface /311

In this case

$$\Psi_\infty = \Psi_t \Psi_M \Psi_a \left(1 - \frac{b}{b_{\text{crit}}}\right)^2, \tag{A-80}$$

where

$$\Psi_t = \left(\frac{2}{\sqrt{\frac{T_w}{T^*_w}}+1}\right)^2; \quad \Psi_M = \left[\frac{\operatorname{arctg} M_\infty \sqrt{r\frac{k-1}{2}}}{M_\infty \sqrt{r\frac{k-1}{2}}}\right]^2;$$

$$\Psi_\alpha = \left(\frac{2}{\sqrt{\psi_\alpha}+1}\right)^2;$$

$$b_{\text{crit}\,\infty} = b_{\substack{\text{crit}\,\infty \\ \alpha=0}} \frac{3}{1+2\psi_\alpha}; \tag{A-81}$$

$b_{\substack{\text{crit}\,\infty \\ \alpha=0}}$ is defined by formula (A-79).

When the boundary conditions are similar, the triple analogy holds:

$$\Psi_\infty = \Psi_{S\infty} = \Psi_{D\infty}. \tag{A-82}$$

Formula for the thermal permeability parameter:

$$b_t = b_{t\,\text{exp}} - \frac{Kb_{i\,\text{crit}}}{2\Psi_t\Psi_M}\left(\sqrt{\frac{4\Psi_t\Psi_M}{Kb_{i\,\text{crit}}}+1}-1\right), \tag{A-83}$$

where

$$K = \frac{i_w - i'}{i^*_w - i_w}.$$

Turbulent Gas Boundary Layer on a Permeable Surface of Weak Curvature

For the case b = const (T_w = const) (subsonic velocities):

$$c_f = \frac{\Psi_\infty B \bar{w}_0^{\varkappa m}}{\left[\frac{1+m}{2} B\,\text{Re}_{\delta w}(\Psi_\infty + b)\int_0^{\bar{x}} \bar{w}_0^{1+(1+m)\varkappa}\,d\bar{x}\right]^{\frac{m}{1+m}}}. \tag{A-84}$$

For an axisymmetric boundary layer: /312

$$c_f = \frac{\Psi_\infty B w_0^{-\varkappa m}}{\left[\frac{1+m}{2} B\,\text{Re}_{\delta w}\,\bar{D}^{(1+m)}(\Psi_\infty + b)\int_0^{\bar{x}} \bar{w}_0^{1+(1+m)\varkappa}\,\bar{D}^{m+1}\,dx\right]^{\frac{m}{1+m}}}. \tag{A-85}$$

The coefficients m and B are taken from Table 1.1;

$$\varkappa = 1 + H = 1 + H_0\psi_t(1+0{,}05b).$$

For critical injection:

$$\mathrm{Re}^{**}_{w} = \bar{w}_0^{-n}\left[\frac{1+m}{2} B\,\mathrm{Re}_{0w} b_{\mathrm{crit}} \int_0^{\bar{x}} \bar{w}_0^{1+(1+m)n}\, d\bar{x}\right]^{\frac{1}{1+m}}; \tag{A-86}$$

$$j_{w\,\mathrm{crit}} = \rho_0 w_0 \frac{B b_{xp}}{2\,(\mathrm{Re}^{**}_{cr})^m} \tag{A-87}$$

Integral of the energy equation for a plane boundary layer:

$$\mathrm{Re}^{**}_{i} = \frac{1}{\Delta i}\left\{\frac{1+m}{2\,\mathrm{Pr}^{0,75}} B\mathrm{Re}_{00} \int_{\bar{x}_0}^{\bar{x}} U\,(1-U^2)^{\frac{1}{k-1}} b_i\,(1 + K)\,\Delta i^{1+m}\, dx + (\mathrm{Re}^{**}_{i}\,\Delta i)^{1+m}_{\bar{x}_0}\right\}^{\frac{1}{1+m}}. \tag{A-88}$$

For the subsonic region with T_w = const and T' = const ($\mathrm{Re}^{**}_T = 0$ at $\bar{x} = 0$):

$$\mathrm{Re}^{**}_{Tw} = \left\{\frac{1+m}{2\,\mathrm{Pr}^{0,75}} Bb_T\,(1+K)\,\mathrm{Re}_{0w} \int_0^{\bar{x}} \bar{w}_0\, d\bar{x}\right\}^{\frac{1}{m+1}}. \tag{A-89}$$

Mass flow of injected gas:

$$j_w = \rho_0 w_0\,\mathrm{St}_0\, b_i, \tag{A-90}$$

where

$$\mathrm{St}_0 = \frac{B}{2\,(\mathrm{Re}^{**}_{iw})^m};\quad \mathrm{Re}^{**}_{iw} = \mathrm{Re}^{**}_{i}\left(\frac{\mu_{cr}}{\mu^*}\right).$$

For subsonic velocities and T_w = const:

$$j_w = \rho_0 w_0 \frac{\frac{B}{2} b_T}{[b_T\,(1+K)]^{\frac{m}{m+1}}\left[\frac{B\,(m+1)}{2\,\mathrm{Pr}^{0,75}}\mathrm{Re}_{01}\int_0^{\bar{x}} \bar{w}_0\, d\bar{x}\right]^{\frac{m}{m+1}}}. \tag{A-91}$$

In the neighborhood of the bow point ($\tilde{w}_0 = c\bar{x}$): /313

$$j_{0w} = \frac{\rho_{02} w_{01} c\,\frac{B}{2}\, b_T^{\frac{1}{m-1}}\,\bar{x}^{0,5}}{(1+K)^{\frac{m}{m+1}}\left[\frac{B\,(m+1)}{2\,\mathrm{Pr}^{0,75}}\frac{\mathrm{Re}_0\, c}{2}\right]^{\frac{1}{1+}}}. \tag{A-92}$$

Chemical reactions on the surface of a body:

$$b_{i1} = \frac{(C_i^0)_e - (C_i^0)_w}{(C_i^0)_w}. \tag{A-93}$$

Gas enthalpy at a thermally insulated wall:

$$i_w = i_e + b_{i1} i_\Sigma^0 \ldots \tag{A-94}$$

Integral of the energy equation (subsonic velocities, i_w = const) for a plane boundary layer.

$$\mathrm{Re}^{**}_{iw} = \left\{ \frac{1+m}{2\,\mathrm{Pr}^n} \Psi_\infty (1 + b_{i1}) \mathrm{Re}_{ew} \int_0^{\bar{x}} \bar{u}_e^{\,m}\, d\bar{x} \right\}^{\frac{1}{m+1}} \ldots, \tag{A-95}$$

for a nozzle:

$$\mathrm{Re}^{**}_{iw} = \frac{1}{D} \left[\frac{B(1+m)}{2\,\mathrm{Pr}^n} \Psi_\infty (1 + b_{i1}) \mathrm{Re}_e \int_0^{\bar{x}} (D)^{-0.75}\, d\bar{x} \right]^{\frac{1}{m+1}}, \tag{A-96}$$

where

$$\mathrm{Re}_e = \frac{4G}{\pi \mu_w D_{\mathrm{crit}}}.$$

The intensity of burnup of the material:

$$J_w = \rho_e u_e b_{i1} \Psi_\infty \frac{B}{2\,\mathrm{Pr}^n (\mathrm{Re}^{**}_{iw})^m}. \tag{A-97}$$

A.1.3. Influence of a Longitudinal Pressure Gradient

The limit critical parameters in the turbulent boundary layer separation section (constant density) are

$$\left(-f \frac{\delta}{\delta^{**}}\right)_{\mathrm{crit}} = 0.062; \quad \left(\frac{\delta^*}{\delta}\right)_{\mathrm{crit}} = 0.3;$$
$$\left(\frac{\delta^{**}}{\delta}\right)_{\mathrm{crit}} = 0.16; \quad H_{\mathrm{crit}} = 1.87; \quad f = -0.01.$$

Frictional drag law in the diffusion region: /314

$$\Psi_f = [1 - \sqrt{f(2-f)}]. \tag{A-98}$$

Influence of non-isothermicity and compressibility on the critical parameters:

1. Subsonic velocities:

$$\frac{\left(\frac{\delta}{\delta^{**}} f\right)_{\mathrm{crit}}}{\left(\frac{\delta}{\delta^{**}} f\right)_{\mathrm{crit}0}} = \left(\frac{2}{\sqrt{\Psi} + 1}\right)^2. \tag{A-99}$$

2. Supersonic velocities:

$$\frac{\left(\frac{\delta}{\delta^{**}} f\right)_{\text{crit}}}{\left(\frac{\delta}{\delta^{**}} f\right)_{\text{crit0}}} = \frac{1}{\psi^* - 1}\left[\arcsin \frac{2(\psi^* - 1) + \Delta\psi}{\sqrt{4(\psi^* - 1)(\psi^* + \Delta\psi) + (\Delta\psi)^2}} - \arcsin \frac{\Delta\psi}{\sqrt{4(\psi^* - 1)(\psi^* + \Delta\psi) + (\Delta\psi)^2}}\right]^2. \tag{A-100}$$

Approximation formulas:

$$\frac{\left(\frac{\delta}{\delta^{**}} f\right)_{\text{crit}}}{\left(\frac{\delta}{\delta^{**}} f\right)_{\text{crit0}}} \approx \left\{\frac{1}{4}[\psi^{*,5} + 1]^2 + \frac{1}{6} r \frac{k-1}{2} M_0^2\right\}^{-1}. \tag{A-101}$$

For the subsonic velocity region:

with $\psi < 1$

$$H_{\text{crit}} = H_{\text{crit0}}\psi; \quad \frac{f_{\text{crit}}}{f_{\text{crit0}}} = \psi^{-0,5}; \tag{A-102}$$

with $\psi > 1$

$$\frac{H_{\text{crit}}}{H_{\text{crit0}}} = 1 + \frac{1,32}{H_{\text{crit0}}}(\psi - 1); \quad \frac{f_{\text{crit}}}{f_{\text{crit0}}} = \frac{1}{\psi}. \tag{A-103}$$

For the supersonic velocity region:

with $\Delta\psi < 0$:

$$H_{\text{crit}} = 2,41\psi^* + 1,38\Delta\psi - 0,52; \tag{A-104}$$

with $\Delta\psi = 0$:

$$\frac{f_{\text{crit}}}{f_{\text{crit0}}} = \psi^{*-1,53}. \tag{A-105}$$

Dynamic Boundary Layer on a Curvilinear Surface

Integral of the momentum equation:

$$\mathrm{Re}^{**}_{\infty} = \exp\left(-\frac{J}{1+m}\right)\left[(m+1)\frac{B}{2}\mathrm{Re}_{\infty}\int_0^{\bar{x}}(\Psi_t\Psi_M)_{\infty} \times \left(\frac{\mu_w}{\mu_{\infty}}\right)^m U(1-U^2)^{\frac{1}{k-1}}\exp(J)\,d\bar{x}\right]^{-\frac{1}{m+1}}, \tag{A-106}$$

/315

where

$$J = (m+1)\int (1 + H_{crit})\frac{d\bar{w}_*}{\bar{w}_*}.$$

Local friction coefficient:

$$c_f = \Psi_{l\infty}\Psi_{M\infty}\Psi_{f\infty}\frac{B}{(\mathrm{Re}^{**}_{**})^m}\left(\frac{\mu_w}{\mu_{**}}\right)^m. \tag{A-107}$$

Boundary-layer shape parameter:

$$f = \frac{\mathrm{Re}^{**}_{**}}{\mathrm{Re}_{**}U^2(1-U^2)^{\frac{1}{k-1}}}\frac{dU}{dx}. \tag{A-108}$$

For subsonic velocities (T_w = const):

$$\mathrm{Re}^{**}_w = \bar{w}_0^{-\varkappa}\left[\frac{1+m}{2}B\mathrm{Re}_{0w}\Psi_{f\infty}\int_0^{\bar{x}}\bar{w}_0^{1+(1+m)\varkappa}\,d\bar{x}\right]^{\frac{1}{1+m}}, \tag{A-109}$$

where $\varkappa = 1 + H_{crit}$.

Local friction coefficient:

$$c_f = \Psi_{l\infty}\Psi_f B(\mathrm{Re}^{**}_w)^{-m}; \tag{A-110}$$

$$f = \frac{\mathrm{Re}^{**}_w}{\mathrm{Re}_{*0w}\bar{w}_*}\frac{d\bar{w}_*}{d\bar{x}}. \tag{A-111}$$

Area of a plane subsonic diffusor with pre-separation friction:

$$\bar{F} = \left[1 + \frac{0{,}0387}{\delta^{**}_1}(x - x_1)\right]^{1/3{,}87}. \tag{A-112}$$

For the case of intense wall cooling ($\psi \to 0$, $H_{crit} \to 0$):

$$\bar{F} = \left[1 + \frac{0{,}02}{\delta^{**}_1}(x - x_1)\right]^{1/2}. \tag{A-113}$$

A.1.4. Joint Influence of a Longitudinal Pressure Gradient and Gas Injection

Limit frictional-drag law (constant shape parameters):

$$\Psi = \left(1 - \frac{b}{4}\right)^2[1 - \sqrt{J(2-J)}], \tag{A-114}$$

where

$$J = f/f_{crit};$$

/316

$$\frac{f_{crit}}{f_{crit0}} = \frac{4}{\pi^2}\left[\arccos\left(\frac{b}{b_{crit0}}\right)\right]^2. \tag{A-115}$$

A.1.5. Turbulent Boundary Layer in the Initial Section of a Cylindrical Duct with Impermeable Walls (Subsonic Velocities T_w = const)

Length of the initial section:

$$\frac{\bar{x}_{init}}{Re_0^{0.25}} = \frac{0.8\psi + 0.55}{\psi^{0.187}}, \tag{A-116}$$

where

$$Re_\delta = 4G/\pi D\mu_\delta.$$

Velocity in the potential flow core (m = 0.25, B = 0.0256):

$$[(1 + 1.3\psi)\,1.25 + 1]\left[4(\bar{w}_\delta - 1)^{0.25} - \frac{1}{\sqrt{2}}\ln\frac{(\bar{w}_\delta - 1)^{0.5} + \sqrt{2}(\bar{w}_\delta - 1)^{0.25} + 1}{(\bar{w}_\delta - 1)^{0.5} - \sqrt{2}(\bar{w}_\delta - 1)^{0.25} + 1} - \sqrt{2}\,\mathrm{arctg}\frac{\sqrt{2}(\bar{w}_\delta - 1)^{0.25}}{1 - (\bar{w}_\delta - 1)^{0.5}}\right] - (1 + 1.3\psi)\frac{(\bar{w}_\delta - 1)^{1.25}}{\bar{w}_\delta} = \frac{0.4\psi^{1.25}\bar{x}}{(\sqrt{\psi} + 1)^2\,Re_{0w}^{0.25}}. \tag{A-117}$$

Reynolds number over the momentum loss thickness:

$$Re^{**}_w = \frac{Re_{\delta w}(\bar{w}_\delta - 1)}{5.2\psi}. \tag{A-118}$$

Local friction coefficient:

$$c_f = \Psi_\infty \frac{0.0256}{(Re^{**}_w)^{0.25}}. \tag{A-119}$$

Reynolds number over the energy loss thickness:

$$Re^{\delta\delta}_{Tw} = \frac{Re_{\delta\tau}(\bar{w}_\delta - 1)}{5.2\psi}\left\{(2.3 + 1.3\psi) - \frac{1.25 + 1.62\psi}{(\bar{w}_\delta - 1)^{1.25}} \times \left[4(\bar{w}_\delta - 1)^{0.25} - \sqrt{2}\,\mathrm{arctg}\frac{\sqrt{2}(\bar{w}_\delta - 1)^{0.25}}{1 - (\bar{w}_\delta - 1)^{0.5}} - \frac{1}{\sqrt{2}}\ln\frac{(\bar{w}_\delta - 1)^{0.5} + \sqrt{2}(\bar{w}_\delta - 1)^{0.25} + 1}{(\bar{w}_\delta - 1)^{0.5} - \sqrt{2}(\bar{w}_\delta - 1)^{0.25} + 1}\right]\right\}^{0.8}. \tag{A-120}$$

Local values of the Stanton number: /317

$$St = \Psi_\infty \frac{0.0128}{(Re^{\delta\delta}_{Tw})^{0.25}\,Pr^{0.75}}. \tag{A-121}$$

A.1.6. Friction and Heat Transfer in a Stabilized Gas Flow in a Pipe

Coefficient of friction and heat-transfer:

$$\left(\frac{c_f}{c_{f0}}\right)_{\overline{Re}_{DW}} = \left(\frac{St}{St_0}\right)_{\overline{Re}_{DW}} = \left(\frac{2}{\bar{\psi}^{0,8}+1}\right)^2, \tag{A-122}$$

where

$$\overline{Re}_{DW} = \rho_W \bar{u} D / \mu_W; \ \bar{\psi} = T_W / \bar{T}.$$

or

$$\overline{Nu} = 0,023 \overline{Re}^{0,8} \overline{Pr}^{0,4} \bar{\psi}^{-0,27}, \tag{A-123}$$

where

$$\overline{Nu} = \alpha D / \bar{\lambda}; \ \overline{Re} = \bar{\rho} \bar{u} D / \bar{\mu}; \ \bar{\psi} = T_{cr} / \bar{T}.$$

A.1.7. Effectiveness of Gas Screens

Initial Cooled Section

1. Plate:

$$\Theta = \left(1 + 15,5 \frac{x - x_1}{x}\right)^{-0,8}. \tag{A-124}$$

2. Curvilinear surface:

$$\Theta_{\bar{x}} = \left\{ 1 + \frac{\beta_{max}^{1+m}}{\Theta_{\bar{x}}^{1+m}} \times \frac{\int_{\bar{x}_1}^{\bar{x}} \Psi_\infty \left(\frac{\mu_W}{\mu_\infty}\right)^m U (1 - U^2)^{\frac{1}{k-1}} \Theta_{\bar{x}}^{1+m} d\bar{x}}{Re_{00}^m \left[\int_0^{\bar{x}_1} \Psi_\infty \left(\frac{\mu_W}{\mu_\infty}\right)^m U (1 - U^2)^{\frac{1}{k-1}} d\bar{x}\right]^{m+1}} \right\}^{-\frac{1}{m+1}}. \tag{A-125}$$

Injection of a Cooled Gas Through a Porous Section

1. Flow past a plate; subsonic velocities:

/318

$$\Theta = \left[1 + \frac{0,25 \, Re_{\Delta x}}{Re_W^{1,25} (1 + K_1)^{1,25}}\right]^{-0,8}. \tag{A-126}$$

2. Flow past a curvilinear surface:

$$\Theta_\Sigma = \left\{ 1 + \frac{0{,}25\,\mathrm{Re}_{\infty\infty}\Psi_{t1}\left(\frac{\mu_{w1}}{\mu_{\infty\infty}}\right)^{0{,}25}\int_{\bar{x}_1}^{\bar{x}} \Psi_M U\,(1-U^2)^{\frac{1}{k-1}}\,d\bar{x}}{(1+K_1)^{1{,}25}\,\mathrm{Re}_{w1}^{1{,}25}} \right\}^{-0{,}8} \tag{A-127}$$

3. Gas flow in a supersonic nozzle:

$$\Theta_\Sigma = \left\{ 1 + \frac{0{,}25\,\mathrm{Re}_{\infty\infty}\Psi_{t1}\left(\frac{\mu_{w1}}{\mu_{\infty\infty}}\right)\int_{\bar{x}_1}^{\bar{x}} \Psi_M\,(\bar{D})^{m-1}\,d\bar{x}}{(1+K_1)^{1{,}25}\,\mathrm{Re}_{w1}^{1{,}25}\,(\bar{D})^{1{,}25}} \right\}^{-0{,}8} \tag{A-128}$$

Injection of a Cooling Gas Through a Slot

1. Flow past a plate; subsonic velocities:

$$\Theta = \left[1 + 0{,}24\,\mathrm{Re}^{-0{,}25}\,\frac{w_0\,(x-x_1)}{w_1 S}\right]^{-0{,}8}. \tag{A-129}$$

2. Supersonic flow past a curvilinear surface:

$$\Theta = \left[1 + \frac{0{,}016\beta^{1{,}25}\Psi_{t1}\left(\frac{\mu_{w1}}{\mu_{\infty\infty}}\right)^{0{,}25}\mathrm{Re}_{\infty\infty}\int_{\bar{x}_1}^{\bar{x}} \Psi_M U\,(1-U^2)^{\frac{1}{k-1}}\,d\bar{x}}{\mathrm{Re}_{\infty\infty}^{1{,}25}} \right]^{-0{,}8}. \tag{A-130}$$

3. Gas flow in a supersonic nozzle:

$$\Theta = \left[1 + \frac{0{,}016\beta^{1{,}25}\Psi_{t1}\left(\frac{\mu_{w1}}{\mu_{\infty\infty}}\right)^{0{,}25}\mathrm{Re}_{\infty\infty}}{(\mathrm{Re}_{\infty\infty})^{1{,}25}\,(\bar{D})^{1{,}25}}\int_{\bar{x}_1}^{\bar{x}} \Psi_M\,(\bar{D})^{m-1}\,d\bar{x} \right]^{-0{,}8}. \tag{A-131}$$

Heat Transfer in the Presence of a Gas Screen

/319

In this case

$$\mathrm{St}_\infty = \frac{B}{2}\,\mathrm{Re}_T^{\infty\infty -m}\,\mathrm{Pr}^{-n}, \tag{A-132}$$

where

$$\mathrm{Re}^{\infty\infty}{}_T = \frac{1}{\left[\Theta - \frac{T_\infty - T_{w1}}{T_\infty - T_{w1}}\right]}\left\{ \frac{(m+1)\,B}{2\,\mathrm{Pr}^{0{,}75}}\,\mathrm{Re}_D \int_{\bar{x}_1}^{\bar{x}} \left[\Theta - \frac{T_\infty - T_w}{T_\infty - T_{w1}}\right]^{m+1} \bar{w}_0\,d\bar{x} + (\mathrm{Re}_T^{\infty\infty})_{\bar{x}=\bar{x}_1}^{m+1} \right\}^{\frac{1}{m+1}}; \tag{A-133}$$

$$q_w = St_\infty \rho_\infty w_\infty (T_\infty - T_{w1}) \left[\theta - \frac{T_\infty - T_w}{T_\infty - T_{w1}} \right]. \quad \text{(A-134)}$$

Effectiveness of a Gas Screen and Heat Transfer on a Chemically Reacting Surface with Tangential Injection of Inert Gas into the Boundary Layer

Limit heat-transfer laws:

for $\psi_1 < 1$:

$$\Psi = \frac{M^*_w}{M_\infty} \frac{T_\infty}{T^*_w} \frac{4}{b^*_1 (1 - \psi_1)} \left[\ln \frac{\sqrt{(1-\psi_1)(1+b^*_1)} + \sqrt{b^*_1}}{\sqrt{1-\psi_1} + \sqrt{b^*_1 \psi_1}} \right]^2; \quad \text{(A-135)}$$

$$b_{sp} = \frac{M^*_w}{M_\infty} \frac{T_\infty}{T^*_w} \frac{1}{1-\psi_1} \left[\ln \frac{1+\sqrt{1-\psi_1}}{1-\sqrt{1-\psi_1}} \right]^2; \quad \text{(A-136)}$$

for $\psi_1 > 1$:

$$\Psi = \frac{M_w}{M_\infty} \frac{T_\infty}{T^*_w} \frac{4}{b^*_1 (\psi_1 - 1)} \left[\operatorname{arctg} \sqrt{\frac{(\psi_1 - 1)(1 + b^*_1)}{b^*_1}} - \operatorname{arctg} \sqrt{\frac{\psi_1 - 1}{b^*_1 \psi_1}} \right]^2; \quad \text{(A-137)}$$

$$b_{crit} = \frac{M_w}{M_\infty} \frac{T_\infty}{T^*_w} \frac{1}{\psi_1 - 1} \left(\arccos \frac{2 - \psi_1}{\psi_1} \right)^2. \quad \text{(A-138)}$$

For an impermeable wall:

$$\Psi_s = \frac{M^*_w}{M_\infty} \frac{T_\infty}{T^*_w} \left(\frac{2}{\sqrt{\psi_1} + 1} \right)^2. \quad \text{(A-139)}$$

Burn-up of surface in the presence of a screen:

$$j_w = b^*_1 \Psi \frac{B}{2} Re_D^{\infty - m} Sc \left(\frac{\mu_w}{\mu_\infty} \right)^m \rho_\infty w_\infty. \quad \text{(A-140)}$$

where

/320

$$Re_D^\infty = \frac{1}{\overline{\Delta C}} \left[\frac{B(m+1)}{2 Sc^n} \int_0^{\bar{x}} Re_L \left(\frac{\mu_w}{\mu_\infty} \right)^m \Psi (1 + b^*_1) \overline{\Delta C}^{m+1} d\bar{x} \right]^{\frac{1}{m+1}}. \quad \text{(A-141)}$$

Turbulent Wall Jet ($w_s/w_0 >> 1$)

Local friction coefficient:

$$c_f = \frac{0.0825}{(Re_m)^{0.2}}. \quad \text{(A-142)}$$

Local Stanton number:

$$St = \frac{\alpha}{\rho_e w_e c_{p0}} = \frac{0,12\Psi^{0,8}\left(\frac{\mu_w}{\mu_e}\right)^{0,2}}{Re_x^{0,2}\bar{x}^{0,8}\,Pr^{0,6}}, \qquad \text{(A-143)}$$

where $\alpha = \frac{q_w}{T_w - T_w^*}$ and T_w^* is the temperature on the axis of the free turbulent jet.

Burn-up of the surface in the turbulent wall jet:

$$i_{ex} = \frac{0,12b_1\rho_e w_e \Psi^{0,8}}{\bar{x}^{0,36}\,Re_x^{0,2}\,Pr^{0,6}}\left(\frac{\mu_w}{\mu_e}\right)^{0,2}. \qquad \text{(A-144)}$$

A.2. RELATIVE LIMIT LAW OF FRICTIONAL DRAG ON A PERMEABLE PLATE IN A COMPRESSIBLE GAS FLOW [Calculations by (5-4-2)] /321

Air-air

Ψ	b_1 = 0	0,1	0,3	0,7	1	2	5	7	10	50	100	1 000
						M = 0						
0,05	2,6610	2,5620	2,3910	2,1260	1,9720	1,6150	1,0970	0,9199	0,7490	0,2440	0,1390	0,0188
0,1	2,2990	2,2090	2,0550	1,8170	1,6800	1,3610	0,9096	0,7552	0,6118	0,1916	0,1078	0,0139
0,5	1,3650	1,3040	1,2010	1,0450	0,9562	0,7556	0,4829	0,3950	0,3130	0,0905	0,0496	0,0060
1	1,0000	0,9267	0,8678	0,7492	0,6824	0,6331	0,3346	0,2716	0,2137	0,0601	0,0326	0,0039
3	0,5310	0,5039	0,4586	0,3914	0,3541	0,2721	0,6660	0,1340	0,1045	0,0284	0,0153	0,0018
5	0,3779	0,3580	0,3248	0,2759	0,2489	0,1900	0,1152	0,0924	0,0718	0,0193	0,0112	0,0012
10	0,2277	0,2153	0,1946	0,1644	0,1478	0,1120	0,0672	0,0537	0,0415	0,0110	0,0059	0,0006
15	0,1657	0,1565	0,1412	0,1190	0,1068	0,0807	0,0480	0,0384	0,0297	0,0078	0,0042	0,0005
20	0,1312	0,1238	0,1116	0,0938	0,0842	0,0634	0,0377	0,0300	0,0232	0,0061	0,0032	0,0004
						M = 1						
0,05	2,4670	2,3744	2,2150	1,9683	1,8251	1,4923	1,0136	0,8501	0,6926	0,2259	0,1292	0,0176
0,1	2,1524	2,0680	1,9230	1,6997	1,5707	1,2727	0,8522	0,7079	0,6722	0,1780	0,1013	0,0132
0,5	1,3115	1,2533	1,1544	1,0042	0,9189	0,7262	0,4645	0,3799	0,3012	0,0873	0,4790	0,0058
1	0,9648	0,9105	0,8429	0,7277	0,6629	0,5180	0,3253	0,2642	0,2079	0,0586	0,0318	0,0038
3	0,5227	0,4961	0,4515	0,3853	0,3486	0,2680	0,1641	0,1321	0,1030	0,0280	0,0151	0,0017
5	0,3736	0,3540	0,3211	0,2728	0,2461	0,1880	0,1140	0,0914	0,0710	0,0192	0,0102	0,0012
10	0,2261	0,2138	0,1933	0,1633	0,1468	0,1113	0,0668	0,0534	0,0413	0,0109	0,0059	0,0007
15	0,1649	0,1567	0,1405	0,1184	0,1063	0,0803	0,0479	0,0382	0,0293	0,0078	0,0042	0,0005
20	0,1306	0,1233	0,1111	0,0935	0,0838	0,0631	0,0376	0,0299	0,0231	0,0061	0,0032	0,0004
						M = 2						
0,05	2,0381	1,9602	1,6265	1,6202	1,5010	1,2249	0,8307	0,6967	0,5678	0,1866	0,1071	0,0148
0,1	1,8168	1,7445	1,6210	1,4311	1,3217	1,0700	0,7146	0,5953	0,4815	0,1523	0,0862	0,0113
0,5	1,1757	1,1244	1,0355	0,9001	0,8243	0,6517	0,4176	0,3419	0,2713	0,0791	0,0435	0,0053
1	0,8892	0,8475	0,7769	0,6709	0,6113	0,4779	0,3007	0,2444	0,1926	0,0545	0,0297	0,0035
3	0,4994	0,4740	0,4315	0,3684	0,3333	0,2564	0,1572	0,1266	0,0987	0,0269	0,0145	0,0017
5	0,3615	0,3425	0,3108	0,2641	0,2383	0,1821	0,1106	0,0887	0,0689	0,0186	0,0099	0,0011
10	0,2216	0,2095	0,1894	0,1601	0,1440	0,1092	0,0656	0,0524	0,0406	0,0108	0,0058	0,0007
15	0,1625	0,1534	0,1385	0,1167	0,1049	0,0792	0,0473	0,0377	0,0291	0,0077	0,0041	0,0005
20	0,1291	0,1218	0,1098	0,0924	0,0829	0,0625	0,0272	0,0296	0,0228	0,0060	0,0032	0,0004

(cont'd)

ϕ	h_1											
	0	0,1	0,3	0,7	1	2	5	7	10	50	100	1 000
						M = 4						
0,05	1,2430	1,1935	1,1091	0,9800	0,9060	0,7363	0,4976	0,4172	0,3404	0,1134	0,0658	0,0096
0,1	1,1519	1,1047	1,0244	0,9019	0,8318	0,6718	0,4485	0,3740	0,3031	0,0976	0,0558	0,0077
0,5	0,8476	0,8097	0,7454	0,6483	0,5935	0,4699	0,3025	0,2483	0,1977	0,0586	0,0325	0,0040
1	0,6844	0,6523	0,5982	0,5169	0,4712	0,3693	0,2335	0,1904	0,1504	0,0432	0,0237	0,0029
3	0,4257	0,4042	0,3681	0,3145	0,2849	0,2196	0,1353	0,1091	0,0853	0,0235	0,0127	0,0015
5	0,3208	0,3040	0,2760	0,2348	0,2120	0,1624	0,0989	0,0795	0,0619	0,0168	0,0090	0,0010
10	0,2053	0,1942	0,1757	0,1486	0,1337	0,1015	0,0611	0,0489	0,0379	0,0101	0,0054	0,0007
15	0,1535	0,1450	0,1309	0,1104	0,0992	0,0750	0,0449	0,0358	0,0277	0,0073	0,0039	0,0004
20	0,1233	0,1164	0,1049	0,0884	0,0793	0,0598	0,0357	0,0284	0,0220	0,0058	0,0031	0,0004
						M = 6						
0,05	0,7786	0,7467	0,6924	0,6099	0,5630	0,4561	0,3075	0,2578	0,2105	0,0710	0,0417	0,0064
0,1	0,7378	0,7669	0,6544	0,5748	0,5296	0,4269	0,2849	0,2378	0,1931	0,0632	0,0364	0,0052
0,5	0,5913	0,5647	0,5197	0,4520	0,4139	0,3281	0,2122	0,1747	0,1396	0,0422	0,0235	0,0030
1	0,5032	0,4997	0,4599	0,3805	0,3471	0,2726	0,1734	0,1417	0,1124	0,0328	0,0181	0,0022
3	0,3446	0,3273	0,2983	0,2554	0,2315	0,1790	0,1108	0,0896	0,0703	0,0196	0,0106	0,0012
5	0,2715	0,2575	0,2340	0,1993	0,1801	0,1383	0,0847	0,0682	0,0532	0,0146	0,0078	0,0009
10	0,1835	0,1736	0,1571	0,1330	0,1198	0,0912	0,0551	0,0441	0,0342	0,0092	0,0049	0,0005
15	0,1408	0,1330	0,1202	0,1014	0,0912	0,0691	0,0414	0,0331	0,0256	0,0068	0,0036	0,0004
20	0,1149	0,1085	0,0979	0,0824	0,0740	0,0559	0,0334	0,0266	0,0206	0,0055	0,0029	0,0003
						M = 8						
0,05	0,5218	0,4999	0,4629	0,4069	0,3752	0,3034	0,2042	0,1713	0,1399	0,0478	0,0283	0,0045
0,1	0,8003	0,4790	0,4429	0,3884	0,3576	0,2879	0,1921	0,1605	0,1305	0,0432	0,0252	0,0038
0,5	0,4225	0,4034	0,3712	0,3229	0,2956	0,2447	0,1524	0,1257	0,1007	0,0309	0,0174	0,0022
1	0,3727	0,3552	0,3259	0,2820	0,2575	0,2026	0,1296	0,1062	0,0845	0,0251	0,0139	0,0017
3	0,2748	0,2611	0,2382	0,2042	0,1853	0,1436	0,0895	0,0725	0,0571	0,0161	0,0087	0,0010
5	0,2252	0,2136	0,1943	0,1657	0,1499	0,1155	0,0710	0,0574	0,0449	0,0124	0,0067	0,0008
10	0,1603	0,1517	0,1375	0,1166	0,1051	0,0802	0,0486	0,0390	0,0303	0,0082	0,0044	0,0005
15	0,1265	0,1195	0,1081	0,0913	0,0822	0,0624	0,0386	0,0301	0,0233	0,0062	0,0033	0,0004
20	0,1051	0,0992	0,0896	0,0756	0,0679	0,0514	0,0308	0,0246	0,0190	0,0051	0,0027	0,0003
						M = 10						
0,05	0,3711	0,3553	0,3287	0,2886	0,2859	0,2147	0,1446	0,1212	0,0991	0,0342	0,0204	0,0035
0,1	0,3581	0,3428	0,3166	0,2773	0,2552	0,2053	0,1370	0,1145	0,0932	0,0312	0,0183	0,0028
0,5	0,3125	0,2984	0,2745	0,2387	0,2187	0,1737	0,1132	0,0936	0,0752	0,0234	0,0133	0,0018
1	0,2824	0,2692	0,2471	0,2139	0,1954	0,1541	0,0989	0,0813	0,0648	0,0196	0,0109	0,0014
3	0,2198	0,2089	0,1907	0,1637	0,1487	0,1156	0,0724	0,0588	0,0464	0,0133	0,0072	0,0009
5	0,1859	0,1764	0,1605	0,1372	0,1243	0,0959	0,0594	0,0480	0,0376	0,0105	0,0057	0,0006
10	0,1385	0,1311	0,1189	0,1010	0,0911	0,0697	0,0425	0,0342	0,0266	0,0072	0,0039	0,0004
15	0,1122	0,1061	0,0960	0,0812	0,0732	0,0557	0,0337	0,0269	0,0209	0,0056	0,0030	0,0003
20	0,0949	0,0896	0,0810	0,0684	0,0615	0,0465	0,0281	0,0224	0,0174	0,0046	0,0025	0,0002
						M = 12						
0,05	0,2766	0,2647	0,2448	0,2147	0,1977	0,1596	0,1074	0,0902	0,0739	0,0252	0,0155	0,0028
0,1	0,2678	0,2562	0,2365	0,2071	0,1904	0,1531	0,1022	0,0855	0,0697	0,0236	0,0139	0,0022
0,5	0,2388	0,2280	0,2097	0,1824	0,1671	0,1329	0,0868	0,0718	0,0578	0,0182	0,0104	0,0014
1	0,2195	0,2093	0,1921	0,1664	0,1621	0,1200	0,0774	0,0637	0,0509	0,0156	0,0087	0,0011
3	0,1778	0,1691	0,1544	0,1327	0,1206	0,0940	0,0592	0,0482	0,0381	0,0110	0,0061	0,0007
5	0,1541	0,1462	0,1332	0,1140	0,1033	0,0800	0,0497	0,0403	0,0317	0,0089	0,0050	0,0005
10	0,1193	0,1130	0,1025	0,0872	0,0788	0,0604	0,0370	0,0298	0,0232	0,0064	0,0036	0,0004
15	0,0989	0,0936	0,0847	0,0718	0,0647	0,0494	0,0299	0,0240	0,0187	0,0051	0,0027	0,0003
20	0,0850	0,0803	0,0727	0,0614	0,0553	0,0420	0,0253	0,0203	0,0158	0,0042	0,0023	0,0002
Helium-air												
						M = 0						
0,05	2,6607	2,3524	2,0411	1,7192	1,5853	1,2456	0,8277	0,6906	0,5599	0,1801	0,1026	0,0138
0,1	2,2987	2,0332	1,7600	1,4746	1,3378	1,0546	0,6887	0,5703	0,4586	0,1420	0,0797	0,0102
0,5	1,3648	1,2087	1,0399	0,8583	0,7709	0,5922	0,3699	0,3008	0,2372	0,0678	0,0370	0,0044
1	0,9933	0,9411	0,7556	0,6193	0,5538	0,4206	0,2579	0,2082	0,1630	0,0453	0,0245	0,0029
3	0,5310	0,4714	0,4030	0,3272	0,2907	0,2172	0,1298	0,1038	0,0805	0,0216	0,0116	0,0013
5	0,3778	0,3356	0,2866	0,2317	0,2054	0,1525	0,0903	0,0720	0,0556	0,0148	0,0079	0,0009
10	0,2277	0,2024	0,1726	0,1390	0,1228	0,0905	0,0530	0,0421	0,0324	0,0085	0,0045	0,0005
15	0,1657	0,1474	0,1256	0,1009	0,0891	0,0655	0,0381	0,0302	0,0232	0,0060	0,0032	0,0003
20	0,1312	0,1167	0,0994	0,0798	0,0703	0,0515	0,0299	0,0237	0,0182	0,0047	0,0025	0,0003

(cont'd)

φ	b_1											
	0	0,1	0,3	0,7	1	2	5	7	10	50	100	1 000
						M = 1						
0,05	2,4670	2,1814	1,8922	1,5929	1,4497	1,1527	0,7654	0,6384	0,5178	0,1669	0,0952	0,0129
0,1	2,1524	1,9039	1,6480	1,3802	1,2519	0,9865	0,6441	0,5334	0,4291	0,1332	0,0749	0,0097
0,5	1,3115	1,1616	0,9995	0,8249	0,7410	0,5693	0,3558	0,2894	0,2284	0,0654	0,0357	0,0043
1	0,9647	0,8552	0,7339	0,6016	0,5380	0,4087	0,2507	0,2025	0,1586	0,0441	0,0239	0,0028
3	0,5227	0,4640	0,3968	0,3221	0,2862	0,2139	0,1279	0,1023	0,0794	0,0213	0,0114	0,0013
5	0,3736	0,3319	0,2834	0,2292	0,2031	0,1508	0,0893	0,0712	0,0550	0,0146	0,0078	0,0009
10	0,2261	0,2010	0,1714	0,1380	0,1220	0,0899	0,0527	0,0418	0,0322	0,0084	0,0045	0,0005
15	0,1649	0,1467	0,1250	0,1004	0,0886	0,0651	0,0379	0,0301	0,0231	0,0060	0,0032	0,0003
20	0,1306	0,1162	0,0990	0,0795	0,0700	0,0514	0,0298	0,0236	0,0181	0,0047	0,0025	0,0003
						M = 2						
0,05	2,0381	1,8027	1,5629	1,3137	1,1946	0,9480	0,6283	0,5241	0,4251	0,1379	0,0790	0,0108
0,1	1,8167	1,6074	1,3909	1,1638	1,0551	0,8305	0,5421	0,4491	0,3615	0,1130	0,0638	0,0083
0,5	1,1767	1,0423	0,8969	0,7403	0,6651	0,5112	0,3200	0,2605	0,2058	0,0593	0,0325	0,0039
1	0,8892	0,7882	0,6766	0,5548	0,4962	0,3772	0,2318	0,1874	0,1469	0,0411	0,0223	0,0026
3	0,4994	0,4433	0,3792	0,3079	0,2736	0,2046	0,1225	0,0981	0,0761	0,0205	0,0110	0,0012
5	0,3615	0,3211	0,2743	0,2219	0,1957	0,1461	0,0866	0,0691	0,0534	0,0142	0,0076	0,0008
10	0,2216	0,1970	0,1680	0,1353	0,1195	0,0882	0,0517	0,0411	0,0316	0,0083	0,0044	0,0005
15	0,1624	0,1445	0,1232	0,0989	0,0873	0,0642	0,0374	0,0297	0,0228	0,0059	0,0032	0,0003
20	0,1291	0,1147	0,0979	0,0785	0,0693	0,0508	0,0296	0,0234	0,0179	0,0046	0,0025	0,0003
						M = 4						
0,05	1,2430	1,1002	0,9528	0,7983	0,7244	0,5724	0,3778	0,3150	0,2557	0,0841	0,0487	0,0070
0,1	1,1518	1,0198	0,8819	0,7363	0,6666	0,5235	0,3414	0,2830	0,2283	0,0726	0,0414	0,0056
0,5	0,8476	0,7511	0,6465	0,5339	0,4797	0,3692	0,2321	0,1895	0,1501	0,0440	0,0243	0,0030
1	0,6844	0,6068	0,5212	0,4278	0,3829	0,2917	0,1802	0,1460	0,1148	0,0326	0,0178	0,0021
3	0,4257	0,3779	0,3234	0,2630	0,2338	0,1753	0,1054	0,0845	0,0657	0,0179	0,0096	0,0011
5	0,3207	0,2849	0,2435	0,1972	0,1749	0,1302	0,0775	0,0618	0,0479	0,0128	0,0069	0,0008
10	0,2054	0,1826	0,1558	0,1255	0,1110	0,0820	0,0482	0,0383	0,0295	0,0078	0,0041	0,0004
15	0,1535	0,1365	0,1164	0,0936	0,0826	0,0608	0,0355	0,0282	0,0216	0,0056	0,0030	0,0003
20	0,1233	0,1097	0,0935	0,0751	0,0662	0,0486	0,0283	0,0224	0,0172	0,0045	0,0024	0,0003
						M = 6						
0,05	0,7786	0,6896	0,5968	0,4988	0,4519	0,3559	0,2343	0,1953	0,1596	0,0528	0,0308	0,0047
0,1	0,7378	0,6535	0,5649	0,4709	0,4259	0,3337	0,2175	0,1805	0,1458	0,0471	0,0271	0,0038
0,5	0,5913	0,5241	0,4513	0,3728	0,3351	0,2583	0,1631	0,1334	0,1061	0,0316	0,0176	0,0022
1	0,5033	0,4463	0,3835	0,3152	0,2823	0,2156	0,1339	0,1088	0,0859	0,0247	0,0136	0,0016
3	0,3447	0,3060	0,2620	0,2134	0,1899	0,1428	0,0863	0,0694	0,0542	0,0149	0,0080	0,0009
5	0,2716	0,2412	0,2053	0,1673	0,1485	0,1109	0,0663	0,0530	0,0412	0,0111	0,0060	0,0007
10	0,1835	0,1631	0,1392	0,1124	0,0994	0,0736	0,0434	0,0345	0,0267	0,0071	0,0038	0,0004
15	0,1407	0,1252	0,1068	0,0859	0,0759	0,0559	0,0328	0,0260	0,0200	0,0053	0,0028	0,0003
20	0,1149	0,1022	0,0871	0,0700	0,0618	0,0454	0,0265	0,0210	0,0161	0,0042	0,0022	0,0002
						M = 8						
0,05	0,5218	0,4623	0,3999	0,3337	0,3021	0,2374	0,1560	0,1308	0,1057	0,0355	0,0210	0,0033
0,1	0,5003	0,4434	0,3831	0,3190	0,2883	0,2256	0,1470	0,1220	0,0987	0,0323	0,0187	0,0028
0,5	0,4225	0,3746	0,3227	0,2666	0,2397	0,1850	0,1172	0,0962	0,0766	0,0232	0,0130	0,0017
1	0,3727	0,3305	0,2842	0,2338	0,2095	0,1603	0,1001	0,0815	0,0645	0 0189	0,0104	0,0013
3	0,2748	0,2440	0,2091	0,1705	0,1520	0,1146	0,0697	0,0562	0,0439	0,0122	0,0066	0,0008
5	0,2252	0,2000	0,1711	0,1390	0,1236	0,0925	0,0556	0,0446	0,0347	0,0095	0,0051	0,0006
10	0,1603	0,1425	0,1217	0,0983	0,0871	0,0646	0,0382	0,0305	0,0236	0,0063	0,0034	0,0004
15	0,1264	0,1125	0,0960	0,0773	0,0684	0,0505	0,0297	0,0236	0,0182	0,0048	0,0026	0,0003
20	0,1050	0,0935	0,0797	0,0641	0,0566	0,0417	0,0244	0,0194	0,0149	0,0039	0,0021	0,0002
						M = 10						
0,05	0,3711	0,3289	0,2844	0,2371	0,2145	0,1684	0,1105	0,0922	0,0750	0,0255	0,0151	0,0025
0,1	0,3581	0,3174	0,2742	0,2282	0,2061	0,1612	0,1050	0,0872	0,0706	0,0233	0,0136	0,0021
0,5	0,3125	0,2772	0,2388	0,1974	0,1775	0,1371	0,0872	0,0716	0,0572	0,0176	0,0099	0,0013
1	0,2824	0,2505	0,2151	0,1774	0,1591	0,1220	0,0765	0,0624	0,0496	0,0147	0,0082	0,0010
3	0,2198	0,1952	0,1674	0,1367	0,1219	0,0922	0,0564	0,0455	0,0357	0,0101	0,0055	0,0006
5	0,1859	0,1651	0,1414	0,1150	0,1023	0,0768	0,0464	0,0373	0,0291	0,0080	0,0043	0,0005
10	0,1385	0,1231	0,1052	0,0852	0,0755	0,0661	0,0334	0,0267	0,0207	0,0055	0,0030	0,0003
15	0,1122	0,0997	0,0852	0,0687	0,0608	0,0450	0,0265	0,0212	0,0164	0,0043	0,0023	0,0003
20	0,0949	0,0844	0,0720	0,0580	0,0812	0,0378	0,0222	0,0176	0,0136	0,0036	0,0019	0,0002

U.S. GOVERNMENT PRINTING OFFICE: 1974—635-043/15

(cont'd)

ϕ	b_1											
	0	0,1	0,3	0,7	1	2	5	7	10	50	100	1 000
						M = 12						
0,05	0,2766	0,2452	0,2120	0,1767	0,1598	0,1253	0,0823	0,0687	0,0559	0,0192	0,0115	0,0020
0,1	0,2678	0,2374	0,2051	0,1706	0,1540	0,1204	0,0784	0,0652	0,0528	0,0176	0,0104	0,0016
0,5	0,2388	0,2118	0,1826	0,1509	0,1358	0,1049	0,0669	0,0550	0,0440	0,0137	0,0077	0,0010
1	0,2196	0,1948	0,1676	0,1381	0,1239	0,0951	0,0598	0,0489	0,0389	0,0117	0,0065	0,0008
3	0,1778	0,1579	0,1355	0,0108	0,0989	0,0749	0,0460	0,0373	0,0293	0,0084	0,0046	0,0005
5	0,1540	0,1368	0,1172	0,0955	0,0851	0,0640	0,0389	0,0313	0,0245	0,0068	0,0037	0,0004
10	0,1193	0,1060	0,0907	0,0735	0,0652	0,0486	0,0290	0,0233	0,0181	0,0049	0,0026	0,0003
15	0,0989	0,0879	0,0751	0,0607	0,0537	0,0399	0,0236	0,0189	0,0146	0,0039	0,0021	0,0002
20	0,0850	0,0756	0,0646	0,0521	0,0461	0,0341	0,0200	0,0159	0,0123	0,0033	0,0017	0,0002
Hydrogen-air												
						M=0						
0,05	2,6608	2,5482	2,3717	2,1057	1,9524	1,5965	1,0845	0,9095	0,7409	0,2409	0,1376	0,0185
0,1	2,2987	2,1977	2,0386	1,7998	1,6628	1,3471	0,8995	0,7487	0,6049	0,1894	0,1066	0,0138
0,5	1,3648	1,2980	1,1923	1,0355	0,9471	0,7478	0,4778	0,3906	0,3095	0,0895	0,0490	0,0059
1	0,9933	0,9424	0,8615	0,7425	0,6760	0,5278	0,3310	0,2887	0,2114	0,0595	0,0323	0,0038
3	0,5310	0,5018	0,4555	0,3880	0,3509	0,2695	0,1648	0,1326	0,1033	0,0281	0,0151	0,0017
5	0,3778	0,3565	0,3229	0,2735	0,2467	0,1882	0,1141	0,0914	0,0710	0,0191	0,0102	0,0011
10	0,2277	0,2144	0,1933	0,1630	0,1465	0,1110	0,0665	0,0531	0,0411	0,0109	0,0058	0,0007
15	0,1657	0,1559	0,1403	0,1180	0,1059	0,0799	0,0477	0,0380	0,0293	0,0077	0,0041	0,0005
20	0,1312	0,1233	0,1108	0,0931	0,0834	0,0628	0,0374	0,0297	0,0229	0,0060	0,0032	0,0004
						M = 1						
0,05	2,4670	2,3619	2,1973	1,9495	1,8069	1,4764	1,0023	0,8405	0,6848	0,2233	0,1277	0,0173
0,1	2,1524	2,0574	1,9079	1,6836	1,5551	1,2593	0,8408	0,7000	0,5657	0,1776	0,1001	0,0129
0,5	1,3115	1,2473	1,1457	0,9951	0,9101	0,7187	0,4595	0,3758	0,2979	0,0863	0,0473	0,0057
1	0,9647	0,9152	0,8367	0,7212	0,6566	0,5127	0,3218	0,2613	0,2058	0,0579	0,0315	0,0037
3	0,5227	0,4940	0,4483	0,3820	0,3455	0,2654	0,1624	0,1306	0,1018	0,0277	0,0149	0,0017
5	0,3736	0,3525	0,3190	0,2706	0,2440	0,1862	0,1129	0,0905	0,0703	0,0190	0,0101	0,0012
10	0,2261	0,2229	0,1920	0,1619	0,1456	0,1102	0,0661	0,0528	0,0409	0,0108	0,0058	0,0006
15	0,1649	0,1551	0,1396	0,1174	0,1054	0,0796	0,0475	0,0378	0,0292	0,0077	0,0041	0,0005
20	0,1306	0,1228	0,1104	0,0927	0,0831	0,0626	0,0372	0,0296	0,0229	0,0060	0,0032	0,0003
						M = 2						
0,05	2,0381	1,9500	1,8120	1,6048	1,4861	1,2120	0,8215	0,6889	0,5614	0,1842	0,1058	0,0146
0,1	1,8168	1,7357	1,6083	1,4176	1,3087	1,0587	0,7067	0,5886	0,4761	0,1505	0,0852	0,0112
0,5	1,1767	1,1190	1,0277	0,8926	0,8164	0,6450	0,4030	0,3381	0,2683	0,0782	0,0429	0,0052
1	0,8892	0,8436	0,7712	0,6650	0,6055	0,4731	0,2975	0,2418	0,1904	0,0640	0,0293	0,0035
3	0,4994	0,4720	0,4285	0,3652	0,3303	0,2539	0,1556	0,1253	0,0977	0,0266	0,0144	0,0016
5	0,3615	0,3411	0,3087	0,2619	0,2362	0,1804	0,1095	0,0878	0,0682	0,0184	0,0098	0,0011
10	0,2216	0,2087	0,1882	0,1587	0,1427	0,1082	0,0649	0,0518	0,0401	0,0107	0,0057	0,0006
15	0,1625	0,1528	0,1376	0,1157	0,1039	0,0784	0,0468	0,0373	0,0288	0,0076	0,0041	0,0005
20	0,1291	0,1214	0,1091	0,0916	0,0822	0,0619	0,0368	0,0293	0,0226	0,0059	0,0032	0,0003
						M = 4						
0,05	1,2430	1,1875	1,1004	0,9008	0,8971	0,7286	0,4921	0,4126	0,3365	0,1121	0,0651	0,0095
0,1	1,1586	1,0992	1,0165	0,8935	0,8237	0,6648	0,4436	0,3699	0,2997	0,0965	0,0552	0,0076
0,5	0,8476	0,8058	0,7399	0,6426	0,5879	0,4651	0,2992	0,2456	0,1955	0,0580	0,0321	0,0040
1	0,6844	0,6494	0,5938	0,5123	0,4668	0,3655	0,2310	0,1883	0,1488	0,0427	0,0234	0,0028
3	0,4257	0,4024	0,3655	0,3119	0,2823	0,2175	0,1339	0,1079	0,0844	0,0232	0,0126	0,0015
5	0,3207	0,3027	0,2742	0,2328	0,2101	0,1608	0,0979	0,0786	0,0612	0,0166	0,0089	0,0010
10	0,2054	0,1934	0,1746	0,1473	0,1325	0,1006	0,0605	0,0484	0,0375	0,0100	0,0053	0,0006
15	0,1535	0,1444	0,1301	0,1095	0,0983	0,0743	0,0444	0,0355	0,0274	0,0073	0,0039	0,0004
20	0,1233	0,1160	0,1043	0,0877	0,0786	0,0593	0,0353	0,0282	0,0217	0,0057	0,0031	0,0003

(cont'd)

ϕ	b_1											
	0	0,1	0,3	0,7	1	2	5	7	10	50	100	1 000
						M = 6						
0,05	0,7787	0,7430	0,6872	0,6044	0,5776	0,4514	0,3041	0,2550	0,2081	0,0702	0,0412	0,0063
0,1	0,7378	0,7035	0,6995	0,5696	0,5245	0,4225	0,2818	0,2352	0,1909	0,0625	0,0361	0,0052
0,5	0,5913	0,5621	0,5159	0,4480	0,4099	0,3248	0,2099	0,1728	0,1380	0,0417	0,0233	0,0023
1	0,5033	0,4775	0,4368	0,3772	0,3439	0,2699	0,1716	0,1402	0,1112	0,0325	0,0179	0,0022
3	0,3446	0,3260	0,2963	0,2532	0,2294	0,1773	0,1097	0,0887	0,0695	0,0194	0,0105	0,0012
5	0,2716	0,2564	0,2324	0,1977	0,1786	0,1370	0,0838	0,0675	0,0526	0,0144	0,0078	0,0009
10	0,1835	0,1729	0,1561	0,1320	0,1188	0,0903	0,0545	0,0437	0,0339	0,0091	0,0049	0,0005
15	0,1408	0,1325	0,1194	0,1006	0,0904	0,0684	0,0410	0,0328	0,0254	0,0067	0,0036	0,0004
20	0,1149	0,1081	0,0973	0,0818	0,0734	0,0554	0,0331	0,0264	0,0204	0,0054	0,0029	0,0003
						M = 8						
0,05	0,5218	0,4975	0,4594	0,4033	0,3716	0,3003	0,2021	0,1694	0,1384	0,0472	0,0280	0,0045
0,1	0,5003	0,4767	0,4396	0,3850	0,3542	0,2850	0,1900	0,1587	0,1291	0,0428	0,0249	0,0037
0,5	0,4225	0,4015	0,3685	0,3200	0,2929	0,2323	0,1507	0,1244	0,0996	0,0306	0,0172	0,0022
1	0,3727	0,3536	0,3236	0,2796	0,2551	0,2006	0,1282	0,1051	0,0836	0,0248	0,0138	0,0017
3	0,2748	0,2599	0,2365	0,2024	0,1836	0,1422	0,0885	0,0718	0,0564	0,0159	0,0087	0,0010
5	0,2252	0,2127	0,1930	0,1644	0,1486	0,1143	0,0703	0,0567	0,0444	0,0123	0,0066	0,0007
10	0,1603	0,1511	0,1366	0,1156	0,1042	0,0794	0,0481	0,0386	0,0300	0,0081	0,0043	0,0005
15	0,1265	0,1191	0,1074	0,0906	0,0815	0,0618	0,0372	0,0298	0,0231	0,0062	0,0033	0,0004
20	0,1051	0,0989	0,0890	0,0750	0,0673	0,0509	0,0305	0,0244	0,0188	0,0050	0,0027	0,0003
						M = 10						
0,05	0,3711	0,3536	0,3263	0,2860	0,2634	0,2125	0,1429	0,1199	0,0980	0,0338	0,0202	0,0034
0,1	0,3581	0,3410	0,3142	0,2748	0,2527	0,2032	0,1355	0,1133	0,0922	0,0309	0,0181	0,0028
0,5	0,3125	0,2970	0,2725	0,2366	0,2166	0,1720	0,1120	0,0925	0,0743	0,0232	0,0131	0,0017
1	0,2824	0,2680	0,2453	0,2121	0,1936	0,1525	0,0979	0,0804	0,0642	0,0193	0,0108	0,0014
3	0,2198	0,2080	0,1894	0,1623	0,1473	0,1145	0,0717	0,0582	0,0459	0,0131	0,0072	0,0009
5	0,1859	0,1756	0,1595	0,1360	0,1232	0,0950	0,0587	0,0475	0,0373	0,0104	0,0057	0,0007
10	0,1385	0,1306	0,1181	0,1002	0,0903	0,0690	0,0420	0,0338	0,0263	0,0072	0,0039	0,0004
15	0,1122	0,1057	0,0951	0,0856	0,0725	0,0551	0,0333	0,0267	0,0207	0,0056	0,0030	0,0003
20	0,0949	0,0893	0,0805	0,0678	0,0609	0,0462	0,0278	0,0222	0,0172	0,0046	0,0025	0,0003
						M = 12						
0,05	0,2766	0,2635	0,2430	0,2128	0,1959	0,1580	0,1062	0,0892	0,0730	0,0255	0,0153	0,0027
0,1	0,2678	0,2549	0,2347	0,2052	0,1886	0,1515	0,1011	0,0846	0,0689	0,0233	0,0137	0,0022
0,5	0,2388	0,2269	0,2882	0,1808	0,1656	0,1315	0,0859	0,0711	0,0572	0,0181	0,0103	0,0014
1	0,2195	0,2084	0,1907	0,1650	0,1507	0,1189	0,0766	0,0630	0,0504	0,0154	0,0086	0,0011
3	0,1778	0,1683	0,1533	0,1315	0,1195	0,0931	0,0585	0,0477	0,0377	0,0109	0,0060	0,0007
5	0,1541	0,1456	0,1323	0,1130	0,1024	0,0792	0,0492	0,0399	0,0313	0,0089	0,0048	0,0006
10	0,1193	0,1125	0,1018	0,0865	0,0781	0,0598	0,0366	0,0295	0,0230	0,0063	0,0034	0,0004
15	0,0989	0,0932	0,0842	0,0712	0,0642	0,0489	0,0297	0,0238	0,0185	0,0050	0,0027	0,0003
20	0,0850	0,0801	0,0722	0,0609	0,0548	0,0416	0,0251	0,0201	0,0156	0,0042	0,0022	0,0003

REFERENCES

1. Abramovich, G. N. Theory of Turbulent Jets. Moscow, Phys.-Math. Press, 1960.
2. Avduevskiy, V. S. Bull. Acad. Sci. USSR Div. Tech. Sci. Mech. and Mach. Const., No. 4, 1960.
3. Avduevskiy, V. S. Bull. Acad. Sci. USSR. Power Engr. and Transportation, No. 5, 1967.
4. Alad'ev, I. T. Bull. Acad. Sci. USSR. Div. Tech. Sci., No. 11, 1951.
5. Ambrok, G. S. J. Tech. Phys., Vol. XXVII, No. 9, 1957.
6. Belyanin, N. M. Appl. Math. and Tech. Phys., No. 4, 1964.
7. Baryshev, Yu. V. and Rozhdestvenskiy, V. I. et al. Bull. Acad. Sci. USSR. Fluid and Gas Mech., No. 2, 1972.
8. Styrikovich, M. A., Mostinskiy, I. L. and Vizel, Ya. M. High-Temperature Phys., Vol. 6, No. 4, 1968.
9. Volchkov, E. P., Kutateladze, S. S. and Leont'ev, A. I. Appl. Math. and Tech. Phys., No. 2, 1965.
10. Volchkov, E. P., Kutateladze, S. S. and Leont'ev, A. I. Ibid, No. 4, 1966.
11. Volchkov, E. P., Zaulichnyy, S. G., Kutateladze, S. S. and Leont'ev, A. I. Ibid, No. 2, 1967.
12. Volchkov, E. P. and Levchenko, V. Ya. Ibid, No. 5, 1965.
13. Volchkov, E. P., Kutateladze, S. S., Levchenko, V. Ya. and Leont'ev, A. I. Ibid, No. 3, 1966.
14. Volchkov, E. P., Zaulichnyy, S. G., Leont'ev, A. I. and Sinaiko, E. I. Combustion and Explosion Physics, No. 2, 1967.
15. Volchkov, E. P. Paper read at the International Seminar in Herzegnovy, Jugoslavia, 1969.
16. Volchkov, E. P., Zaulichnyy, S. G., Leont'ev, A. I. and Sinaiko, E. I. High-Temperature Physics, Vol. 8, No. 1, 1970.
17. Volkov, Yu. M., Malyuta, D. D. and Panchenko, V. P. Trans. of the Atomic Energy Inst.
18. Vasil'ev, D. N. Appl. Math. and Tech. Phys., No. 3, 1971.
19. Van Dyke, Milton D. Perturbation Methods in Fluid Mechanics. New York, Academic Press, 1964.
20. Ginzburg, I. P. Bulletin of Leningrad State Univ., No. 7, 1963.
21. Ginzburg, I. P. and Kust'yaninova, N. S. J. Engr. Phys., Vol. IX, No. 4, 1965.
22. Gol'clshtik, M. A. and Kutateladze, S. S. In the book: Wall Turbulence. Novosibrisk, Press of the Sib. Branch of the Acad. Sci. USSR, 1968.
23. Gukhman, A. A. and Dyukshin, N. V. Principles of the Theory of Heat Exchange in a High-Speed Gas Flow. State Machine-Construction Lit. Press, 1950.
24. Gurfnik, M. M. Mechanics. Bull. Acad. Sci. USSR, No. 5, 1965.
25. Dorodnitsyn, A. A. Appl. Math. and Mech., Vol. VI, No. 6, 1942.
26. Dedyakin, B. V. and Lel'chuk, V. L. Thermal Power Engineering, No. 9, 1959.
27. Ermolaev, I. K. and Fadeev, V. A. Trans. of the Moscow Advanced Technol. Institute, No. 6, 1970.
28. Zhukauskas, A., Makaryavichus, V. and Shlanchauskas, A. Heat Transfer of Pipe Clusters in a Cross Flow of Fluid. Vilnius, "Mintis" Press, 1968.
29. Zysina-Molozhen, L. S. and Loskova, I. N. In the book: Heat and Mass Transfer. Vol. 1, Moscow, "Energy" Press, 1968.
30. Ievlev, V. M. Proc. Acad. Sci. USSR, Vol. 86, No. 6, 1952.
31. Ievlev, V. M. Ibid, Vol. 87, No. 1, 1952.

32. Ievlev, V. M. Bull. Acad. Sci. USSR. Fluid and Gas Mech., No. 1, 1970.
33. Il'in, L. N. Boiler Turbine Construction, No. 1, 1951.
34. Ivashchenko, N. I. Thermal Power Eng., No. 2, 1958.
35. Idel'chuk, I. E. Handbook on Hydraulic Drag. Moscos-Leningrad, State Power Press, 1960.
36. Kalikhman, L. E. Turbulent Boundary Layer on a Curvilinear Surface in a Gas Flow. Defence Press, 1956.
37. Kalikhman, L. E. Appl. Math. and Mech., Vol. X, No. 4, 1946.
38. Kalikhman, L. E. J. Tech. Phys., Vol. XXV, No. 11, 1955.
39. Kibardin, Yu. A., Juznetsov, S. A. and Shumyatskiy, V. Ya. Atlas of Gas-dynamic Functions at High Velocities and Temperatures for Air Flows. Moscow-Leningrad, State Power Lit. Press, 1961.
40. Karman, T. von. In the book: Gas Dynamics. Joint State Sci-Tech. Publ. House, 1939.
41. Kutateladze, S. S. Thermal Power Engineering, No. 7, 1956.
42. Kutateladze, S. S. Appl. Math. and Tech. Phys., No. 1, 1960.
43. Kutateladze, S. S. Principles of Heat Transfer Theory. Novosibirsk, Publ. House of the Sib. Branch of the Acad. Sci. USSR, 1970.
44. Kutateladze, S. S. and Leont'ev, A. I. Turbulent Boundary Layer of a Compressible Gas. Novosibirsk, Publ. House of Sib. Branch of the Acad. Sci. USSR, 1962.
45. Kutateladze, S. S., Leont'ev, A. I. et al. In the book: Friction and Heat- and Mass Transfer in a Turbulent Boundary Layer. Novosibirsk, Publ. House of the Sib. Branch of the Acad. Sci. USSR, 1964.
46. Kutateladze, S. S., Leont'ev, A. I. and Pimenov, A. K. High-Temperature Physics, No. 4, 1966.
47. Kutateladze, S. S., Zaulichnyy, E. G. and Leont'ev, A. I. Appl. Math. and Tech. Phys., No. 4, 1967.
48. Kutateladze, S. S. and Borishanskiy, V. M. Manual on Heat Transfer. Moscow-Leningrad, State Power Lit. Press, 1959.
49. Kutateladze, S. S. In the book: Wall Turbulence. Novosibirsk, Publ. House of the Sib. Branch of the Acad. Sci. USSR, 1968.
50. Kolmogorov, A. N. Proc. Acad. Sci. USSR, Vol. 30, No. 4, 1941.
51. Komarov, V. P. and Leont'ev, A.I. High-Temperature Phys., Vol. 8, No. 3, 1970.
52. Kozlov, L. V. Bull. Acad. Sci. USSR. Div. Tech. Sci. Mech. and Machine Const., Nos. 2 and 4, 1963.
53. Kosterin, S. I. and Koshmarov, Yu. A. J. Tech. Phys., Vol. XXIX, No. 7, 1959.
54. Kosterin, S. I., Kozhinov, I. A. and Leont'ev, A. I. Thermal Power Engr., No. 3, 1958.
55. Kosterin, S. I., Leont'ev, A. I. and Fedorov, V. K. Ibid, No. 7, 1961.
56. Kruzhilin, G. N. J. Tech. Phys., No. 3, 1936.
57. Landau, L. D. and Lifshits, E. M. Continuum Mechanics. Moscow, State Tech. Lit. Press, 1953.
58. Loitsyanskiy, L. G. Fluid and Gas Mechanics. Moscow, "Science" Press, 1970.
59. Lykov, A. V. and Mikhailov, Yu. A. Theory of Heat and Mass Transfer. Moscow-Leningrad, State Power Lit. Press, 1963.
60. Leont'ev, A. I. In the book: Problems of Power Engineering. Moscow, Acad. Sci. USSR, 1959.
61. Leont'ev, A. I. and Fedorov, V. K. J. Eng. Phys., Vol. 4, No. 8, 1961.

62. Leont'ev, A. I. "Limit Laws of Friction and Heat Exchange in a Turbulent Boundary Layer." Doctor of Technical Sciences Diss., Sib. Branch, Acad. Sci. USSR, 1962.
63. Leont'ev, A. I., Mironov, B. P. and Lugovskoy, P. P. J. Eng. Phys., Vol. 10, No. 4, 1966.
64. Leont'ev, A. I. and Mironov, B. P. Appl. Math. and Tech. Phys., No. 5, 1965.
65. Leont'ev, A. I. Mironov, B. P. and Fafurin, A. V. Ibid, No. 1, 1967.
66. Leont'ev, A. I., Oblivin, A. N. and Romanenko, P. N. Ibid, No. 5, 1961.
67. Leont'ev, A. I. Mironov, B. P. and Fafurin, A. V. Ibid, No. 4, 1968.
68. Leont'ev, A. I., Mironov, B. P. and Fafurin, A. V. J. Eng. Phys., Vol. 16, No. 4, 1969.
69. Leont'ev, A. I., Mironov, B. P. and Fafurin, A. V. High-Temp. Phys., Vol. 7, No. 6, 1969.
70. Leont'ev, A. I. and Fedorov, V. K. J. Eng. Phys., Vol. 10, No. 5, 1966.
71. Leont'ev, A. I., Fafurin, A. V. and Nikitin, P. V. High-Temp. Phys., Vol. 7, No. 2, 1969.
72. Leont'ev, A. I., Mironov, B. P. and Mukhin, V. A. J. Eng. Phys., Vol. XV, No. 1, 1968.
73. Lapin, Yu. V. Turbulent Boundary Layer in Supersonic Gas Flows. Moscow, "Science" Press, 1970.
74. Mikheev, M. A. Principles of Heat Transfer. Moscow-Leningrad, State Power Lit. Press, 1956.
75. Mironov, B. P. and Lugovskoy, P. P. J. Eng. Phys., Vol. 13, No. 4, 1967.
76. Mironov, B. P., Yarygina, N. I. and Smirnov, M. R. Paper presented at the IV Internat. Conf. on Heat Transfer, Paris, 1970.
77. Motulevich, V. P. J. Eng. Phys., Vol. III, No. 8, 1960.
78. Motulevich, V. P. In the book: Physical Gas Dynamics, Heat Transfer and the Thermodynamics of High-Temperature Gases. Moscow, Acad. Sci. USSR, 1962.
79. Motulevich, V. P. J. Eng. Phys., Vol. XIV, No. 1, 1968.
80. Motulevich, V. P. Paper presented at the International Seminar at Herzernovg, Jugoslavia, 1969.
81. Mugalev, V. P. Trans. of the Moscow Phys.-Tech. Inst., No. 4, 1959.
82. Mugalev, V. P. Bull. of Advanced Educat. Insts. Aviation Technol., No. 3, 1959.
83. Mugalev, V. P. In the book: Heat and Mass Transfer. Vol. I, Moscow, "Energy" Press, 1968.
84. Mukhin, V. A., Sukomel, A. S. and Velichko, V. I. J. Eng. Phys., Vol. 5, No. 11, 1962.
85. Petukohv, B. S. and Kirillov, V. V. Thermal Power Eng., No. 5, 1960.
86. Petukhov, B. S., Detlaf, A. A. and Kirillov, V. V. J. Tech. Phys., Vol. XXIV, No. 10, 1954.
87. Petukhov, B. S., Kirillov, V. V., Tsü, Tsu-Siang, and Maidanik, V. N. High-Temp. Phys., Vol. 3, No. 1, 1965.
88. Romanenko, P. N. and Semenov, Yu. P. Thermal Power Eng., No. 1, 1966.
89. Romanenko, P. N. Heat Exchange and Friction in Gradient Fluid Flow. Moscow, "Energy" Press, 1964.
90. Romanenko, P. N. and Kharchenko, V. N. Appl. Math. and Tech. Phys., No. 1, 1963.
91. Sedov, L. I. Similarity and Dimension Methods in Mechanics. Moscow, State Tech. Lit. Publ. House, 1954.
92. Sovershennyy, V. D. Bull. Acad. Sci. USSR. Fluid and Gas Mech., No. 3, 1968.

93. Fafurin, A. V. and Krechetnikov, Yu. O. Bull. Advanced Educat. Insts. Aviation Technology, No. 2, 1969.
94. Fedyaevskiy, K. K. and Ginevskiy, A. S. J. Tech. Phys., Vol. 2, 1967.
95. Frankel, F. and Vlishel, V. Trans. of the Central Aero-Dynamics Inst., No. 321, 1937.
96. Kharchenko, V. N. Ibid, No. 1068, 1967.
97. Chernyy, G. G. Gas Flow at High Supersonic Velocity. Moscow, State Phys.-Math. Publ. House, 1959.
98. Shirokov, M. F. J. Tech. Phys., No. 1, 1937.
99. Shirokov, M. F. Physical Principles of Gas Dynamics and Application of Gas Dynamics to Heat-Transfer and Friction Processes. Moscow, State Phys.-Math. Publ. House, 1958.
100. Schlichting, H. Boundary-Layer Theory. N. Y., McGraw-Hill, 1955.
101. Baker, E. Influence of Mass Transfer on Surface Friction at Porous Surface. TWF/R/3 Imperial College, 1967.
102. Bartle, R. E., Leadon, B. M. In: Proc. of the 1962 Heat Transfer and Fluid Mech. Inst. Stanford University Press, 1962.
103. Bartle, R. E., Leadon, B. M. JAS, Vol. 27, No. 1, 1960.
104. Baylay, F. J. and Turner, A. B. J. Roy. Aero. Soc., Vol. 72, No. 696, 1968.
105. Black, Sarnecki. Aeron. Res. Council, Vol. 20, p. 501, 1958.
106. Bradfield, W. S. and De Coursin, D. V. JAS, Vol. 23, No. 3, 1956.
107. Bradshaw, P., Ferriss, D. H. and Atwell, N. P. J. Fluid Mech. Vol. 28, pt 3, 1967.
108. Brebner, G. C. and Badley, I. A. ARC RM, No. 2886, 1952.
109. Brinich, P. F. and Diaconis, N. S. NACA TN, No. 2742, 1952.
110. Buri, A. Eine Berechnungsgrundlage für die turbulente Grenzschicht bei beschleunigter und verzögerter Strömung. Disseration, Zürich, 1931.
111. Campbell, D. A. and Perkins, H. C. Int. J. Heat Mass Transfer, Vol. 11, No. 6, 1968.
112. Carlson, L. W. and Talmor, E. Int. J. Mass Transfer, Vol. 11, No. 11, 1968.
113. Chapman, D. and Kester, R. JAS, Vol. 20, No. 7, 1953.
114. Chin, G. H., Skirvin, S. C., Hayes, L. E. and Burgraff, U. R. J. Heat Transfer. Trans. ASME, ser. V, Vol. 83, No. 2, 1961.
115. Clarke, J. H., Menkes, H. R. and Libby, P. A. JAS, Vol. 22, No. 4, 1955.
116. Clauser, F. JAS, Vol. 21, No. 2, 1954.
117. Clemmow, D. H. ARC 14051, RM 1568, 1951.
118. Coles, D. JAS, Vol. 21, No. 7, 1954.
119. Cope, W. F. Proc. Roy. Soc., Vol. 215A, No. 1120, 1952.
120. Coulson, G. M. and Richardson, G. F. Chem. Eng., Vol. 1, p. 257, 1954.
121. Crocco, L. AIAA J., Vol. 1, No. 12, 1963.
122. Crocco, L. J. of the Amer. Rocket Society, Vol. 22, No. 6, 1952.
123. Culik, F. E. C. JAS, Vol. 28, No. 9, 1961.
124. Dahman, S. NACA TN, No. 2667, 1952.
125. Danberg, T. E., Winkler, E. M. and Chang, P. K. Proc. of the 1965 Heat Transfer and Fluid Mech. Inst., Stanford Univ. Press, 1965.
126. Denison, R. M. J. Aerospace Sci., Vol. 28, No. 6, 1961.
127. Deisler, R. G. NACA TN, No. 2138, 1950.
128. Donaldson, C. P. NACA TN, No. 2962, 1952.
129. O'Donnell, R. M. NACA TN, No. 3122, 1954.
130. Dorrance, W. and Dore, F. JAS, Vol. 21, No. 6, 1954.
131. Dorrance, W. Viscous Hypersonic Flow. New York, San Francisco, Toronto, London, 1962.

132. Van Driest, E. R. JAS, Vol. 18, No. 3, 1951.
133. Van Driest, E. R. ZAMP, Vol. IX, p. 233-248, 1958.
134. Dunberg, I., Winkler, E. and Chomg, P. K. Heat Transfer and Fluid Mech. Inst. Los Angeles, Calif., Stanford, University Press, 1965.
135. Durgin, F. H. JAS, Vol. 26, No. 6, 1959.
136. Eichhorn, R., Eckert, E. R. and Anderson, A. Trans. ASME, Ser. C, Vol. 82, No. 4, 1960.
137. Fage, A. ARC RM, No. 1852, 1938.
138. Fallis, B. JAS, Vol. 20, No. 9, 1953.
139. Fernandez, F. L. and Zukoski, E. E. AIAA 6th Aerospace Sciences Meeting, New York, January, AIAA Paper, No. 68-129, 1968.
140. Fogarpli, R. P. and Saydah, A. R. AIAA J. Vol. 4, No. 6, 1966.
141. Friedman, J. Jet Propulsion, No. 79, 1949.
142. Furua, G. Memoirs of the Faculty of Engineering of Nagoya Univ., Japan, Vol. 10, No. 1, 1963.
143. Goldstein, R. G., Rask, R. B. and Eckert, E. R. G. Int. J. Heat Mass Transfer, Vol. 9, No. 12, 1966.
144. Goldstein, R. G., Shavit, G. and Chen, T. S. Trans. ASME, Ser. C. Vol. 87, No. 3, 1965.
145. Green, L. and Nali, K. L. JAS, Vol. 26, No. 11, 1959.
146. Grootenhuis, P. J. Roy. Aero. Soc., Vol. 63, No. 578, 1959.
147. Hakkinen, R. J. NACA TN, No. 3486, 1955.
148. Hacker, D. S. Jet Propulsion, Vol. 26, No. 9, 1956.
149. Hacker, D. S. Amer. Soc. Mech. Engrs. Paper, 58A-249, 1958.
150. Hall, N. A. and Price, H. In: Int. Dev. in Heat Transfer, Colorado, 1961.
151. Hartnett, J. P. Trans. ASME, Vol. 77, No. 8, 1955.
152. Hartnett, J. P., Birkebak, R. C. and Eckert E. R. G. J. Heat Transfer Trans ASME, Ser. C, Vol. 82, No. 3, 1961.
153. Hartnett, J. P. and Sastri, V. M. K. Heat Transfer in Transpired Turbulent Boundary Layers. International Summer School. Heat and Mass Transfer in Turbulent Boundary Layer, 1968.
154. Hill, F. K. JAS, Vol. 23, No. 1, 1956.
155. Hill, F. K. Physics of Fluids, Vol. 2, No. 6, 1959.
156. Jeromin, L. J. Fluid Mecy. Vol. 31, No. 1, 1968.
157. Jonsson, V. K. and Baker R. G. Imperial College TWF/TN/50. August 1968.
158. Jonsson, V. K. and Scott, C. I. Univ. of Minnesota. HTL TR-63, July 1965.
159. Kays, W. M. Convective Heat and Mass Transfer. McGraw-Hill, 1966.
160. Knuth, E. L. Jet Propulsion, Vol. 24, No. 6, 1954.
161. Knuth, E. L. and Dershin, H. Int. J. Heat Mass Transfer, Vol. 6, No. 12, 1963.
162. Korkegi, R. H. JAS, Vol. 23, No. 2, 1956.
163. Kulgein, N. G. J. of Fluid Mech. Vol. 12, pt. 3, 1962.
164. Kutateladze, S. S. and Leontiev, A. I. Turbulent Boundary Layers in Compressible Gases. London, 1964.
165. Laganelli, A. L., and Hartnett, J. P. Trans. ASME, Ser. V. Vol. 90, No. 4, 1968.
166. Launder, B. E. Massachusetts Inst. of Tech. Gas Turbine Lab. Rep. No. 71, 1963.
167. Launder, B. E. and Lockwood, F. C. Trans. ASME, Ser. V., Vol. 91, No. 2, 1969.
168. Leadon, B. M. and Scott, C. J. JAS, Vol. 23, No. 8, 1956.
169. Leadon, B. M. and Bartle, E. R. JAS, Vol. 27, No. 3, 1960.

170. Lees, L. Combustion and Propulsion. Third AGARD Colloqium, N. Y., p. 451-498, 1958.
171. Wolf, H. and Lehman, G. H. Jet Propulsion, Vol. 27, pt. I, 1957.
172. Librizzi, G. and Cresci, R. I. AIAA J., Vol. 2, No. 4, 1964.
173. Lobb, R. K., Winkler, E. M. and Persh, J. JAS, Vol. 22, No. 1, 1955.
174. Leontiev, A. I. In: Heat and Mass Transfer in Turbulent Boundary Layers. Advances in Heat Transfer, Vol. III, Academic Press, New York, p. 33-39, 1966.
175. Maise, G. and McDonald H. AIAA J. Vol. 6, No. 1, 1968.
176. Matting, E. W., Chapman, D. R., Nycolm, J. R. and Thomas, A. S. NASA, TR-R-82, 1961.
177. McEligot, D. M., Magee, P. M. and Leppert, G. ASME Papers, 64-HT-12, No. 1, 1965.
178. McLafferty, G. H. and Barber, R. E. J. Aerospace Sci., Vol. 29, No. 1, 1962.
179. Mickley, A. L., Ross, R. C., Squyers, A. L. and Stewart, W. E. NACA TN, No. 3208, 1954.
180. Mickley, A. L. and Davis, P. S. Rep. NACA Contract 6228, 1955.
181. Micley, H. S. and Davis, P. S. NACA TN, No. 4017, 1957.
182. Moffat, R. G. and Kays, W. M. Int. J. Heat and Mass Transfer, Vol. 11, No. 10, 1968.
183. Monaghan, R. J. ARCC, p. 45, 1950.
184. Moore, D. R. and Harkness, I. AIAA J, Vol. 3, No. 4, 1965.
185. Myers, G. E., Schauer, I. I. and Eustis, R. H. J. Basic Eng., Trans. ASME, Ser. D, Vol. 85, No. 1, 1963.
186. Nathan, Ness. JAS, Vol. 28, No. 8, 1961.
187. Nichiwaki, N., Hirata, M. and Tsuchida, A. J. Eng. Power, 675, 1961.
188. Nikuradse, J. VDI Forschungsheft, No. 356, 1932.
189. Olson, R. M. and Sparrow, E. M. A.I. Ch. E. J., Vol. 9, No. 6, 1963.
190. Pappas, C. C. NACA TN, No. 3222, 1954.
191. Pappas, C. C. and Okuno, A. F. JAS, Vol. 27, No. 5, 1960.
192. Pappas, C. C. and Okuno, A. F. NADA TN, N D 2230, 1964.
193. Papell, S. S. and Trout, A. M. NACA TN, N D—9, 1959.
194. Perkins, H. C. and Worsoe-Schmidt, P. Int. J. Heat Mass Transfer, Vol. 8, No. 7, 1965.
195. Pinkel, B. A. Trans. ASME, Vol. 76, No. 2, 1954.
196. Prandtl, L. ZAMM, Bd 5, 136, 1925.
197. Rannie, W. D. JAS, Vol. 23, No. 5, 1956.
198. Reshotko, E. and Tucker, M. NACA TN, No. 4154, 1957.
199. Reynolds, W. C., Kays, W. M. and Kline, S. J. Trans. ASME, Ser. C, Vol. 82, No. 4, 1960.
200. Romanenko, P. N. and Kharchenko, V. N. Int. J. Heat Mass Transfer, Vol. 6, No. 8, 1963.
201. Rosenbaum, H. and Margolis, D. P. Phys. of Fluids, Vol. 10, No. 6, 1967.
202. Rose, P. H., Probstein, R. F. and Adams, M. C. JAS, Vol. 25, No. 12, 1958.
203. Rubesin, M. W., Maybew, R. C. and Varga, S. A. NACA TN, No. 2305, 1951.
204. Rubesin, M. W., Pappas, C. C. and Okuno, A. F. NASA RM, A 55, December 1955.
205. Rubesin, M. W. NACA TN, No. 3341, 1954.
206. Rubesin, M. W. and Pappas, C. C. NACA TN, No. 4149, 1968.
207. Saarias, M. AIAA J., Vol. 6, No. 8, 1968.
208. Sastri, V. M. K. and Hartnett, J. P. In: Progress in Heat and Mass Transfer, Pergamon Press, Vol. 2, p. 213-223, 1969.

209. Szablewski, W. ZAMM, Bd 31, 131, 1951.
210. Scott, C. G., Eckert, E. R. G., Jonsson, V. K. and Yang, G. W. Heat Transfer Lad. Rep., HTL—TR, No. 55, 1964.
211. Schubaner, G. B. and Klebanoff, P. S. NACA Rep., No. 1030, 1950.
212. Shigemitsu, Y. J. Phys. Soc. Japan, Vol. 12, No. 2, 1957.
213. Schutz-Grunow, F. ZAMM, Bd 35, 309, 1956.
214. Seban, R. A. Trans. ASME, Ser. C, Vol. 82, No. 4, 1960.
215. Seban, R. A. and Back, L. H. Int. J. Heat Mass Transfer, Vol. 3, No. 2, 1961.
216. Seban, R. A. and Back. L. H. J. Heat Transfer, Vol. 84, No. 1, 1962.
217. Sigalla, A. J. Roy. Aero. Soc., Vol. 62, No. 576, 1958.
218. Sigalla, A. Aircraft Eng., Vol. 30, No. 351, 1958.
219. Roger, L., Simpson, R. L., Moffat, R. J. and Kays, W. M. Int. J. Heat Mass Transfer, Vol. 12, No. 7, 1969.
220. Simpson, R. L., Whitten, D. G. and Moffat, R. J. Int. J. Heat Mass Transfer, Vol. 13, No. 1, 1970.
221. Smith, F. and Harrop, R. R.A.E. TN Aeronaut., No. 1759, 1946.
222. Snodgrass, R. B. Jet Propulsion, Vol. 25, No. 12, 1955.
223. Sommer, S. C. and Chort, B. J. JAS, Vol. 23, No. 6, 1956.
224. Spalding, D. B. J. Appl. Mech., Trans. ASME, Ser. C., Vol. 28, No. 3, 1961.
225. Spalding, D. B. Convective Mass Transfer, Arnold, London, 1963.
226. Spalding, D. B., Auslander, D. M. and Sundaram, T. R. Paper Presented at A.G.A.R.D. Combustion and Propulsion Colloquium, London, 1963.
227. Spalding, D. B. and Chi, S. W. J. Fluid Mech., Vol. 18, pt. 1, 1964.
228. Spalding, D. B. AIAA J., Vol. 3, No. 5, 1965.
229. Spalding, D. B. and Patankar, S. V. Heat and Mass Transfer in Boundary Layers Morgan—Crampian, London, 1967.
230. Sparrow, E. M. and Cess, R. D. Radiation Heat Transfer. Brooks/Cole Pub. Comp., California, 1966.
231. Spence, D. A. JAS, Vol. 23, No. 1, 1956.
232. Squire, L. C. J. Fluid Mech., Vol. 37, pt. 3, 1969.
233. Stivenson, T. N. AIAA J., Vol. 2, No. 8, 1964.
234. Stratford, B. S. J. Fluid Mech., Vol. 5, pt. 1, 1959.
235. Stollery, G. L. and El—Ehwany, A. A. Int. J. Heat Mass Transfer, Vol. 8, No. 1, 1965.
236. Tewfik, O. E. AIAA J., Vol. 1, No. 6, 1963.
237. Tewfik, O. E. et al. Thermal Diffusion Effects on Energy Transfer in Turbulent Boundary Layer with Helium Injection, Proc. of the 1962 Heat Transfer and Fluid Mech. Inst., Stanford University Press, 1962.
238. Torii, K. et al. Third Int. Heat Transfer Conf., Chicago, Paper No. 85, August 1966.
239. Turcotte, D.L. J. Aerospace Sci., Vol. 27, No. 9, 1960.
240. Townsend, A. A. The Structure of the Turbulent Shear Flow, Cambridge University Press, 1956.
241. Waiter, S. A. and Le Blanc, L. P. SD 68—635, October, 1968.
242. Wallis, G. B. The Inst. of Mech. Eng. Proceed., Vol. 180, pt. I, No. 1, 1965-66.
243. Wallis, G. B. Int. J. Heat Mass Transfer, Vol. 11, No. 3, 1968.
244. Whitten, D. G. et al. Rep. NHMT-3, Stanford Univ., 1967.
245. Wilson, R. E. JAS, Vol. 17, No. 9, 1950.
246. Winkler, E. M. J. Appl. Mech. Trans. ASME, Ser. E., Vol. 28, No. 2, 1961.
247. Whitte, A. B. and Harper, E. G. AIAA J., Vol. 1, No. 2, 1963.
248. Wolf H. J. Heat Transfer, Trans. ASME, Ser. C., No. 11, 1959.

249. Wooldridge, C. E. and Muzzy, R. G. AIAA J., Vol. 4, No. 11, 1966.
250. Woodruff, L. W. and Lorenz, G. C. AIAA J., Vol. 4, No. 6, 1966.
251. Jakob, M. et al. Trans. ASME, Vol. 72, 1950.
252. Yuan, S. W. and Barazotti, A. Heat Transfer Fluid, Mech. Inst. Berkeley, p. 25-39, 1958.
253. Young, B. B. and Janssen, E. JAS, Vol. 19, No. 4, 1952.
254. Zellnik, H. E. and Churchill, S. W. A.I. Ch. E. J., Vol. 4, No. 1, 1960.
255. Zaric, S. International Summer School, Heat and Mass Transfer in Turbulent Boundary Layer, Boris Kidric Institute of Nuclear Sciences, 1968.
256. Goldstein, R. G., Eckert, E. R. G. and Wilson, D. T. Trans. ASME, Ser. B, Vol. 90, No. 4, 1968.
257. Burus, W. K. and Stollery, G. L. Int. J. Heat Mass Transfer, Vol. 12, No. 8, 1969.
258. Pichal, M. Strojnicky Casopis, Rocnik XVI, cislo 2, 1965.
259. Spivak, H. M. Aero Phys. Lab., Nor. Am. Aviation Rep., NOCM-615 CAL-1052, 1950.
260. Brinich, P. F. and Diaconis, N. S. Nat. Adv. Comm. Aero., Wash., Tech. Note No. 2742, 1952.
261. Monagan, R. J. and Jonson, J. E. Aero. Res. Counc., London, No. CP64, 1952.
262. Monagan, R. J. and Cooke, J. R. Aero. Res. Counc., London, No. CP39 and CP140, 1953.
263. Goddard, F. E. J. Aerospace Sci., Vol. 26, No. 1, 1959.
264. Abbot. AGARD Memo. A. G/8M4, 1953.

Translated for the National Aeronautics and Space Administration by Scripta Technica, Inc. NASw-2484.

U.S. GOVERNMENT PRINTING OFFICE: 1974—635-043/15